Gene Delivery with Amphiphilic Lower Generation Polypropylenimine Dendrimer

Katherine Bolton

2007

University of Strathclyde Glasgow

A thesis submitted in fulfilment of the requirements of the degree of Doctor of Philosophy

Department of Pharmaceutical Sciences
University of Strathclyde

Acknowledgments

First and foremost I would like to thank Prof. Ijeoma Uchegbu and Dr. Andreas Schätzlein for their vital guidance and support over the past few years. Thank you for allowing me to explore this subject with such impunity. You have taught me much more than research tools – you have changed the way I think.

Grateful thanks to Dr. Paul Gellert and Dr. Clive Washington of AstraZeneca UK for their personal input and company sponsorship.

I extend my thanks to Dr. Dave Watson (University of Strathclyde) for mass spectra, Dr. Laurence Tetley (University of Glasgow) for electron microscope images and Miss. Ya Tsz Anne Chim in the laboratories of Prof. Martyn C Davies (University of Nottingham) for atomic force microscope images.

Thank you to Dr. Christine Dufès and Mrs. Carol McCormack for imparting valuable skills and knowledge along with my senior researchers: Dr. Xiaozhong Qu, Dr. Vitaliy Khutoryanskiy, Dr. Pei Lee Kan, Dr. Dennis Wong, Dr. Woei Ping Cheng, Dr. Pui Ee Wong and Dr. Mazen El-Hammadi. Thank you also to all the technicians in the Department of Pharmaceutical Sciences and the Beatson Laboratories who made this work possible.

Finally, thank you to my husband Jered for his unwavering support.

Table of Contents

1. Introduction 15

1.1. Gene Therapy 15

1.1.1. Background 15

1.1.2. Clinical developments 16

1.1.3. The ideal gene medicine 18

1.1.4. Viral gene delivery 18

1.1.5. Non-viral gene delivery 19

1.1.5.1. Barriers to non-viral gene delivery 19

1.1.5.2. Naked DNA 20

1.1.5.3. Cationic lipids 21

1.1.5.4. Cationic polymer 23

1.1.5.5. Amphiphilic polymer 24

1.1.5.6. Targeting strategies 25

1.1.5.7. Dendrimers 25

1.1.5.8. Polyproylenimine (PPI) dendrimer 27

1.2. Aims and Objectives 30

2. Synthesis and Characterisation of Amphiphilic DAB-16 32

2.1. Introduction 32

2.1.1. Alkylation reaction 33

2.1.2. Nuclear Magnetic Resonance (NMR) spectroscopy 33

2.1.3. Mass Spectroscopy (MS) 34

2.1.4. Elemental Analysis (EA) 35

2.1.5. Ultraviolet-Visible Spectrophotometry with hydrophobic probe 36

2.1.6. Photon Correlation Spectroscopy (PCS) 37

2.1.7. Transmission Electron Microscopy (TEM) 38

2.2. Materials 39

2.3. Methods 40

2.3.1. Synthesis of cetyl DAB-16 (cDAB-16) 40

2.3.2. ^{1}H NMR 40

2.3.3. ESIMS 40

2.3.4. EA 42

2.3.4.1. Determination of C, H and N 42
2.3.4.2. Determination of Br content 42
2.3.5. Preparation of self-assembled structures 42
2.3.6. Determination of Critical Aggregation Concentration (CAC) 43
2.3.7. PCS 43
2.3.8. TEM 43
2.3.8.1. Negative stain TEM 44
2.3.8.2. Freeze fracture TEM 44
2.4. Results 45
2.4.1. Product yield 45
2.4.2. ^{1}H NMR 45
2.4.3. ESIMS 48
2.4.4. EA 52
2.4.5. Self-assembly 53
2.4.6. Determination of CAC 53
2.4.7. PCS 54
2.4.8. TEM 57
2.5. Discussion and conclusions 60
3. DNA Complexation Studies 63
3.1. Introduction 63
3.1.1. Plasmid DNA production 65
3.1.1.1. Culture and harvest of *Escherichia coli* 66
3.1.1.2. Extraction of plasmid DNA 66
3.1.1.3. Endotoxin removal 66
3.1.1.4. Purification of plasmid DNA 67
3.1.1.5. Determination of plasmid yield and purity 67
3.1.2. Isothermal Titration MicroCalorimetry 67
3.1.3. Ethidium Bromide exclusion assay 70
3.1.4. Agarose gel retardation assay 71
3.2. Materials 72
3.3. Methods 73
3.3.1. pDNA synthesis and purification 73

3.3.2. Isothermal Titration Microcalorimetry (ITC) 73
3.3.3. Preparation of complexes 74
3.3.4. Ethidium Bromide exclusion assay 74
3.3.5. Agarose gel retardation assay 75
3.4. Results 76
3.4.1. Plasmid quality and purity 76
3.4.2. ITC 76
3.4.2.1. The influence of pH 76
3.4.2.2. Proton transfer 80
3.4.2.3. Overview of binding profiles 83
3.4.2.4. Apparent binding enthalpies 85
3.4.3. Ethidium bromide exclusion assay 87
3.4.4. Agarose gel retardation assay 90
3.5. Discussion and conclusions 93
4. Physicochemical Characterisation of Complexes 97
4.1. Introduction 97
4.1.1. PCS 98
4.1.2. Zeta potential 98
4.1.3. Precipitation profiling 100
4.1.4. Atomic Force Microscopy (AFM) 100
4.1.5. Biological challenge 102
4.1.5.1. Glycosaminoglycan (GAG) 102
4.1.5.2. Nuclease 103
4.1.5.3. Serum 103
4.2. Materials 104
4.3. Methods 105
4.3.1. Preparation of complexes 105
4.3.2. PCS and zeta potential 105
4.3.3. Precipitation profiling 105
4.3.4. AFM 106
4.3.5. Biological challenge 106
4.3.5.1. Heparin 106

4.3.5.2. Nuclease 106
4.3.5.3. Serum 107
4.4. Results 108
4.4.1. PCS and zeta potential 108
4.4.1.1. Dendrimer profiles 108
4.4.1.2. Environmental conditions – pH 111
4.4.1.3. Environmental conditions – salt and serum 112
4.4.2. Precipitation profiling 114
4.4.3. AFM 117
4.4.4. Biological challenge 123
4.4.4.1. Heparin 123
4.4.4.2. Nuclease resistance 124
4.4.4.3. Serum resistance 127
4.5. Discussion and conclusions 129
5. In vitro biological characterisation 133
5.1. Introduction 133
5.1.1. Biocompatibility 134
5.1.1.1. Haemocompatibility 134
5.1.1.2. Cytotoxicity 135
5.1.2. Cell transfection 136
5.2. Materials 138
5.3. Methods 140
5.3.1. Cell culture maintenance (A431, PC-3, B16 F10) 140
5.3.2. pDNA synthesis and purification 140
5.3.3. Preparation of complexes 140
5.3.4. Haemocompatibility assay 140
5.3.5. MTT reduction assay 141
5.3.6. Reporter gene assays 142
5.3.6.1. β-Galactosidase activity 143
5.3.6.2. Firefly Luciferase activity 143
5.3.6.3. Total cell protein 144
5.3.7. Statistical analysis 144

5.4. Results 145
5.4.1. Haemocompatibility 145
5.4.2. Cytotoxicity 148
5.4.3. Transfection assays 152
5.4.3.1. The role of excess dendrimer in transfection 152
5.4.3.2. Choice of promoter 154
5.4.3.3. Transfection profiles 154
5.4.3.4. Serum effects 157
5.5. Discussion and conclusions 159
6. In vivo biological characterisation 162
6.1. Introduction 162
6.1.1. Toxicity determination 162
6.1.2. Quantification of Luciferase transgene expression 163
6.1.2.1. In vivo 163
6.1.2.2. Ex vivo 164
6.2. Materials 165
6.3. Methods 166
6.3.1. Dose ranging 166
6.3.2. Cell culture and tumour induction 166
6.3.3. Preparation and administration of treatments 167
6.3.4. Quantification of Luciferase transgene expression 167
6.3.4.1. Living Imaging® 167
6.3.4.2. Ex vivo analysis 168
6.4. Results 169
6.4.1. Dose ranging 169
6.4.2. Luciferase transgene expression 169
6.4.2.1. Animal weights 169
6.4.2.2. Total cell protein 170
6.4.2.3. Whole animal perfusion 171
6.4.2.4. Ex vivo biodistribution analysis 172
6.4.2.5. IVIS® quantitative analysis 173
6.4.2.6. *Ex vivo/ in vivo* correlation 178

6.5. Discussion and conclusions 179
7. Conclusions and further work 181
7.1. Conclusions 181
7.2. Further work 188

List of Tables

Table 1 Materials and suppliers used in Chapter 2 39

Table 2 Product yield 45

Table 3 Principal mass spectrum peaks identified for cDAB-16 product 50

Table 4 Elemental analysis of cDAB-16 * = No. of mol cetyl groups per 100 mol PPI groups 52

Table 5 Z average mean diameter and PI of cDAB-16 aggregates after manufacture (5mg.mL^{-1}), cholesterol added ranging from 0 - 10mg/mL (n=3). 55

Table 6 Z average mean diameter and PI of cDAB-16 vesicles 24 h after manufacture (5mg.mL^{-1}), cholesterol added ranging from 2.5 - 10mg/mL (n=3) 55

Table 7 Materials and suppliers used in Chapter 3 72

Table 8 Measured ΔH_{app} for carrier interaction with pDNA (verified independently). Carriers injected into pDNA (6.67 mM PPI/PEI into 1.5mM bps) at 25°C in phosphate buffer (pH 7.4, I = 10mM) (raw data not shown). 86

Table 9 Summary of N: P ratios at which key carrier-DNA complex events occur when visualised on a 1% agarose gel. 90

Table 10 Materials and suppliers used in Chapter 4 104

Table 11 Hydrodynamic diameter (nm) and surface zeta potential (mV) of complexes (PPI 30 N: P/ PEI 6 N: P, pDNA 50 μg.mL^{-1}) in differing solution pH. 112

Table 12 Materials and suppliers used in Chapter 5 139

Table 13 Mean IC_{50} values for dendrimer formulations in A431 cells (n=3) 149

Table 14 Mean IC_{50} values for dendrimer formulations in PC-3 cells (n=3) 149

Table 15 Mean IC_{50} values for dendrimer formulations in B16 F10 cells (n=3) 149

Table 16 Materials and suppliers used in Chapter 6 165

List of Figures

Figure 1 Indications addressed by gene therapy clinical trials..... 16
Figure 2 Vectors used in gene therapy clinical trials 17
Figure 3 Subcellular trafficking of non-viral gene delivery system (polymer-based)20
Figure 4 Chemical structures of several cationic lipids (a) and helper lipids (b) applied in cationic lipid gene delivery. Adapted from [33] 22
Figure 5 Cationic polymers used for gene delivery (a) branched poly(ethylenimine) (PEI) (b) fractured PAMAM dendrimer (c) Poly-L-lysine (PLL). Adapted from [41] 24
Figure 6 Poly(propylene imine) dendrimer synthesis by divergent strategy [55]..... 27
Figure 7 Structure of DAB-16-Am (PPI G3) [59] 28
Figure 8 Hydrophobic probes (i) pyrene (ii) methyl orange 37
Figure 9 Synthesis of cetyl DAB-16 (cDAB-16) 41
Figure 10 ^{1}H NMR spectrum of cDAB-16 in CD_3OD (* = solvent peak) and proton assignments. 46
Figure 11 ^{1}H-^{1}H COSY 90 of cDAB-16 in CD_3OD (* = solvent peaks). For proton assignments please see Figure 10 47
Figure 12 Electrospray ionisation mass spectrum of DAB-16-Am 49
Figure 13 Electrospray ionisation mass spectrum of cDAB-16 51
Figure 14 MO wavelength shift with cDAB-16 concentration. The midpoint of the transition between the non-aggregated and aggregated λ_{max} corresponds to the CAC of cDAB-16. Values pooled from two independent experiments. 54
Figure 15 Size distribution graph for cDAB-16 vesicles 5mg.mL^{-1} containing cholesterol 2.5mg.mL^{-1} (molar ratio 0.4) 56
Figure 16 Negative stain transmission electron micrographs of cDAB-16 vesicles (5mg.mL^{-1} in water). (i) x50,000 magnification (densely populated). (ii) x20,000 magnification (sparsely populated). 58
Figure 17 (i) Schematic illustration of lamellar structures (imaged in Figure 16(i) & (ii)) 59
Figure 18 Molecular model of PPI G3 dendrimer-DNA binding [59]..... 64
Figure 19 (a) A schematic diagram of a typical cell arrangement in an ITC. (b) Performing a titration and example of raw data output [122] 68

Figure 20 Structure of ethidium bromide (Eth Br) and illustration of Eth Br stacking between DNA base pairs 71
Figure 21 pCMVsport β-Galactosidase vector map [146] 73
Figure 22 Main: DAB-16-Am injected into pDNA (8.89mM PPI: 0.29mM bps) at 25°C, all in phosphate buffer (I = 10mM) adjusted to (i) pH 3 (ii) pH 7 (iii) pH 11. Inset: corresponding raw ITC. (iv) ΔH_{app} versus solution pH for DAB-16-Am..... 79
Figure 23 (i) DAB-16-Am injected into pDNA (6.67mM PPI: 1.5mM bps) at 25°C, pH 7.4, I = 10mM in (i) TRIS buffer (ii) HEPES buffer (iii) phosphate buffer (iv) ΔH_{ion} versus ΔH_{app} for DAB-16-Am 82
Figure 24 (i)-(iv) Enthalpograms for all carriers over N:P ratio 0-6 (y axis values adjusted for baseline); 8.16 mM PPI/PEI into 0.29 mM bps, pH 7.4, 25°C in phosphate buffer (I = 10mM) 84
Figure 25 Binding of DAB-16-Am to DNA probed by Eth Br after 0.5-168 h (N: P ratio 0.125-5) 88
Figure 26 Binding of cDAB-16 to DNA probed by Eth Br after 0.5-168 h (N: P ratio 0.125-5) 88
Figure 27 Binding of cDAB-16 vesicles probed by Eth Br after 0.5-168 h (N: P ratio 0.125-5) 89
Figure 28 Mean reduced fluorescence of Eth Br in DNA solution after incubation with carriers for 0.5 h (N: P ratio 0.125-5) (n= 3)..... 89
Figure 29 DAB-16-Am. Upper gel – Coomassie stain. Lower gel – Eth Br stain..... 91
Figure 30 ExGen 500. Upper gel – Coomassie stain. Lower gel – Eth Br stain..... 91
Figure 31 cDAB-16. Upper gel – Coomassie stain. Lower gel – Eth Br stain. 92
Figure 32 cDAB-16 vesicles. Upper gel – Coomassie stain. Lower gel – Eth Br stain. 92
Figure 33 Schematic representation of the structure of the electrical double layer according to Stern's theory [104]. (ψ_o = surface potential, ψ_d = stern potential, δ = stern layer thickness, ζ = zeta potential, κ = ionic boundary layer). 99
Figure 34 Schematic representation of an AFM system with a moveable cantilever [201] 101
Figure 35 Size and zeta potential analysis of DAB-16-Am-DNA complexes 0.5-60 N:P pH 7.4 109

Figure 36 Size and zeta potential analysis of cDAB-16 -DNA complexes 0.5-60 N: P pH 7.4 110
Figure 37 Size and zeta potential analysis of cDAB-16 vesicles -DNA complexes 0.5-60 N: P pH 7.4 110
Figure 38 Hydrodynamic diameter (nm) of carriers at a final DNA concentration of 25 μg.mL^{-1} (PPI 30 N: P/ PEI 6 N: P) in differing environments. HBD = formed in HEPES buffered dextrose; HBD x10 = formed in HBD, diluted x10 into HBD; DMEM x10 = formed in HBD, diluted x10 into DMEM; DMEM = formed in DMEM; 50% FBS = formed in HBD, diluted x10 into DMEM: FBS 1: 1 v/v. 113
Figure 39 Variation in DNA solubility complexed with DAB-16-Am at N: P ratios 0.1-30 at three DNA concentrations. 115
Figure 40 DAB-16-Am NP 0.5-30 (250μg.ml^{-1} DNA) and amine levels (pH 7.4) . 116
Figure 41 cDAB-16 NP 0.05-30 (250μg.ml^{-1} DNA) and amine levels (pH 7.4) 116
Figure 42 Centre = free plasmid DNA. Route a = condensation by DAB-16-Am, route b = condensation by cDAB-16 and route c = condensation by cDAB-16 vesicles (all after 15 min incubation). 117
Figure 43 TM-AFM images in 5% dextrose solution (pH 10). DAB 16-Am –DNA complex at 30 N: P ratio; where scale bar in (a) is 500 nm and (b) is 100 nm. Z = 10 nm in (a) and Z = 15 nm in (b) 119
Figure 44 TM-AFM images in 5% dextrose solution (pH 10). Cetyl-DAB 16 –DNA complexes at 30 N: P ratio; where scale bar in (a) is 500 nm and (b) is 100 nm. Z = 10 nm in (a) and Z = 15 nm in (b) 119
Figure 45 TM-AFM images in 5% dextrose solution (pH 10). Cetyl DAB 16-vesicles –DNA complexes at 30 N: P ratio. Where scale bar in (a) is 500 nm and (b) is 100 nm. Z-scale for (a) = 35 nm and (b) = 15 nm 120
Figure 46 DAB-16-Am-DNA complexes, 30 N: P, pH 7.4, 15-20 min incubation Z = 10nm for both images. 121
Figure 47 Cetyl-DAB-16-DNA complexes, 30 N: P, pH 7.4, 15-20 min incubation. Z = 10nm for both images. 122
Figure 48 '– HEP' = carriers at 30 N: P (DAB-16-Am, cDAB-16 and cDAB-16 vesicles), 6N:P (ExGen 500) and 2 N:P (DOTAP); '+ HEP' = carrier complexes with

1% w/v heparin sodium (25°C, 10 min); '+ HEP + HEAT' = with 1% w/v heparin sodium (70°C, 16 h) 123
Figure 49 DNase I sensitivity of pDNA in the presence of carriers..... 126
Figure 50 DNA degradation in the presence of 50% v/v foetal bovine serum (FBS) with carriers..... 128
Figure 51 Suggested initial binding configurations for the three dendrimer species based on studies in Chapter 3 and Chapter 4. 131
Figure 52 The EIF1α/HTLV Luc (enhanced) expression plasmid..... 137
Figure 53 The CMV Luc (enhanced) expression plasmid 137
Figure 54 Mean ± SE haemolytic activity (%) of carriers at concentrations from 0.001 – 10 mg.mL^{-1}. 0% = PBS solution, 100% = Triton-X 100 1% v/v (n=3). 146
Figure 55 Mean ± SE haemolytic activity (%) of lower generation PPI dendrimers free or complexed with pDNA (30 N: P) (n=3) 147
Figure 56 Mean ± SE A431 % cell viability (CV) versus free dendrimer concentration (n=3) 150
Figure 57 Mean ± SE A431 % CV versus dendrimer complexed with pDNA (30 N: P) (n=3) 150
Figure 58 Mean ± SE B16 F10 % cell viability (CV) versus free dendrimer concentration (n=3) 151
Figure 59 Mean ± SE PC-3 % cell viability (CV) versus free dendrimer concentration (n=3) 151
Figure 60 Mean ± SE (n = 6) transfection efficiency of DAB-16-Am with varied N: P ratio (columns); with fraction of total dendrimer in supernatant (line)..... 153
Figure 61 Comparison of transfection efficiencies (mean ± SE) of complete DAB-16-Am-pDNA complexes versus supernatant complexes with varied N: P ratio (n = 6). 153
Figure 62 Expression profiles for pCMV and pEIF1α-Luc plasmid (1 μg DNA) alone or complexed with ExGen (6 N: P) or DAB-16-Am (30 N: P) (Mean values ± SE, n = 3). 154
Figure 63 Transfection profile of cDAB-16: 1,2,6 and 30 N: P with 1μg pEIF1α/HTLV-Luc. ExGen: 6 N: P with 0.3 μg pEIF1α/HTLV-Luc. Blank: DMEM.

(All columns). Plotted against % cell viability (line) as determined by BCA assay (Mean values ± SE, n=5)..... 155
Figure 64 Transfection profile of DAB-16-Am: 1,2,6 and 30 N: P with 1μg pEIF1α/HTLV-Luc. ExGen: 6 N: P with 0.3 μg pEIF1α/HTLV-Luc. Blank: DMEM. (All columns). Plotted against % cell viability (line) as determined by BCA assay (Mean values ± SE, n=5)..... 156
Figure 65 Luciferase expression achieved by carriers in A431, PC-3 and B16 F10 cells. BL = DMEM. Luc = EIF1α/HTLV-Luc 0.5 μg. ExGen = ExGen 500: pLuc (6 N: P, 0.3 μg). D16 = DAB-16-Am: pLuc (30 N: P, 0.5 μg). CD16 = cDAB-16: pLuc (30 N: P, 0.5 μg). CC16 = cDAB-16 vesicles: pLuc (30 N: P, 0.5 μg) (Mean values ± SE, n = 6)..... 157
Figure 66. The reduction of carrier transfection efficiencies in A431 cells (0.5 μg pEIF1α/HTLV-Luc) upon addition of 50% v/v serum (statistical significances are as follows: * p = 0.001 ** p ≤ 0.02 *** p ≤ 0.05) (Mean values ± SE, n = 3)..... 158
Figure 67. Illustration of photon transport of light from an internal source to the visible position on the surface of the animal. This surface image is observed [267]. 164
Figure 68 Animal weights (g) recorded at 0, 24 and 48h post i.v. injection with carrier formulations: Blank = HBD pH 7.4, pLuc = EIF1α/HTLV –Luc (50 μg), ExGen 500 = ExGen 500: pLuc (6 N: P), DAB-16-Am = DAB-16-Am: pLuc (30 N: P), cDAB-16 = cDAB-16: pLuc (30 N: P), cDAB-16 vesicles = cDAB-16 vesicles: pLuc (30 N: P). (Mean values ± SE, n=3 animals/group)..... 170
Figure 69 Total protein content (mg) per 0.2 mL organ lysate measured by BCA assay (Mean values ± SE, n = 15 animals)..... 171
Figure 70 Ex vivo luciferase analysis of liver or lung lysates 24 h after injection with DAB-16-Am 30 N: P with EIF1α/HTLV –Luc (50 μg) (n=2), ExGen 500 6N: P with EIF1α/HTLV –Luc (50 μg) (n=2) or Blank = HBD (pH 7.4) (n=2) with or without whole animal perfusion. 172
Figure 71 Ex vivo luciferase analysis of organ lysates 48 h after injection with: Blank = HBD pH 7.4, pLuc = EIF1α/HTLV –Luc (50 μg), ExGen 500 = ExGen 500: pLuc (6 N: P), DAB-16-Am = DAB-16-Am: pLuc (30 N: P), cDAB-16 = cDAB-16: pLuc

(30 N: P) (Mean values ± SE, n = 3 with the exception of one animal in the cDAB-16 group removed from the study). 173
Figure 72 ROIs measured for lungs and tail at 24 h in mouse treated with ExGen-pLuc (6 N: P) 174
Figure 73 ROIs measured for lungs and tail at 48 h in mouse treated with ExGen-pLuc (6 N: P) 174
Figure 74 In vivo luciferase activity in the lung for carriers BL = blank, pLuc = ElF1α/HTLV –Luc (50 μg), ExGen = ExGen 500: pLuc (6 N: P), D16 = DAB-16-Am: pLuc (30 N: P), CD16 = cDAB-16: pLuc (30 N: P), CC16 = cDAB-16 vesicles: pLuc (30 N: P) (Mean values ± SE, n=3) at (a) 24 h and (b) 48 h. 176
Figure 75 In vivo luciferase activity in the tail for carriers BL = blank, pLuc = ElF1α/HTLV-Luc, ExGen = ExGen 500: pLuc (6 N: P), D16 = DAB-16-Am: pLuc (30 N: P), CD16 = cDAB-16: pLuc (30 N: P), CC16 = cDAB-16 vesicles: pLuc (30 N: P) (Mean values ± SE, n=3) at (a) 24 h and (b) 48 h. 177
Figure 76 Ex vivo – in vivo correlation between 64 tail and lung samples at 48 h post injection. 178

Abstract

In this work a novel lower generation amphiphilic polypropylenimine (PPI) dendrimer with good aqueous solubility was developed and tested as a gene delivery agent. PPI dendrimer generation 3 (DAB-16-Am) was substituted with a low level of cetyl chains (less than 5 molar percent) by reaction with 1-bromohexadecane under carefully controlled conditions. Structural characterisation was carried out using nuclear magnetic resonance spectroscopy, mass spectrometry and elemental analysis. Cetylated DAB-16 spontaneously self-assembled in an aqueous environment and in the presence of cholesterol (50% w/w) formed unilamellar vesicles of approximately 50nm in diameter. Cetylation tripled the DNA binding capacity of the dendrimer, supporting the hypothesis that the presence of hydrophobic alkyl chains would improve the packaging of DNA by the dendrimer. Apparent DNA binding enthalpies were also significantly more favourable. The size, surface charge and morphologies of the resulting complexes were found to be dependent upon the composition of the dendrimer. Cetylated dendrimer was able to stabilise complexes against electrostatic disruption but differing biophysical characteristics of complexes did not influence the protection of DNA against nuclease activity. The introduction of hydrophobic moieties increased the haemolytic potential of the dendrimer and enhanced cytotoxic effects in three immortalised cell lines. Cetylated DAB-16 formulations were able to transfect these cell lines although the dendrimer dose applied to cells must balance intracellular access and toxicity. Cetylated DAB-16 was also well tolerated when administered intravenously at doses required for *in vivo* gene delivery. These features suggest that cetylated DAB-16 has a potential application in anti-tumour gene therapy.

1. Introduction

1.1. Gene Therapy

1.1.1. Background

The discovery of the complementarity of deoxyribonucleic acid (DNA) by Watson and Crick in 1953 [1, 2] led to understanding of the mechanism of hereditary and an explosion of new developments in the areas of biochemistry and genetics.

To date the entire human genome has been mapped (3 billion DNA base pairs sequenced and between 20-25,000 genes identified) and as a result of the availability of this genetic information many potential disease targets have been identified [3]. Gene therapy is "the deliberate introduction of genetic material into human somatic cells for therapeutic, prophylactic or diagnostic purposes" (UK Gene Therapy Advisory Committee, 2004). There are two main approaches: direct introduction of genes into target cells in the body (*in vivo* gene therapy) or modification of target cells outside patients which are then re-implanted (*ex vivo* gene therapy) [4].

Initially the concept of gene therapy was limited to monogenic (single gene) recessive disorders such as cystic fibrosis, the most common life threatening inherited condition in the UK. In this technique, copies of the healthy gene are introduced into cells *in vivo* in order to produce sufficient functional protein product to compensate for its defective counterpart [4]. Successes in the treatment of Severe Combined Immunodeficiency Disease (SCID) have been widely publicised in the UK, requiring *ex vivo* transformation of haematopoietic stem cells and their autologous transplantation [4].

As the genetic basis for multifactoral diseases such as cancers is being expounded application of gene therapy to these conditions represents potential cures for the most frequent causes of death in this country.

1.1.2. Clinical developments

Gene therapy clinical trials have been carried out in the United Kingdom for over a decade, first targeting monogenic diseases but now overtaken in number by cancer gene therapy trials and widely extending to cardiovascular and infectious diseases. According to the clinical trials database of the Journal of Gene Medicine website [5] most current trials (to date, 1309) are in early development phases and currently 67% of clinical trial protocols are in the area of oncology (Figure 1).

The most efficient and specific vehicles utilised for introducing and maintaining foreign gene expression in a tissue are viruses, and of all trials maintained in this database, 23% use retroviruses and 25% adenoviruses to deliver the gene of interest (Figure 2).

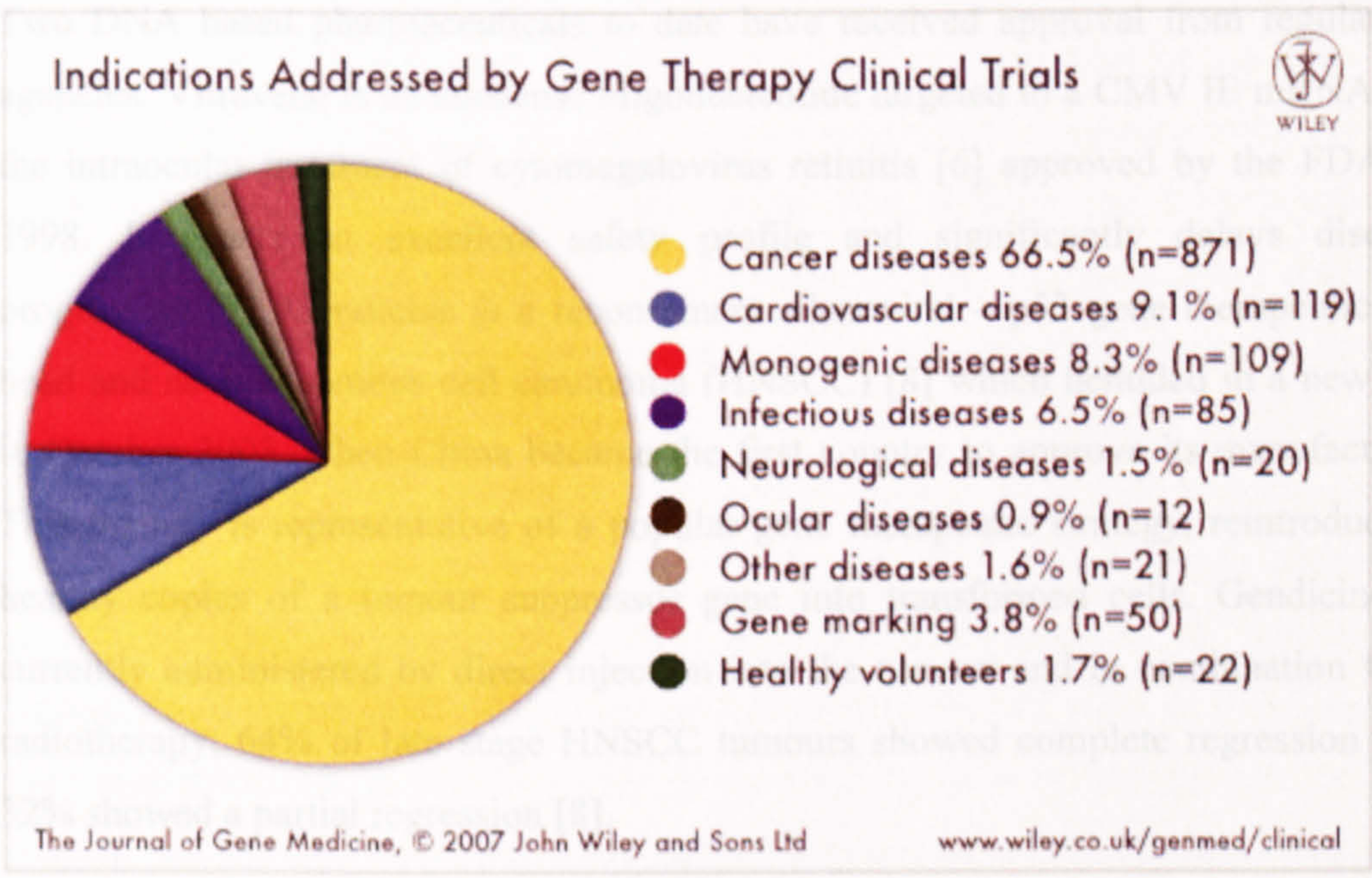

Figure 1 Indications addressed by gene therapy clinical trials

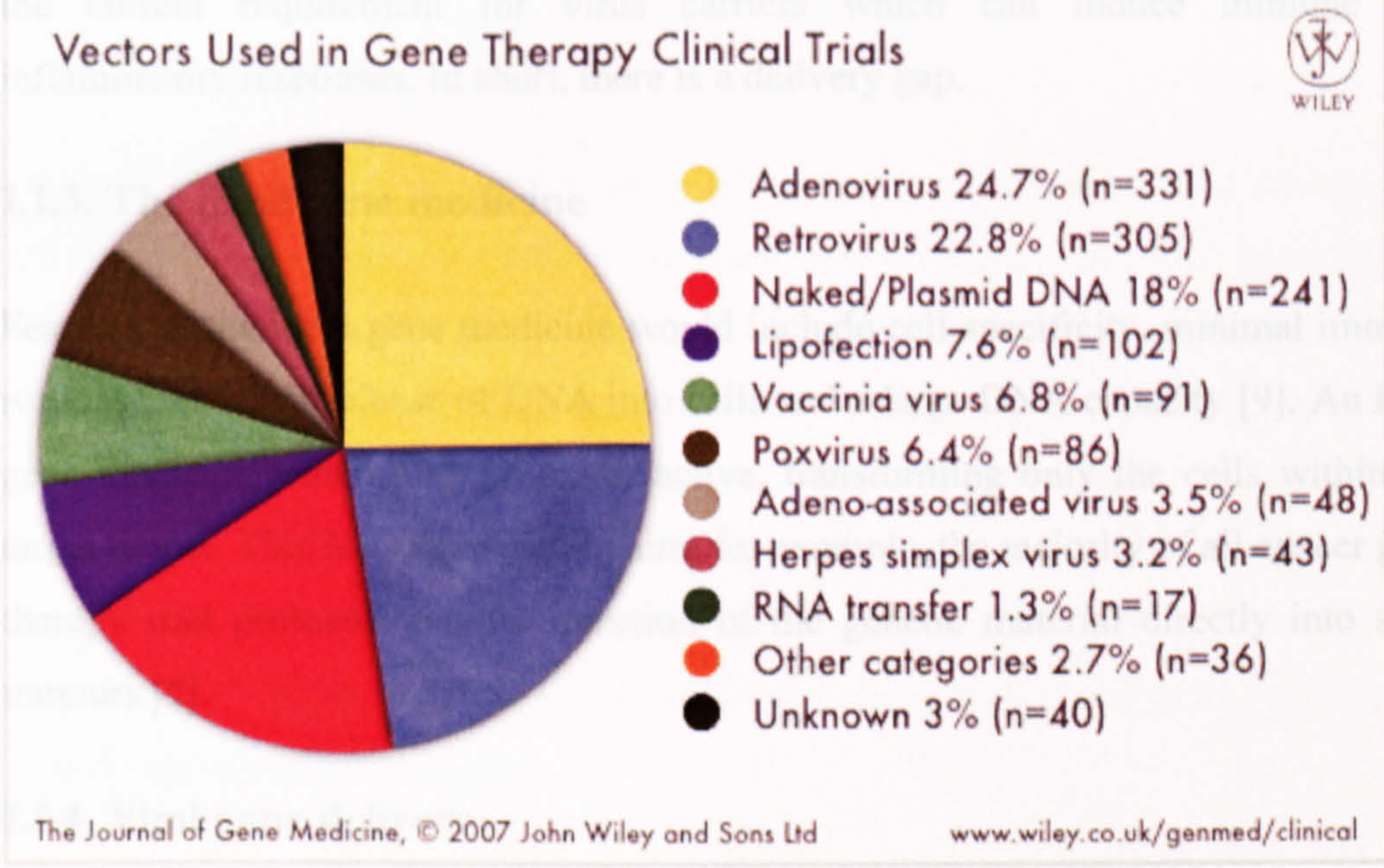

Figure 2 Vectors used in gene therapy clinical trials

Two DNA based pharmaceuticals to date have received approval from regulatory agencies. Vitravene is an antisense oligonucleotide targeted to a CMV IE mRNA for the intraocular treatment of cytomegalovirus retinitis [6] approved by the FDA in 1998. It boasts an excellent safety profile and significantly delays disease progression [7]. Gendicine is a recombinant adenoviral – p53 gene therapeutic for head and neck squamous cell carcinoma (HNSCC) [8] which heralded in a new era in October 2003, when China became the first country to approve its manufacture. This therapy is representative of a popular gene therapeutic strategy, reintroducing healthy copies of a tumour suppressor gene into transformed cells. Gendicine is currently administered by direct injection into the tumour and in combination with radiotherapy, 64% of late stage HNSCC tumours showed complete regression and 32% showed a partial regression [8].

After 15 years of investigation, one could ask why so few therapies have progressed beyond early stage clinical trials. The focus on multigene disorders such as cardiovascular disease poses an inherent problem for a single gene strategy, but some of the biggest obstacles are the short lived nature of gene therapy in the organism and

the current requirement for virus carriers which can induce immune and inflammatory responses. In short, there is a delivery gap.

1.1.3. The ideal gene medicine

Features of the ideal gene medicine would include cell specificity, minimal immune response, efficient release of DNA into cells and a large DNA capacity [9]. An ideal gene medicine would also be orally active, transforming only the cells within the target tissue. This is a rather distant aim, for example, the majority of all cancer gene therapy trial protocols require injection of the genetic material directly into solid tumours [5].

1.1.4. Viral gene delivery

Viral vectors such as attenuated viruses, adenoviruses and retroviruses are efficient in delivery of nucleic acid to specific cell types (as little as one viral particle is required to transfect a dividing cell) [10] and have been developed for use in *ex vivo* and *in vivo* gene therapy [5]. The only reported side effect of the successful product Gendicine over five years of clinical trials was self-limiting fever; however adenoviral vectors have been reported to cause serious immunological reactions which escalate with necessary repeated administration, including one tragic loss of life in a gene therapy trial for ornithine transcarboxylase deficiency (OTCD) [11]. Retroviruses have found success in gene therapy clinical trials, able to permanently restore a functioning immune system to sufferers of X-linked severe combined immunodeficiency disease (X-SCID) through reintroduction of autologous haematopoietic stem cells transfected *ex vivo* with a healthy copy of the defective gene. However, retroviruses randomly incorporate the gene of interest into the host genome and cases of insertional carcinogenesis as a result of this therapy have been reported, requiring greater caution in further trials [12]. As a result, non-viral vectors have been studied as an attractive alternative.

1.1.5. Non-viral gene delivery

The major classes of non-viral vectors that have demonstrated useful transfection efficiencies (whilst still thousands of times less efficient than viral systems) are naked DNA [13] and DNA formulated with cationic lipids (lipoplexes) [14] or polymers (polyplexes) [15]. No specific host immune response has been produced after administration of these vectors and episomal placement of delivered DNA favours safe, acute treatment. The chemical composition of these carriers can be carefully controlled and they are capable of complexing DNA of any size in large quantities [9]. Some of the obstacles that the designers of these technologies must circumvent are outlined below.

1.1.5.1. Barriers to non-viral gene delivery

The stability of a non-viral delivery system in the extracellular biological milieu, particularly after intravenous administration, must be both physical and chemical to allow the therapeutic payload to reach its target tissue. Endogenous, negatively-charged molecules such as glycosaminoglycans and serum albumin can release DNA from a positively charged binding agent and nucleases present in the extracellular environment degrade exposed DNA within minutes [16, 17]. Also, non-specific interactions with scavenging immune system components lead to aggregation and sequestration of particulates and prevent access to target organs [18].

Once proximity to the target organ is achieved, the complexes must extravasate and cross the target organ interstitium. Target cell internalisation necessitates association with the cell surface. The non-viral carrier must then stimulate the process of endocytosis. Following internalisation, the intracellular vesicles containing the external particle become structures called endosomes responsible for returning recycled material to the cell surface [19]. Therefore, the non-viral systems must escape these structures into the cytoplasm where further intracellular nucleases await [20]. The systems must then be trafficked towards the nucleus, at which point a further barrier is encountered, the nucleolar membrane. Access to the nucleus is either dependent on cell division when the nuclear envelope breaks down or through

tiny pores in the nuclear membrane [21]. At this point the DNA payload must have been released to allow access by the transcription apparatus [22-27], eventually assembling the desired protein and, in large enough quantities, producing the desired therapeutic effect (Figure 3).

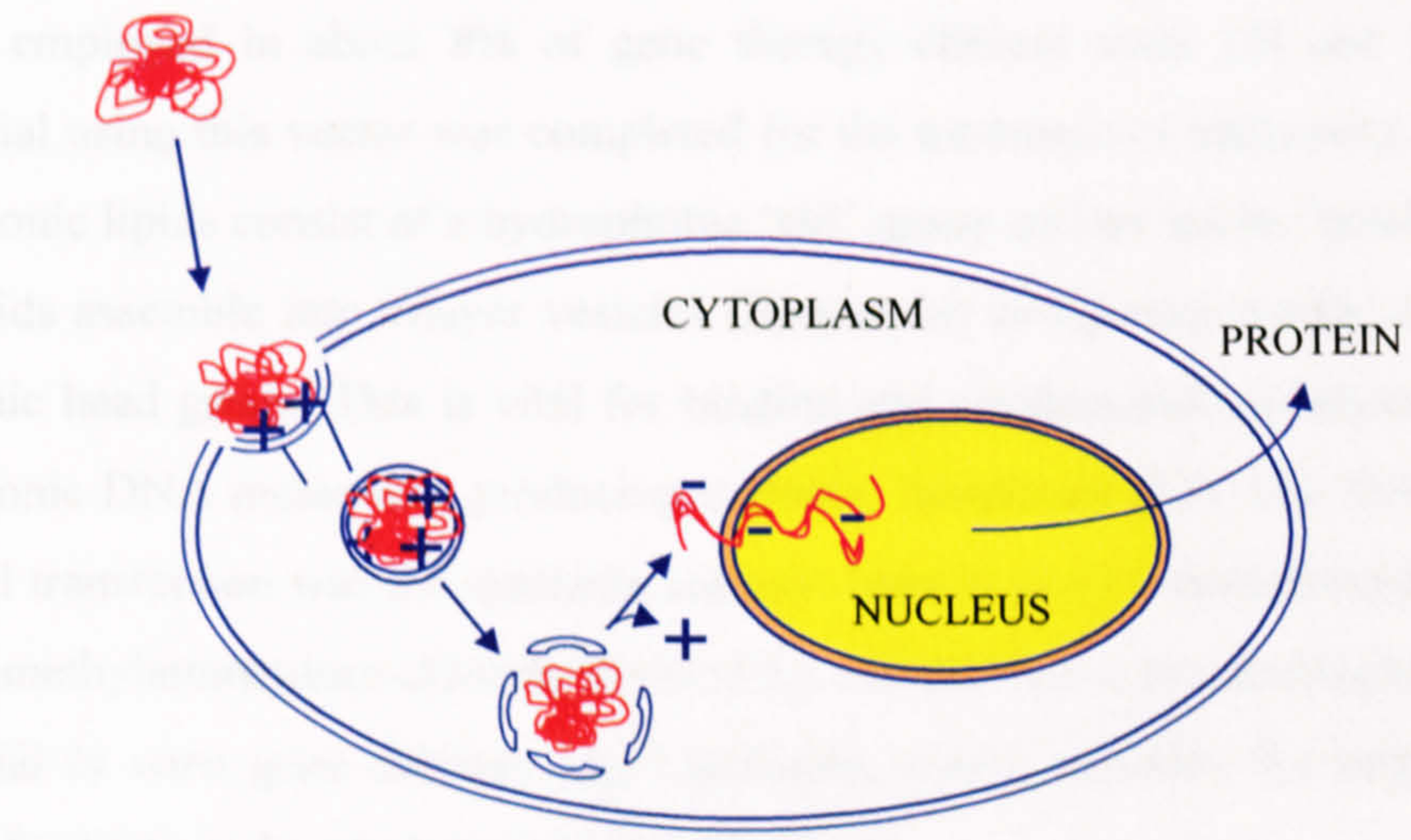

Figure 3 Subcellular trafficking of non-viral gene delivery system (polymer-based)

1.1.5.2. Naked DNA

Physical methods of gene delivery remain popular due to the lack of immunogenicity of naked DNA [9], triggered by the work of Wolff *et al.* in 1990 who demonstrated that naked DNA could transfect smooth muscle cells, in some cases with the effect persisting for more than two months [13]. Since then all manner of physical techniques have been exploited. Hydroporation relies on the generation of hydrodynamic pressure from large volume intravenous injections to efficiently transfect liver cells [28]. *In vivo* electroporation employs the use of pulses of electric current to increase cell permeability to a plasmid DNA following direct tissue or intravenous injection [29]. Also, five clinical trials of naked plasmid DNA are currently being carried out using 'gene gun' (high pressure particle bombardment) technology [5].

These techniques are each limited by a lack of targeting ability, physical damage to tissues and also the continuing susceptibility of plasmid DNA to nuclease degradation *in vivo* [9].

1.1.5.3. Cationic lipids

According to the Journal of Gene Medicine database, cationic liposomes are currently employed in about 8% of gene therapy clinical trials [5] and the first clinical trial using this vector was completed for the treatment of melanoma in 1993 [30]. Cationic lipids consist of a hydrophobic 'tail' group and an amine 'head' group. These lipids assemble into bilayer vesicles (liposomes) in aqueous media, exposing the cationic head group. This is vital for binding and condensation (compaction) of large, anionic DNA molecules, producing colloidal lipoplexes [31]. The first to find use in cell transfection was the synthetic cationic lipid N-[1-(2,3-dioleyloxy)propyl]-N,N,N-trimethylammonium chloride (DOTMA), and this led to the development of a commercial *in vitro* gene delivery kit, Lipofectin, which includes the helper lipid DOPE to facilitate endosomal escape [32] (Figure 4).

(a)

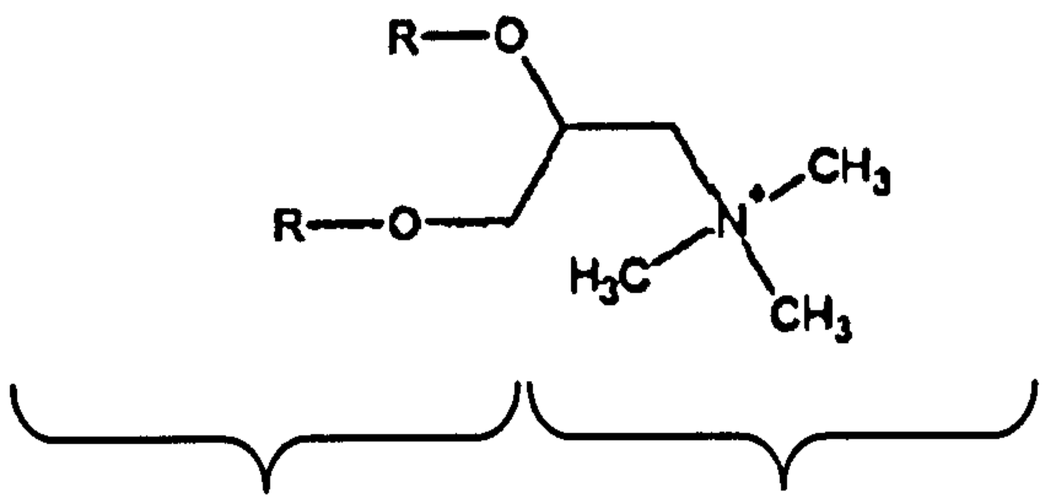

DOTMA

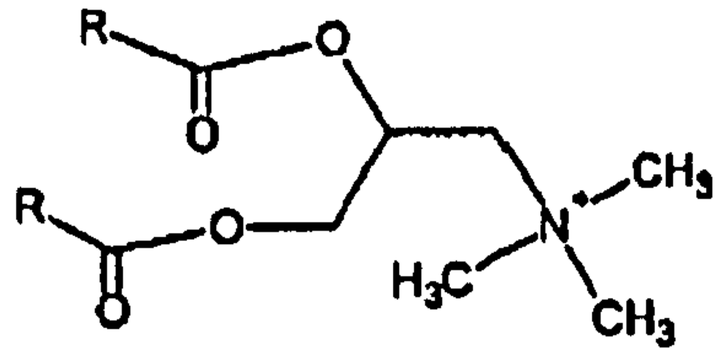

DOTAP

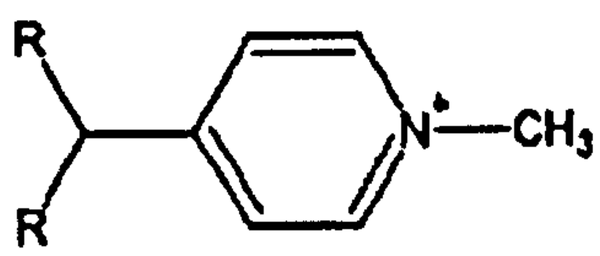

SAINT2

(b)

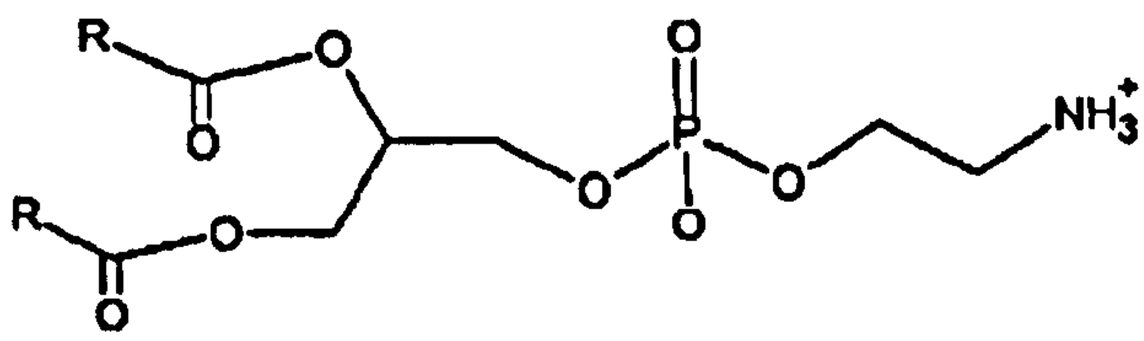

DOPE

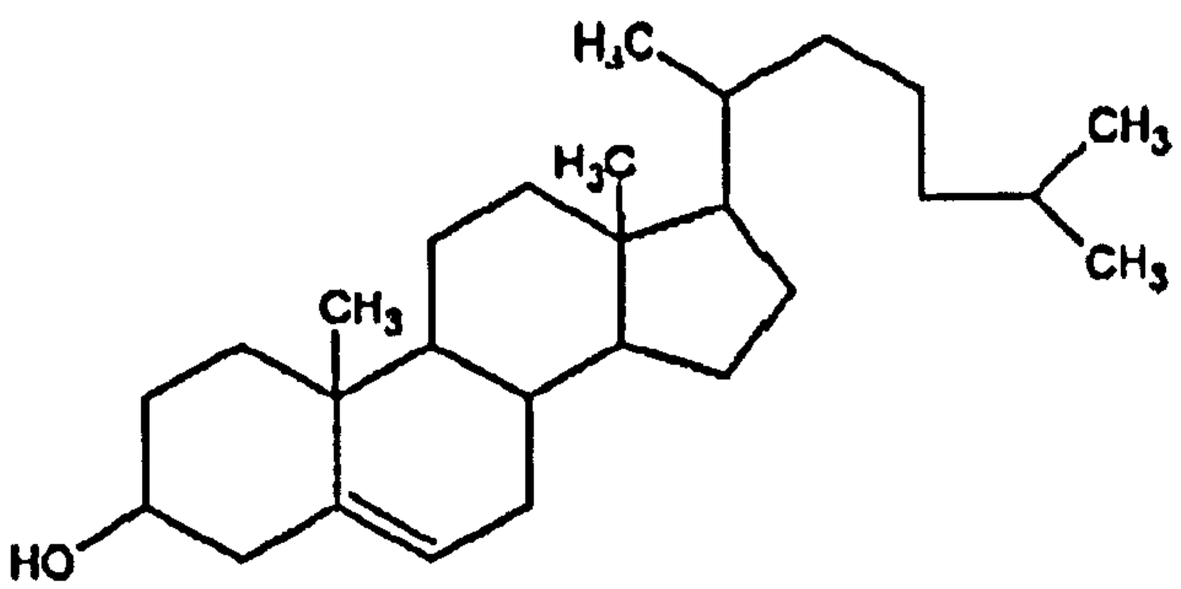

Cholesterol

Figure 4 Chemical structures of several cationic lipids (a) and helper lipids (b) applied in cationic lipid gene delivery. Adapted from [33]

Lipoplexes have been shown to protect genetic material from degradation by plasma nucleases where intravenous administration is required to reach otherwise inaccessible organs. However, these lipoplexes must retain a positive surface zeta potential required for non-specific cellular entry via endocytosis (their fusogenic properties allow endosomal escape and subsequent nuclear trafficking) [34]. As a result they are cleared rapidly from the circulation by the reticuloendothelial system and accumulate in the lung capillary bed, resulting in gene expression mainly in the lung endothelium [14]. A balance must also be struck between good access to the cell cytoplasm and damage to the cell membrane and essential cellular anions. Toxicity has been a major limitation for their use as *in vivo* gene delivery systems [9].

1.1.5.4. Cationic polymer

Cationic polymers are also able to condense DNA effectively (forming polyplexes) and polymeric structures allow tight control of macroscopic characteristics of polyplexes [35]. These were used before lipoplexes to transform cells *in vitro* but progress has been slow due to the low efficiency of previously examined systems, such as poly-L-lysine (PLL) which required the use of helper substances such as the endosomolytic agent chloroquine for efficacy [36]. Polymeric gene carriers are unused in clinical trials with the exception of linear polyethylenimine (L-PEI) which was used to administer a therapeutic plasmid intravesicularly to treat bladder carcinoma in two patients with demonstrable success and no detectable toxicity from the carrier [37]. Second generation polycations such as L-PEI are one of the most efficient groups of synthetic transfection agents. These are potentially superior vehicles of therapeutic genes when compared with lipoplexes [38]. However, these cationic polymers still display cytotoxicity due to their surface charge and resulting instability interaction of polyplexes with anionic blood components allowing release of free polymer [39]. It is widely held that the failure of the amino acid based PLL was due to a lack of endosomal escape facility [35]. PEI contains protonable nitrogens which cause a chloride ion influx as the pH falls within the endosome, causing an osmotic membrane rupture and preventing lysosomal degradation of the transported DNA [40].

(a)

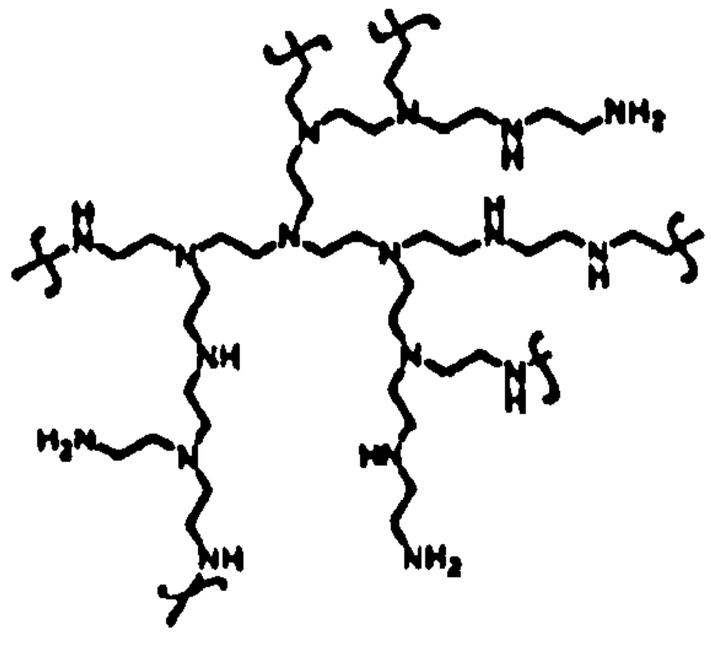

(b)

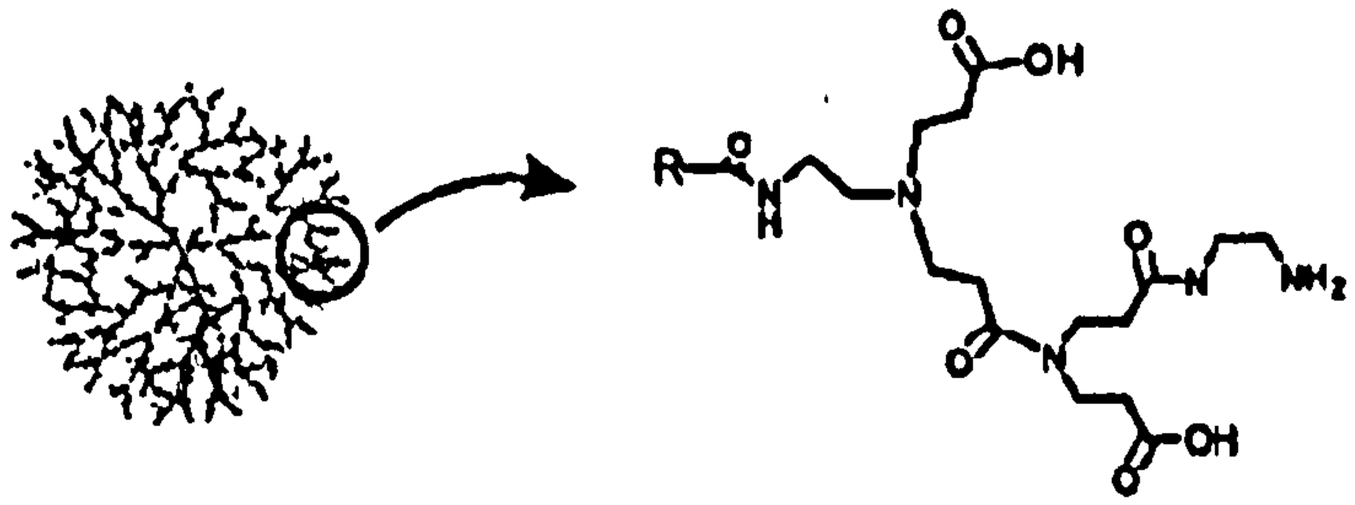

(c)

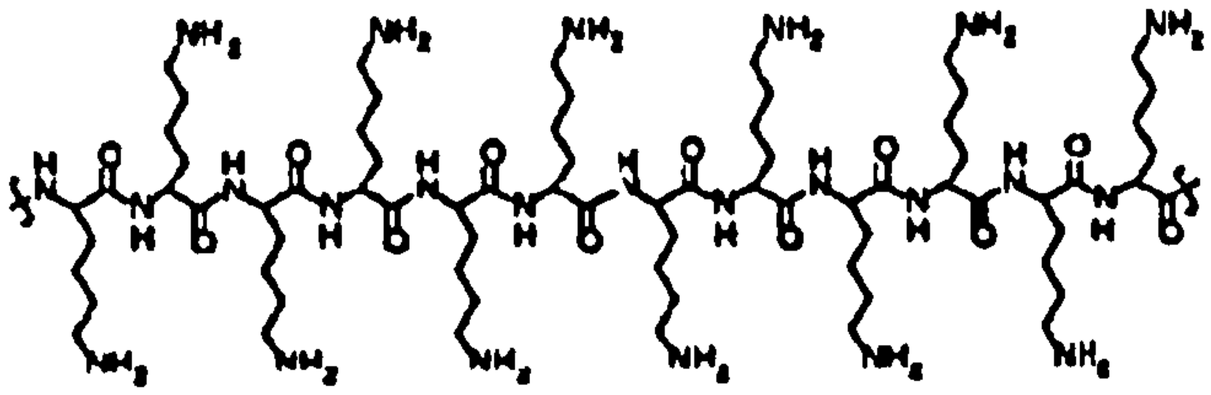

Figure 5 Cationic polymers used for gene delivery (a) branched poly(ethylenimine) (PEI) (b) fractured PAMAM dendrimer (c) Poly-L-lysine (PLL). Adapted from [41]

1.1.5.5. Amphiphilic polymer

Liposomalisation can concentrate the cationic charge on the liposomal surface available for DNA condensation, therefore vectors combining the advantages of both liposomes and polycations have been investigated, lipopolyplexes. Cationic polymeric vesicles consisting of poly-L-lysine (PLL) or poly-L-ornithine (PLO) modified with hydrophilic (mPEG) and hydrophobic (palmitoyl) groups can be formed in the presence of cholesterol [36]. These have been shown to be less toxic than the unmodified polymers and can be used to deliver genes *in vivo* without the aid of lysomotropic agents [42], probably as a result of their amphiphilic nature.

Cetylated low molecular weight polyethylenimine (PEI) has been shown to self-assemble in the presence of helper lipids [43] and produced superior *in vitro* transfection of COS-1 cells when compared with Lipofectamine at low ratios of liposome/DNA and high DNA dose. Injection of these 'polycation liposomes' via the portal vein of mice was shown to produce reporter gene expression in the liver [43]. Lipidic PLL complexed with DNA was found to produce more efficient in vitro transfection than Lipofectin [44] and vesicles of dendritic PLL, described as 'dendrisomes', have more recently been investigated for encapsulation of hydrophilic drug [45].

1.1.5.6. Targeting strategies

Targeting is a general strategy to improve the specificity of a formulation and it is deemed to be a necessary component of a 'virus-like' particle [46-48]. The head groups of cationic lipid and polymeric structures are amenable to modification with targeting ligands such as transferrin [15, 49] and galactose [50], which could interact with receptors upregulated on the surface of a transformed cell or present on a hepatocyte, respectively. Obviously these strategies are rendered much more effective if interaction with the biological milieu is prevented. Approaches to shield the complex and improve the plasma circulation half life include the incorporation of hydrophilic polymers such as polyethylene glycol (PEG) [15, 51] and poly[N-(2-hydroxypropyl)methacrylamide] (pHPMA) [52] onto the surface; adequate circulatory time will allow the complex to reach its target organ. Judicious promoter selection can also avoid transgene expression within non-target cells. Transcription targeting is one example of using target associated promoter elements [53]. Other targeting structures for consideration include nuclear localisation signal (NLS) peptides containing amino acid portions that bind to importins to facilitate transfer through the nuclear pore [9].

1.1.5.7. Dendrimers

Dendrimers (the term arises from the Greek "dendron" = tree and "meros" = part) are macromolecular compounds that consist of a series of branches around an inner core. The first synthesis of such complexity was reported in 1978 by Buhelier *et al.* [54].

Dendrimer have unique properties; ideally they are almost perfectly monodisperse with a highly branched three-dimensional architecture [55]. The first dendritic structures to be thoroughly investigated were Tomalia's polyamidoamine (PAMAM) dendrimers, one of two commercially available frameworks, the other being polypropylenimine dendrimers (diaminobutamine dendrimers or DABs) which are also constructed divergently. Synthesis begins with a multifunctional core (usually 1, 4-diaminobutane) and extends in five 'generations' of branching to the periphery or outer shell [55]. These ranges of cationic (amine functionalised) dendrimers have been extensively studied as gene delivery agents [56-59]. They are amenable to derivatisation themselves and offer multiple attachment sites for drug or targeting ligand [60, 61]. Other dendrimers are constructed from monomers as required. Amphipathic asymmetric dendrimers consisting of dendritic PLL are an example of these [62]. These dendrimers have also demonstrated *in vitro* transfection ability and have in some cases been further modified with a lipidic core. The characteristics of resulting 'dendriplexes' with DNA have been recorded [63].

PAMAM dendrimer transfection efficiency was found to be dependent on the positive charge of the dendrimer and its flexibility. Gebhart and Kabanov report that partially degraded PAMAM dendrimer (commercially avaliable as SuperFect) is one of the most efficient DNA delivery polycations [57, 64] and has been used for delivery of antisense oligonucleotides [56]; however it exhibits significant cytotoxicity. Generation 3 PAMAM dendrimer has been shown to be less cytotoxic in a reference cell line than linear PEI and PLL [39]. It contains within its structure tertiary amines available for endosomal buffering (there is evidence that these dendrimers also cause chloride accumulation in the late endosome [40]) but demonstrates poor transfection efficiencies at this lower generation [64].

Interestingly the applications of dendrimers outside gene therapy are extremely broad and include drug delivery [60] including oral application [65], diagnostic imaging (particularly magnetic resonance imaging, MRI) [66], tissue repair scaffolds [67], anti-microbials [68] and liquid crystalline biosensory systems [69].

1.1.5.8. Polyproylenimine (PPI) dendrimer

Polypropylenimine dendrimers were first synthesised by Vögtle *et al.* in 1978 as previously mentioned [54]. This synthetic approach is based on a repetitive reaction sequence of the double Michael addition of amine to acrylonitrile, followed by reduction of the nitriles to primary amines. However, it was only 15 years later that a modified reinterative two-stage process achieved synthesis of up to 10kg PPI dendrimer per batch up to the fifth generation dendrimer, these then becoming commercially available as Astramol® [70] (Figure 6).

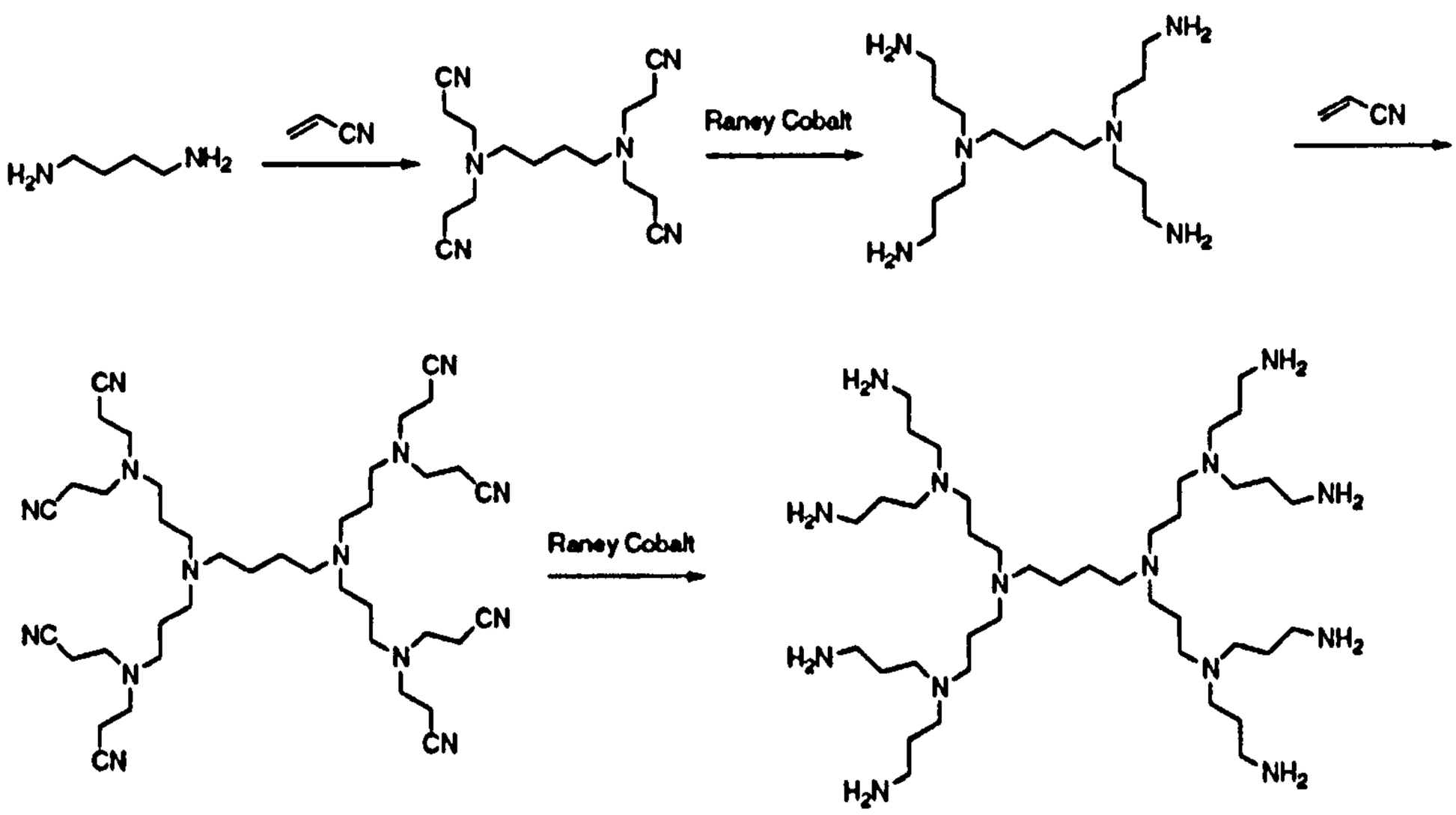

Figure 6 Poly(propylene imine) dendrimer synthesis by divergent strategy [55]

PPI or DAB dendrimer have interesting physical properties, the solubility of the dendrimer largely being determined by the end group but also the non-polar branches making amine-terminated dendrimers (DAB-4-Am to DAB-64-Am) soluble in water, methanol (polar protic solvent) and toluene (non-polar, aprotic solvent) [70]. All dendrimers consist of inner tertiary amines located at branching points of the various dendritic shell and basicity is one of the most dramatic properties of the PPI dendrimers. Titration experiments have shown that is possible to protonate all nitrogen atoms up to the fifth generation dendrimer, DAB-64-Am, and that there are two equivalence points: pKa values of 10.0 for primary amines and 5.7 for tertiary amines [70]. DAB-16-Am (3rd generation dendrimer, 16 terminal amine groups) is the particular focus of this work and shown in Figure 7. The radius of this spherical

dendrimer as measured by small angle neutron scattering (SANS) is close to 1nm [70].

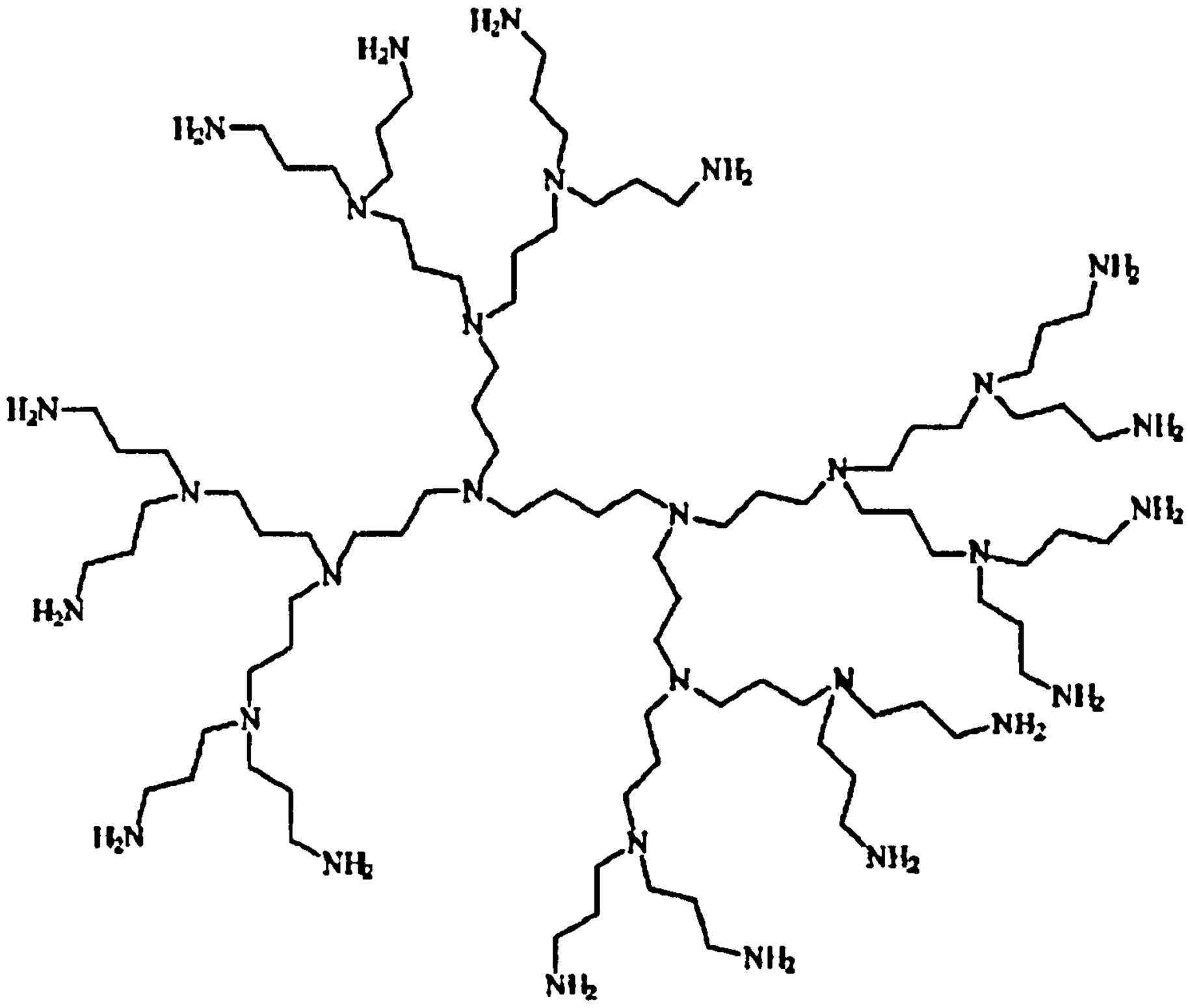

Figure 7 Structure of DAB-16-Am (PPI G3) [59]

Lower generation (generation 2 and 3) polypropylenimine dendrimers have been used for gene and oligonucleotide delivery [58, 59, 71]. As previously mentioned, these dendrimers contain 100% protonable nitrogens and DAB-16-Am is able to completely condense DNA. This is noteworthy as these are small dendritic molecules; transfection efficiency does not usually reside with molecules of this size. It is suggested that the flexibility and the multivalency of the molecule contribute to this unique ability [59].

This group has reported that DAB-16-Am produces an *in vitro* cytotoxicity comparable with the cationic liposomal formulation DOTAP and at the lowest DNA doses used DAB-16-Am was as transfection efficient as DOTAP. DAB-8-Am (2nd generation, 8 terminal amine groups) had a comparable efficiency at the highest

doses used. A real influence of molecular size was seen on gene transfer and cytotoxicity as lower generations have a reduced excess of anion binding sites [59].

Quarternisation has been used to reduce the toxicity of polymers [72, 73] and has also been applied as an approach to PPI dendrimers, improving biocompatibility but exhibiting a deleterious effect on transfection efficiency when compared with DAB-16-Am [74]. Interestingly, adminstration of DAB-16-Am-DNA dendriplexes via the tail vein to mice was found to produce preferential liver expression of the reporter gene, in contrast with a commercial linear PEI formulation which resulted in high levels of gene expression in the lung tissue [74]. It would appear that PPI dendrimers are still able to bind serum components such as proteins but are forming smaller aggregates as a result. These proteins are thought to act as opsonins which encourage rapid clearance into the liver, probably by Kupffer cell scavengers [75]. Also the most permeable vascular beds are those of the liver and spleen where intercellular spaces of 100nm have been reported [9]. This feature may be advantageous as the liver is the principal site for metabolism and synthesis of many essential proteins.

Intravenous injection of PPI G3 (DAB-16-Am) dendriplexes to CD1 nude mice bearing skin sarcoma (A431) cell xenografts has also been shown to result in a localisation of gene expression in the tumours and caused significant regression of these distant tumours when combined with a tumour necrosis factor alpha (TNFα). expression plasmid, with no apparent signs of toxicity [53]. The use of DAB-16-Am to deliver a minimum P-53 derived apoptotic peptide also leading to tumour regression *in vivo* [76] may now lead to the development of an effective clinical treatment involving the PPI G3 carrier for a broad range of malignant diseases.

1.2. Aims and Objectives

Gene therapy of currently incurable diseases requires the development of safe and effective gene delivery systems. While the most efficient gene transfer vehicles are undoubtedly viruses, the widespread use of viruses is limited by safety concerns and their lack of targeting ability. As a result non-viral vectors are being studied as attractive alternatives. Gene [59] and oligonucleotide [58, 71] transfer ability has been found with the lower generation (generation 2 – DAB-8-Am and generation 3 – DAB-16-Am) polypropylenimine dendrimers and their derivatives. Also, unusually, *in vivo* DAB-16-Am targets gene expression to either the liver [74] or distant tumours [53, 76].

Further enhancement of DNA binding and transfection efficiencies of DAB-16-Am is paramount. Secondly, improvements are sought in the stability of the DAB-16-Am-DNA complexes, particularly at close to isoelectric ratios and at the high concentrations that are required for *in vivo* experimentation (for example, 2mg plasmid DNA was complexed with L-PEI in 10mL for treatment of bladder carcinoma [37]). Also, this work aims to produce a tool to test the "lung avoidance" hypothesis [74], which opines that the small size and non-amphiphilic nature of this dendrimer is responsible for the lack of aggregation in the blood and hence the non localisation of gene expression within the lung capillaries.

Low levels of amphiphilic substitution conferred to polymeric systems have previously been shown to induce self-assembly whilst maintaining aqueous solubility and increase the efficiency of transfection of a number of cell lines [77-82]. They also report that inclusion of the neutral helper lipid cholesterol in formulations favours self-assembly of these amphiphiles into bilayer vesicles. Vesicles are stable systems, unlike micelles, which can mitigate the damage to biological structures which often results from hydrophobic derivatisation [83] and can further improve transfection efficiencies [80, 84].

The principal objective of this work is therefore to synthesise and characterise a novel, water-soluble amphiphilic gene delivery agent derived from the low molecular weight dendrimer DAB-16-Am. Structural characterisation will be carried out using NMR spectroscopy, electrospray ionisation mass spectroscopy and elemental analysis.

The processes of DNA binding will be further explored and condensation by the parent dendrimer DAB-16-Am will be compared with that of cDAB-16 and cDAB-16 vesicles. It is postulated that the phenomenon of cooperativity through short range hydrophobic interactions would improve the DNA-binding efficiencies of the amphiphile formulations, as seen in the literature [77, 85, 86].

The physicochemical properties of the resulting dendrimer-DNA complexes at various molar ratios will be explored [87]. The parameters to be examined are hydrodynamic diameter, surface zeta potential and DNA tertiary structure. Improvements are sought in the stability of the DAB-16-Am-DNA complexes at close to isoelectric ratios and the tendency to proximity aggregate at concentrations commonly required for *in vivo* experimentation; therefore carrier and concentration dependent solubility of complexed DNA will be assessed. The impact of the pH environment on complex size will be considered along with dilution effects, ionic environment and biological challenges to transfection.

Then, the haemocompatibility of each dendrimer species will be examined, along with cytotoxic effects and the efficiency of transfection of three immortalised cell lines. Finally, the *in vivo* toxicity and organ biodistribution profile of gene expression produced by the amphiphilic dendrimer gene carrier will be profiled in order to determine whether it could be a suitable gene delivery agent for human use; particularly with a view towards therapeutic cancer gene therapy.

2. Synthesis and Characterisation of Amphiphilic DAB-16

2.1. Introduction

Lower generation (G2 and G3) polypropylenimine (PPI) dendrimers of unprecedented low molecular weight (<2,000Da) have gained recognition as effective gene transfer agents [58, 59]. PPI G3 (DAB-16-Am) has had demonstrable success as an *in vivo* carrier of therapeutic plasmid DNA [53]. Quaternisation of dendrimer surface primary amines has previously been explored as a method to further improve transfection efficiencies [74].

Low levels of amphiphilic substitution conferred to polymeric systems have been shown to induce self-assembly whilst maintaining aqueous solubility and increase the efficiency of transfection of a number of cell lines [77-82]. Wang *et al.* advise derivatisation with a low level (<5 mol %) of cetyl (16 carbon) chains in order to maintain aqueous solubility and promote micellar structures using the related polymer poly(ethylenimine) [88]. They also report that inclusion of the neutral helper lipid cholesterol in formulations favours self-assembly of these poly(ethylenimine amphiphiles into bilayer vesicles. Vesicles are stable systems, unlike micelles, and their stability can mitigate the damage to biological structures which often results from hydrophobic derivatisation [83] and can further improve transfection efficiencies [80, 84].

The aim of this chapter is therefore to synthesise and characterise a novel amphiphilic gene delivery agent derived from the low molecular weight dendrimer DAB-16-Am. Structural characterisation will be carried out using NMR spectroscopy, electrospray ionisation mass spectroscopy and elemental analysis. The propensity of the derivative for self-assembly in aqueous media, with or without the neutral helper lipid, cholesterol, will be assessed using UV-Vis. spectrophotometry (with methyl orange as a hydrophobic probe), photon correlation spectroscopy and transmission electron microscopy.

2.1.1. Alkylation reaction

Amphiphilic nature was conferred to DAB-16-Am (PPI G3) via grafting of long hydrophobic alkyl chain(s) onto the hydrophilic dendrimer shell. In this work alkylation was performed using cetyl bromide according to the modified protocol of Nöding *et al.* [89] as a single phase reaction in tetrahydrofuran (THF). In this reaction cetyl bromide is attacked at its electrophilic carbon centre by a dendrimer nitrogen lone pair (most reactive from the primary amine shell) and nucleophilic substitution proceeds via a S_N2 mechanism [90]. In an effort to limit the extent of formation of multiply substituted dendrimer molecules, DAB-16-Am and cetyl bromide were reacted at a 5:1 molar ratio.

2.1.2. Nuclear Magnetic Resonance (NMR) spectroscopy

The atomic nucleus utilised for Nuclear Magnetic Resonance (NMR) spectroscopy in this work is ^1H (proton, 99.98% natural abundance) which has been studied since the beginnings of NMR spectroscopy and has been used for the identification of the majority of organic compounds [91, 92]. The proton can adopt two possible spin (energy) states in a static magnetic field (B_0), orientated parallel or anti-parallel to the field. The difference in potential energy between these two states is dependent upon the strength of the field B_0. Transition between the two states occurs at a single resonant frequency and this value is specific to the atomic nucleus (at an applied field strength of 2.348 T the resonant frequency of ^1H is 100MHz) but is also influenced by the electron density in the environment of each chemically distinct proton in the structure [92].

In order to detect and accurately measure these nuclear resonances a sample is perturbed using a pulsed radiofrequency (RF) signal applied at 90° to the static magnetic field B_0, generating an oscillating magnetic field (B_1) which covers a range of frequencies. This pulse of rotating magnetisation induces a signal from each proton type which then diminishes in intensity to zero. The detected signals make up the free induction decay (FID) spectrum which is then converted to the frequency spectrum by Fourier transformation (FT). The deviation of each peak from the

frequency of an internal standard, usually tetramethylsilane (TMS), is then divided by the operating frequency to give the chemical shift (δ), expressed in parts per million (ppm). As TMS is allocated δ0, ^{1}H absorption peaks will usually appear downfield between δ0-10. Structures are assigned according to peak positions and multiplicities; integration of peak area gives the relative abundance of detected protons with great accuracy [91]. Also, two adjacent nuclei can interact ('couple') with each other which can be deduced from measurement of a coupling constant, J, or through the use of ^{1}H-^{1}H COrrelated SpectroscopY (COSY) 90, a two dimensional NMR experiment [93].

A disadvantage is that deuterated solvent (containing the ^{2}H isotope, 0.02% natural abundance) must be used to dissolve the sample without interference and to maintain a steady field, which adds to the expense of this complex procedure [91].

2.1.3. Mass Spectroscopy (MS)

Mass Spectroscopy (MS) relies on the chemical reactivity of a molecule and therefore is not a true spectroscopic method, but it is an extremely sensitive technique (mass spectra can be obtained with only a few micrograms of sample) which assists in structural elucidation [92, 94]. A mass spectrometer is designed to vapourise the compound of interest, produce ionic forms of the compound and then separate and detect these ions according to their mass/ charge (*m/ z*) ratio, thus generating a mass spectrum [92]. In this work a quadrupole mass spectrometer is used to analyse molecular ions generated using positive electrospray ionisation (ESI).

ESI is an excellent technique for the generation of quasi-molecular ions from large polar molecules and is used to achieve complete molecular characterisation of PPI dendrimers and their side products [70]. A water/ methanol/ volatile organic acid mixture of low pH containing the analyte is first sprayed through a capillary needle, forming positively charged droplets in an applied potential difference. Quasi-molecular ions of the analyte molecules ($[M + H]^{+}$) are formed and released from the droplets upon solvent evaporation and then carried by an electric field to the ion analyser [92]. The electrospray process produces a distribution of molecular ion

charged states (the number of charged species reflecting the number of protonation sites) and very little fragmentation. Multiply charged ions of otherwise too heavy molecules can enter the detection range of the quadrupole mass spectrometer (*m/ z* maximum of ca. 4000, although best up to *m/ z* 1000) allowing molecular weight determination [92].

The population distribution in the spray is accurately reflected in the intensity of the peaks in the mass spectrum. The most abundant peak is arbitrarily assigned an abundance of 100% and is termed the base peak. However, without an internal standard these abundances cannot be related to concentration and the technique remains qualitative [92, 94].

2.1.4. Elemental Analysis (EA)

Elemental analysis is an important technique used to determine the elemental content of organic compounds [95]. Historically, gravimetric analysis of combusted and oxidised product was used to determine the quantity of carbon or hydrogen that was initially present in a sample. Analysers today can precisely measure elemental C, H, N and S content in a single run (although in this work only the elements C, H and N are quantified). These operate by dynamic flash combustion of a sample (~2mg) sealed in a tin capsule. The encapsulated sample is dropped into a preheated ceramic crucible in the presence of an O_2/He mixture, upon which the capsule melts and the sample is rapidly oxidised at 1800°C. Optimised catalysts complete the oxidation process and the resulting mixture of CO_2, H_2O and N_2 is chemically cleaned of interferences such as halogens, separated by gas chromatography and each component measured with a thermal conductivity detector [95].

For quantification of halogen content (bromide in this work), the combustion process is completed in an O_2 flask containing the appropriate adsorbents to produce an aqueous solution of bromide ions, the concentration of which is then determined by potentiometric titration [96].

2.1.5. Ultraviolet-Visible Spectrophotometry with hydrophobic probe

Ultraviolet (UV) and visible (Vis) electromagnetic radiation is absorbed by many organic compounds, energising electron transitions between molecular orbitals of differing energy states [92, 94]. For the purpose of UV-Vis spectrophotometry a conjugated double bond or aromatic system is the preferred absorbing structure (or chromophore), which reduces the separation of the energy states through π-bond electron delocalisation and can therefore be activated by less energetic, longer wavelengths (in the UV and Vis regions, 190-350nm and 350-700nm respectively). The total amount of incident light absorbed by a chromophore is proportional to the number of absorbing molecules in the light path and the path length, therefore UV-Vis spectrophotometry is usually employed in the area of quantitative analysis [94]

The technique requires a monochromatic light source, automatically scanning through a wavelength range, to pass through a solution in a sample cell which is then detected by a photomultiplier tube and converted into an electrical current. A matched sample cell containing only solvent is used to correct for solvent absorption [92]. A spectral plot of wavelength (nm) versus absorbance intensity (au) allows identification of the maximum absorption wavelength (λ_{max}). A change of solvent medium or a loss of conjugation can cause a hypsochromic (blue) shift of an absorption maximum to a shorter wavelength. A bathochromic (red) shift to a longer wavelength may again be caused by a change of solvent medium or extension of the chromophore by conjugation [92].

Characteristic shifts in λ_{max} are exploited in many applications of UV-Vis spectrophotometry. One such application is the detection of hydrophobic regions formed in an aqueous solution when amphiphilic agents (for example, surfactants) aggregate. This requires the use of a hydrophobic probe such as the azo dye, methyl orange (MO, Figure 8) [73, 97-102]. When transferred from bulk water into the hydrophobic interior of an aggregate, such as a micelle, MO undergoes a hypsochromic shift in the λ_{max} of long-wavelength absorption bands which can be readily detected using this technique. A likely explanation for this blue shift is the formation of 'H-aggregates' of dye molecules at interfacial regions with a parallel,

higher energy orientation [103]. For the purpose of analysis, the concentration at the midpoint of the wavelength transition between non-aggregated and aggregated states is termed the critical aggregation concentration (or CAC). At this point sufficient amounts of monomer are present to provide the thermodynamic drive to overcome short-range, intermolecular repulsive forces [97, 101].

(i) 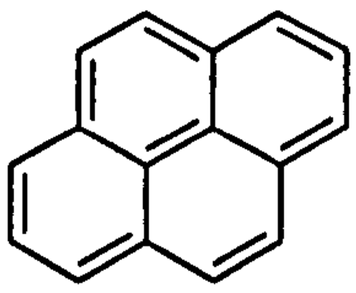

(ii) 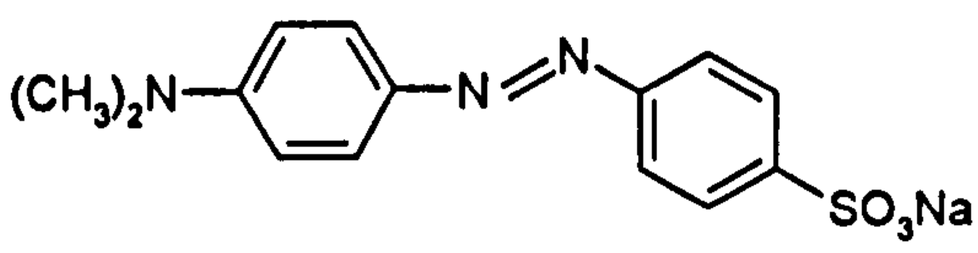

Figure 8 Hydrophobic probes (i) pyrene (ii) methyl orange

2.1.6. Photon Correlation Spectroscopy (PCS)

Light scattered by a colloidal population has an intensity, polarisation and angular distribution dependent on many characteristics of the particles [104]. Photon correlation spectroscopy (PCS) exploits light scattering to size particles (with diameters in the range 1-5000nm) based on the measurement of their Brownian motion [105]. Brownian motion is a constant random thermal motion, closely related to the diffusion coefficient of a particle and the larger the particle, the slower this motion. This motion is detected by measuring the the fluctuation in the intensity of the scattered light from an incident beam (in this example, a He/ Ne laser) over time. Light scattering is detected using a photomultipler, and the time dependent light intensity fluctuations are analysed to give the size distribution of a particle population. This information, together with the temperature and the viscosity of the suspending medium allows calculation of particle size [105]. Light scattering measurements are also dependent on the shape of particles (usually approximated as spherical), their interactions with other particles and also the difference between the refractive index (RI) of the particles and their dispersant medium [104].

PCS measures the hydrodynamic radius (Z) of a particle which is generally a few nanometres larger than the geometric radius of a sphere due to solvation effects.

Experimental difficulties include the elimination of dust contamination, as these relatively large particles scatter light strongly and introduce significant error [104].

2.1.7. Transmission Electron Microscopy (TEM)

Particles in the colloidal size range (generally between 1-1000nm) may be observed directly with an electron microscope, which functions in an analogous way to a light microscope [104]. Transmission electron microscopy (TEM) involves irradiation of a very thin specimen (<1μm) mounted on an electron-transparent grid with a monochromatic beam of electrons. These electrons are generated by thermoionic discharge, energy filtered with a magnetic 'prism' to enhance image contrast, transported in a positive electric field and focused on the sample using a magnetic 'lens'. Some of these electrons are transmitted through the less dense regions of the sample (others are scattered out of the field of view) and then detected using a fluorescent screen, thus generating structural and morphological information [104].

TEM is a technique well utilised in the biological and physical sciences alike, although organic materials are relatively electron-transparent (due to low atomic density) therefore contrast must be further enhanced [104]. A negative stain can be used to deposit heavy metal atoms on the sample surface (usually uranium or vanadium) for this purpose. Replication of the sample surface by shadowing with a heavy metal is also a technique used in this work to examine vesicle surfaces producing a three dimensional effect. Other limitations of this technique for biological applications include the requirement for samples to be thoroughly dried before observation (to prevent vapour interfering with the transmission of the electron beam) which can introduce artefacts. The electron beam itself can also cause degradation of organic samples, giving rise to misleading images [104].

2.2. Materials

DAB-16-Am (PPI Generation 3) MW 1686.7 g mol^{-1}	Sigma Aldrich Co., UK
1-bromohexadecane (cetyl bromide) MW 305.35 g mol^{-1}, d 0.999 g cm^{-3}	Sigma Aldrich Co., UK
Sodium hydroxide pellets MW 40.0 g mol^{-1}	BDH; VWR International, UK
Tetrahydrofuran	Riedel-de-Haën; Sigma Aldrich Co., UK
Methanol	Fluka; Sigma Aldrich Co., UK
Deuterated solvents	Sigma Aldrich Co., UK
Methyl orange MW 327.3g mol^{-1}	Sigma Aldrich Co., UK
Sodium tetraborate decahydrate (borax) MW 201.2 g mol^{-1}	Sigma Aldrich Co., UK
Dextrose, anhydrous MW 180.2 g mol^{-1}	Sigma Aldrich Co., UK
Cholesterol MW 386.7 g mol^{-1}	Sigma Aldrich Co., UK
Polystyrene beads 100nm mean diameter	Sigma Aldrich Co., UK
Methylamine vanadate 2% w/v (NanoVan)	Nanoprobes Inc., USA

Table 1 Materials and suppliers used in Chapter 2

2.3. Methods

2.3.1. Synthesis of cetyl DAB-16 (cDAB-16)

1-bromohexadecane (cetyl bromide, 36 μL, 1.2 x 10^{-4} mol) was added to 1 g (5.9 x 10^{-4} mol) DAB-16-Am (PPI G3) in a suitable volume (50 mL) of tetrahydrofuran (THF). The mixture was reacted under reflux (Electromantle MA, Electrothermal, UK) at 70°C for 48 h with continuous stirring in a fume cupboard. Sodium hydroxide pellets (2g, 0.05 mol) were dissolved in a suitable volume of methanol (25 mL) overnight and added to the cooled reaction mixture. This was then heated under reflux at 70°C for a further 24 h and allowed to cool to room temperature before rotary evaporation of solvent (Heizbad WB Laborota 4000, Heidolph, Germany) at 60°C under reduced pressure. The product was air-dried overnight before it was dispersed in distilled water (50 mL), exhaustively dialysed against distilled water (5 L) with 6 changes over 24 h (Visking tubing with molecular weight cut off (MWCO) 12,000-14,000Da, Medicell Int. Ltd., UK) and then freeze dried for approximately 72 h (Modulyo A-230, Savant Instruments Inc., USA). For synthetic scheme see Fig. 2.

2.3.2. ^{1}H NMR

cDAB-16 (5 - 10 mg mL^{-1}) in deuterated methanol (CD_3OD) was submitted to the Department of Applied Chemistry at the University of Strathclyde for ^{1}H NMR and ^{1}H–^{1}H COrrelation SpectroscopY (COSY) 90 experiments on a Bruker AMX 400 MHz spectrometer (Bruker Instruments, UK). Proton assignments for DAB-16 by Chai *et al.* [106] and Schätzlein *et al.* [74] were consulted.

2.3.3. ESIMS

cDAB-16 (approximately 5 mg) was dissolved in methanol/0.1% formic acid (1:1) and infused directly into a TSQ 7000 triple quadrupole mass spectrometer (ThermoQuest, USA) with the electrospray ionisation (ESI) needle held at 4.5 kV and capillary temperature at 250°C.

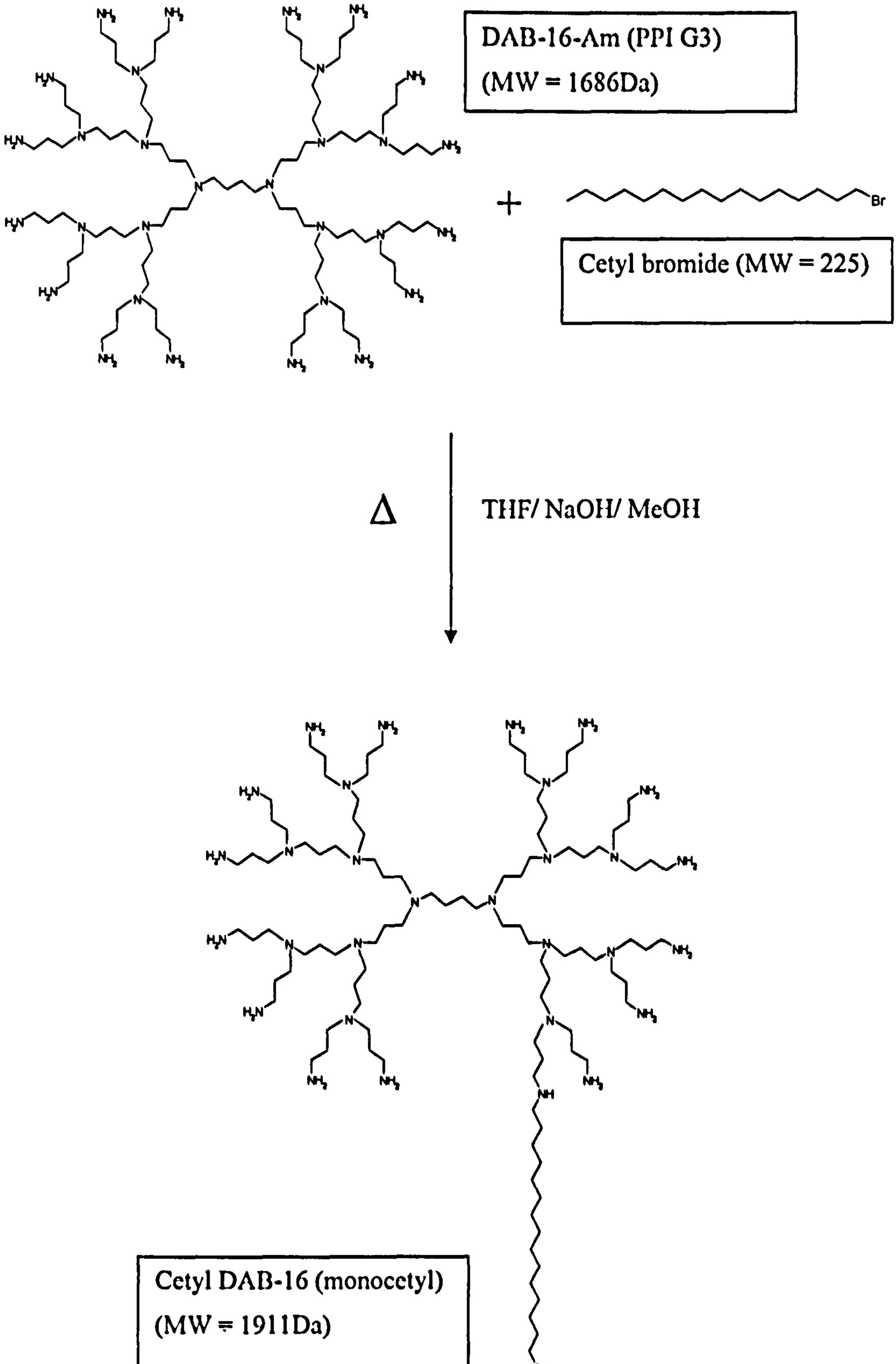

Figure 9 Synthesis of cetyl DAB-16 (cDAB-16)

2.3.4. EA

Elemental analysis was conducted at the Department of Pure and Applied Chemistry at the University of Strathclyde.

2.3.4.1. Determination of C, H and N

Simultaneous determination of carbon, hydrogen and nitrogen was performed on a Perkin-Elmer 2400 analyser (Perkin Elmer Instruments, UK). Each dendrimer sample (2 mg) was wrapped in tin foil and combusted at 1800°C in pure oxygen. Combustion products were catalysed and interferences removed before being swept away into the detector zone where each element was separated in a gas chromatographic column and eluted as CO_2, H_2O and N_2 respectively. Detected signals were then converted into the percentage of elements found. The degree of dendrimer alkylation was determined from the ratio of C:H:N in the product.

2.3.4.2. Determination of Br content

cDAB-16 samples were also tested for residual bromide content using the oxygen-flask combustion method [96]. Each sample (5 mg) was combusted in an oxygen flask containing hydrogen peroxide (H_2O_2) and potassium hydroxide (KOH) as absorbents. After 30 minutes the flask was flushed with distilled water. Ethanol was added and the solution acidified before titration with mercuric nitrate using diphenylcarbazone as the indicator. Lastly, the bromine content was calculated as a percentage of sample weight.

2.3.5. Preparation of self-assembled structures

Self-assembled structures were prepared by probe sonication (Soniprep 150, Sanyo Gallenkamp, UK) of 5mg.mL^{-1} cDAB-16 in distilled water (1 – 2 mL) for 5 min at 75% of full power. To form vesicles, cholesterol was then added (final concentration 2 - 10 mg.mL^{-1}) and the dispersion further sonicated for two periods of 5 min at 75% of full power.

2.3.6. Determination of Critical Aggregation Concentration (CAC)

Methyl orange (1.64mg) and borax (1.526g) were dissolved in distilled water (200 mL) to make 25μM methyl orange in 0.02 M borate buffer (pH 9.4). This solution was used to prepare dendrimer samples in the concentration range 0.0001 mg ml^{-1} – 12.5 mg ml^{-1} for probe sonication (section 2.3.5). Samples were protected from light and incubated for 1 h at room temperature (25°C) before scan analysis (350 nm – 600 nm) on a UV-Vis spectrophotometer (Unicam UV 300 spectrophotometer, UK). Samples dissolved in methyl orange solution were blanked at each concentration against identically treated samples in buffer to cancel non-specific, concentration-dependent absorption of visible light by the dendrimer primary amines.

2.3.7. PCS

Measurement of Z average (mean hydrodynamic) diameter and polydispersity of freshly prepared cDAB-16 aggregates (5 mg mL^{-1}) and vesicles (as in section 2.3.5) was carried out at 25°C and at a fixed angle of 90° using a photon correlation spectrometer (Malvern Zetasizer 3000HS_A, Malvern Instruments, UK). Three measurement runs were carried out for each sample, each consisting of 10 sub-runs to which autoCONTIN® analysis was applied. Medium refractive index (RI) was set as 1.33. A latex bead standard (Sigma Aldrich Ltd, UK) of 100nm mean diameter (diluted approximately x1000 in distilled water) was used to calibrate the spectrometer before each experiment.

2.3.8. TEM

TEM was performed at the Institute of Biomedical and Life Sciences at the University of Glasgow using an energy filtering transmission electron microscope (LEO 912 Omega EF-TEM, Leo Electron Microscopy Ltd., UK) operated at 120 kV supplying electrons of zero energy loss. cDAB-16 aggregates (5 mg mL^{-1}) and vesicles (5 mg mL^{-1} cDAB-16 containing 2.5 mg mL^{-1} dispersed cholesterol) were prepared freshly for analysis in distilled water as described in section 2.3.5.

2.3.8.1. Negative stain TEM

A droplet of the sample was applied to a carbon-coated grid and allowed to adsorb before blotting. This process was then repeated with methylamine vanadate 2% w/v (NanoVan) negative stain before imaging.

2.3.8.2. Freeze fracture TEM

The sample was rapidly cryofixed and fractured in liquid nitrogen before shadowing of the fractured surface with evaporated platinum at an angle of 45° under vacuum. A second coat of carbon was applied before the metal replica was 'released' from the sample using dilute acid. The final replica was then carefully washed and dried and mounted on a copper grid before imaging.

2.4. Results

2.4.1. Product yield

DAB-16-Am is a colourless oil but the cetylated product was recovered as a clear, yellow-orange gel. Orange colouration is characteristic of this modification [89, 107] and indicates extended electronic conjugation length resulting from the addition of the alkyl group to the dendrimer amine network [92]. The cetylated product retains solubility in the polar solvent methanol (up to a maximum of 10mg.mL^{-1}) and solubility in water. The average yield weight and quantitative percentage yield of cetyl DAB-16 are calculated below (Table 2).

	Yield weight (mg)	Percentage yield (%)
Mean ± St. dev. (n = 3 batches)	331.6 ± 82.8	32.0 ± 8.0

Table 2 Product yield

2.4.2. ^{1}H NMR

The presence of cetyl moieties was confirmed by ^{1}H NMR signals at δ_H0.90 and δ_H1.29, which can be assigned to the methyl protons and aliphatic γ-methylene protons of the cetyl chain. The chemical shifts are assigned as follows:

δ_H0.90 = -C$\underline{H}_3$, δ_H1.29 = -CH$_2$-(C$\underline{H}_2$)$_n$-CH$_3$, δ_H1.47 = N-CH$_2$-C$\underline{H}_2$-C$\underline{H}_2$-CH$_2$-N-, δ_H1.65 = -N-CH$_2$-C$\underline{H}_2$-CH$_2$-N, δ_H2.46 = -N-C$\underline{H}_2$-CH$_2$-C$\underline{H}_2$-N-, δ_H2.74 = -CH$_2$-C$\underline{H}_2$-NH$_2$, δ_H3.10 = -(C$\underline{H}_2$)$_3$-NH$^+$, δ_H3.26-3.31 = -C$\underline{H}_2$-NH$_3^+$, δ_H3.40-3.60 = -C$\underline{H}_2$-Br (Figure 10).

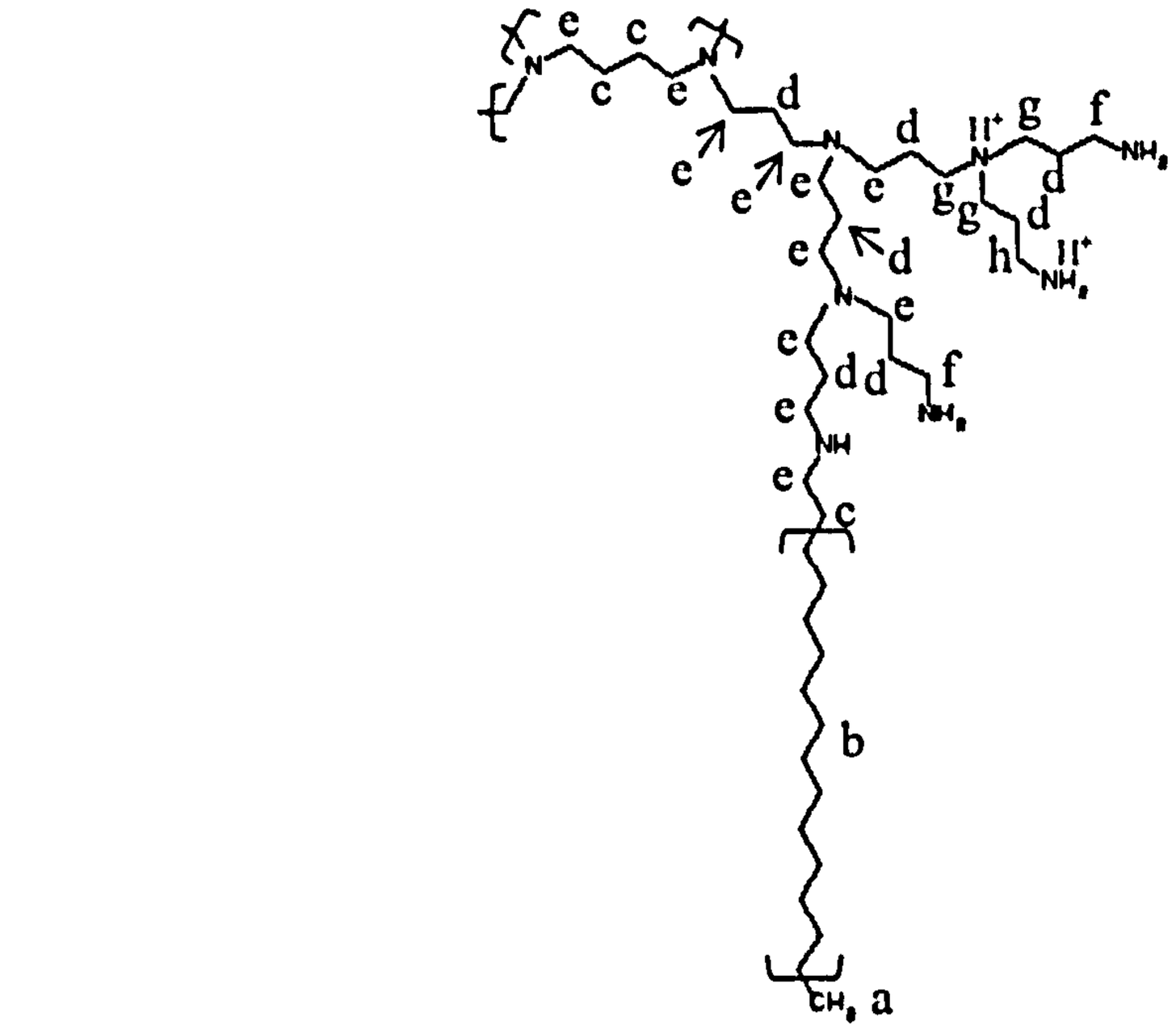

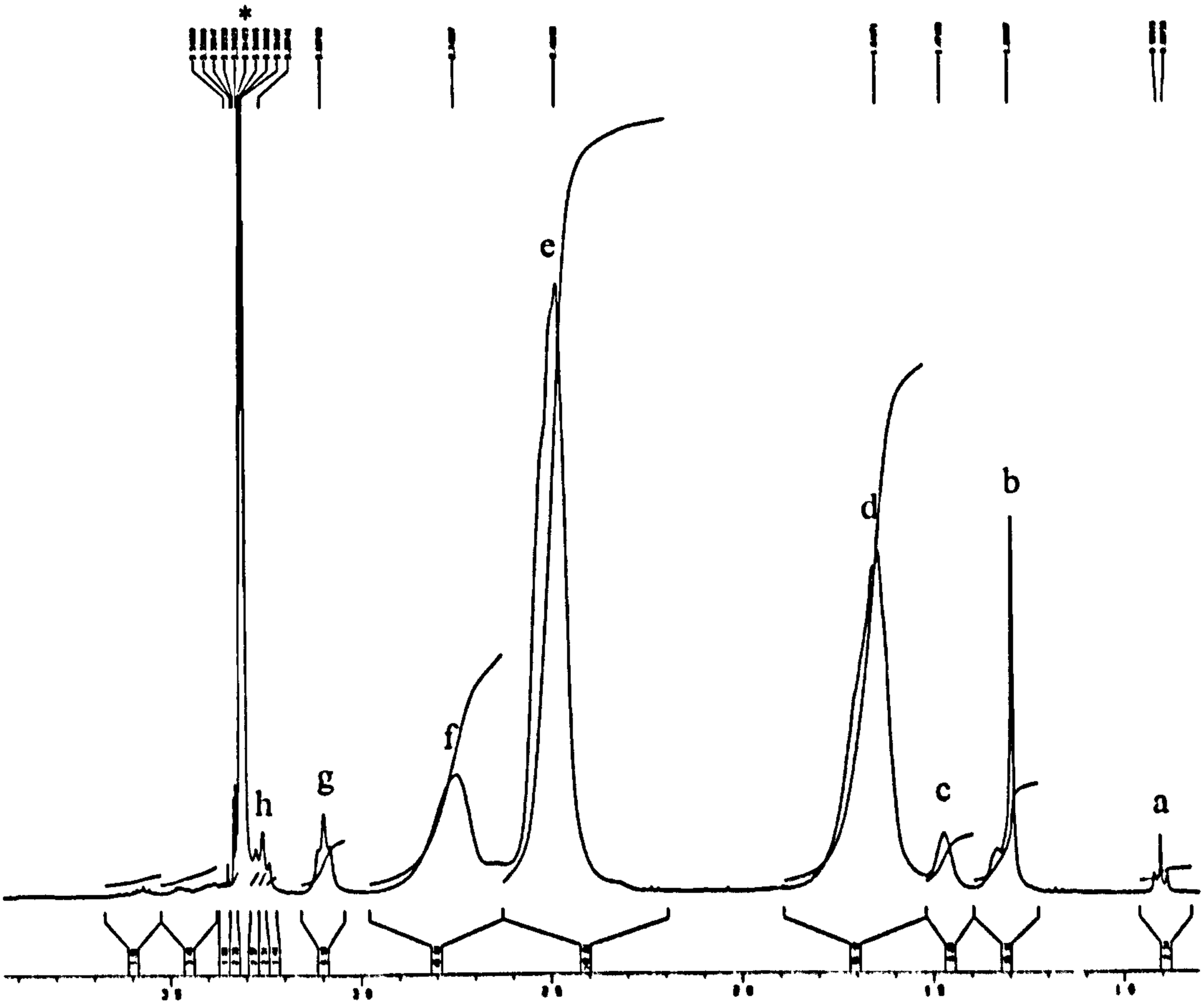

Figure 10 ^{1}H NMR spectrum of cDAB-16 in CD_3OD (* = solvent peak) and proton assignments.

Proton assignments were confirmed using ^{1}H-^{1}H COSY 90 (Figure 11). As previously stated, integration of peak area gives the relative abundance of detected protons [91] therefore the extent of alkyl substitution can be estimated from Figure 10. The proton ratio of peak f (dendrimer termini): peak a (methyl) is calculated to be 27.6: 1, which approximates 1.1 alkyl chains per dendrimer molecule. A small amount of ammonium functions are detected at dendrimer termini; their contribution is not included in this calculation. These could be due to protonation of primary amines (which may also occur to a lesser extent with tertiary amines) in the presence of a small quantity of residual water (δ_{H}4.90, see Figure 11) or association with residual bromide ions (δ_{H}3.40-3.60); although it is notable that residue of the initial reactant alkyl bromide is hardly detectable in Figure 10. Ammonium functionalities could also result from multiple alkylations at one reactive centre leading to tri-cetylated products, although under these reaction conditions this is expected to be limited. Attachment of the cetyl chain cannot be confirmed using this technique.

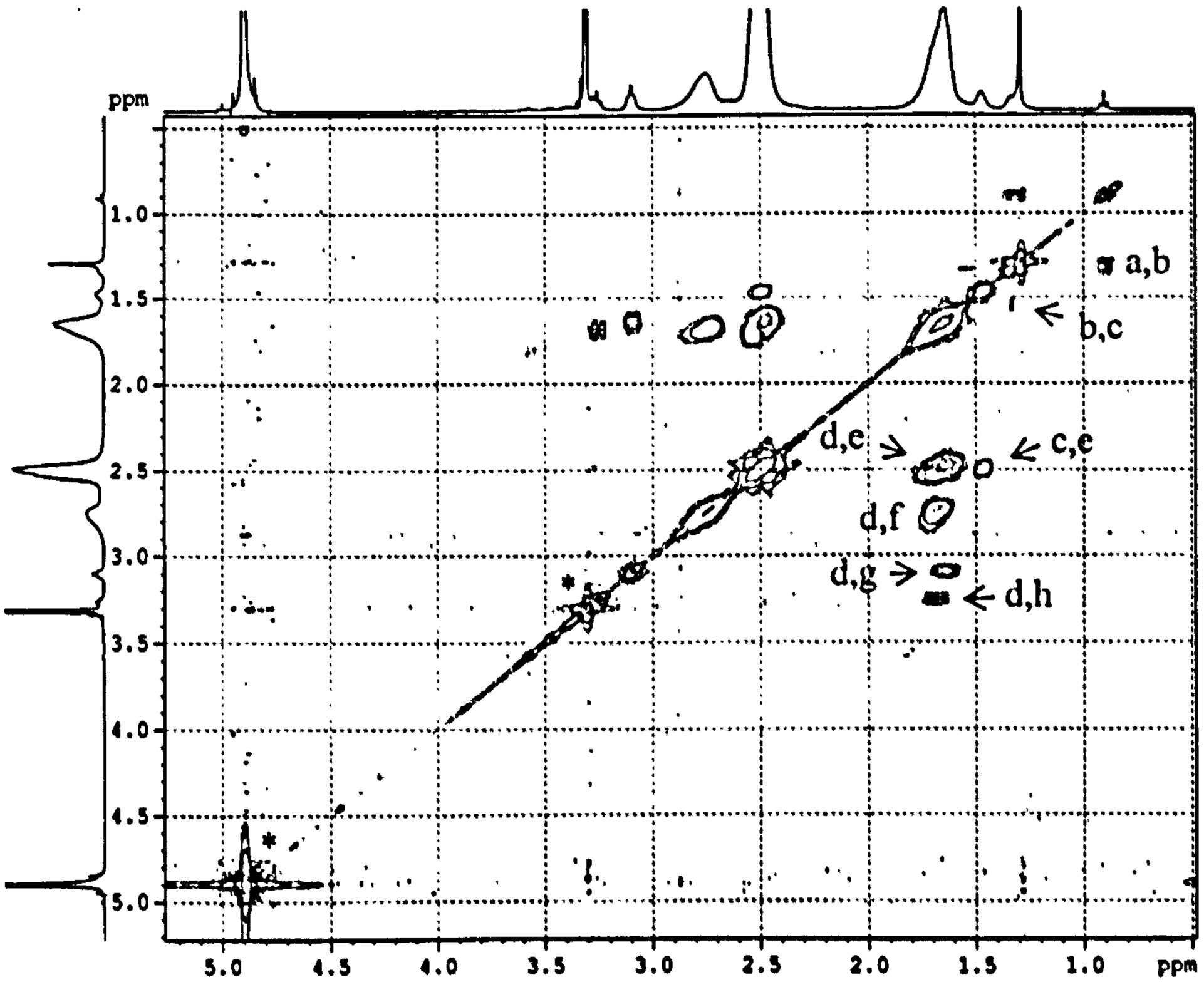

Figure 11 ^{1}H-^{1}H COSY 90 of cDAB-16 in CD_3OD (* = solvent peaks). For proton assignments please see Figure 10

2.4.3. ESIMS

First, a high resolution electrospray ionisation mass spectrum was taken to confirm the purity of the principal starting reactant, DAB-16-Am (Figure 12). Using this technique the molecular weight of DAB-16-Am is calculated to be 1686.72 Da (ideal molecular weight: 1686.79 Da). Also detectable on the spectrum are dendrimer molecules with losses of multiples of polypropylenimine units (e.g. $[M - (58)_n + H]^+$), most likely the outer dendrimer branches. PPI dendrimers possess some statistical defects as a result of divergent synthesis [70] and this experimental procedure can further promote fracturing of branches [92].

The significant peaks identified on the mass spectrum of cDAB-16 (Figure 13) are tabulated below (Table 3). Importantly, ESIMS is able to confirm attachment of cetyl chain(s). Species identified include DAB-16-Am and its mono-, di- and tri-cetylated forms. The base peak at *m/z* 1686.4 (assigned 100% abundance) represents the singly-charged, pseudo-molecular ion of the parent dendrimer, DAB-16-Am. The relative abundance of peaks representing the pseudo-molecular ions of monocetylated DAB-16 and DAB-16-Am suggest that they are the most abundant dendrimer species in the sample. However, due to the limited mass detection range of this technique (up to *m /z* ca. 2000) singly protonated species of di- and tri- cetylated DAB-16 cannot be detected at all. Tricetyl DAB-16 is only detectable as a $[M + 2H]^{2+}$ pseudo-molecular ion with a very low relative abundance (*m/ z* 1180.8, see Figure 13). Also, this profile may be a reflection of the likely relative solubilities of the cetylated constituents in the polar solvent methanol (DAB-16-Am > monocetyl DAB-16 > dicetyl DAB-16 > tricetyl DAB-16) therefore firm conclusions cannot be drawn.

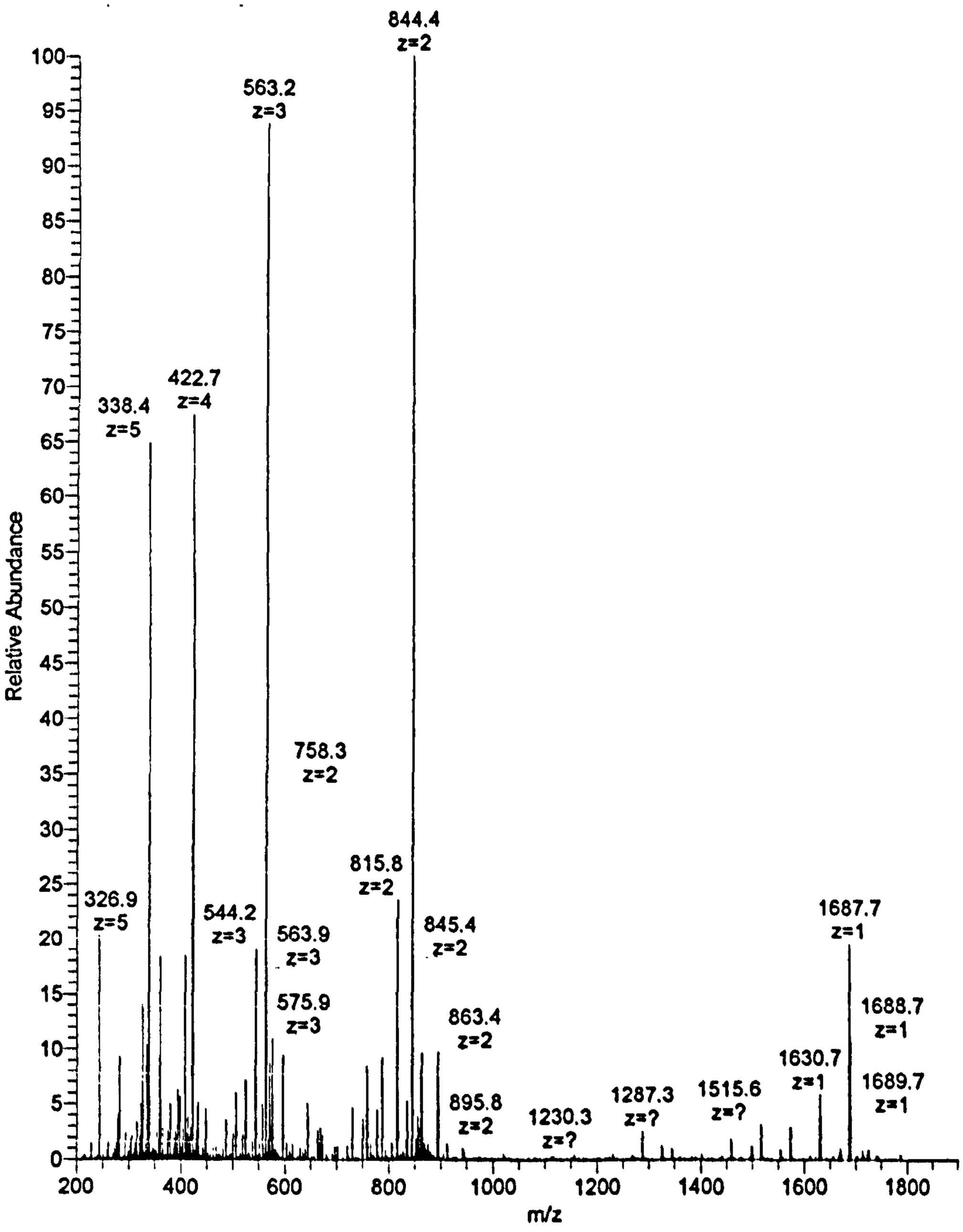

Figure 12 Electrospray ionisation mass spectrum of DAB-16-Am

Dendrimer species	*m/z* ratio	Fragment
DAB-16-Am *MW = 1686.4 Da*	1686.4 (base peak) 1629.3 1572.2 1515.2 1458.2 1345.0 1287.0 844.0 815.4 563.1	$[M + H]^+$ $- CH_2CH_2CH_2NH_2$ $- (CH_2CH_2CH_2NH_2)_2$ $- (CH_2CH_2CH_2NH_2)_3$ $- (CH_2CH_2CH_2NH_2)_4$ $- (CH_2CH_2CH_2NH_2)_5$ $- (CH_2CH_2CH_2NH_2)_6$ $[M + 2H]^{2+}$ $- CH_2CH_2CH_2NH_2$ $[M + 3H]^{3+}$
Monocetyl DAB-16 *MW = 1911.5 Da*	1911.5 1854.4 1796.4 956.1 927.6 637.9 478.8	$[Monocetyl + H]^+$ $- CH_2CH_2CH_2NH_2$ $- (CH_2CH_2CH_2NH_2)_2$ $[Monocetyl + 2H]^{2+}$ $- CH_2CH_2CH_2NH_2$ $[Monocetyl + 3H]^{3+}$ $[Monocetyl + 4H]^{4+}$
Dicetyl DAB-16 *MW = 2136.4 Da*	1068.2 712.7	$[Dicetyl + 2H]^{2+}$ $[Dicetyl + 3H]^{3+}$
Tricetyl DAB-16 *MW = 2361.6 Da*	1180.8	$[Tricetyl + 2H]^{2+}$

Table 3 Principal mass spectrum peaks identified for cDAB-16 product

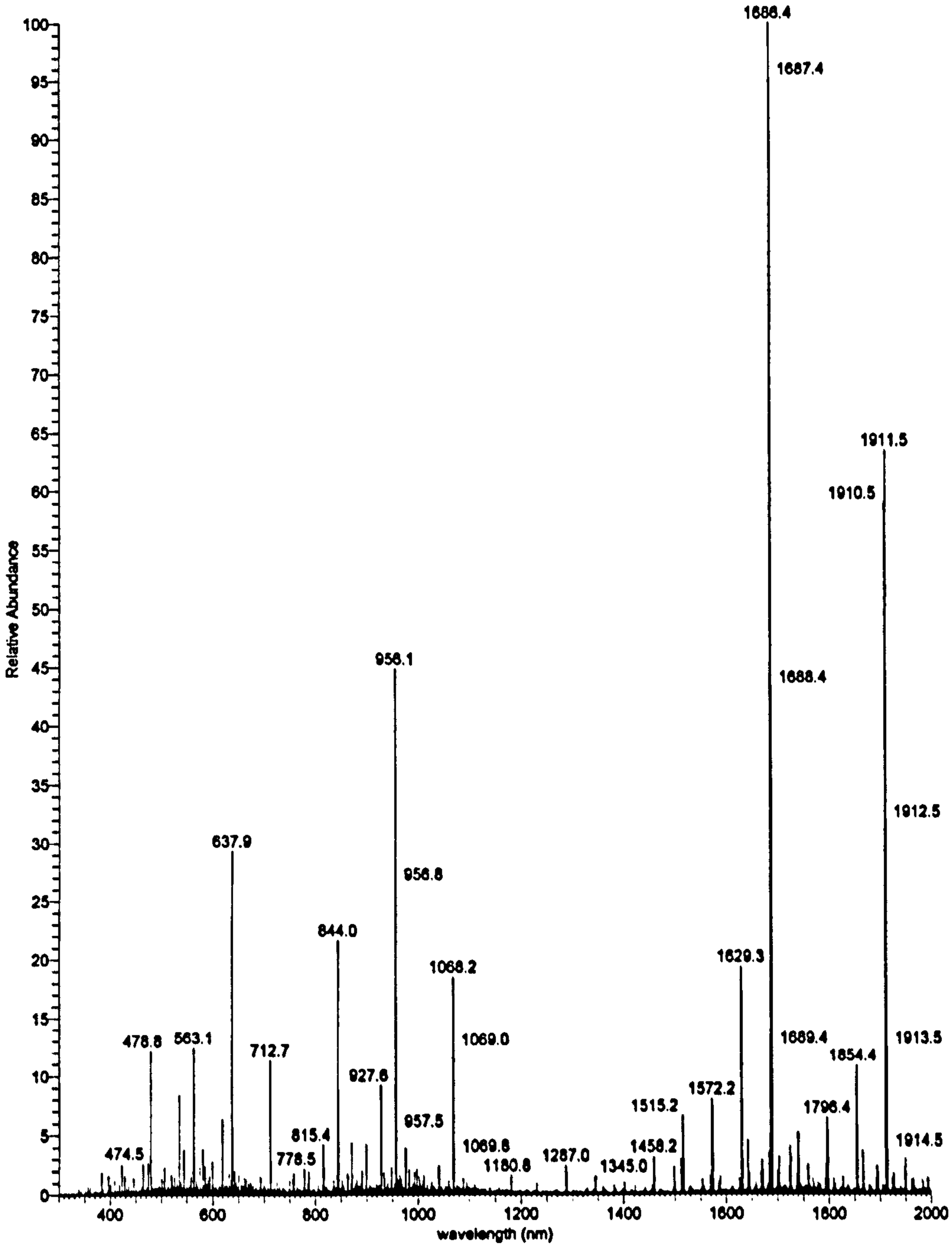

Figure 13 Electrospray ionisation mass spectrum of cDAB-16

2.4.4. EA

In this work, elemental analysis was used to accurately calculate the level of dendrimer cetylation. The elements that compose the dendrimer are quantified (C, H and N) and also a possible contaminant, Br, arising from the initial reactant cetyl bromide. The results of elemental analysis for three batches of cDAB-16 are compared with the theoretical compositions of DAB-16-Am and monocetyl DAB-16 in Table 4.

	Theoretical (DAB-16-Am)	Theoretical (monocetyl DAB-16)	Actual Mean ± St. dev., n = 3 batches
% C	62.63	65.31	54.90 ± 7.77
% H	12.33	12.56	11.51 ± 1.63
% N	24.91	21.98	18.24 ± 1.18
% Br	0	0	0.48 ± 0.47
% CHN	100	100	84.65 ± 13.45
C/ N ratio	2.51	3.47	3.20 ± 1.10
Molar % cetylation*	0	3.45	3.75 ± 2.33
No. of cetyl chains per dendrimer molecule	0	1	1.09 ± 0.67

Table 4 Elemental analysis of cDAB-16 * = No. of mol cetyl groups per 100 mol PPI groups

The mean C/ N ratio and mean number of chains per dendrimer molecule for the three cDAB-16 batches produced agree with the theoretical values for monocetyl DAB-16 (Table 4). However, for accuracy, in further experimental work the average molecular weight used is calculated from elemental analysis of each individual batch of cDAB-16. Upon analysis the element Br was undetectable in one batch produced and just within detection range in the remaining two batches (Table 4).

2.4.5. Self-assembly

Probe sonication was selected to promote spontaneous formation of assembled structures, although cDAB-16 dissolves immediately to form a colourless to pale yellow, clear solution. Yellow colouration increases with increasing acidity of the solution due to extension of the dendrimer conjugation length by amine protonation [92]. Brief sonication periods were employed as described in 2.3.5. Upon addition of cholesterol, white particles were visible in the cDAB-16 vesicle formulation, but following two further sonication periods a translucent dispersion was produced.

2.4.6. Determination of CAC

In this experiment methyl orange (MO) exhibited an absorption maximum of 465nm in aqueous, consistent with literature values [73, 97, 99, 101, 103]. A hypsochromic shift of this maxima to 438nm in the presence of cDAB-16 (Figure 14) indicates the presence of persistent aggregates containing hydrophobic domains, for example, micelles [73]. This a modest decrease when compared with hypsochromic shifts recorded for more hydrophobic compounds, which concurs with the retained hydrophilic character of cDAB-16 [100]. A sigmoidal fit of the curve (Figure 14) allows identification of the transition region between non-aggregated and aggregated states and the concentrations that this region spans. The midpoint of this transition is assigned to the concentration at which self assembly begins to occur (the CAC), estimated to be 0.62mg.mL^{-1} (0.32mM).

It was confirmed prior to experimentation that the structure of DAB-16-Am itself has no effect on MO lambda max at the concentrations studied. However, DAB-16-Am is able to solubilise the smaller fluorescent probe, pyrene (Figure 8) within its branch network when the dendrimer is present in concentrations above approximately 0.5 mg.mL^{-1} (data not shown). This is supported by literature observations that sites close to the core of DAB-32-Am and DAB-64-Am dendrimers are able to solubilise pyrene [108] therefore this technique was not included for quantitative determination of hydrophobic domains formed upon aggregation. PPI dendrimers also display a

degree of intrinsic fluorescence in media with neutral to low pH which can interfere with fluorescent techniques [109].

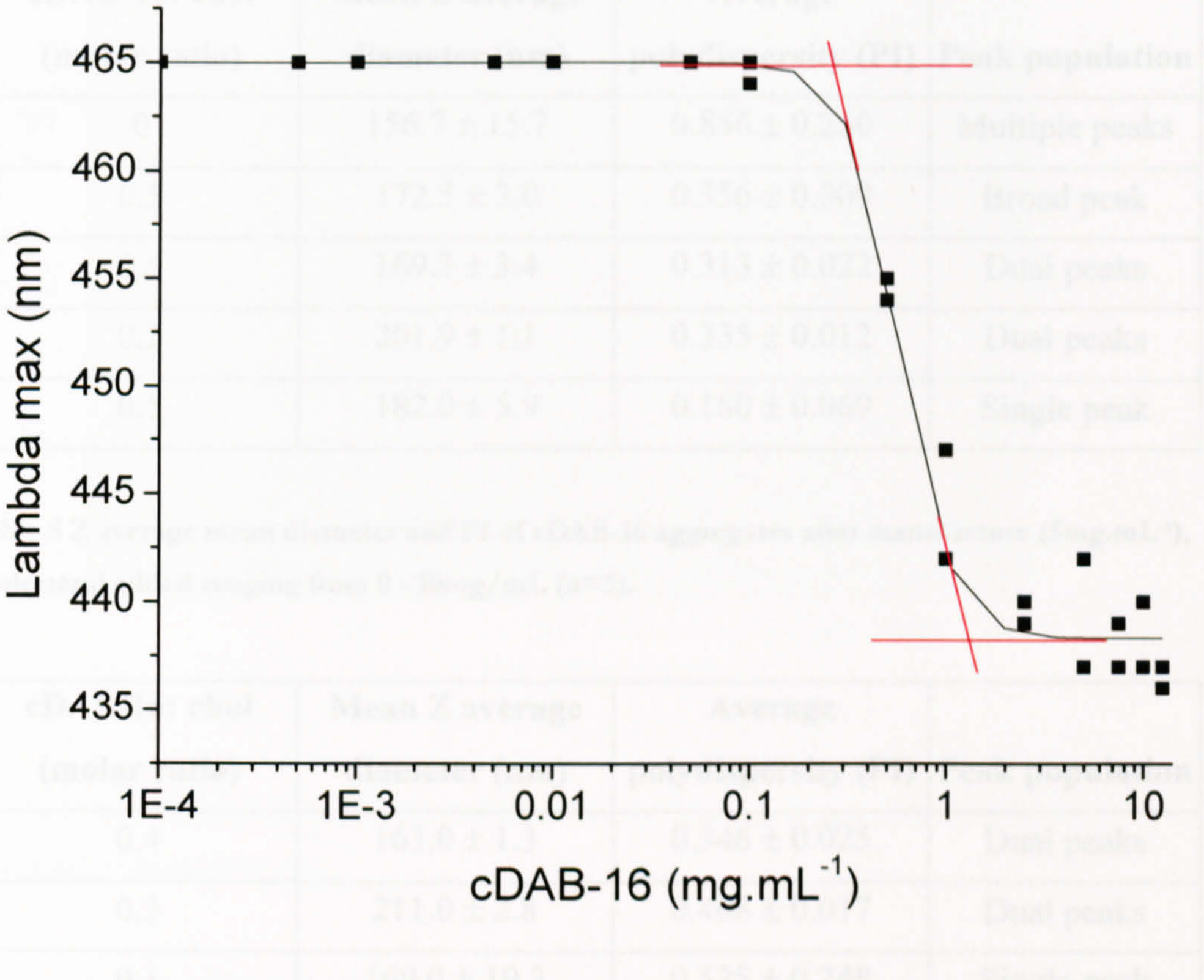

Figure 14 MO wavelength shift with cDAB-16 concentration. The midpoint of the transition between the non-aggregated and aggregated λ_{max} corresponds to the CAC of cDAB-16. Values pooled from two independent experiments.

2.4.7. PCS

PCS data is expressed as a size distribution graph of the particle size versus the intensity of light scattered by particles in each size range. The Z average diameter and polydispersities of freshly prepared cDAB-16 aggregates and vesicles are listed in Table 5. Selected vesicle formulations were sized a further 24 h later to assess their colloidal stability (Table 6). The cumulant mean size (Z average mean diameter) arises from the hydrodynamic diameter of the vesicles. The accuracy of the particle size distribution is represented by the polydispersity index (PI) which ranges from 0 to 1. A PI value of 0.7 or more is an indication of an inaccurate size result but

a moderate PI value between 0.3 and 0.4 is acceptable for colloidal systems [105]. All values were measured in triplicate.

cDAB-16: chol (molar ratio)	Mean Z average diameter (nm)	Average polydispersity (PI)	Peak population
0	156.7 ± 15.7	0.856 ± 0.250	Multiple peaks
0.5	172.5 ± 3.0	0.356 ± 0.009	Broad peak
0.4	169.3 ± 3.4	0.313 ± 0.022	Dual peaks
0.2	201.9 ± 1.1	0.335 ± 0.012	Dual peaks
0.1	182.0 ± 5.9	0.160 ± 0.069	Single peak

Table 5 Z average mean diameter and PI of cDAB-16 aggregates after manufacture (5mg.mL^{-1}), cholesterol added ranging from 0 - 10mg/mL (n=3).

cDAB-16: chol (molar ratio)	Mean Z average diameter (nm)	Average polydispersity (PI)	Peak population
0.4	163.0 ± 1.3	0.346 ± 0.025	Dual peaks
0.2	211.0 ± 2.8	0.408 ± 0.017	Dual peaks
0.1	169.0 ± 19.3	0.525 ± 0.248	Single peak

Table 6 Z average mean diameter and PI of cDAB-16 vesicles 24 h after manufacture (5mg.mL^{-1}), cholesterol added ranging from 2.5 - 10mg/mL (n=3)

After sonication all formulations of cDAB-16 assembled into particles that could be sized using PCS. Without the inclusion of cholesterol cDAB-16 forms structures with a wide polydispersity. The addition of cholesterol to the formulation in all cases increased the size of the assemblies which concurs with the literature and may be due to an increase in monomer aggregation number [36, 80]. The broad distribution of sizes at a molar ratio of 0.5 (Table 5) indicates that no distinct vesicle populations have been formed. Above this molar ratio, the vesicles exist in two populations which are represented by peaks at about 50nm (with greatest intensity) and 300nm (Figure 15).

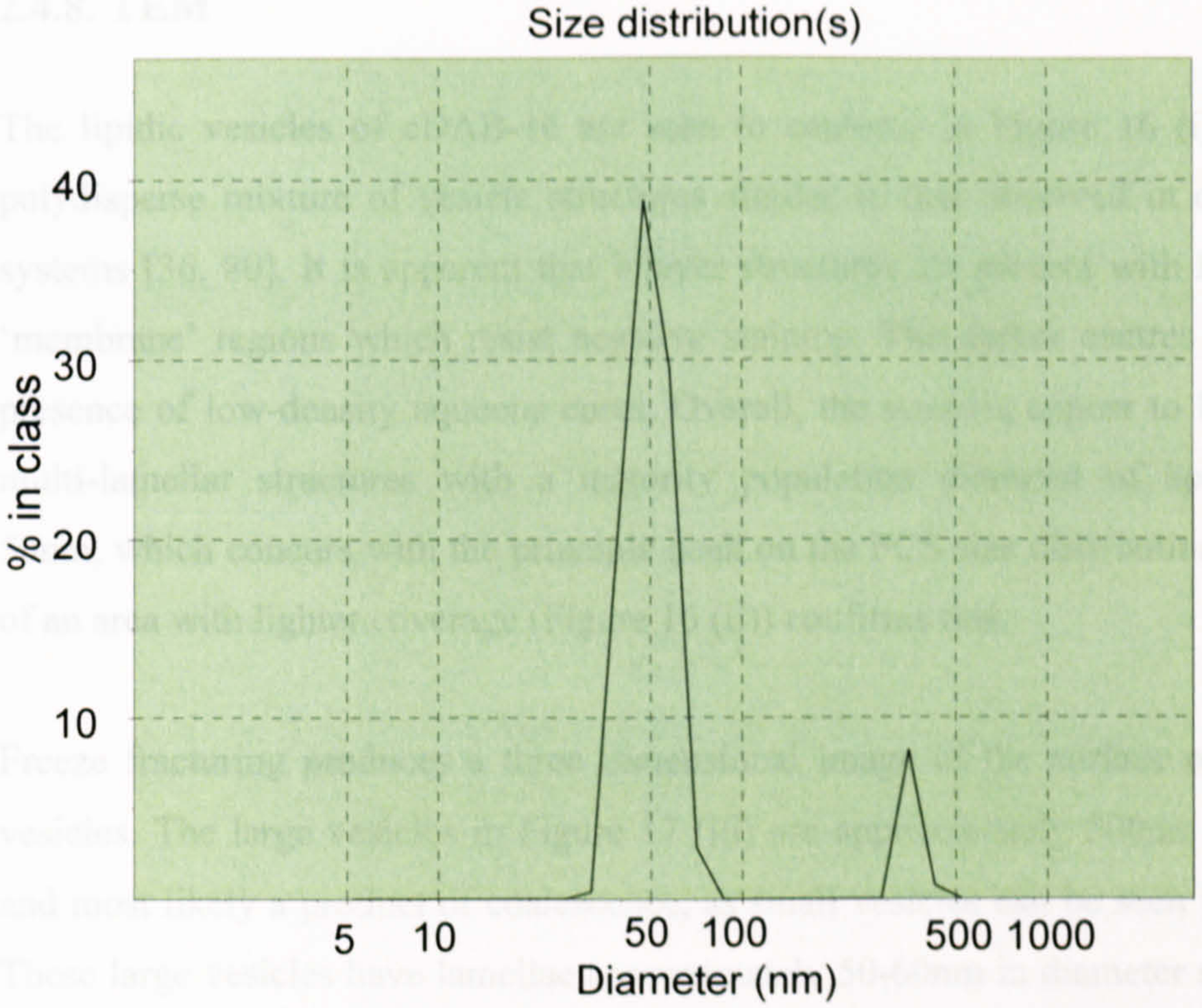

Figure 15 Size distribution graph for cDAB-16 vesicles 5mg.mL^{-1} containing cholesterol 2.5mg.mL^{-1} (molar ratio 0.4)

It appears that adding further amounts of cholesterol collapses these two populations into a single population peak (seen at a 0.1 cDAB-16: cholesterol molar ratio in Table 5). This could be because the amount of cholesterol included is in such large excess that cDAB-16 is now being incorporated into cholesterol aggregates. This formulation does not retain its stability at 24 h unlike the other vesicle formulations in Table 6. Aggregates produced at this molar ratio were very polydisperse after refrigeration for 24 h and cholesterol had visibly fallen out of the dispersion. The most stable formulation that gave the smallest particle size contained a 0.4 molar ratio of cDAB-16: cholesterol (5mg cDAB-16: 2.5mg cholesterol, Figure 15). This formulation was taken forward into further experiments and always prepared immediately before use.

2.4.8. TEM

The lipidic vesicles of cDAB-16 are seen to coalesce in Figure 16 (i) forming a polydisperse mixture of vesicle structures similar to that observed in other lipidic systems [36, 80]. It is apparent that bilayer structures are present with high-density 'membrane' regions which resist negative staining. The darker centres suggest the presence of low-density aqueous cores. Overall, the vesicles appear to be disc-like, multi-lamellar structures with a majority population diameter of approximately 50nm, which concurs with the principle peak on the PCS size distribution. An image of an area with lighter coverage (Figure 16 (ii)) confirms this.

Freeze fracturing produces a three dimensional image of the surface of individual vesicles. The large vesicles in Figure 17 (iii) are approximately 500nm in diameter and most likely a product of coalescence, as small vesicles can be seen inside them. These large vesicles have lamellae approximately 50-60nm in diameter suggesting a thickness of approximately four bilayers (Figure 17 (ii)) and each has a large aqueous core. Bilayer structures can be seen etched and shaded onto the surface of the vesicles.

(i)

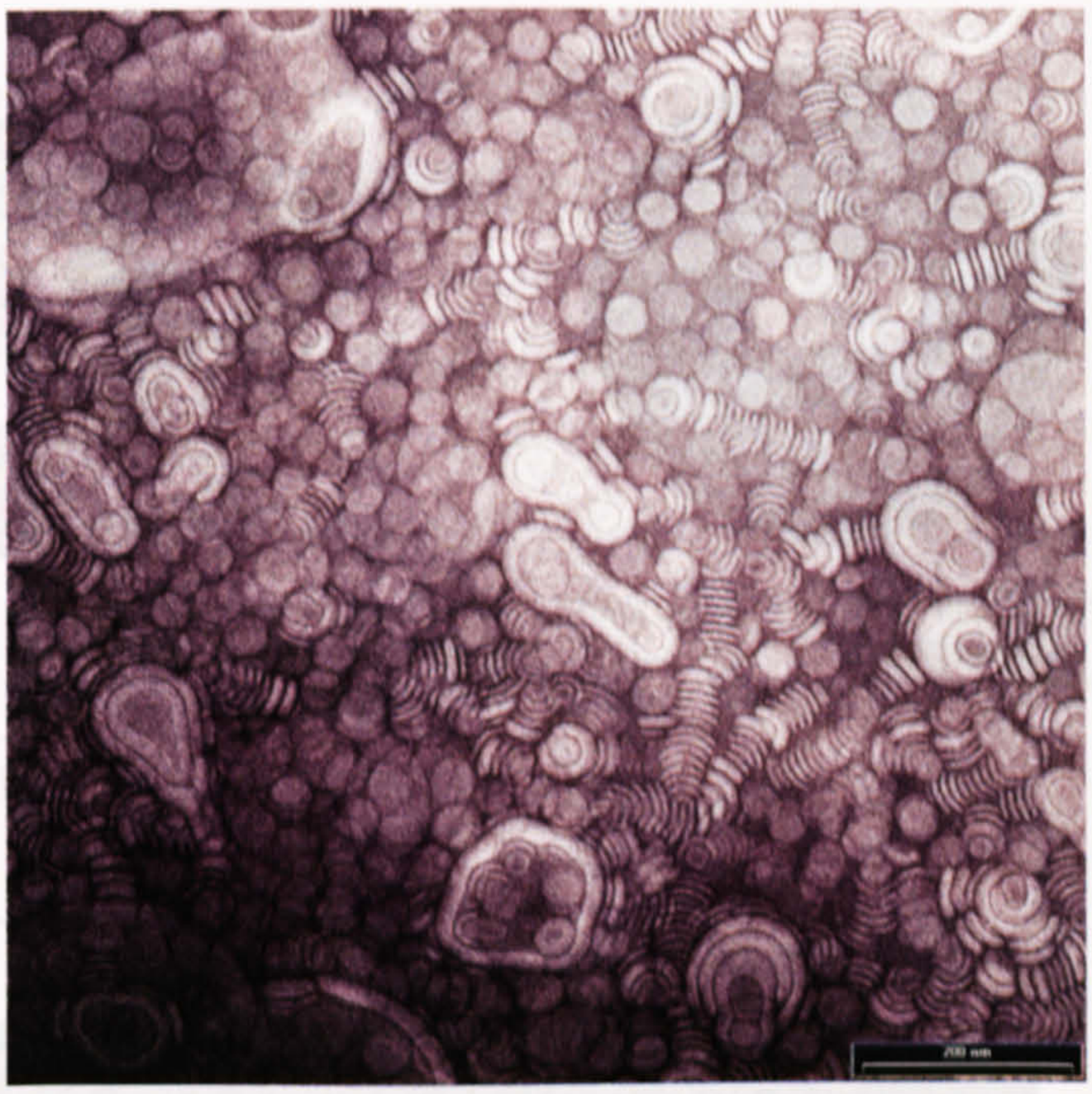

(ii)

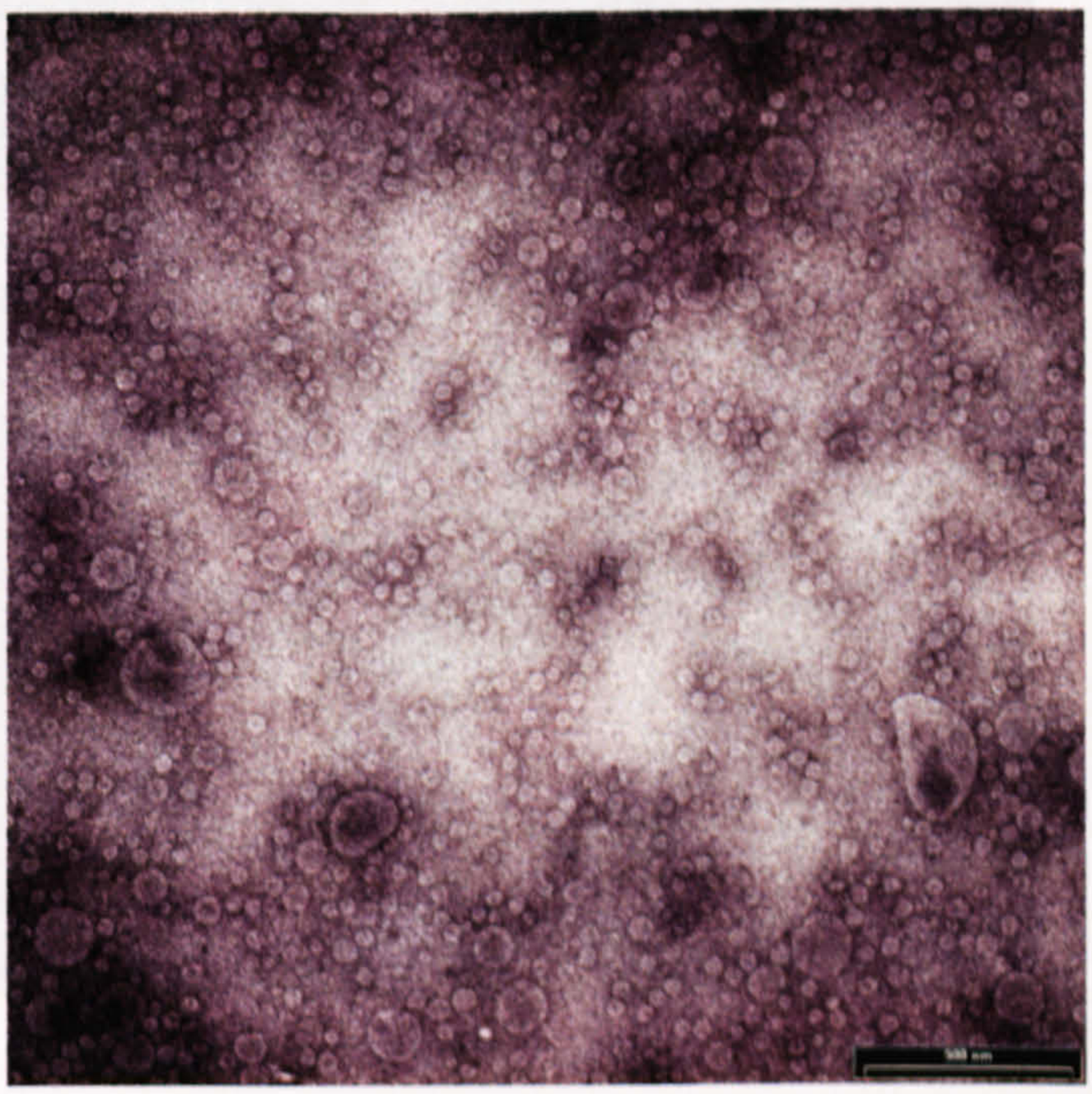

Figure 16 Negative stain transmission electron micrographs of cDAB-16 vesicles (5mg.mL^{-1} in water). (i) x50,000 magnification (densely populated). (ii) x20,000 magnification (sparsely populated).

(i)

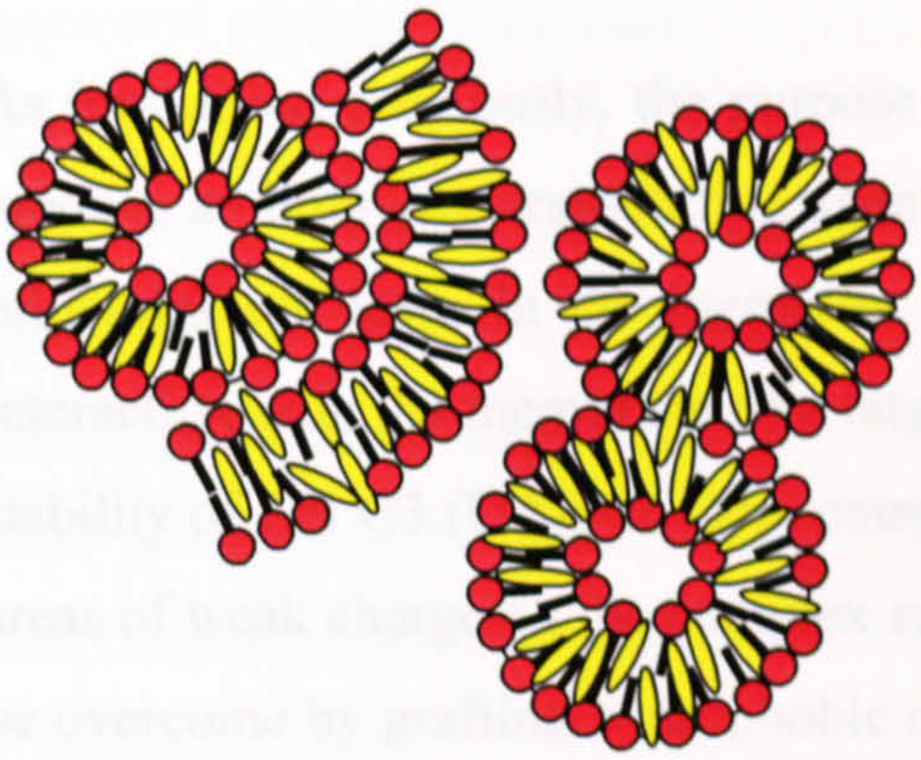

(ii)

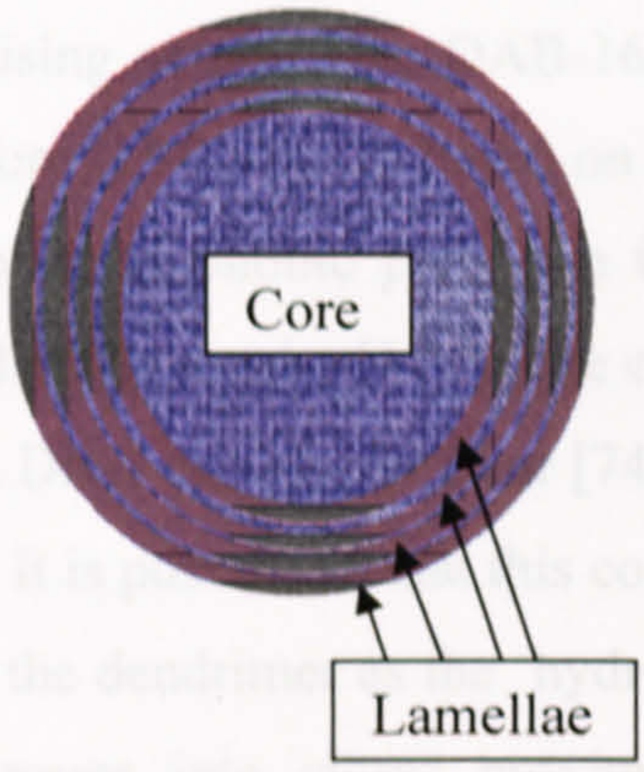

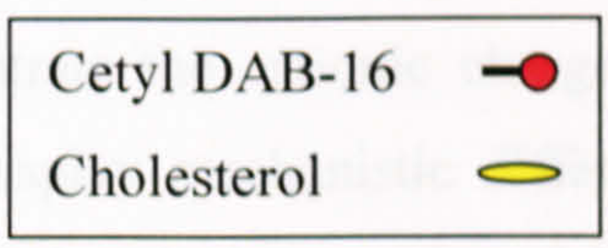

(iii)

Figure 17 (i) Schematic illustration of lamellar structures (imaged in Figure 16(i) & (ii)). (ii) Schematic illustration of large multilamellar vesicle. (iii) Freeze fracture transmission electron micrograph of large, multilamellar cDAB-16 vesicles. x30,000 magnification.

2.5. Discussion and conclusions

As introduced previously, the purpose of synthesising amphiphilic DAB-16 was to produce an improved transfection agent derived from DAB-16-Am based on rational principles set down in the literature. Inclusion of hydrophobic parts can improve interaction with the membrane of a target cell facilitating uptake [110]. The colloidal stability of PPI G3 (DAB-16-Am) complexes with DNA can also be poor [74] due to areas of weak charge on the complex surface [59]. It is postulated that this could also be overcome by grafting hydrophobic chains onto the dendrimer as the 'hydrophobic effect' [104] will bring the dendrimer head groups into closer proximity and concentrate the cationic charges available for DNA binding. Crucially, cDAB-16 may display mechanistic differences which allow links to be forged between the physicochemical properties of the dendrimers and their biological effects.

The cDAB-16 product contains a statistical distribution of low levels of cetylation based around a mean value. Therefore this product exists as a mixture and although the use of preparative LC–MS (chromatographic separation followed by MS analysis of each fraction) may be able to separate single populations [70], the final yield would almost certainly preclude use in biological applications. Rather, a population average value is used for quantitation but with careful attention to the polydispersity of these systems.

This population average value can be altered through variation of starting reactant molar ratio and also the dialysis volume and tubing molecular weight cut off (MWCO) value. A MWCO value of 12-14 KDa was selected to allow free movement of the underivatised DAB-16-Am dendrimer from the cDAB-16 product whilst retaining the aggregated amphiphilic molecules. It appears that exhaustive dialysis over 24 h was successful in drastically reducing the level of DAB-16-Am remaining but DAB-16-Am has not been completely removed (Table 3). It may be that the parent dendrimer remains associated with the aggregates in the dialysis medium which then hinder its removal. The residue of cetyl bromide that remains

after this process, however, is barely detectable by ^{1}H NMR and quantitative elemental analysis of bromide.

The ^{1}H NMR and EA data agree an average level of derivatisation of 1.1 cetyl chains per dendrimer molecule. ESIMS data (Table 3 and Figure 13) give some indication that there is very little tri-cetylated product in the mixture although this cannot be taken as quantitative. As anticipated, the average substitution level is very low (3.75 mol %) and cDAB-16 is expected to exhibit characteristics favouring association into vesicle structures.

Probe sonication was successfully employed to produce self-assembled systems from cDAB-16. The benefits of probe sonication, when compared with solvent evaporation methods, include improvements in formulation biocompatibility (as organic residues are not present) and rapid promotion of stable preparations of aggregates [80]. A small CAC value (0.32mM) has been estimated (Figure 14) for cDAB-16 in aqueous, low ionic strength media using the hydrophobic probe, MO. Further proof of the presence of these assemblies is taken from PCS measurements as a particulate population is detected with a low mean Z average hydrodynamic diameter (Table 5). These amphiphilic structures tend to be fluid-like, with molecules in constant thermal motion within the aggregate, thus it is difficult to assign a definitive size or shape to them [111]. Importantly though, this potential for hydrophobic interaction may alter the microstructures that are formed upon complexation of cDAB-16 with plasmid DNA.

The Z average mean hydrodynamic diameter of cDAB-16 vesicles (2: 1 cDAB-16: cholesterol weight ratio) correlated well with the estimated diameter of the main vesicle population from TEM images (Figure 16). The size peak with the most intensity was that of 50nm, representing uni-lamellar vesicles which appeared disc-like on these images. Visible coalescence of individual vesicles to form multi-lamellar vesicles (Figure 17 (iii)) could account for the presence of a vesicle population with Z average mean size of 300nm (Figure 15). These vesicles are

expected to behave differently to the cDAB-16 aggregates in biological systems, again providing a tool for the formation of structure-activity relationships.

In conclusion, cDAB-16 was successfully synthesised with the required low level of cetylation to promote dynamic aggregation processes in aqueous media but also to retain good aqueous solubility. It consists of a heterogeneous population of monomers with respect to cetylation levels. It can form stable vesicle assemblies in the presence of cholesterol and thus will be an excellent tool alongside the parent dendrimer DAB-16-Am for the examination of structure-biological activity relationships.

3. DNA Complexation Studies

3.1. Introduction

The behaviour of DNA molecules in solution fascinates scientists, and not just because they are the repository of our genetic blueprint. DNA has a long effective persistence length (i.e. it is a very stiff molecule) due to an effective density of one negative charge every 0.17nm of its length under physiological conditions [112]. However, in spite of predicted strong intermolecular repulsions, several higher-ordered forms of double stranded (duplex) DNA are known in nature [113].

The DNA duplex collapses into a dense, aggregated ψ-phase in aqueous solution merely in the presence of excess salt and inert polymer (or ethanol) due to osmotic pressure [113, 114]. Simple aggregation also occurs in the presence of divalent cations such as Mg^{2+} [115], polyamines [116] and basic polypeptides such as histones. DNA assembled in the nuclei of cells is tightly compacted into chromatin by octets of histones [113]. This is accounted for by the counterion condensation theory proposed by Gerard Manning [117]. In physiological solution, a thin layer of mono- or divalent counterions partially neutralises the DNA phosphates and causes limited relaxation of the DNA helices due to reduced electrostatic repulsion [112]. Release of this counterion layer (and bound water) provides the entropic drive for polyamine binding [118, 119]. Wilson and Bloomfield [115] have demonstrated that for global condensation (collapse) of DNA by linear polymers ~90% of the DNA phosphates must be neutralised. Not only charge neutralised by these agents, DNA can also become spontaneously overcharged by polyamines such as spermine and other polyvalent ions [120]. An attraction is generated between DNA helices due to coordination of multiple ammonium groups, producing particulate DNA complexes.

DAB-16-Am has a particularly large coordination number (30 N) and is therefore is especially suitable for electrostatic interaction with multiple DNA sugar-phosphate backbones via these ammonium functionalities. This process produces particulate dendrimer-DNA complexes (popularly termed 'dendriplexes'). Particulate nature is

vital for efficient cellular delivery of genetic material *in vitro* or *in vivo* [9]. Initial molecular modelling studies have demonstrated that DAB-16-Am is able to wrap around an entire helical turn of DNA spanning both the major and minor groove (Figure 18). An entire helical turn of DNA consists of 10 base pairs and is approximately 34Å in length [121]. Excitingly, the dendrimer tertiary amines have the potential to be involved in DNA binding as well as the more highly ionised primary amines due to the flexibility of PPI dendrimer branches [59]. Core binding is not possible for other commercially-available dendrimers (e.g. PAMAM dendrimers) and larger polymeric gene carriers.

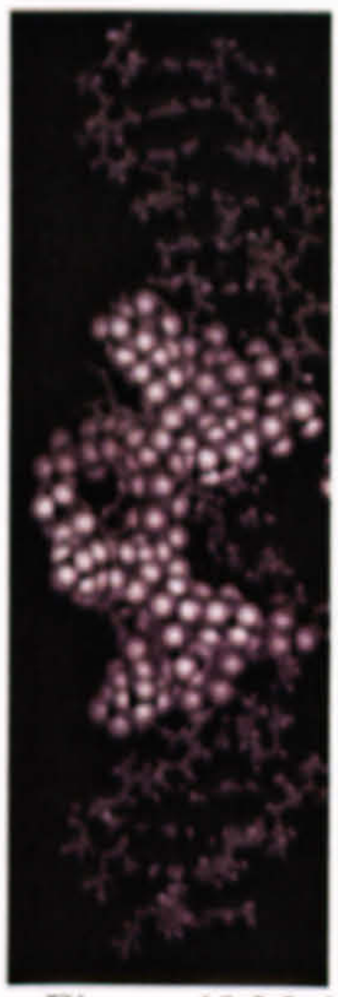

Figure 18 Molecular model of PPI G3 dendrimer-DNA binding [59]

The purpose of this chapter is to further explore the processes of DNA binding and condensation by the parent dendrimer DAB-16-Am immediately and to compare these parameters with those of cDAB-16 and cDAB-16 vesicles. It is important to establish that these amphiphilic formulations can complex DNA into small particles for *in vitro* and *in vivo* transfection. It is also postulated that enhanced dendrimer cooperativity through short range hydrophobic interactions would improve the DNA-binding efficiencies of the amphiphile formulations [77, 85, 86].

Isothermal Titration Microcalorimetry (ITC) is able to detect and accurately measure tiny heats (minimum detectable heat pulse ~0.2μcal) added or removed by thermodynamic processes occurring in the solution state [122]. It will be used to

directly determine apparent binding enthalpies and give insight into the binding-condensation profile (overall described as a complexation profile) as dendrimer is titrated into DNA solutions [123]. An assay utilising the exclusion of a fluorescent DNA intercalator, ethidium bromide, will be used to examine dendrimer-DNA binding. This has been used reliably to probe the interactions between DNA and both dendrimers [59, 124] and cationic amphiphiles [125]. Retardation of DNA migration through an agarose gel will be used to identify the initiation and completion of DNA complexation by a dendrimer species and finally the gel will be stained to determine the point at which excess dendrimer appears (indicating 'overcharging' of the complex) [126].

A large, linear poly(ethylenimine) (L-PEI) (22KDa, ExGen 500) will be included in all experiments for the purpose of comparison. It is a commercial *in vitro* transfection agent generally regarded as the gold standard polymeric carrier as it can mediate high levels of transfection in a range of cell types [127].

The physicochemical properties of the resulting complexes will be examined in Chapter 4.

3.1.1. Plasmid DNA production

Plasmids are self-replicating, extrachromosomal circular dsDNA molecules found in almost all bacteria species [128]. Specific enzymes (gyrases and topoisomerases) control the angle of twist between nucleotides, usually presenting plasmid DNA in a negative supercoiled, compact configuration [121]. Plasmids carry genes that that specify a range of functions including antibiotic resistance. Since the 1970s, vectors for propagation, manipulation and delivery of specific DNA sequences have been constructed with fragments from *Escherichia coli* (*E. coli*) plasmids. All plasmid vectors contain three common features; a replicator, a selectable marker (usually a gene encoding resistance to a particular antibiotic) and a cloning site. Transformation of *E. coli* with a high-copy-number plasmid can produce hundreds of clones per bacterial cell [128]. These can be readily separated out from chromosomal DNA due to their relatively small size (only several kilobases) [121]. The process of plasmid

generation, harvest, removal of chromosomal DNA by alkaline denaturation and finally purification by anion-exchange chromatography is discussed below [129].

3.1.1.1. Culture and harvest of *Escherichia coli*

All plasmids used in this work were produced in the DH5α strain of *E. coli* bacteria grown at 37°C with shaking in complete Luria-Bertani (LB) medium containing a balance of essential nutrients and the selection antibiotic ampicillin to allow efficient proliferation [130]. The cultures were typically harvested by centrifugation 16 h after incubation (the transition time for growth to progress through exponential to stationary stage), achieving a density of ~$2x10^9$ cells per mL [130].

3.1.1.2. Extraction of plasmid DNA

Bacterial cell membranes are commonly lysed using chemical methods, especially ethylenediamine tertaacetate (EDTA) for plasmid preparations, but in this method the anionic detergent sodium dodecyl sulphate (SDS) is used in combination with NaOH, termed alkaline lysis [129, 130]. The high pH (pH 12) also serves to denature genomic DNA by breaking down hydrogen bonds of all DNA molecules except those in the supercoiled state. RNA molecules also have the potential to compete with DNA for resin binding sites; therefore RNase is added to the lysis mixture. Upon neutralisation with potassium acetate these contaminants, including proteins, form a precipitate which can be removed by filtration before the lysate is applied to the anion-exchange column [129, 130].

3.1.1.3. Endotoxin removal

At this stage, a patented endotoxin removal buffer is added to remove endotoxins, or lipopolysaccharides (LPS). These are cell membrane components of the host bacteria *E. coli*. Endotoxins activate the complement cascade in mammals, which can cause fever and endotoxic shock syndrome. The presence of these molecules also sharply reduces cell transfection efficiencies [129, 130].

3.1.1.4. Purification of plasmid DNA

Finally, the lysate is passed through the anion exchange resin which comprises of 100 μm silica beads coated with positively charged diethylaminoethanol (DEAE) groups. These groups bind the plasmid DNA tightly. After the remaining contaminants have been washed out, plasmid DNA is eluted in a high salt buffer and precipitated using ethanol [129, 130].

3.1.1.5. Determination of plasmid yield and purity

DNA concentration can be estimated by UV absorbance spectrophotometry at a wavelength of 260nm, adjusted for non-specific absorbance at 320nm, using the relationship that an A_{260} of 1.0 for a 1cm path length = 50μg.mL^{-1} pure DNA [131]. The total yield is obtained by multiplying the DNA concentration by total sample volume. The A_{260}/A_{280} ratio is a reliable estimate of DNA purity with few limitations and a value of 1.8 – 2.0 is representative of a high-quality DNA sample [131].

3.1.2. Isothermal Titration MicroCalorimetry

Isothermal Titration microCalorimetry (ITC) is a sensitive technique which takes direct measurement of the heat of interactions in solution (i.e. the enthalpy, ΔH) [132] and is used frequently to probe polycation-DNA interaction [123, 126, 133, 134]. In an ITC experiment, two identical cells (one a reaction and one a reference cell) with volume approximately 1.5mL are kept at a constant temperature by heating. Aliquots of a ligand, for example, polycation, are injected into a solution of macromolecule, for example, DNA, in the reaction cell. An exothermic or endothermic enthalpy is associated with the resulting interaction. Thus to maintain a constant temperature the amount of heat supplied to the reaction cell has to be either decreased or increased with respect to the reference cell and it is this change in the rate of heat flow that is measured [122].

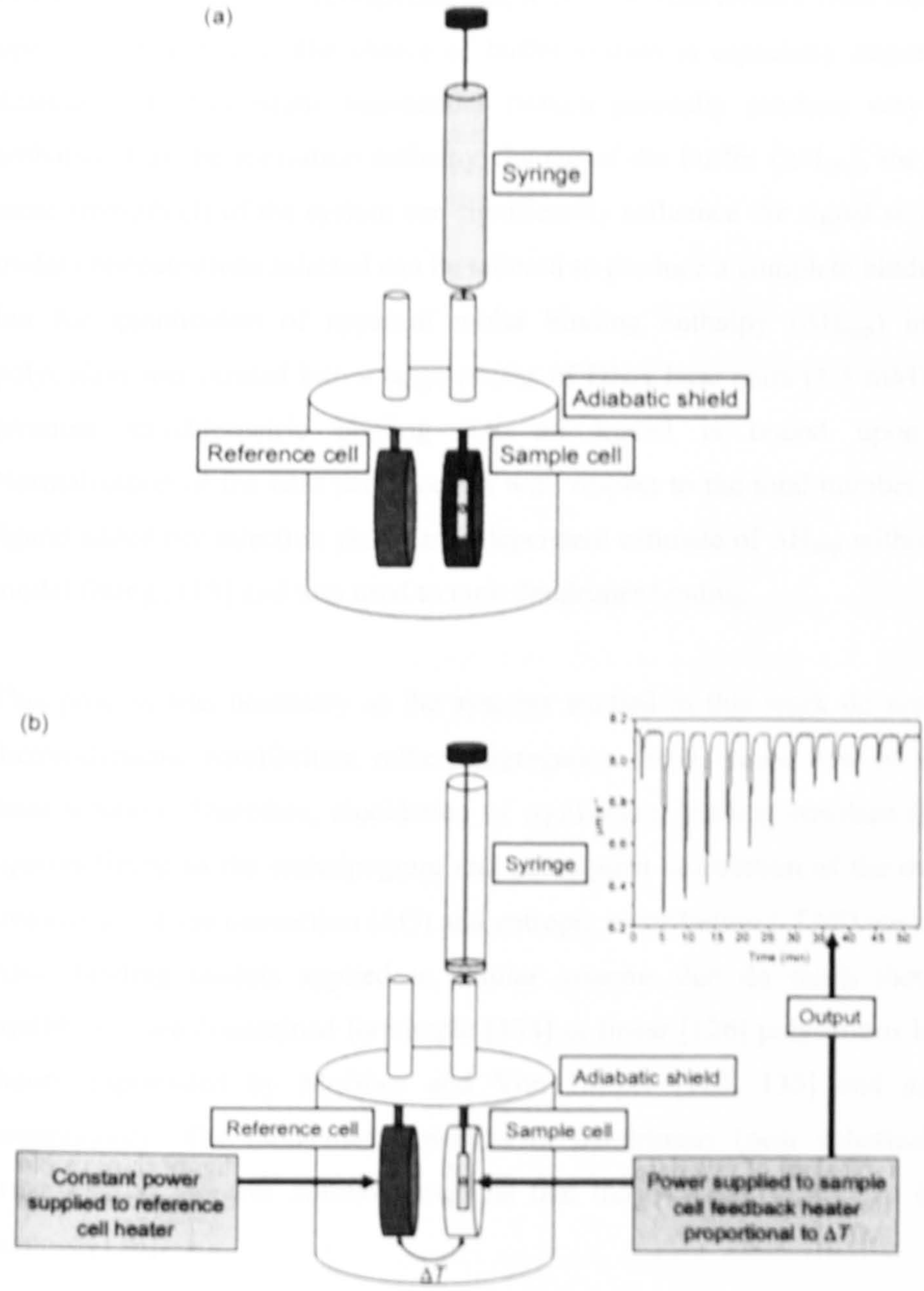

Figure 19 (a) A schematic diagram of a typical cell arrangement in an ITC. (b) Performing a titration and example of raw data output [122]

For successful ITC experiments both the DNA and ligand must be adequately prepared. Plasmid DNA should be very pure ($A_{260}/A_{280} > 1.8$), of accurately determined concentration and exist in a predominantly supercoiled form when visualised on an agarose gel. It is necessary to buffer match ligand solutions and

DNA solutions, usually through dialysis, to prevent interference from dilution effects upon injection [119]. The choice of buffer system is especially important for the detection of electrostatic interactions (which generally produce very low molar enthalpies) as the ionisation enthalpy change of the buffer (ΔH_{ion}), the pH and the ionic strength (I) of the system can significantly influence the signal size [119]. The molar concentrations selected can be tailored to produce a complete binding isotherm but for quantitation of apparent molar binding enthalpy (ΔH_{app}) in this work polycation was titrated into a large excess of DNA base pairs (1.5 mM) in order to promote stoichiometric binding (i.e. all ligand is bound upon injection). Normalisation of the heat per injection with respect to the total number of moles of ligand added per injection yields an independent estimate of ΔH_{app} without statistical model fitting [119] and was used to rank dendrimer binding.

This process was necessary as the systems studied in this work do not proceed to thermodynamic equilibrium; rather, aggregation events cause loss of the complex from solution. Therefore, elucidation of equilibrium binding constant (K_d) by least squares fitting to the enthalpogram and subsequent calculation of the overall Gibbs free energy of the interaction (ΔG) and entropic contribution ($-T\Delta S$) are not possible. Also, binding models applied to similar systems that do reach thermodynamic equilibrium are determined for simple [134] or linear [126] polycations based on the theory expounded by McGhee and Von Hippel [120, 135] and assume non-cooperativity. The molecular dynamics of dendrimers (near spherical, branched structures) in salt-free solutions suggest that these cannot be treated in the same manner [136].

In addition, a study was made of linked protonation effects using ITC [137] to detect the transfer of protons from the buffer species upon DNA binding by DAB-16-Am. To do this, buffer systems with differing ionisation enthalpies (ΔH_{ion}) and good buffering capacity at physiological pH were selected [138, 139] for use at a constant low ionic strength (I = 10mM). The number of protons exchanged (nH^+) and the true binding enthalpy (ΔH_0) can be determined from the contribution to the measured binding enthalpy (ΔH_{app}) [134, 137, 140] according to the relationship:

$$\Delta H_{app} = \Delta H_0 + nH^{\circ}.\Delta H_{dil} \qquad \text{Equation 1}$$

Limitations of the ITC technique are often as a result of its sensitivity; vibration and nearby electronic equipment can interfere with the baseline [119]. Also without extensive degassing of solutions the baseline can be obliterated by bubbles. Due to the large capacity of the cell, and the high concentrations of DNA required for accurate assessment of a system which produces very small heat changes, milligram amounts of DNA are consumed.

3.1.3. Ethidium Bromide exclusion assay

The ethidium bromide (Eth Br) exclusion (or competition) assay exploits the ability of Eth Br, a planar aromatic dye (Figure 20), to intercalate (or insert) between neighbouring base pairs of the DNA duplex [124]. Widom and Baldwin noted the inhibition of cation-induced DNA condensation by Eth Br in 1983 [141]. Eth Br is a very convenient fluorescent spectroscopic probe which has since been widely used to study DNA binding by other species [42, 72, 74, 77, 79, 81, 123, 125, 133, 142, 143]. When intercalated the position of the planar group results in an increase of fluorescent yield with a λ_{max} detectable at ~590nm; upon exclusion from DNA this fluorescence is quenched [124]. DAB-16-Am can bind an entire helical turn of DNA [59] and in doing so prevents the base pair separation which must occur for Eth Br intercalation to take place (Figure 20) [124].

It is noteworthy that this technique is not being used to give information about the condensation process; if this information is required then a fluorescent probe covalently bound to DNA which self-quenches upon proximity, for example fluorescein or rhodamine labelled DNA, would be more appropriate. More unusual methods used to assess the extent of condensation include the use of optical tweezers to determine resistance to DNA strand separation [142, 144, 145].

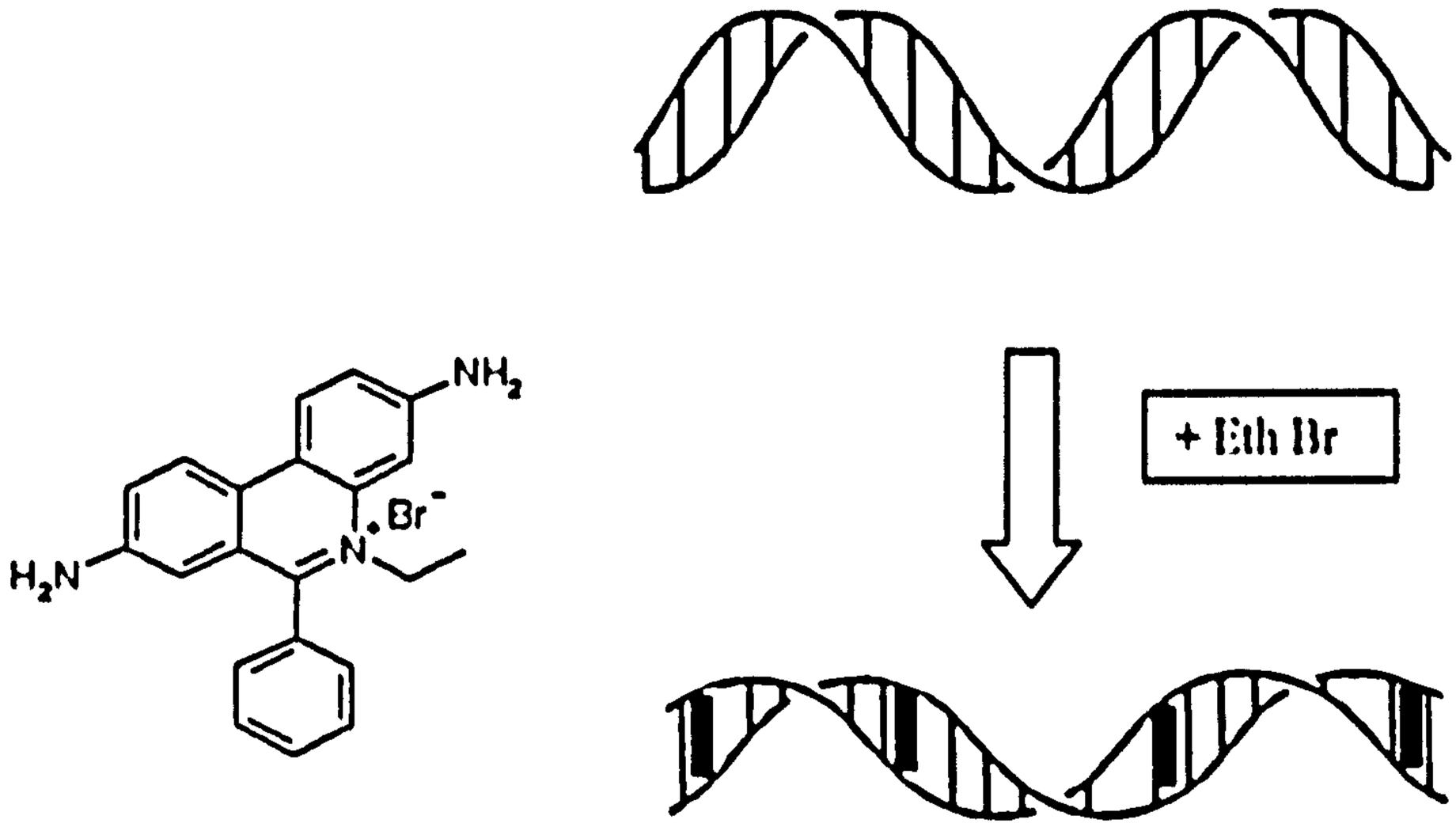

Figure 20 Structure of ethidium bromide (Eth Br) and illustration of Eth Br stacking between DNA base pairs

3.1.4. Agarose gel retardation assay

Agarose analytical gels are composed of a cross-linked network of alternating D- and L-galactose units forming channels up to several hundred nanometers in diameter, the initial concentration of agarose determining the size of these channels. When applied to an agarose gel under the influence of an electric field, carrier-DNA complexes and free DNA migrate through the gel at different rates dependent on the molecular weight and conformation of the DNA, the applied voltage and the composition of the electrophoresis buffer [129]. Visualisation of the distance of migration of plasmid bands using UV irradiation in the presence of Eth Br allows identification of the dendrimer amine: DNA phosphate molar ratio at which charge neutralisation begins to alter DNA mobility and the ratio at which the overall complexation process is complete. The first appearance of excess carrier overcharging of DNA can be detected on the same gel (migrated to the anode) using a brilliant blue stain for amines [126]. A disadvantage of this technique includes the inability to investigate fixed time points and it is possible that the applied potential difference and buffer composition will affect complex structures.

3.2. Materials

DAB-16-Am (PPI Generation 3) MW 1686.7 g mol^{-1}	Sigma Aldrich Co., UK
cDAB-16 (cetylated DAB-16) Average MW 1932.1 g mol^{-1}	Synthesised as in Chapter 2
ExGen 500 MW 22,000 g mol^{-1}	Helena Biosciences, UK
EndoFree Plasmid Giga Kit	QIAGEN, UK
pCMVsport β-Galactosidase	Life Sciences, GibcoBRL, UK
Dextrose, anhydrous	Sigma Aldrich Co., UK
Cholesterol	Sigma Aldrich Co., UK
Ethidium bromide	Sigma Aldrich Co., UK
Agarose; electrophoresis grade	Life Sciences, GibcoBRL, UK
tris-(hydroxymethyl)aminomethane (TRIS) base	Melford Laboratories, UK
Phosphoric acid	BDH Laboratories, UK
Boric acid	Fisher Scientific, UK
(4-(2-hydroxyethyl)-1-piperazineethanesulfonic acid) (HEPES) free acid, 1M (sterile)	Sigma Aldrich Co., UK
Ethylendiamine tetraacetate (EDTA)	Sigma Aldrich Co., UK
Hyperladder I	Bioline Ltd, UK
5x Loading Buffer	Bioline Ltd, UK
Ninhydrin reagent	Sigma Aldrich Co., UK
Methanol	BDH Laboratories, UK
Glacial acetic acid	BDH Laboratories, UK
Coomassie Brilliant Blue G	Sigma Aldrich Co., UK

Table 7 Materials and suppliers used in Chapter 3

3.3. Methods

3.3.1. pDNA synthesis and purification

For binding studies, plasmid DNA (pCMVsport β-Galactosidase, 7.2Kbp) was selectively propagated in *E. coli* grown in LB medium containing 100mg.mL^{-1} ampicillin at 37°C and subsequently purified using a QIAGEN EndoFree Plasmid Giga kit according to the manufacturer's instructions (Section 3.1.1). Precipitated pDNA was re-dissolved overnight in sterile 5% dextrose solution.

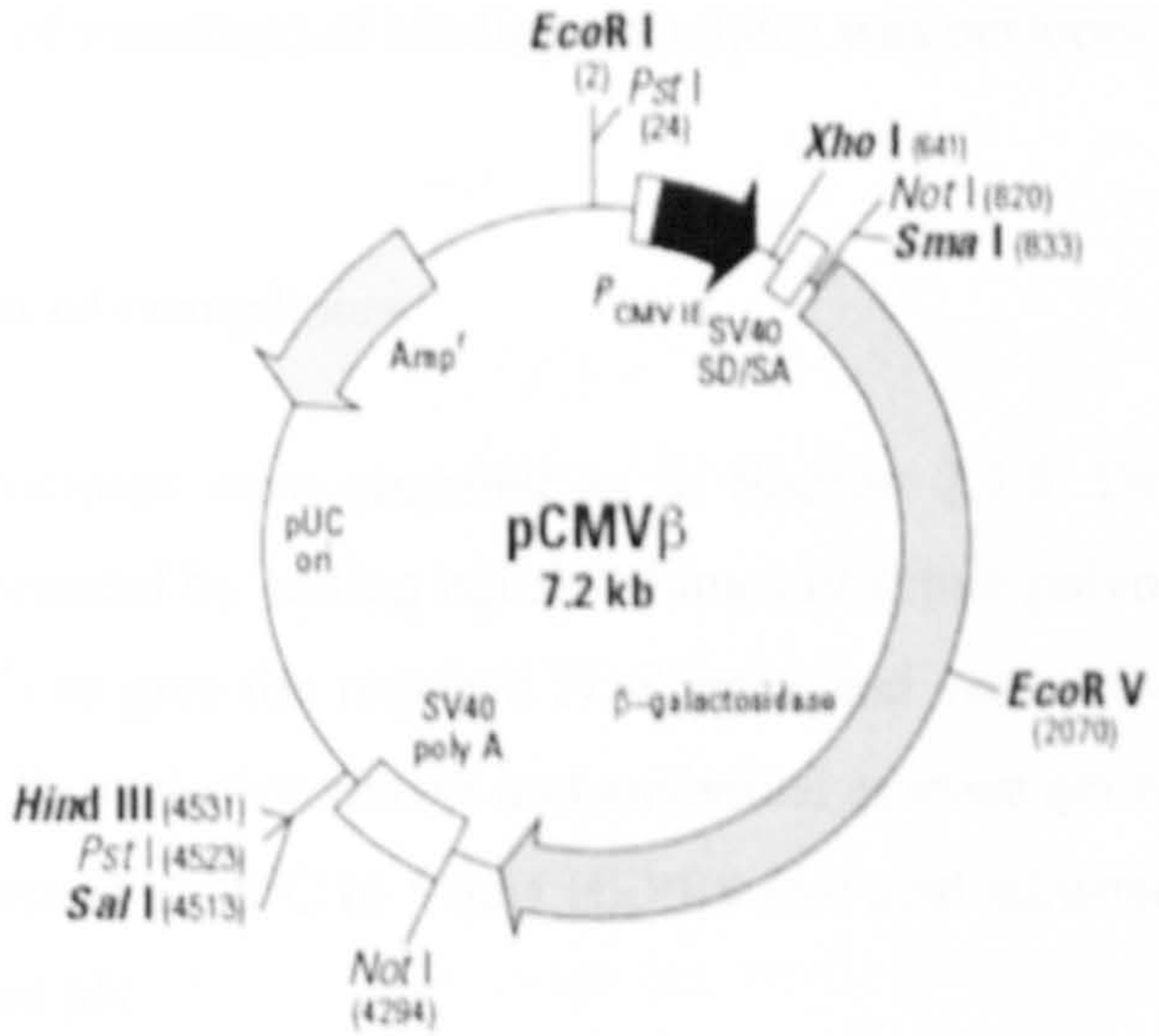

Figure 21 pCMVsport β-Galactosidase vector map [146]

3.3.2. Isothermal Titration Microcalorimetry (ITC)

Calorimetric experiments were performed using a Microcal VP-ITC Microcalorimeter (MicroCal, USA) operated at 25°C. Typically a series of 28 x 10uL injections were made at 300 s intervals into a cell of approximately 1.4mL volume containing either pDNA or blank buffer. Buffer solutions were prepared at I = 10mM (phosphate, HEPES and TRIS) and adjusted to the desired pH ± 0.05 units according to the method of Ellis *et al.* [138] and then sterile filtered. Concentrated samples of pCMVsport β-Galactosidase plasmid DNA (~1mL, up to 3mg.mL^{-1}) were dialysed against 2 L buffer solution with two changes over 48 h at 4°C using dialysis cassettes of 3000Da MWCO, 3mL capacity (Slide-a-lyser, Pierce, IL, USA). The final

equilibrium buffer solution was then used to dissolve dendrimers for reaction and to dilute DNA to the correct concentration based on determination of A_{260}. The amphiphilic dendrimer formulations were prepared by probe sonication as in Section 2.3.5. For examination of ExGen 500, a solution 100mM in PEI units was dialysed against the appropriate buffer solution along with pDNA, then the final PEI concentration was determined using a standard ninhydrin assay developed by Moore and Stein [147, 148]. The concentration of pDNA in the reaction cell was either 0.29 mM or 1.50 mM in base pairs (MW nucleotide pair = 684 $g.mol^{-1}$). Calculation of binding enthalpies was completed using Microcal Origin® Version 7. One-way ANOVA (analysis of variation) of binding enthalpies was performed using Minitab® Version 10.

3.3.3. Preparation of complexes

Self-assembled structures were prepared as in Section 2.3.5. Dendrimer (or PEI) complexes were prepared by adding equal volumes of dilute polymer to dilute DNA (100 – 200$\mu g.mL^{-1}$) to give the required N: P ratio, and vortex mixed for 10 s. For the purpose of Eth Br exclusion assays and analytical agarose gel retardation studies, complexes were formed at 25°C in 5 mM HEPES free acid adjusted with dilute acid/ alkali to the required pH.

Molar nitrogen: phosphate calculations were based on the ratio of no. of mol of PPI groups (e.g. for DAB-16-Am, MW = 56 $g.mol^{-1}$) or PEI groups (MW = 44 $g.mol^{-1}$) to the no. of mol of DNA phosphate groups (1g of DNA contains 3mmol of phosphate).

3.3.4. Ethidium Bromide exclusion assay

The reduced fluorescence of Eth Br was used to probe the binding of DAB-16-Am and its amphiphilic derivatives. Dendrimer nitrogen: DNA phosphate complexes were formed at molar N:P ratios of 0.125-5 (final volume 100µL, final DNA concentration 100$\mu g.mL^{-1}$). At specific time points (0.5, 1, 2, 4, 24 and 168 h) 900µL of Eth Br 0.4$\mu g.mL^{-1}$ was added (final volume 1mL), mixed by inversion and

transferred to a fluorescence cuvette. The fluorescence intensity of each sample was determined using a Perkin-Elmer LS-50B fluorimeter (Perkin-Elmer, UK) at λ_{ex} = 526nm, λ_{em} = 592nm and the extent of Eth Br exclusion expressed in relative units (RU);

$$RU = (F_t - F_0)/(F_e - F_0) \qquad \text{Equation 2}$$

where F_t = fluorescent intensity of Eth Br in sample at time t, F_0 = fluorescent intensity of Eth Br in dilute buffer, F_e = fluorescent intensity of Eth Br in DNA solution (10μg.mL^{-1}).

3.3.5. Agarose gel retardation assay

Complexes (5μL, 0.2μg DNA, N: P ratio 0.25-60) were loaded onto an agarose gel (1% w/v) in 0.5x TBE (TRIS base 45mM: Boric acid 45mM: EDTA 1mM) buffer adjusted to pH 7.4 containing Eth Br (0.5μg.mL^{-1}) and run in x 0.5 TBE buffer (pH 7.4) at 150 V for 45 – 60 min before visualisation using a UV transilluminator (Syngene Gene Genius Bioimaging System, UK). A molecular weight marker, DNA ladder λ-Hind III (Hyperladder I, 2μL) was run for size comparison with 14 regularly spaced bands (10,000 – 200 bp). Following this, polymer was visualised by staining the gel with 1% w/v Coomassie blue dye in water: methanol: glacial acetic acid solution (80:10:10 v/v) and subsequently washed with destain solution (80:10:10 v/v of staining solution without the dye) according to the method of Rungsardthong *et al.* [126]. Images were captured using a Medalight LP400 panel connected to the Syngene Gene Genius Bioimaging System (Syngene,UK).

3.4. Results

3.4.1. Plasmid quality and purity

The quality of pDNA after purification was visually examined using agarose gel electrophoresis. pDNA was confirmed to be predominantly in supercoiled form. Assessment of DNA purity from RNA and protein contaminants consistently gave A_{260}/A_{280} values of >1.8 <2.0, also non-nucleic acid absorbance (detectable at 320nm) was negligible.

3.4.2. ITC

3.4.2.1. The influence of pH

The enthalpograms at each pH (Figure 22 i-iii) are shown for the purpose of illustrating the overall binding profile of DAB-16-Am and for the elucidation of binding stoichiometries at pH 3 and pH 7 (a binding event is not detectable at pH 11 consistent with the findings of Kabanov *et al.* [149]). These were obtained by injection of 8.89 mM PPI units into 0.29 mM DNA base pairs. Apparent binding enthalpies (Figure 22 iv) were more accurately obtained through the injection of 6.67mM PPI units into an excess of DNA base pairs (1.50 mM) (raw data not shown). The mean of the first four injection heats of a constant size minus the blank injection heats (DAB-16-Am into buffer only) were used.

Examination of the binding profile of DAB-16-Am at pH 7 (Figure 22 ii) gives the following information: initial titration of dendrimer into DNA solution provokes an exothermic (-ΔH) event of small magnitude. At a molar N: P ratio of 1 in the reaction cell an endothermic contribution (+ΔH) can be detected on the raw ITC profile which is increasing in magnitude. At an N: P ratio of 1.5 this heat rapidly grows, dominating the enthalpogram, until at N: P 2 it decreases in a stepped manner to zero. These thermodynamic events can be rationalised to real events. The initial, slightly favourable enthalpies are anticipated to arise as a result of electrostatic (ionic) bond formation between the dendrimer primary amines and the DNA phosphate backbone. As increasing amounts of dendrimer are added, this enthalpy becomes less favourable, probably due to electrostatic repulsion from existing

dendrimer molecules bound along the DNA backbone. At the same time, these binding events will create local areas of charge neutralisation and perturb the DNA duplex structure. This is the beginning of the condensation process and accounts for the increasing enthalpic requirement. The sudden increase in this unfavourable enthalpy is likely to coincide with the onset of global condensation and aggregation; interestingly it is at this point that species such as spermine reach a threshold binding density which triggers cooperativity of binding [120] and this does not necessarily represent complete DNA phosphate charge neutralisation. As mentioned previously, the threshold for global DNA collapse is estimated to be approximately 90% neutralisation of DNA phosphates for linear polymers; this particular model also assumes that polycation behaviour remains non-cooperative [115].

This profile differs considerably at pH 3 (Figure 22 i). Along with a more negative binding exotherm and a much smaller enthalpic requirement for DNA structural rearrangement, the resulting complex is stabilised against aggregation processes leading to precipitation. The entire process is complete at 2 N: P and 3 N: P for pH 3 and pH 7 systems respectively. This represents a final amount of 10 moles of DNA phosphate associated with 1 mole of DAB-16-Am at near physiological pH and 15 moles of phosphate associated with 1 mole of DAB-16-Am at pH 3 under these experimental conditions.

A plot of apparent molar binding enthalpy (ΔH_{app}) versus solution pH varies in a linear manner (Figure 22 iv) although this relationship should not be extrapolated beyond this range of values. As expected, ΔH_{app} is greatest at the lowest pH value examined (pH 3), at which all amines within the dendrimer structure are ionised and available for binding in a 'dense shell, open core' conformation [136] and falls to zero by pH 11 in which region the opposite is true [150].

(i)

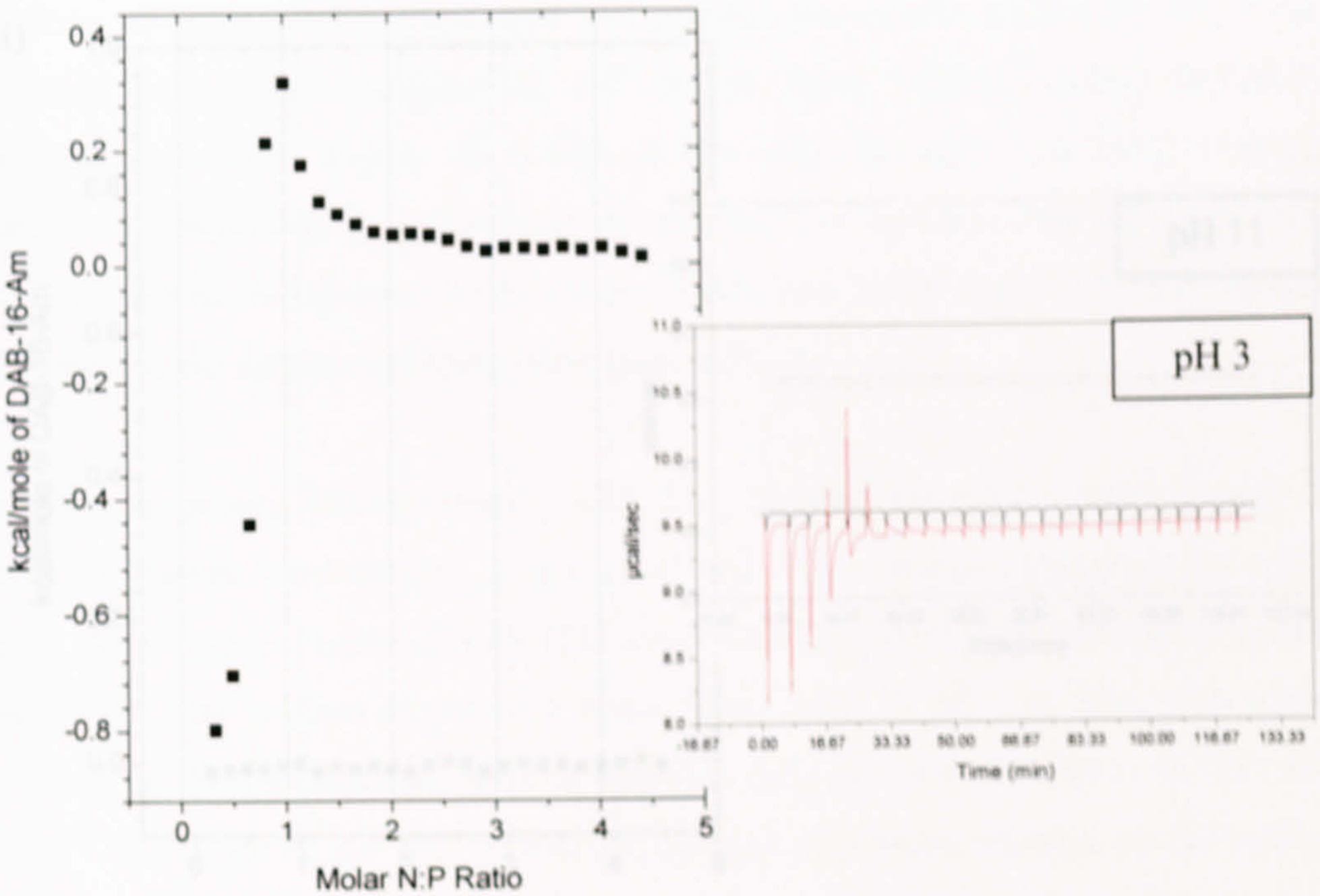
kcal/mole of DAB-16-Am
0.4
0.2
0.0
-0.2
-0.4
-0.6
-0.8
0
1
2
3
4
5
Molar N:P Ratio
pH 3
µcal/sec
11.0
10.5
10.0
9.5
9.0
8.5
8.0
-16.67
0.00
16.67
33.33
50.00
66.67
83.33
100.00
116.67
133.33
Time (min)

(ii)

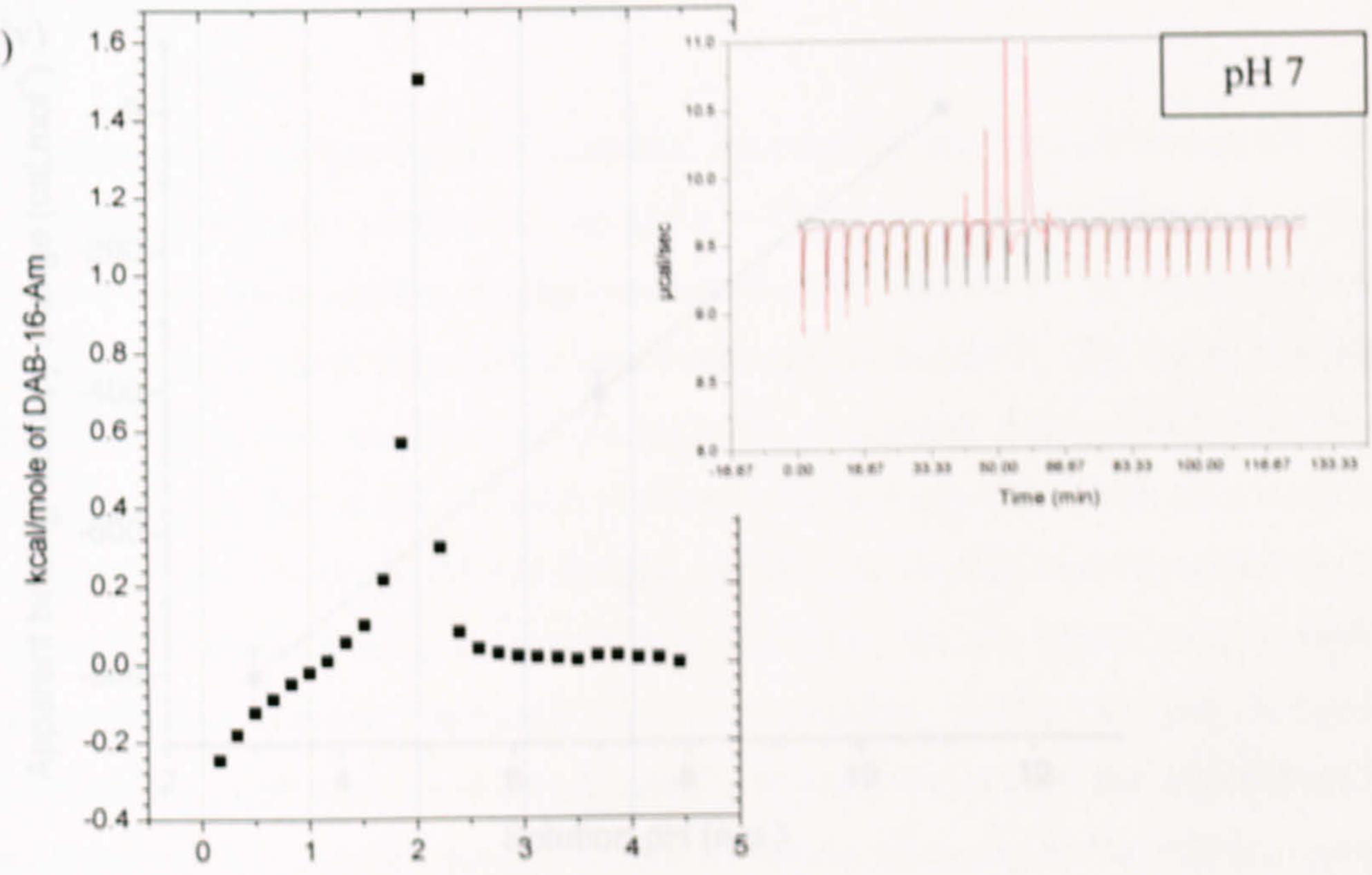
kcal/mole of DAB-16-Am
1.6
1.4
1.2
1.0
0.8
0.6
0.4
0.2
0.0
-0.2
-0.4
0
1
2
3
4
5
Molar N:P Ratio
pH 7
µcal/sec
11.0
10.5
10.0
9.5
9.0
8.5
8.0
-16.67
0.00
16.67
33.33
50.00
66.67
83.33
100.00
116.67
133.33
Time (min)

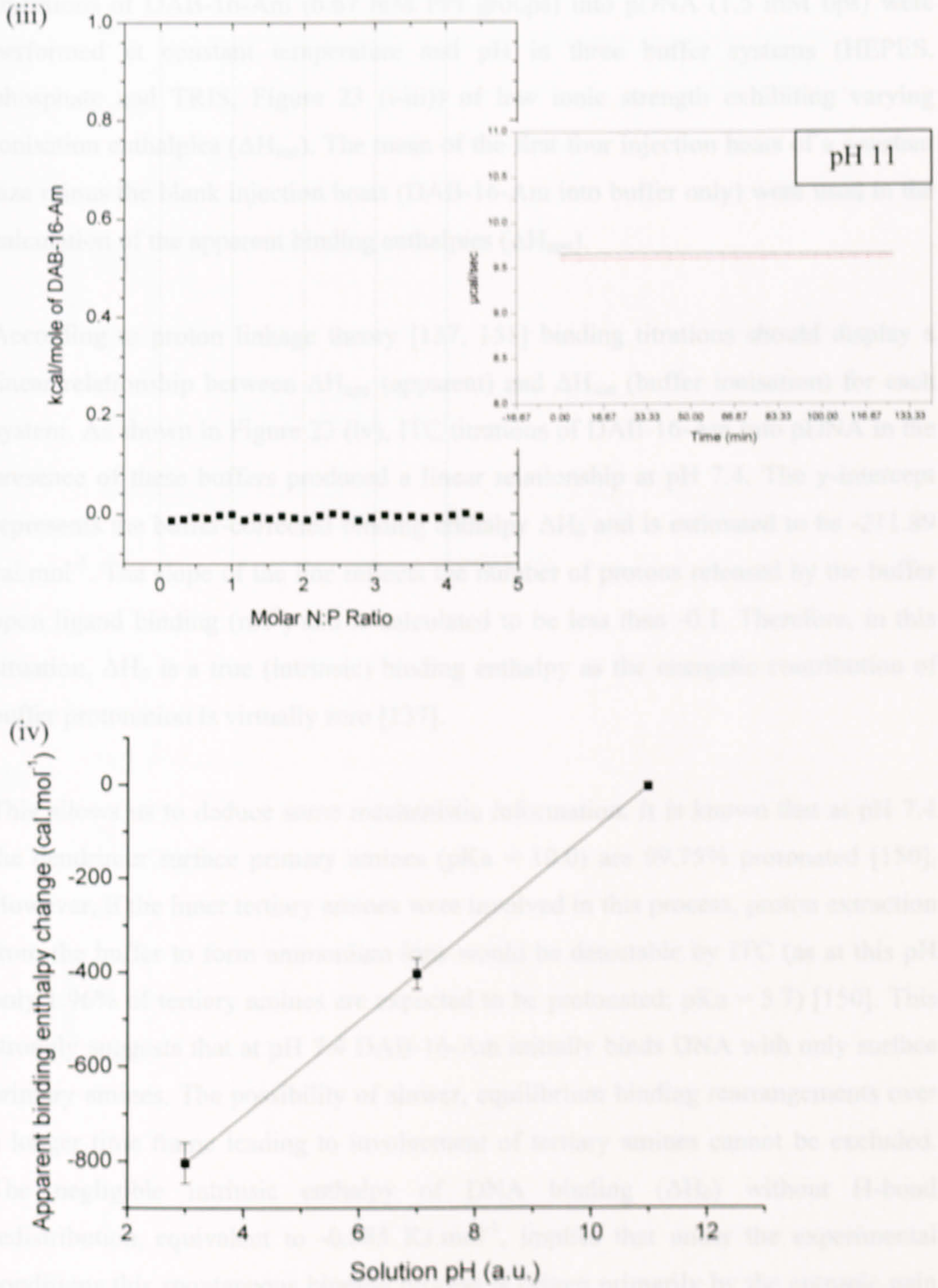

Figure 22 Main: DAB-16-Am injected into pDNA (8.89mM PPI: 0.29mM bps) at 25°C, all in phosphate buffer (I = 10mM) adjusted to (i) pH 3 (ii) pH 7 (iii) pH 11. Inset: corresponding raw ITC. (iv) ΔH_{app} versus solution pH for DAB-16-Am

3.4.2.2. Proton transfer

Injections of DAB-16-Am (6.67 mM PPI groups) into pDNA (1.5 mM bps) were performed at constant temperature and pH in three buffer systems (HEPES, phosphate and TRIS, Figure 23 (i-iii)) of low ionic strength exhibiting varying ionisation enthalpies (ΔH_{ion}). The mean of the first four injection heats of a constant size minus the blank injection heats (DAB-16-Am into buffer only) were used in the calculation of the apparent binding enthalpies (ΔH_{app}).

According to proton linkage theory [137, 151] binding titrations should display a linear relationship between ΔH_{app} (apparent) and ΔH_{ion} (buffer ionisation) for each system. As shown in Figure 23 (iv), ITC titrations of DAB-16-Am into pDNA in the presence of these buffers produced a linear relationship at pH 7.4. The y-intercept represents the buffer-corrected binding enthalpy ΔH_0 and is estimated to be -211.89 cal.mol^{-1}. The slope of the line reflects the number of protons released by the buffer upon ligand binding (nH^+) and is calculated to be less than -0.1. Therefore, in this situation, ΔH_0 is a true (intrinsic) binding enthalpy as the energetic contribution of buffer protonation is virtually zero [137].

This allows us to deduce some mechanistic information. It is known that at pH 7.4 the dendrimer surface primary amines (pKa = 10.0) are 99.75% protonated [150]. However, if the inner tertiary amines were involved in this process, proton extraction from the buffer to form ammonium ions would be detectable by ITC (as at this pH only 1.96% of tertiary amines are expected to be protonated; pKa = 5.7) [150]. This strongly suggests that at pH 7.4 DAB-16-Am initially binds DNA with only surface primary amines. The possibility of slower, equilibrium binding rearrangements over a longer time frame leading to involvement of tertiary amines cannot be excluded. The negligible intrinsic enthalpy of DNA binding (ΔH_0) without H-bond redistribution, equivalent to -0.885 KJ.mol^{-1}, implies that under the experimental conditions this spontaneous binding process is driven primarily by the entropic gain by the system, probably due to the degrees of freedom gained upon displacement of DNA associated water and counterions by the dendrimer molecules (the hydrophobic effect) [122, 152].

(i)

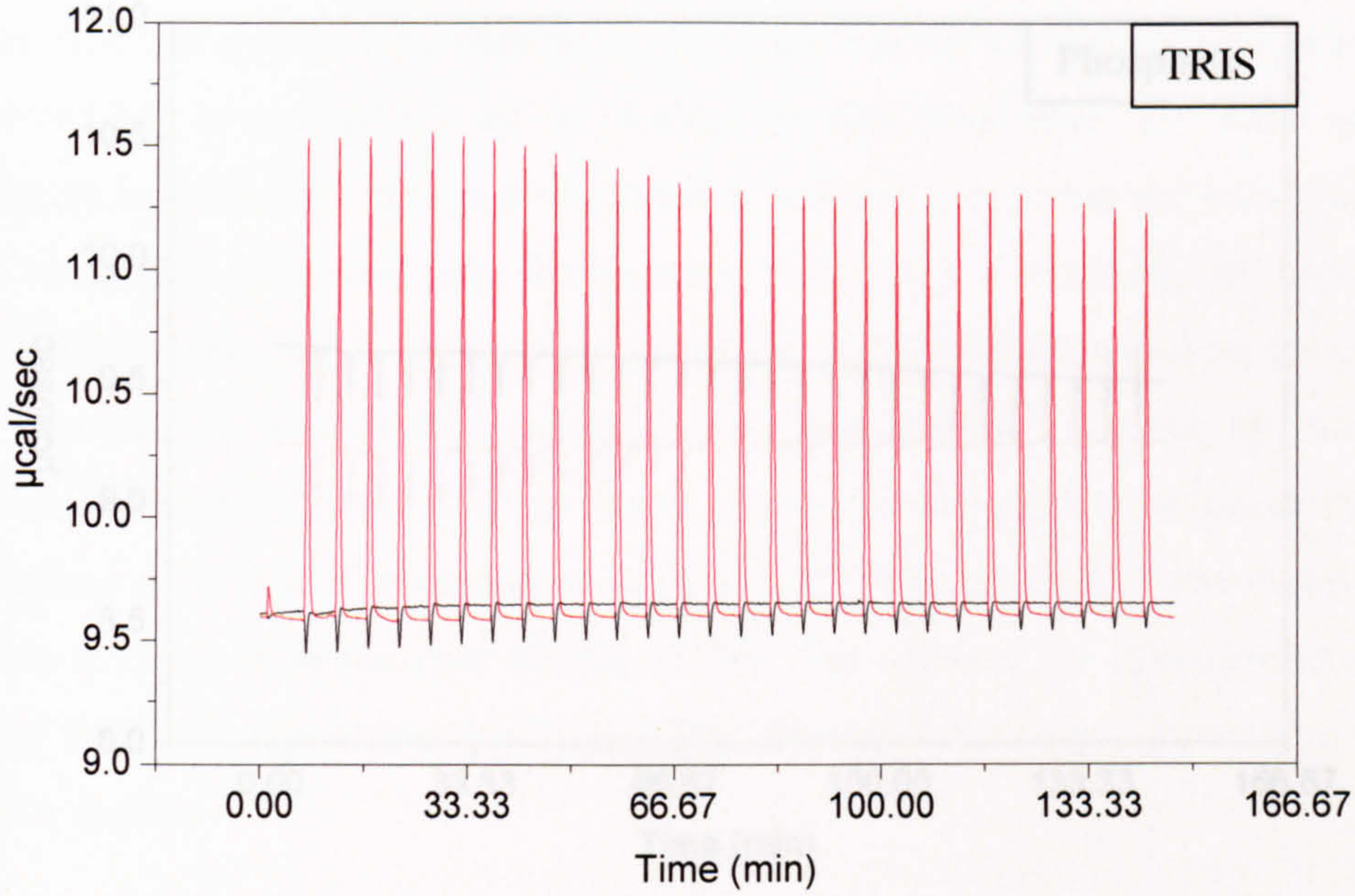
TRIS
12.0
11.5
11.0
10.5
10.0
9.5
9.0
µcal/sec
0.00
33.33
66.67
100.00
133.33
166.67
Time (min)

(ii)

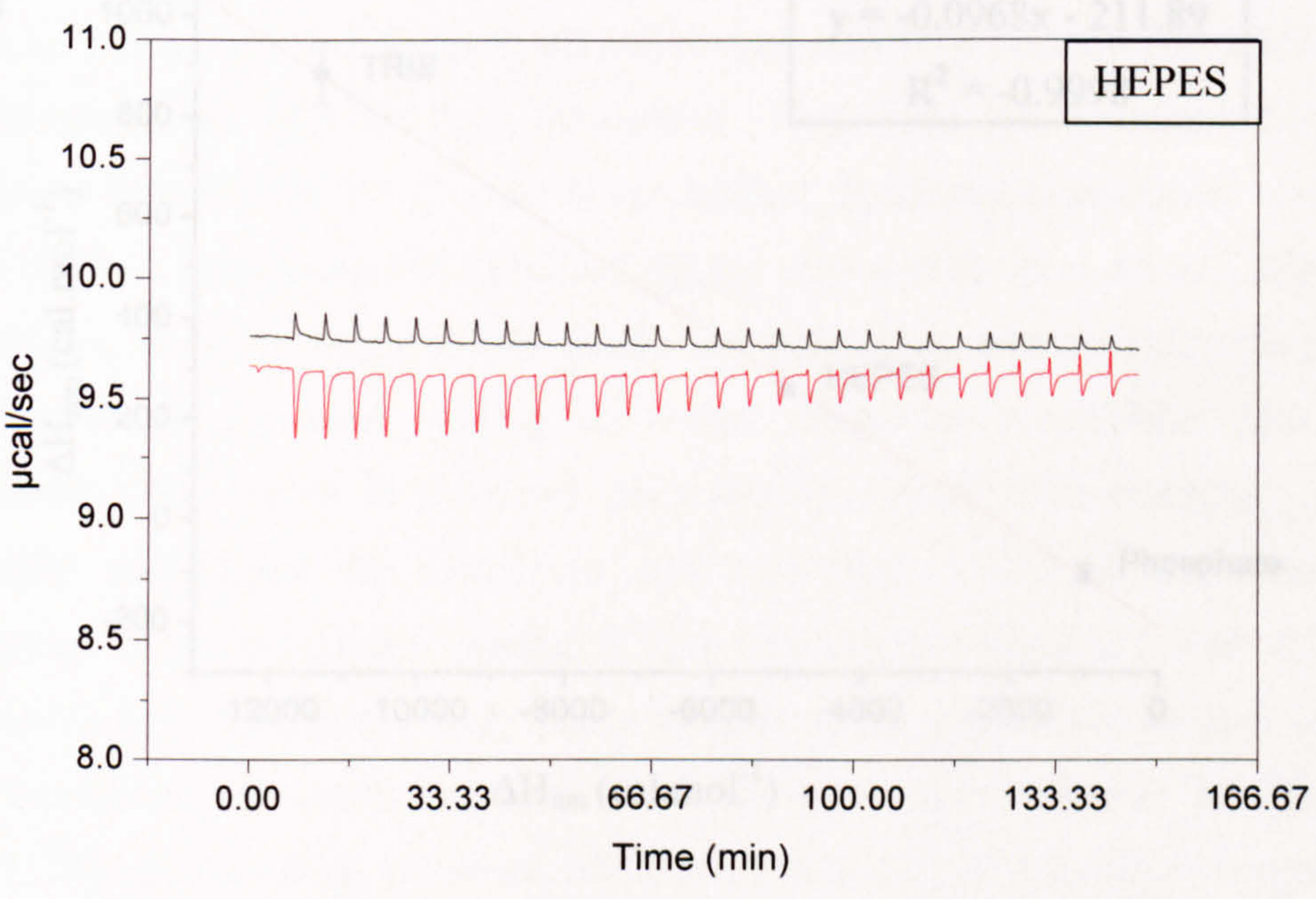
HEPES
11.0
10.5
10.0
9.5
9.0
8.5
8.0
µcal/sec
0.00
33.33
66.67
100.00
133.33
166.67
Time (min)

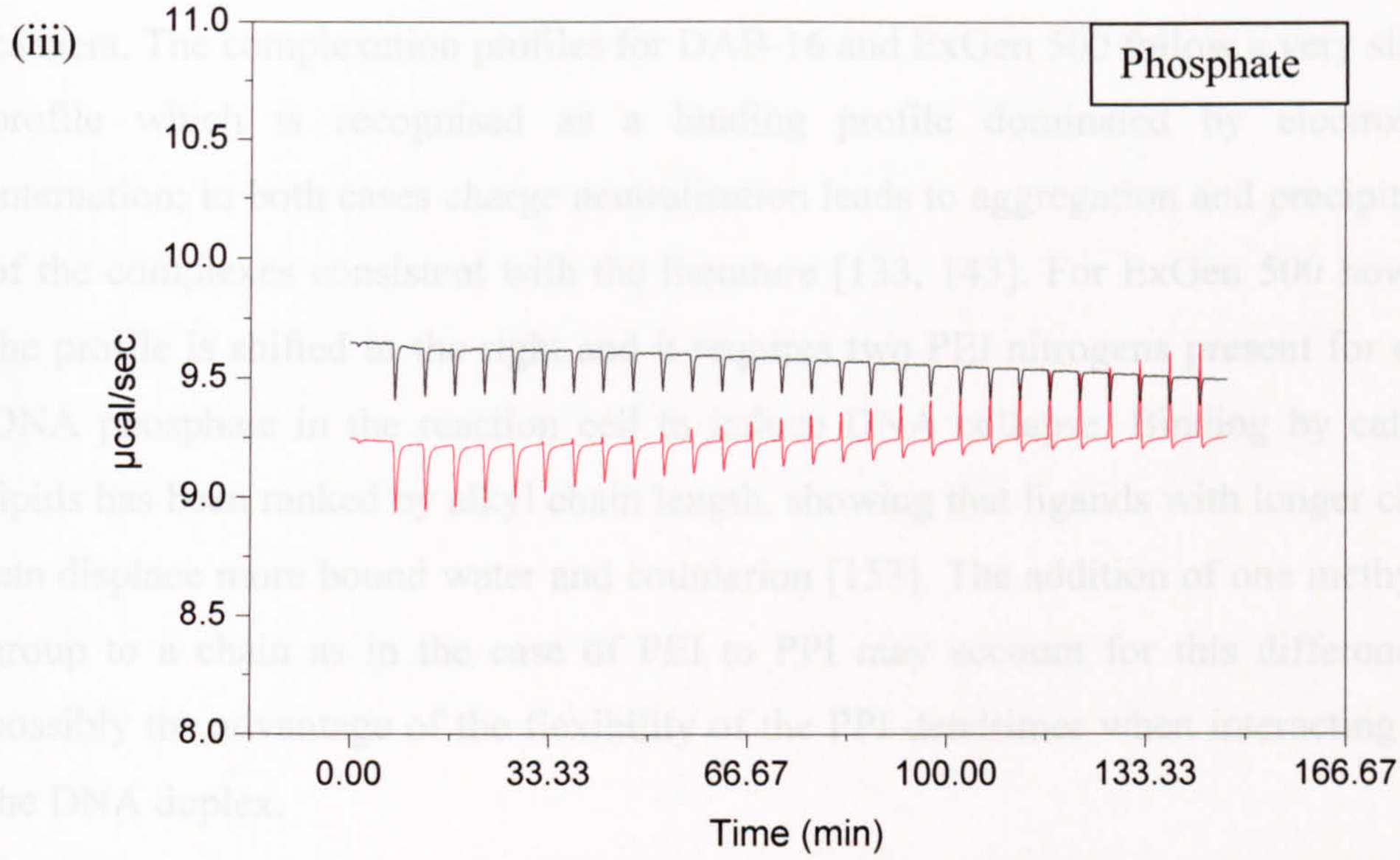

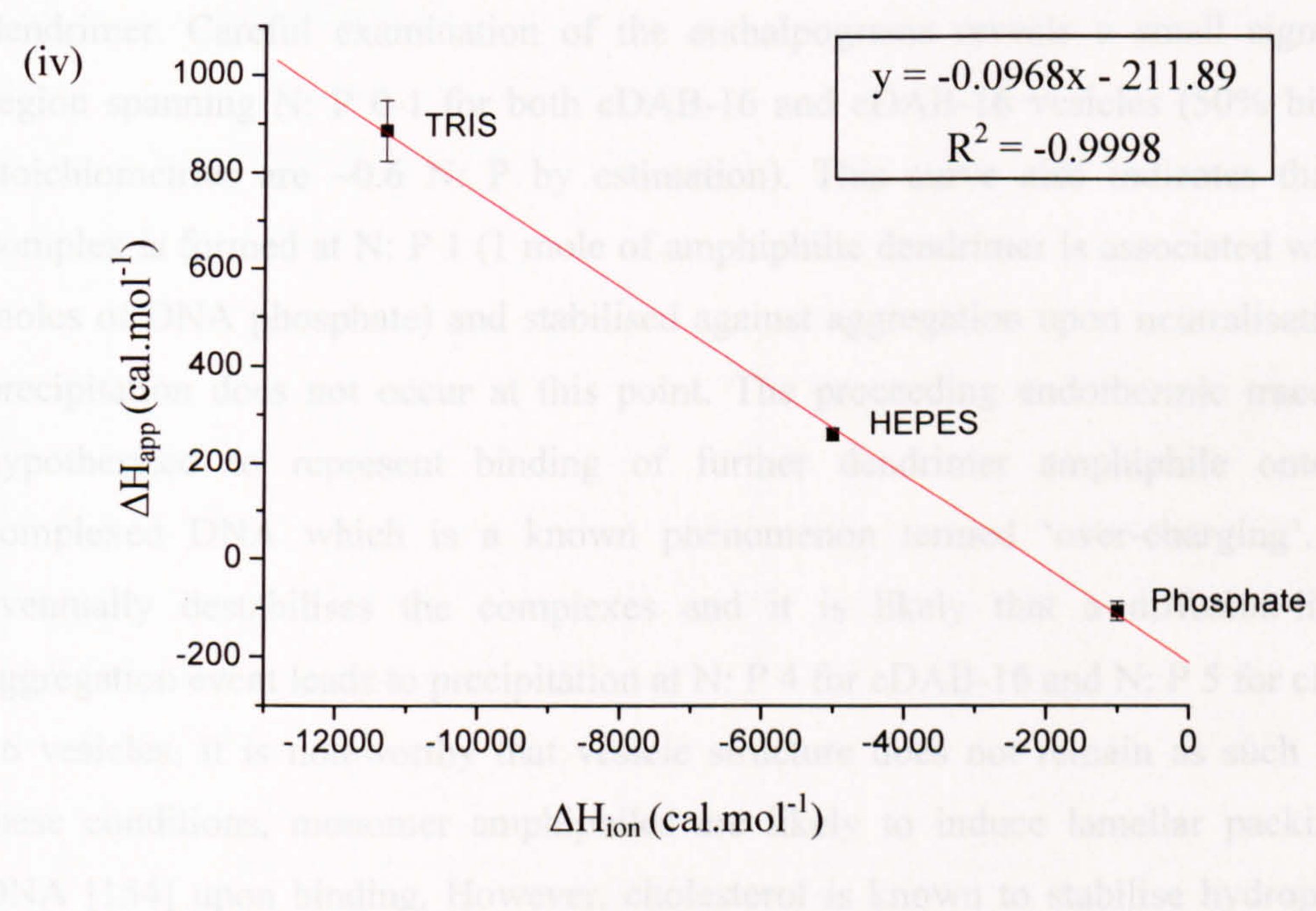

Figure 23 (i) DAB-16-Am injected into pDNA (6.67mM PPI: 1.5mM bps) at 25°C, pH 7.4, I = 10mM in (i) TRIS buffer (ii) HEPES buffer (iii) phosphate buffer (iv) ΔH_{ion} versus ΔH_{app} for DAB-16-Am

3.4.2.3. Overview of binding profiles

Using the enthalpograms from Figure 24 a comparison can be drawn between the carriers. The complexation profiles for DAB-16 and ExGen 500 follow a very similar profile which is recognised as a binding profile dominated by electrostatic interaction; in both cases charge neutralisation leads to aggregation and precipitation of the complexes consistent with the literature [133, 143]. For ExGen 500 however the profile is shifted to the right and it requires two PEI nitrogens present for every DNA phosphate in the reaction cell to induce DNA collapse. Binding by cationic lipids has been ranked by alkyl chain length, showing that ligands with longer chains can displace more bound water and counterion [153]. The addition of one methylene group to a chain as in the case of PEI to PPI may account for this difference or possibly the advantage of the flexibility of the PPI dendrimer when interacting with the DNA duplex.

To analyse the above curves reliance was placed on the change of sign of enthalpy and triggered precipitation events, but this cannot be assumed for amphiphilic dendrimer. Careful examination of the enthalpograms reveals a small sigmoidal region spanning N: P 0-1 for both cDAB-16 and cDAB-16 vesicles (50% binding stoichiometries are ~0.6 N: P by estimation). This curve also indicates that the complex is formed at N: P 1 (1 mole of amphiphilic dendrimer is associated with 30 moles of DNA phosphate) and stabilised against aggregation upon neutralisation as precipitation does not occur at this point. The proceeding endothermic traces are hypothesised to represent binding of further dendrimer amphiphile onto the complexed DNA which is a known phenomenon termed 'over-charging'. This eventually destabilises the complexes and it is likely that a diffusion-limited aggregation event leads to precipitation at N: P 4 for cDAB-16 and N: P 5 for cDAB-16 vesicles. It is noteworthy that vesicle structure does not remain as such under these conditions, monomer amphiphiles are likely to induce lamellar packing of DNA [154] upon binding. However, cholesterol is known to stabilise hydrophobic interactions which would account for the extended profile of the cDAB-16 vesicles formulation before aggregation.

(i) DAB-16-Am

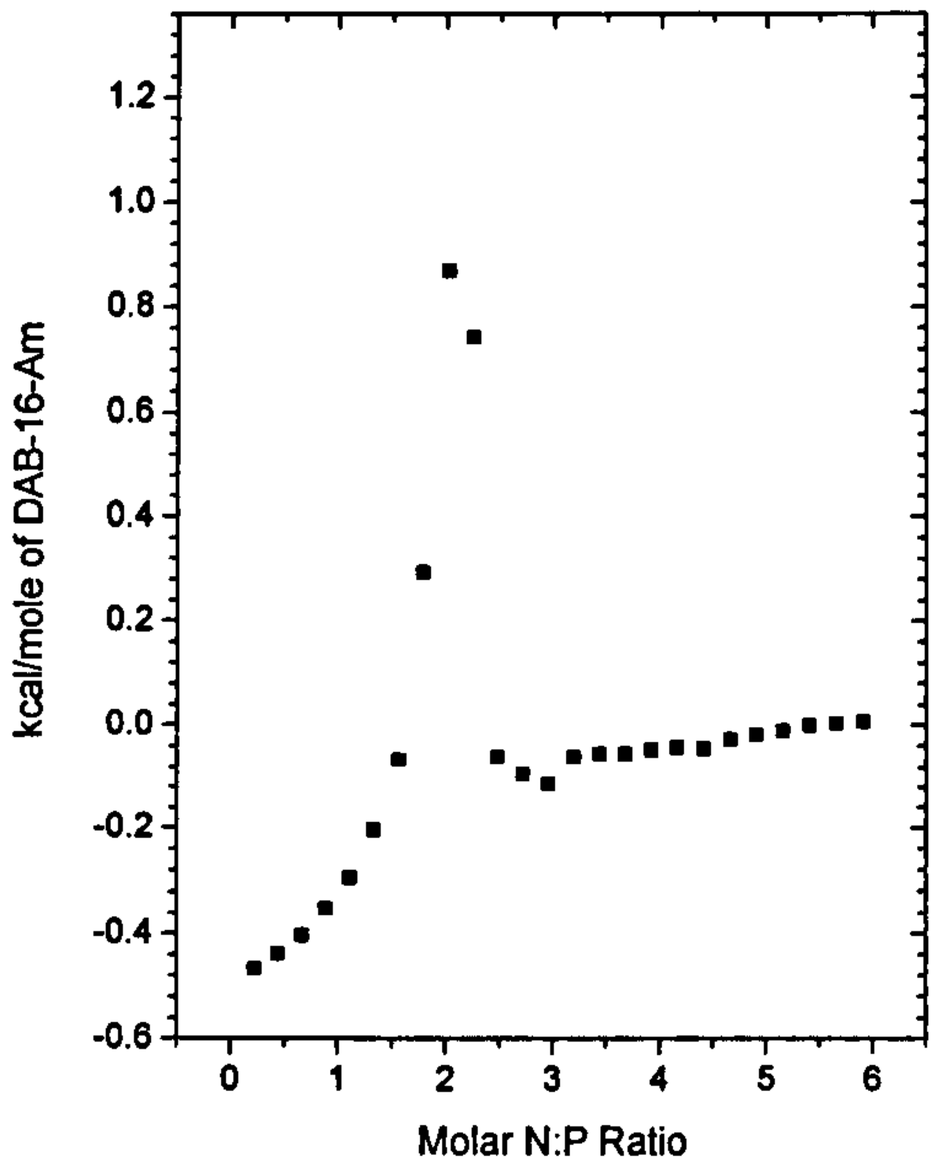

(ii) ExGen 500

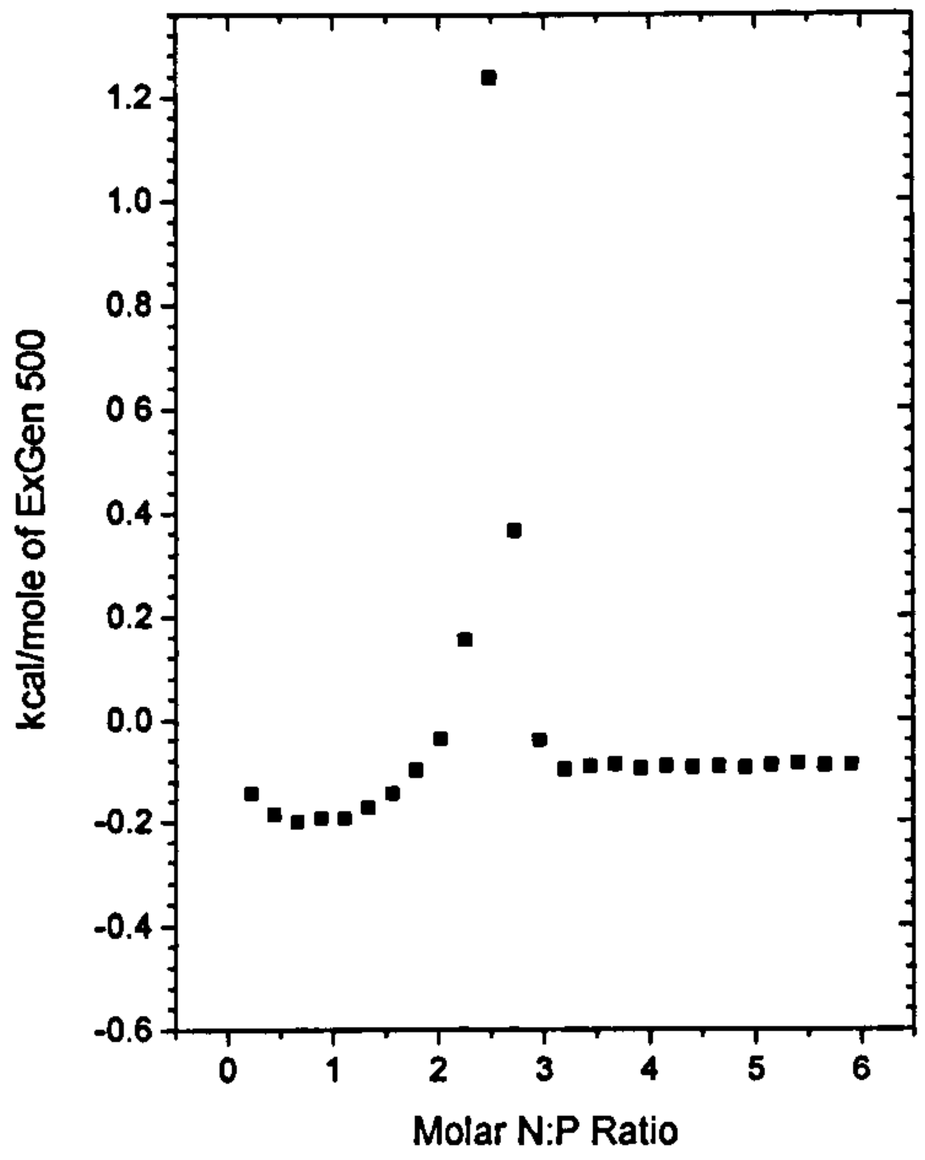

(iii) cDAB-16

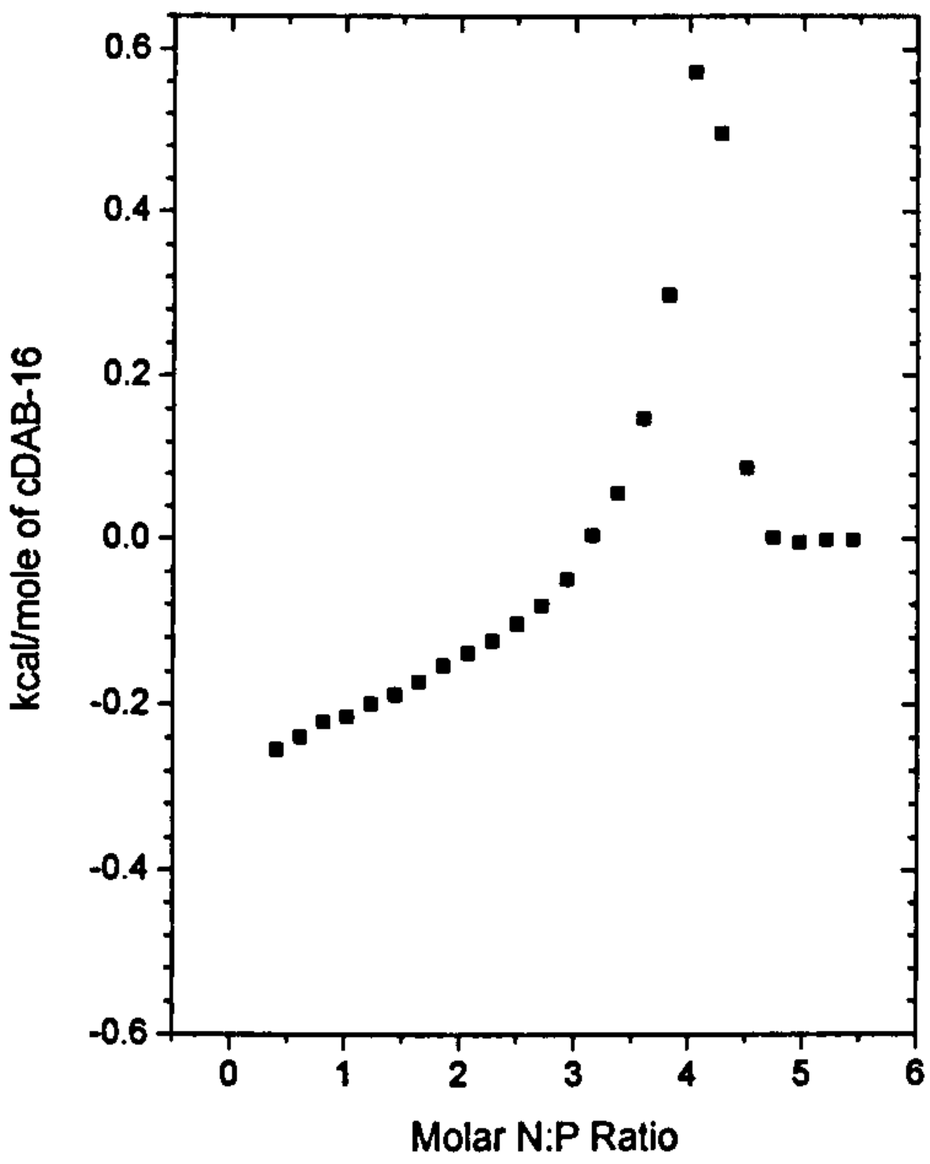

(iv) cDAB-16 vesicles

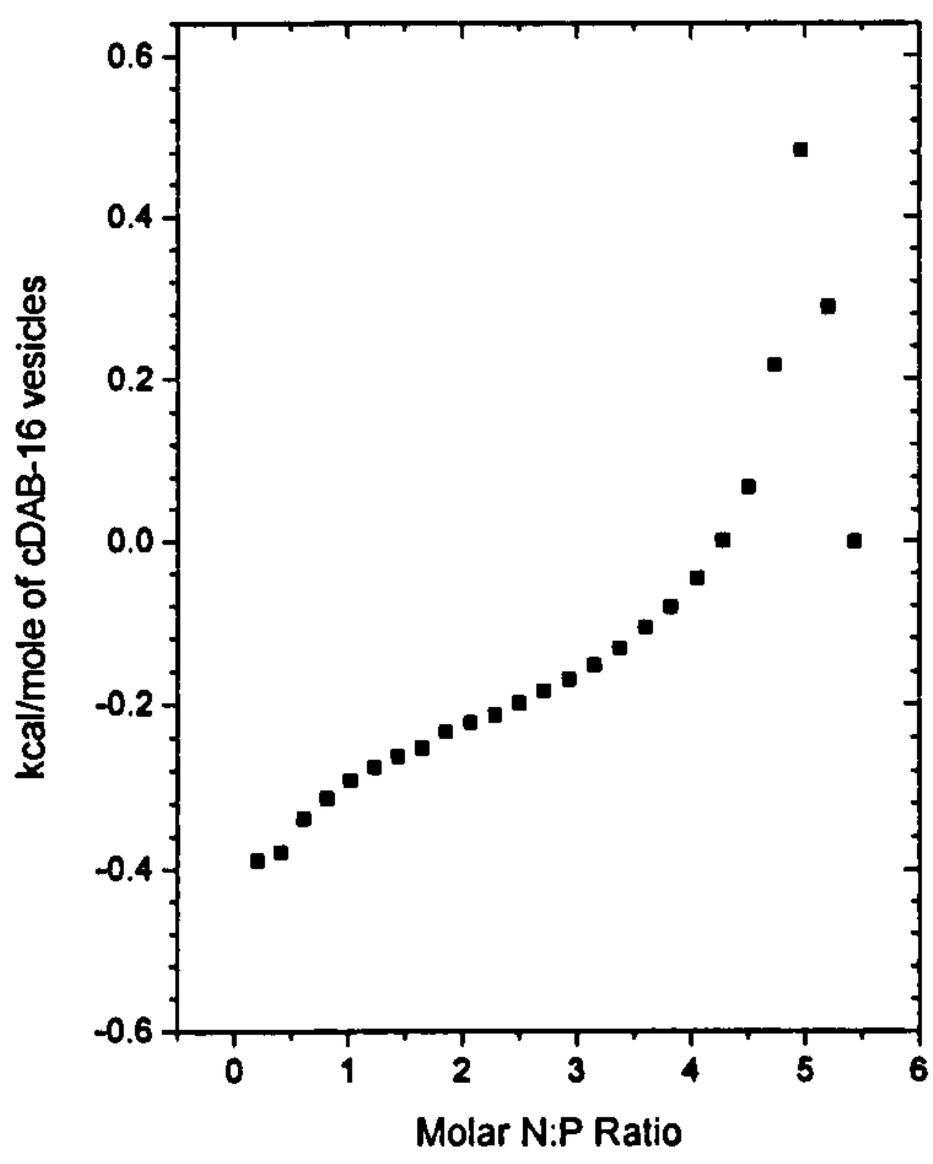

Figure 24 (i)-(iv) Enthalpograms for all carriers over N:P ratio 0-6 (y axis values adjusted for baseline); 8.16 mM PPI/PEI into 0.29 mM bps, pH 7.4, 25°C in phosphate buffer (I = 10mM)

3.4.2.4. Apparent binding enthalpies

Tabulated below (

Table 8) are the apparent pDNA binding enthalpies (ΔH_{app}) of the four carriers DAB-16-Am, cDAB-16, cDAB-16 vesicles and ExGen 500 in low ionic strength phosphate buffer. To obtain these values, each carrier is repeatedly injected into a stoichiometric excess of pDNA in solution. The mean of the first four injection heats (in cal) of a constant size minus the corresponding blank injection heats (carrier injected into buffer only) normalised with respect to the number of moles of carrier per injection is equal to ΔH_{app} ($cal.mol^{-1}$).

The measured enthalpies are small in magnitude indicating that, under these experimental conditions, binding of each carrier to pDNA is virtually enthalpically neutral as has already been seen for DAB-16-Am in section 3.4.2.2. This is consistent with a binding process driven by entropic gain to the system. There is however a small favourable increase in the DNA binding enthalpy of DAB-16 as a result of hydrophobic derivatisation ($p = <0.0001$), but no significant difference in binding enthalpy between the cDAB-16 and cDAB-16 vesicles formulations ($p = 0.374$). This increase in enthalpy release may arise from improved ionic interaction between the amphiphile and the DNA surface as a result of concurrent amphiphile aggregation processes.

ExGen 500 binds DNA with the most negative apparent enthalpy. Linear PEI has an intrinsic negative binding enthalpy [133], as has been determined for DAB-16-Am, but also receives a negative enthalpic contribution from protonation effects. This may account for the more favourable apparent enthalpy when compared with DAB-16-Am, which from the profile in Figure 24 (i) appears to bind more tightly. These binding characteristics may impact on DNA release from complexes within biological systems.

Carrier	ΔH_{app} (cal.mol^{-1}) in PO_4^{2-} buffer
DAB-16-Am	-107.3 ± 19.5
cDAB-16	-282.9 ± 58.7
cDAB-16 vesicles	-249.6 ± 64.6
ExGen 500	-453.2 ± 86.3

Table 8 Measured ΔH_{app} for carrier interaction with pDNA (verified independently). Carriers injected into pDNA (6.67 mM PPI/PEI into 1.5mM bps) at 25°C in phosphate buffer (pH 7.4, I = 10mM) (raw data not shown).

3.4.3. Ethidium bromide exclusion assay

As previously mentioned, Eth Br fluoresces upon insertion into the DNA duplex, and this value is normalised to RU = 1; exclusion of Eth Br is deemed to be complete at RU <0.1. The fluorescent yields of Eth Br in the presence of DAB-16-Am (Figure 25), cDAB-16 (Figure 26) and cDAB-16 vesicles (Figure 27) for a period of 168 h are shown. All carriers were able to completely exclude Eth Br and complexes remained stable in solution during this period. This suggests that these agents could be used over a longer time frame for transfection study. A transfection study over five days with DAB-16-Am showed sustained plasmid DNA expression by cells initially incubated with these complexes [143].

These results also suggest that following initial DNA binding by the dendrimers a further slow equilibrium rearrangement takes place, potentially to involve tertiary amines in a more stable DNA complex. At 168 h DAB-16-Am (Figure 25) can completely exclude Eth Br at 0.5 N: P (compared with a value of 1.5-2 N: P after 0.5 h incubation). cDAB-16 formulations (Figure 26 and Figure 27) achieve 0.25 N: P after 168 h (in contrast with 1 N: P after 0.5 h incubation). At this final time point there is little difference between the binding profiles of the parent and amphiphilic dendrimer; it may be that a minimum complex structure has been reached.

A value for 1.5 N:P was measured for DAB-16-Am after 0.5 h incubation at pH 7.4 (not shown graphically) and confirmed to be near the point of complete Eth Br exclusion for DAB-16-Am (1.5 N: P 90.91 ± 1.07% exclusion; 2 N: P 96.89 ± 0.23% exclusion) concurring with literature values [59].

Figure 28 summarises the Eth Br exclusion efficiencies of the various carriers after 0.5 h incubation with DNA, allowing the relative DNA binding efficiencies of each to be ranked as follows: cDAB-16 (pH 7) = cDAB-16 vesicles (pH 7) > DAB-16-Am (pH 3) = ExGen 500 (pH 3) > DAB-16-Am (pH 7) > ExGen 500 (pH 7).

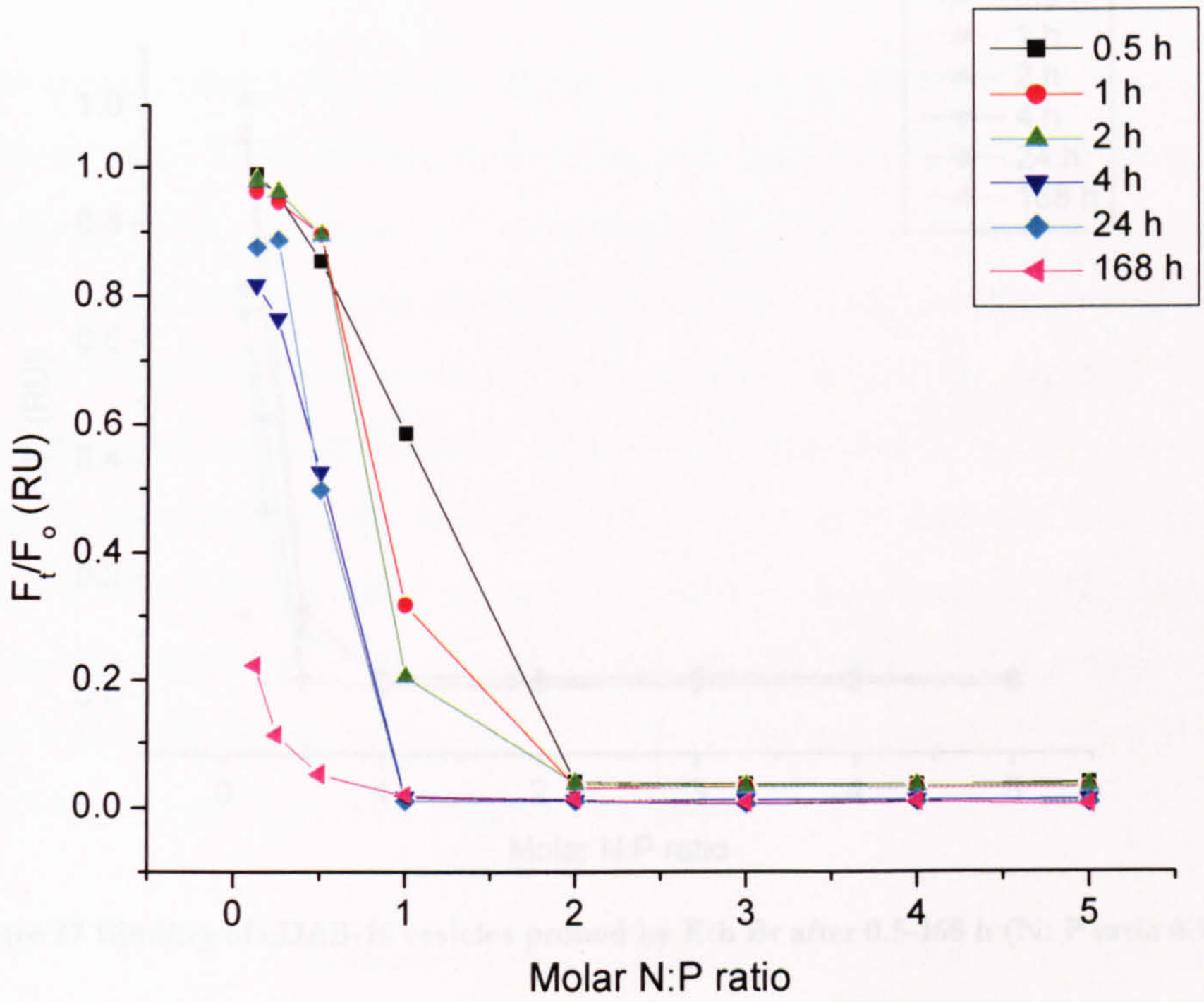

Figure 25 Binding of DAB-16-Am to DNA probed by Eth Br after 0.5-168 h (N: P ratio 0.125-5)

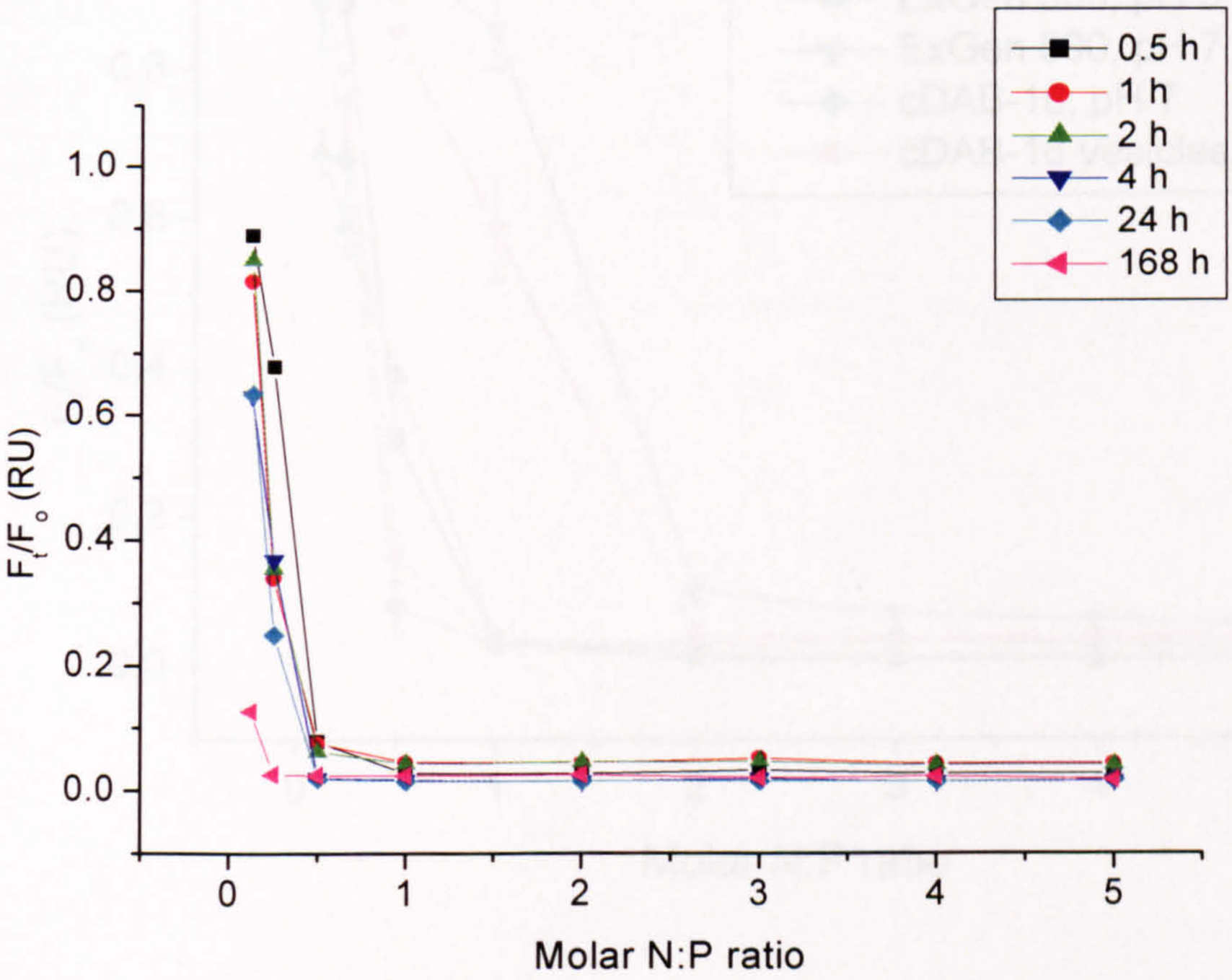

Figure 26 Binding of cDAB-16 to DNA probed by Eth Br after 0.5-168 h (N: P ratio 0.125-5)

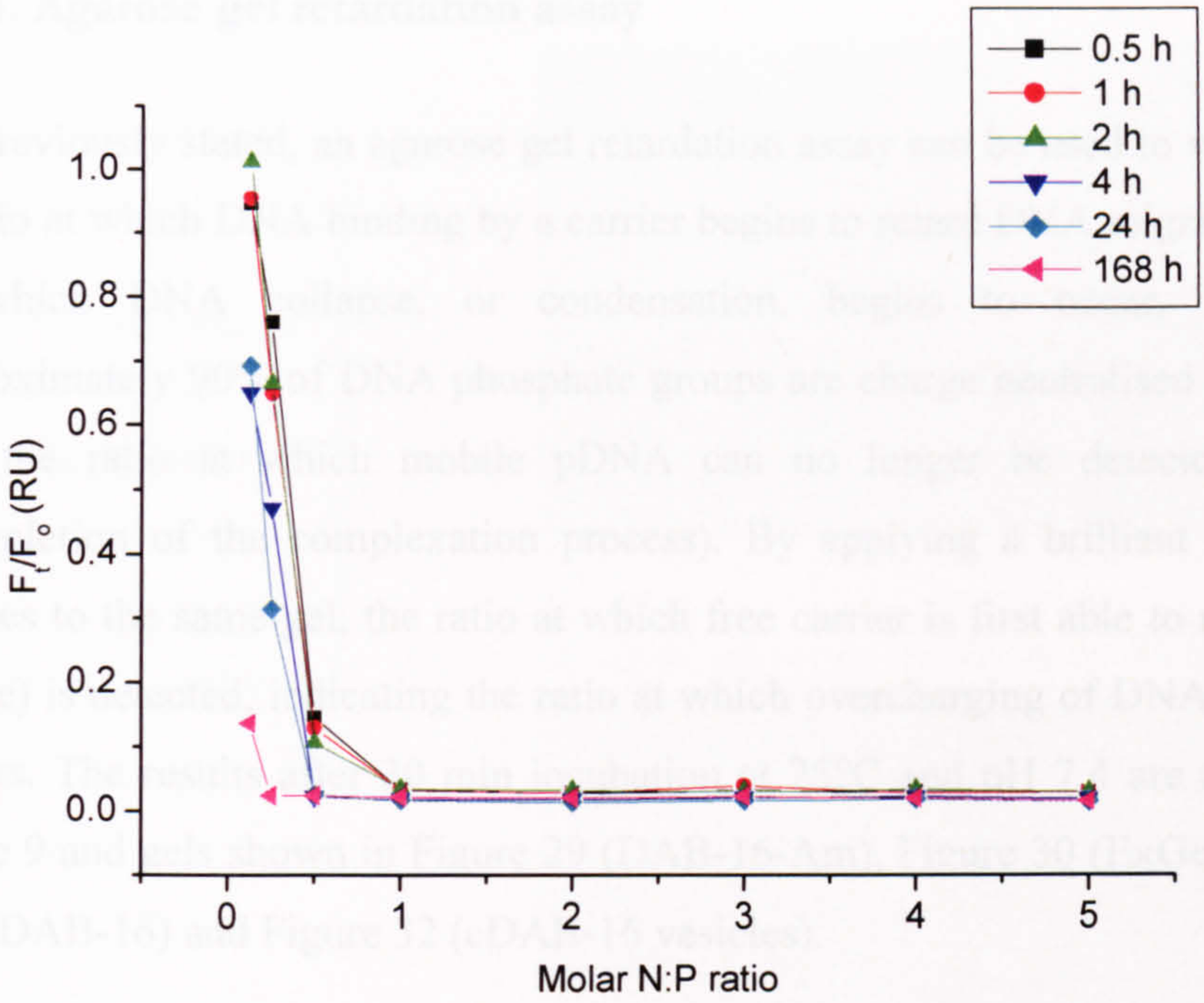

Figure 27 Binding of cDAB-16 vesicles probed by Eth Br after 0.5-168 h (N: P ratio 0.125-5)

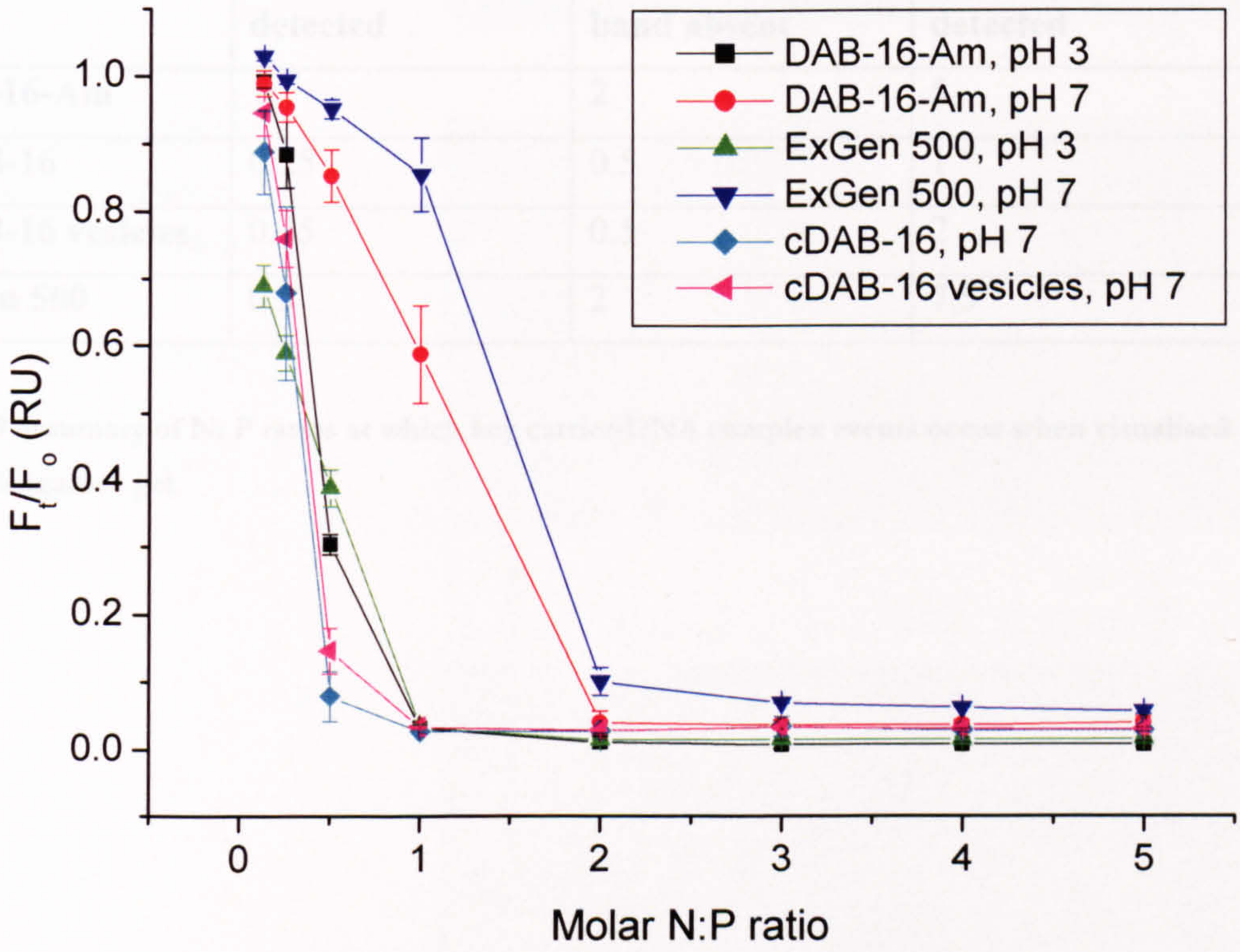

Figure 28 Mean reduced fluorescence of Eth Br in DNA solution after incubation with carriers for 0.5 h (N: P ratio 0.125-5) (n= 3)

3.4.4. Agarose gel retardation assay

As previously stated, an agarose gel retardation assay can be used to visualise the N: P ratio at which DNA binding by a carrier begins to retard DNA migration (the point at which DNA collapse, or condensation, begins to occur, usually when approximately 90% of DNA phosphate groups are charge neutralised by the carrier) and the ratio at which mobile pDNA can no longer be detected on the gel (completion of the complexation process). By applying a brilliant blue stain for amines to the same gel, the ratio at which free carrier is first able to migrate (to the anode) is detected, indicating the ratio at which overcharging of DNA by the carrier occurs. The results after 30 min incubation at 25°C and pH 7.4 are summarised in Table 9 and gels shown in Figure 29 (DAB-16-Am), Figure 30 (ExGen 500), Figure 31 (cDAB-16) and Figure 32 (cDAB-16 vesicles).

	Retarded complex detected	**Migrating pDNA band absent**	**Excess carrier detected**
DAB-16-Am	1	2	5
cDAB-16	0.25	0.5	1
cDAB-16 vesicles	0.25	0.5	2
ExGen 500	0.5	2	7.5

Table 9 Summary of N: P ratios at which key carrier-DNA complex events occur when visualised on a 1% agarose gel.

Figure 29 DAB-16-Am.
Upper gel – Coomassie stain. Lower gel – Eth Br stain.
HYP I = Hyperladder I.
N: P ratio = 0.25-60
Pol = 1mg.mL^{-1} polymer alone

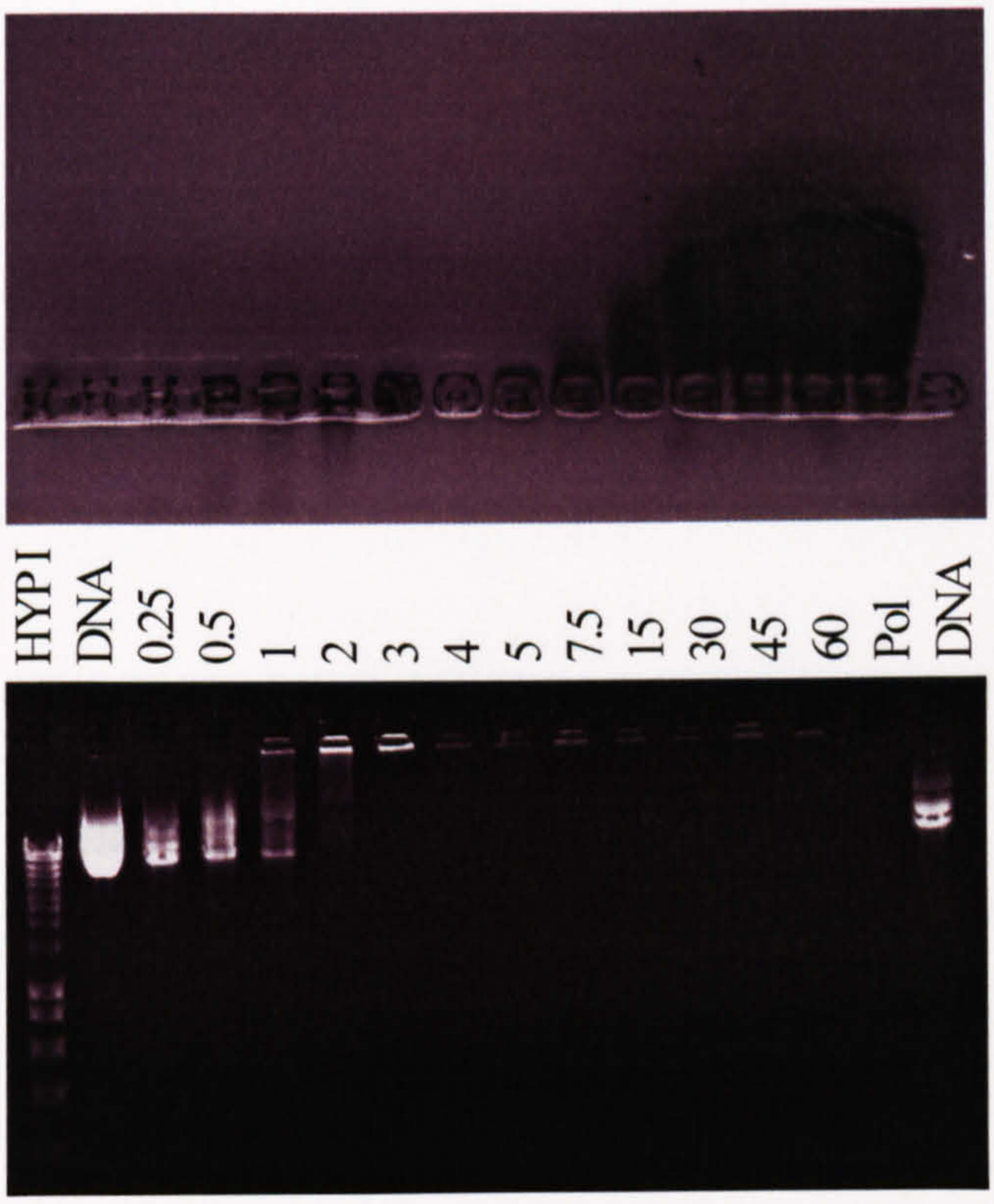

Figure 30 ExGen 500.
Upper gel – Coomassie stain. Lower gel – Eth Br stain.
HYP I = Hyperladder I.
N: P ratio = 0.25-60
Pol = 1mg.mL^{-1} polymer alone

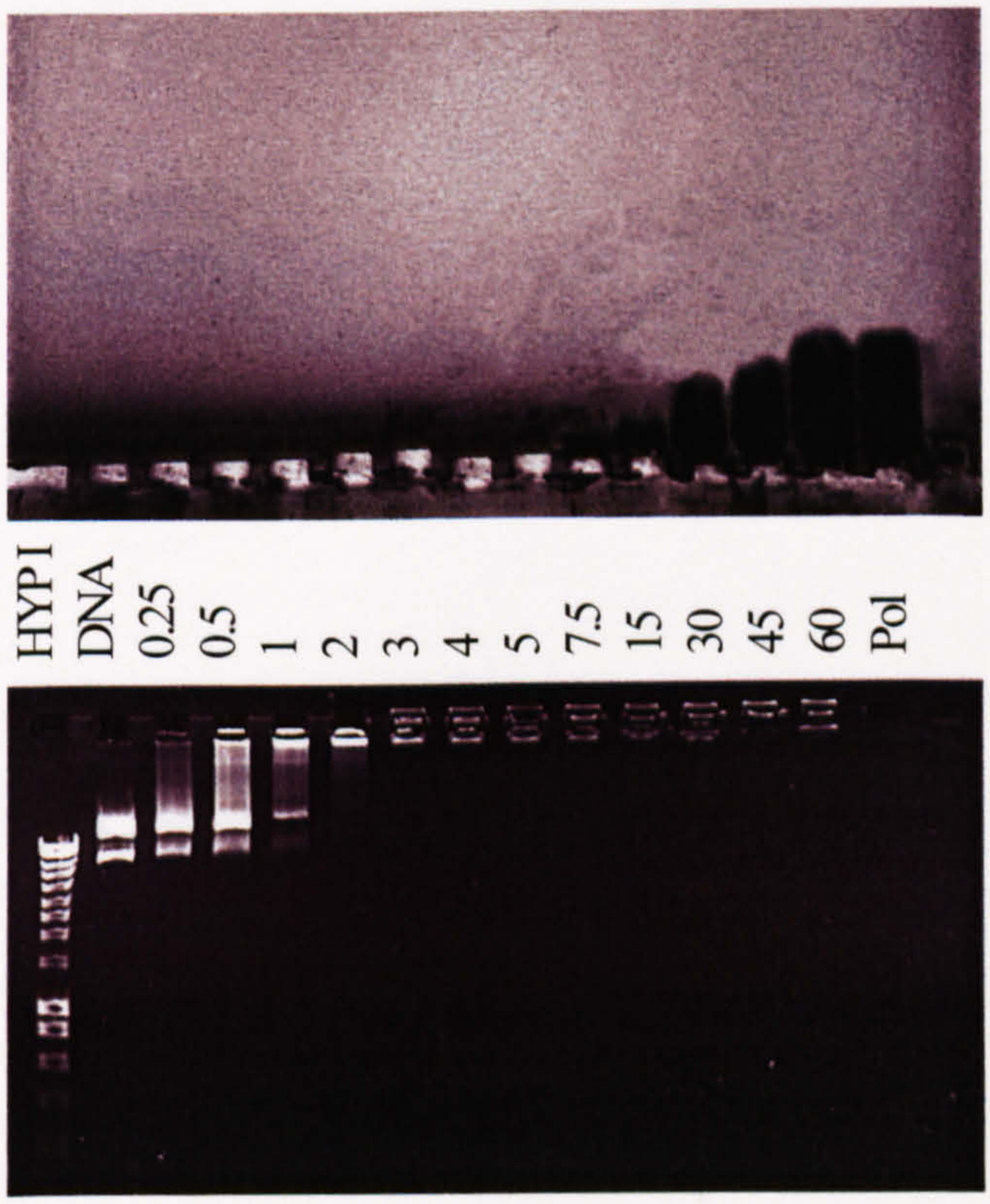

Figure 31 cDAB-16.
Upper gel – Coomassie stain. Lower gel – Eth Br stain.
HYP I = Hyperladder I.
N: P ratio = 0.25-60
Pol = 1mg.mL^{-1} polymer alone

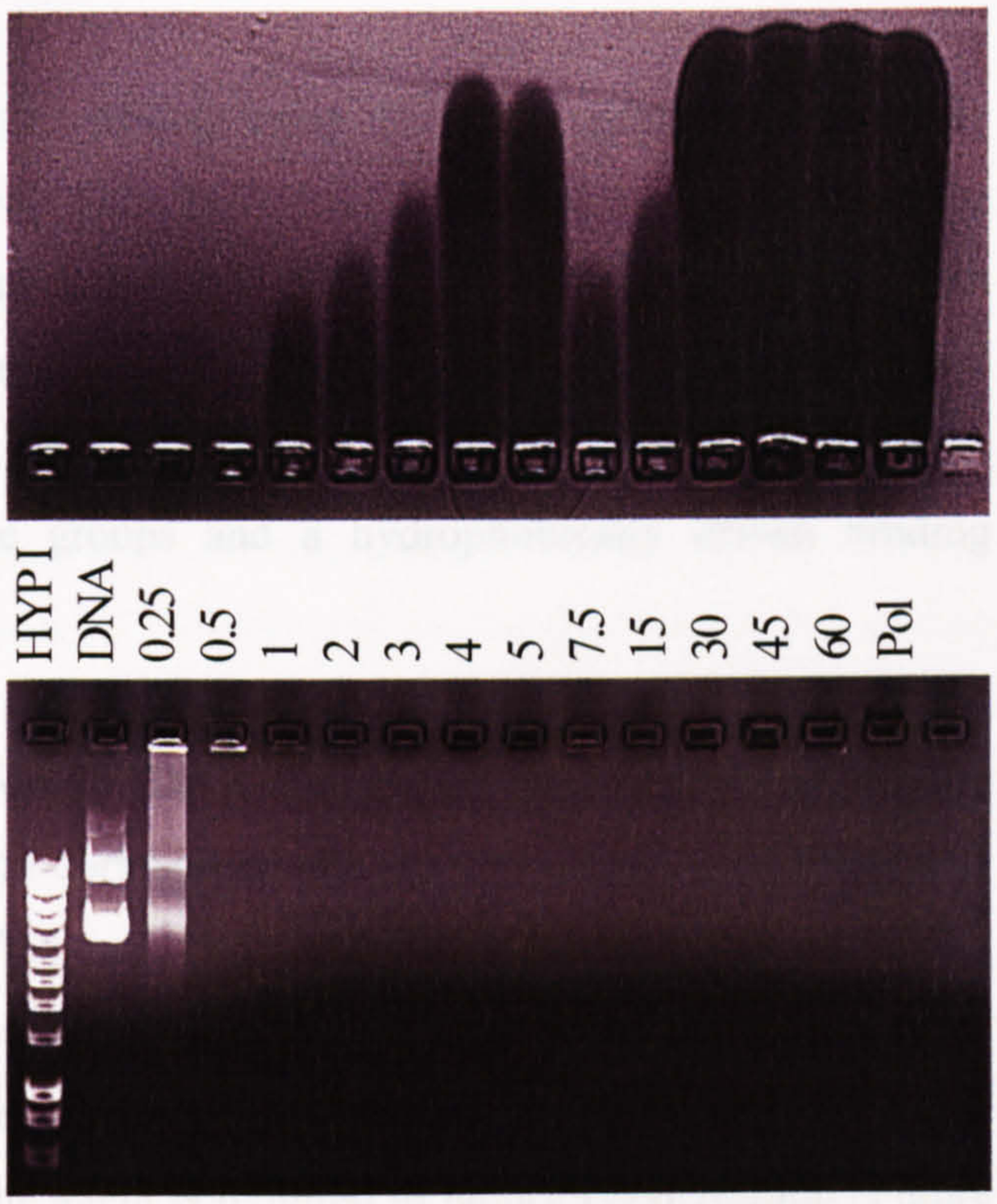

Figure 32 cDAB-16 vesicles. Upper gel – Coomassie stain. Lower gel – Eth Br stain.
HYP I = Hyperladder I.
N:P ratio = 0.25-60
Pol = 1mg.mL^{-1} polymer alone

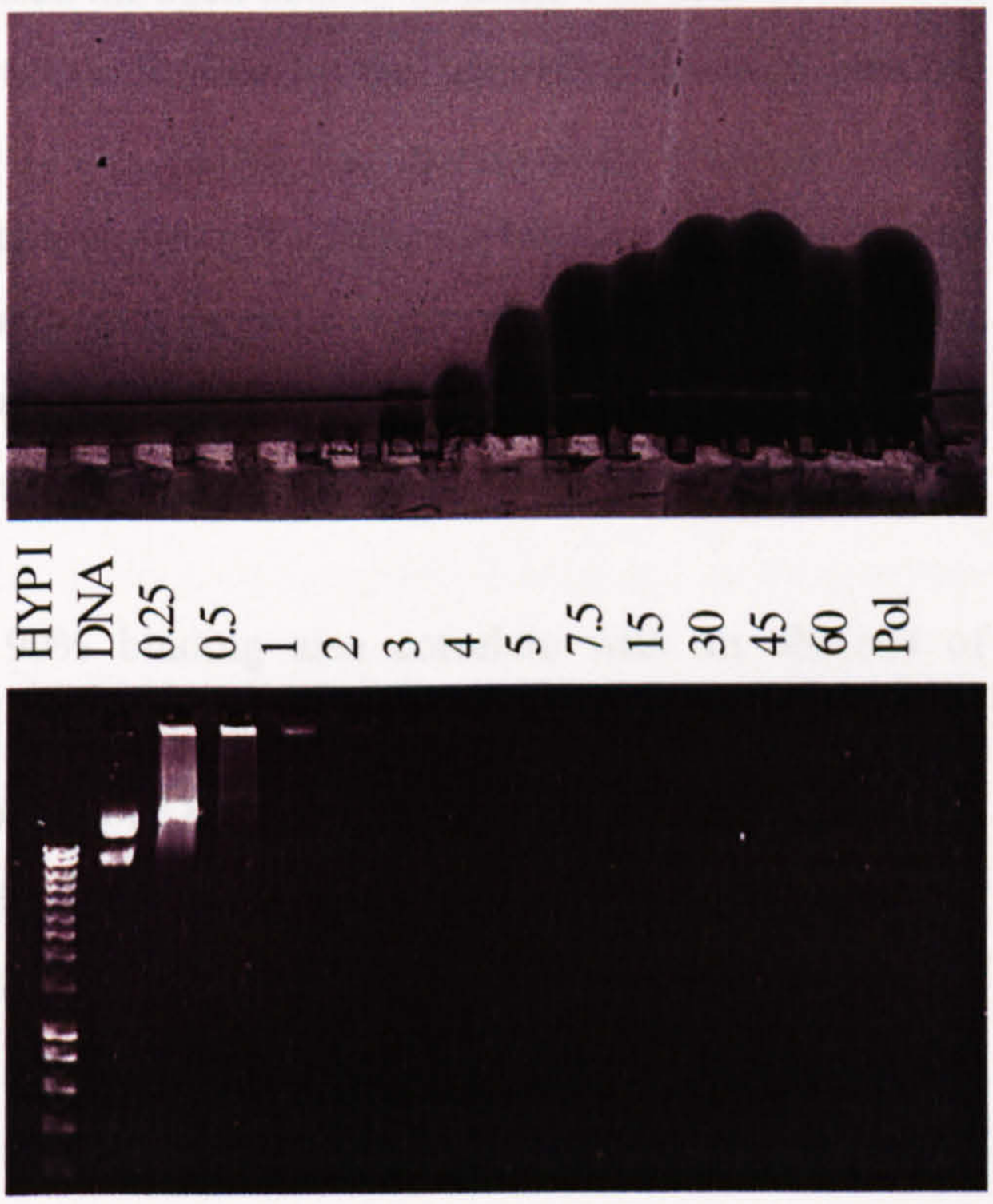

3.5. Discussion and conclusions

After examination of linked proton effects using ITC it is concluded that only dendrimer primary amines are involved in the initial DNA binding reaction under the experimental conditions (I = 10mM, pH 7.4, 25°C) and that this process has an intrinsically small favourable enthalpy of -211.89 cal.mol^{-1} (Figure 23 iv). This result is consistent with electrostatic (ionic) interaction between charged dendrimer ammonium and DNA phosphate groups and a hydrophobically driven binding process [123, 133].

ITC analysis of DNA aggregation by DAB-16-Am and the control ExGen 500 reveals threshold behaviours which correspond with ~90% exclusion of Eth Br at 2 N: P for ExGen 500 (89.94 ± 2.07%) and 1.5 N: P for DAB-16-Am (90.91 ± 1.07%). This result concurs with the previously mentioned observations of Wilson and Bloomfield [115]. DAB-16-Am binds DNA more efficiently than linear PEI under these conditions as less complexing agent is required to induce condensation (Figure 24). It is speculated that the increased nitrogen density of linear PEI does not pose an advantage at this stage of the process, limited by the separation distance between DNA phosphate groups (~3.3Å) [113]. Rather the increased hydrophobic length provided by an additional methylene group in the PPI unit may increase the amount of bound water that is displaced upon unit binding, adding favourable entropy to the system [153]. DAB-16-Am is also an inherently flexible molecule under these conditions [70] which would aid in overcoming steric hindrances to binding.

These values of approximately 90% binding also correlate with an absence of migrating plasmid DNA band on agarose gels (Figure 29 and Figure 30). However, these are not the final molar amounts of DNA phosphate associated with DAB-16-Am and ExGen 500, which is actually 3 N: P (Figure 24). Therefore, DAB-16-Am dendrimer (1 mol) is associated with 10 mol of DNA phosphate at the completion of the complexation reaction. This is not predicted by Eth Br binding assay as binding is complete soon after condensation is initiated, but this N: P ratio does concur with a

complete lack of DNA mobility on agarose gels for DAB-16-Am and ExGen 500 (Table 9).

At pH 3, the DAB-16-Am-DNA condensation process was initiated at 1 N: P and complete at 2 N: P (at the end of complexation, 15 mol of phosphate are bound by 1 mol of dendrimer) on the ITC enthalpogram (Figure 22 i). This was confirmed using Eth Br as the dye was completely excluded from the DNA duplex at 1 N: P (Figure 28). Therefore, DAB-16-Am binds DNA more efficiently at a lower pH. It is known that PPI dendrimers swell into extended conformations upon protonation of primary and tertiary amine groups [70]. It is plausible that inner tertiary amines now have improved access to the DNA backbone. Permanent ionisation of amine groups via methyl quaternisation has been shown to be detrimental to binding of DNA by DAB-16-Am; however this is more likely to be as a result of steric hindrance by the bulky methyl groups [74]. ExGen 500 also produces a similar Eth Br exclusion profile at pH 3 (Figure 28). DAB-16-Am-DNA complexes could benefit from formation at an acidic pH prior to use in other applications; ExGen 500 is already supplied for commercial use in acidic solution.

Examination of the DAB-16-Am-DNA system in various pH conditions and buffers in this work leads to the conclusion that if generations of PPI dendrimer are to be examined in more detail using ITC, experiments should either be undertaken in a buffer with a large ionisation enthalpy (e.g. TRIS, which buffers at physiological pH and has an intrinsic buffer ionisation enthalpy of 11.3 $Kcal.mol^{-1}$) or at a low pH (e.g. pH 3, buffered by citrate which has a ΔH_{ion} contribution of zero and multiple acidic pKa values) to produce binding enthalpies which are several $Kcal.mol^{-1}$ in magnitude. This system cannot be assessed under physiological salt conditions using ITC as the ionic species further attenuate charge persistence lengths, reducing the magnitude of already small electrostatic interactions [136]. Stopped-flow kinetic studies (utilising extrinsic fluorescence or circular dichromism) [155] do not require attainment of binding equilibrium and could also be conducted in conjunction with ITC. For example, simultaneous injection of fluorescently labelled DNA and

polymer solution into a fluorimeter cell allows time course monitoring of the initial DNA binding event at millisecond intervals.

cDAB-16 and cDAB-16 vesicle binding events occur rapidly upon introduction into the microcalorimeter reaction cell containing DNA solution (Figure 24 iii & iv). Eth Br exclusion values at 0.5 N: P of 92.08 ± 3.69 % for cDAB-16 and 85.40 ± 3.35 % for cDAB-16 vesicles (Figure 28) are consistent with the estimated stoichiometries from these enthalpograms and on agarose gels (Figure 31 & Figure 32) both species have completely retarded the mobile plasmid DNA band at 0.5 N: P. Using all the available techniques it can be concluded that the complexation process is complete for both species at 1 N: P (30 mol of phosphate are bound by 1 mol of amphiphilic dendrimer). Dendrimer amphiphile formulations containing cholesterol are likely to form a locally ordered phase such as stacks of lipid bilayer lamellae [154]. The complexes remain soluble at neutrality because of these stabilising hydrophobic interactions [85].

Examination of these systems over a longer time period reveals that at least two stages occur after mixing; first, a fast binding event and structural rearrangement, followed by a slow equilibrium rearrangement phase. After one week of incubation at 25°C cDAB-16 formulations are able to completely exclude Eth Br at approximately 0.25 N: P (Figure 26 & Figure 27) and DAB-16-Am at approximately 0.5 N: P (Figure 25). It is possible that these represent attainment of common minimum structures and that the favourable hydrophobic interactions that arise between the amphiphilic dendrimer derivatives merely served to accelerate the condensation process. It is also hypothesised that the slow equilibrium rearrangement allows tertiary amines to approach DNA phosphate groups and extract buffer protons for binding. The fact that ready protonation of tertiary amines of DAB-16-Am is likely to be responsible for its improved pDNA binding efficiency in a low pH environment supports this hypothesis.

Exploitation of this feature in biological milieu may be difficult however as other influences such as increased ionic strength and enzymatic breakdown will affect this

equilibrium state. These ideas will be addressed, along with the phenomenon of DNA overcharging, in Chapter 4.

In conclusion, the three techniques used in this chapter to study the DNA complexing agents DAB-16-Am, cDAB-16, cDAB-16 vesicles and ExGen 500 (linear PEI) agree closely. The most efficient DNA complexation agents were the cDAB-16 formulations, which tripled the binding capacity of the parent dendrimer. This supports the hypothesis that the presence of hydrophobic alkyl chains would improve the packaging of DNA by the dendrimer.

4. Physicochemical Characterisation of Complexes

4.1. Introduction

Definitive physicochemical parameters of complexed DNA applicable to widely differing carrier systems, which in turn correlate with biological effects such as *in vitro* cell transfection efficiencies, remain elusive [156]. To date, the physical and chemical properties of complexed nucleic acids have been extensively studied in order to build up structure-activity relationships (SAR). Properties that have been correlated with biological activity include: polymer chemical structure [51, 73, 74, 157-160], hydrophobic content [42, 72, 78, 81-83, 161-164] and molecular weight [59, 79, 123, 165, 166]; complex charge ratio [167-170], size [59, 171-174] and internal structure [175-179]; plasmid DNA size [180], DNA tertiary structure [168, 181-185] and solubility [167]; free polymer concentration [167, 186], presence of adjuncts [15, 50, 187, 188], conditions of manufacture [189] and resistance to degradation [190].

It has been shown in Chapter 3 that cDAB-16 formulations bind plasmid DNA more efficiently than the parent dendrimer under the conditions examined; here the physicochemical properties of the resulting dendrimer-DNA complexes at various N: P ratios will be explored. The parameters to be examined are hydrodynamic diameter, surface zeta potential and DNA structural features (using atomic force microscopy). Improvements are sought in the stability of the DAB-16-Am-DNA complexes at close to isoelectric ratios and the tendency to proximity aggregate at concentrations commonly required for *in vivo* experimentation; therefore carrier and concentration dependent solubility of complexed DNA will be assessed. The impact of the pH environment on complex size will be considered along with dilution effects, ionic environment and the presence of serum. Further to this, biological challenges that can reduce transfection efficiencies will be mimicked using heparin, serum and nuclease.

4.1.1. PCS

The size of dendrimer-DNA complexes is an important characteristic and has differing implications for *in vitro* and *in vivo* delivery as for the latter, successful injection (i.e. particles reaching the target site) relies on particulates less than 1 micron in size. The background to the PCS technique was elaborated in Section 2.1.6.

4.1.2. Zeta potential

For the purposes of non-viral gene delivery, complexes usually carry a net cationic charge [156] which facilitates cell uptake through interaction with negatively charged membrane components. Surface charge arises principally from the ionisation of chemical groups and the adsorption of counter ions producing an electrical double layer around the particle. The liquid layer that surrounds the particle can be considered to exist in two parts; an inner region which contains ions strongly bound to the surface (the stern layer) and a diffuse, outer region in which ion distribution is determined by electrostatic effects and Brownian motion [104]. The stern layer moves through the solution with the particle as one unit and the boundary of this layer is termed the 'surface of shear' (see Figure 33). The potential that exists at this distance is known as the zeta (ζ) potential, a product of the true particle charge. The stability of colloidal dispersions is strongly influenced by these charges, opposing long-range, attractive van der Waals forces, the principle cause of aggregation [104].

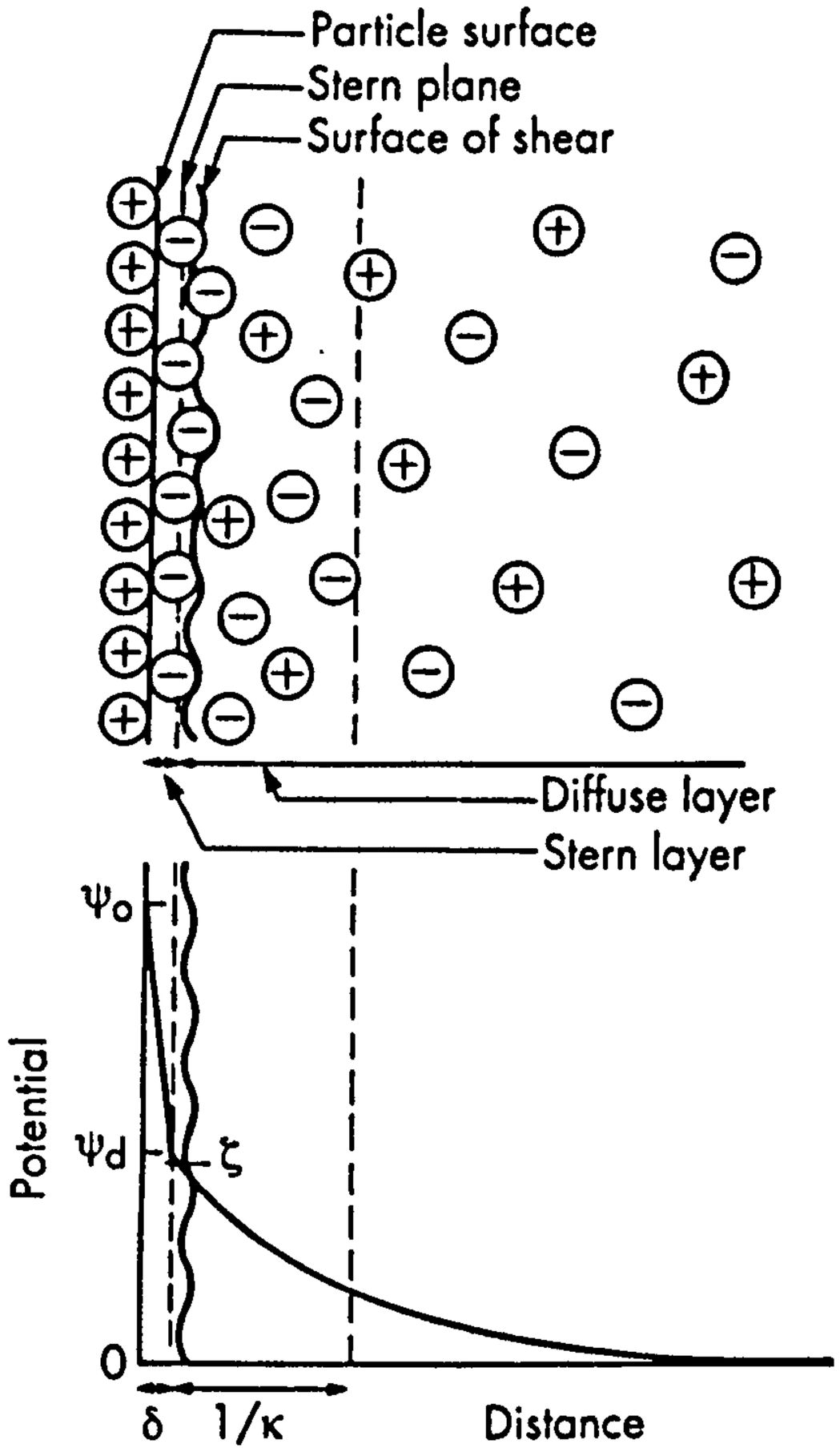

Figure 33 Schematic representation of the structure of the electrical double layer according to Stern's theory [104]. (ψ_o = surface potential, ψ_d = stern potential, δ = stern layer thickness, ζ = zeta potential, $\varkappa$ = ionic boundary layer).

The Malvern Zetasizer uses laser Doppler electrophoresis to measure the electrophoretic mobility (i.e. velocity per unit electric field) of a particle in solution. This constant velocity is the sum of the effect of electrode migration and viscous forces. Two laser beams meet within the sample cell and scattering of this light by the moving particles is detected as photons by a photomultiplier and fed into a digital correlator. This then calculates the zeta potential from the fluctuating intensity patterns [191].

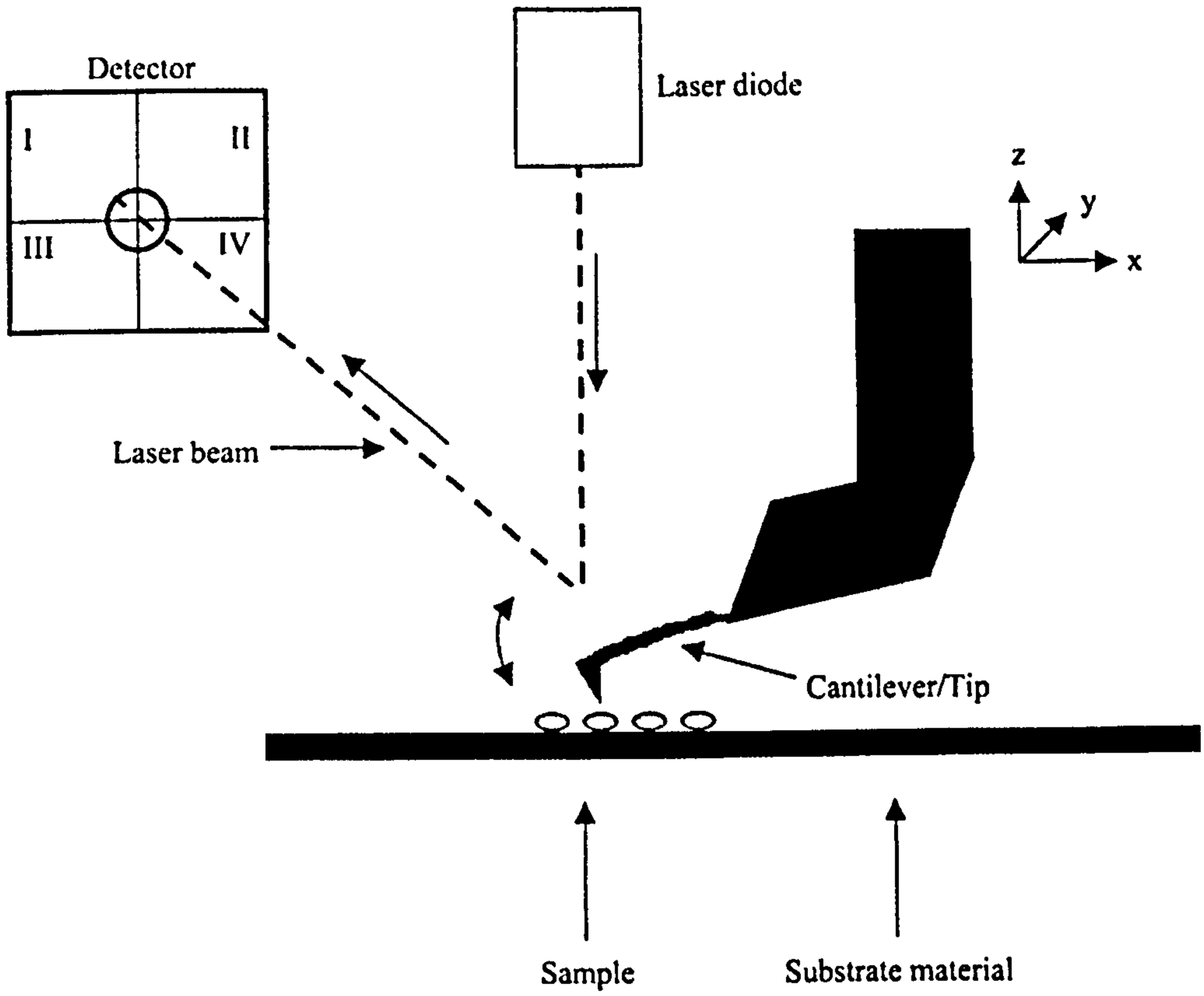

Figure 34 Schematic representation of an AFM system with a moveable cantilever [201]

AFM is the best method to investigate surface topography in three dimensions, to a resolution as high as 0.1nm. The limit to this resolution is due to the cantilever-tip system. TappingMode™ AFM (Digital Instruments, CA) is a key advance in AFM of soft, biological materials. The tip does not come into direct contact with the surface and can be used to examine liquid covered surfaces (as in this work) without any specific sample preparation [201]. When scanning the sample line by line, the vertical movement of the tip is detected by the change in reflection of a laser beam. In addition, the tip makes periodic vertical movements at defined frequencies (Figure 34). From the vertical displacement of the tip and changes in frequency, digital images are generated.

AFM has even been used to observe in real time Eth Br-induced supercoiling and assembly of rod and toridal condensates induced by polycation [202] and degradation

4.1.3. Precipitation profiling

Multi-molecular condensates of DNA can under some conditions be resolubilised by further addition of polymer beyond a second critical stoichiometry [120, 192]. This effect has been observed for different DNA lengths, concentrations and single, double and even triple stranded DNA [193-196]. It should be noted that this phenomenon necessitates the ability of each polycation to form a DNA liquid crystalline phase [194]. In the field of non-viral gene delivery this resolubilisation is attributed to DNA 'overcharging' and is relied upon to produce complexes that remain condensed but approach solution (mono-molecular) state, maintained by electrostatic repulsion [167]. However, it is reported in the literature that resolubilisation of high molecular weight DNA at increased spermine or spermidine concentrations is associated with re-entrant decondensation of individual DNA molecules (termed the 'incomplete ion dissociation mechanism') [193, 194, 196]. Therefore, a DNA condensation profile is not complete without examination of aggregation-solubilisation effects.

To examine these effects, in this work complexes formed at various dendrimer: pDNA ratios and DNA concentrations were subjected to ultracentrifugation to remove any insoluble particulates. The supernatants were then assessed using UV-Vis. spectroscopy at A_{260} to determine soluble DNA concentration and at A_{420} according to an improved 2,4,6-trinitrobenzenesulfonic acid method for enhanced detection of primary amines [197-199] to measure the amount of dendrimer free and incorporated in soluble complexes.

4.1.4. Atomic Force Microscopy (AFM)

Historically, cation-induced toroidal condensation of DNA was studied using techniques such as light scattering, electron microscopy (EM) and circular dichromism (CD) [141, 200]. Atomic Force Microscopy (AFM) is one of a number of scanning probe microscopy techniques which crucially can give information on the size and shape of complexes used in transfection [182, 184].

of condensed DNA complexes exposed to DNase I [203]. Visualisation by EM, which is also commonly used for this purpose, is hampered by the unknown ionic concentration of the DNA environment as the samples are dried which can produce structural artefacts. AFM offers more potential to observe DNA supercoil in a controlled aqueous environment, albeit still confined to two dimensions, immobilised to a substrate [204]. Other advantages include the applicability of AFM in a wide range of environments and the lack of requirement for labelled species in comparison with fluorescence microscopy [205]. The affect of pH and substrate choice on PAMAM dendrimer deformation has been investigated [206, 207] and TM-AFM has been found to be an excellent method to assess dendrimer sample quality. Fang and Hoh [207] do however admit that sampling patterns potentially could pose problems in AFM interpretation.

AFM experiments were carried out by Miss Ya Tsz Anne Chim in the laboratories of Professor Martyn C Davies (Laboratory of Biophysics and Surface Analysis, University of Nottingham).

4.1.5. Biological challenge

4.1.5.1. Glycosaminoglycan (GAG)

The varieties of intracellular and extracellular barriers to gene delivery are manifold [16]. Interestingly, free PEI has been observed in the cytosol [208, 209] and Okuda *et al.* [26] have investigated DNA releasing factors in the cytosol which were found to be soluble proteins. However, a key stage in successful gene delivery is physical interaction with tissue and cell membrane proteoglycans – proteins covalently linked to one or more sulphated or carboxylic glycosaminoglycans (GAGs). The GAGs that have been shown to be detrimental to cellular uptake are principally chondroitin and heparan sulphate [210]. These interfere with the integrity of the complexes, displacing cationic complexing agents. A synthetic GAG, heparin, can be used to assess the stability of the complexes formed against electrostatic disruption [190]. PEI and fractured dendrimer (identified as those agents with endosomal buffering capacity) were most sensitive to DNA relaxation and release by sulphated GAGs whereas cationic lipid formulations, particularly containing the fusogenic agent DOPE were most resistant [211]. In this work the ability of heparin to relax

condensation within complexes was assessed using Eth Br intercalation into released DNA.

4.1.5.2. Nuclease

DNase I is a pancreatic endonuclease which catalyses the hydrolysis of double stranded DNA [212, 213]. It has been shown using X-ray crystallography that DNase I binds in the minor groove of B-form DNA and cleaves DNA at the phosphodiester linkages [214]. It requires the presence of the divalent cations for maximal activity [215] and linked double strand breaks (DSBs) are facilitated in the presence of Mg^{2+}. Present in blood plasma, neutral DNase is an effective barrier against circulating exogenous DNA [216], therefore protection of pDNA from this enzyme is necessary for successful intravenous delivery. Intracellular dangers to transfection also include cytosolic nucleases, reliable evidence suggests [20, 217].

In this work, DNase I will be used to attempt to degrade the DNA within PPI G3 dendrimer complexes as has been done for PAMAM dendrimers [181], PEIs and 1,2-Dioleoyl-3-Trimethylammonium-Propane (DOTAP) [218] and poly(L-Lysine) block co-polymer [219] to name a few. The remaining plasmid will be electrophoresed on an analytical gel.

4.1.5.3. Serum

Following an adapted method by Hill *et al.* [220] protection of DNA from serum nuclease by the carriers will be assessed. Serum proteins are able to modulate transfection efficiencies through DNA complex destabilising effects [221-223]. Incubation in 50% v/v serum was used to mimic the biological situation more closely than a single recombinant serum nuclease.

4.2. Materials

DAB-16-Am (PPI Generation 3)	Sigma Aldrich Co., UK
cDAB-16 (cetylated DAB-16)	See Section 2.3.1
ExGen 500	Helena Biosciences, UK
1,2-Dioleoyl-3-Trimethylammonium-Propane (DOTAP)	Avanti Polar Lipids Inc, AL, USA
pCMVsport β-Galactosidase	Life Sciences, GibcoBRL, UK
Dextrose, anhydrous	Sigma Aldrich Co., UK
Cholesterol	Sigma Aldrich Co., UK
HEPES free acid, 1M (sterile)	Sigma Aldrich Co., UK
Phosphoric acid	BDH Laboratories, UK
2,4,6-trinitrobenzene sulfonic acid (TNBS) reagent	Sigma Aldrich Co., UK
Ethidium bromide	Sigma Aldrich Co., UK
Agarose; electrophoresis grade	Life Sciences, GibcoBRL, UK
TRIS base	Melford Laboratories, UK
EDTA	Sigma Aldrich Co., UK
Boric acid	Fisher Scientific, UK
Hyperladder I	Bioline Ltd, UK
5x Loading Buffer	Bioline Ltd, UK
DNase I recombinant, RNase-free	Roche Diagnostics, UK
DNase I incubation buffer (10x)	Roche Diagnostics, UK
Foetal Bovine Serum (FBS)	Life Sciences, GibcoBRL, UK
Dulbecco's Modified Eagles Medium (DMEM)	Life Sciences, GibcoBRL, UK
Triton X-100	Sigma Aldrich Co., UK
Heparin (sodium salt)	Sigma Aldrich Co., UK
Zeta Potential Standard, ZET 5500	Malvern Instruments Ltd, UK
Polystyrene beads (100nm)	Sigma Aldrich Co., UK

Table 10 Materials and suppliers used in Chapter 4

4.3. Methods

4.3.1. Preparation of complexes

For the purposes of this chapter, self assembled dendrimer formulations were prepared as section 2.3.5. DOTAP liposomes were prepared by dispersing 20mg DOTAP in 10mL water and diluting into the chosen buffer before sonicating the resulting dispersion for 5 min periods at 75% of full power (Soniprep 150, Sanyo Gallenkamp, UK) until it appeared translucent and bluish. Polymer or lipid complexes were prepared by adding equal volumes of dilute stock solution to dilute DNA (100 – 200μg.mL^{-1}) to give the required N: P ratio, and vortex mixing for 10 s.

4.3.2. PCS and zeta potential

Carrier-DNA complexes prepared as in section 4.3.1 in 1mM phosphate buffer (pH 7.4) at molar ratios ranging from 0.5 – 60 N: P were analysed for Z average hydrodynamic diameter and surface zeta potential using a Malvern Zetasizer 3000HS$_A$ (Malvern Instruments Ltd., UK) at 25°C. The zeta potential of a standard (Malvern Instruments Ltd, UK) was analysed and confirmed to be within the stated range (-50mV ± 5mV) before each zeta potential measurement was taken. Final concentrations of complexes were adjusted using buffer to fall within the ideal count range for the instrument. Zeta potential was determined in triplicate with the following parameters: medium viscosity 0.89 cP, dielectric constant 79 and beam mode F(ka) 1.5 (Smoluchowski approximation) [191]. In addition, size and zeta potential measurements were performed on complexes buffered at pH 10 and pH 3. Selected complex formulations were also sized in HEPES buffered dextrose (HBD: 20mM HEPES free acid in 5% dextrose adjusted to pH 7.4), DMEM and after x10 dilution into HBD, DMEM or DMEM: FBS (1: 1 v/v). For details of size analysis please see section 2.3.7.

4.3.3. Precipitation profiling

Complexes prepared in 1mM phosphate buffer (pH 7.4) (1mL) at DNA concentrations ranging from 50 – 500μg.mL^{-1} and various N: P ratios were subjected to preparative ultracentrifugation at 100,000 rpm for 1 h using a Beckman TL-100

ultracentrifuge (Beckman Coulter Ltd, UK). A sample from the top of the supernatant (~2μL) was removed using a quartz capillary tube (Biochrom Ltd, UK) and the absorbance of soluble pDNA read at A_{260} using a GeneQuant DNA/ RNA calculator (Biochrom Ltd, UK). It was confirmed that free dendrimer did not significantly absorb light at A_{260}, although A_{260} values were adjusted for any non-specific absorbance detected at A_{320}. Up to the entire remainder of the supernatant was subjected to UV-Vis spectrophotometry at A_{420} after diluting into assay range using buffer (if required) and incubation with 2,4,6-trinitrobenzene sulfonic acid (TNBS) 0.03M (25 μL reagent per 1mL sample) at 25°C for 30 min. Dendrimer concentrations (the sum of free dendrimer and that contained in soluble complexes) were calculated from a constructed standard curve for each species.

4.3.4. AFM

Dendrimer-DNA complexes at 30 N:P in 5% dextrose solution or HBD pH 7.4 (50μg.mL^{-1} pDNA) were incubated at 25°C for 15 min before immobilisation on freshly cleaved muscovite mica of approximately 1cm^2 and being imaged directly in liquid using a Tapping Mode (TM) AFM on a Nanoscope (IIIa) MultiMode system (Veeco Instruments, CA).

4.3.5. Biological challenge

4.3.5.1. Heparin

The increased fluorescence of Eth Br upon addition of heparin was used to assess the disruption of DNA complexed with DAB-16-Am, its amphiphilic formulations, ExGen 500 and the cationic lipid DOTAP. Pre-formed complexes (80μL) were incubated at 25°C for 10 min or 70°C in a heating block for 16 h following addition of 20 μL 5 % w/v heparin or blank buffer (final DNA concentration 100μg.mL^{-1}). Fluorescence analysis was carried out using Eth Br as described in section 3.3.4.

4.3.5.2. Nuclease

Pre-formed complexes (100μg.mL^{-1} pDNA, 25 μL) were incubated with 2 U DNase I per μg pDNA at 37°C for 0.5, 1, 2, 3 or 4 h in an incubation buffer mixture (40 mM Tris-HCl, 10 mM NaCl, 6 mM $MgCl_2$, 1 mM $CaCl_2$; pH 7.9). The reaction was

stopped and DNA released by the addition of 5 μL EDTA 250 mM followed by 10μL Heparin 5% w/v in Triton-X 100 5 % v/v in water (final volume = 50μL) then heating for 10 min at 70°C. Free plasmid incubated in the absence and presence of DNase I (2 U/ μg pDNA) was included as a control. The success of the enzyme stop and carrier release protocol had previously been confirmed in exploratory experiments. Complexes (0.2 μg pDNA) were loaded onto an agarose gel (1% w/ v) in 0.5x TBE (TRIS base 45mM: Boric acid 45mM: EDTA 1mM) buffer adjusted to pH 7.4 containing Eth Br (0.5μg.mL^{-1}) and run at 150 V for 45 – 60 min before visualisation with a UV transilluminator (Syngene Gene Genius Bioimaging System, UK). A molecular weight marker, DNA ladder λ-Hind III (Hyperladder I, 2μL) was run for size comparison with 14 regularly spaced bands (10,000 – 200 bp).

4.3.5.3. Serum

Pre-formed complexes (100μg.mL^{-1} pDNA) were incubated with FBS (1: 1 v/v) at 37°C for 0.5, 1, 2, 3 or 4 h. The reaction was stopped and DNA released by the addition of 5 μL EDTA 250 mM followed by 10μL Heparin 5% w/v in Triton-X 100 5 % v/v in water to 35μL complexes (final volume = 50μL) then heating for 10 min at 70°C. Free plasmid incubated in the absence and presence of serum was included as a control. Complexes (0.2 μg pDNA) were loaded onto an agarose gel (1% w/ v) in 0.5x TBE (TRIS base 45mM: Boric acid 45mM: EDTA 1mM) buffer adjusted to pH 7.4 containing Eth Br (0.5μg.mL^{-1}) and run at 150 V for 45 – 60 min before visualisation with a UV transilluminator (Syngene Gene Genius Bioimaging System, UK). A molecular weight marker, DNA ladder λ-Hind III (Hyperladder I, 2μL) was run for size comparison with 14 regularly spaced bands (10,000 – 200 bp).

4.4. Results

4.4.1. PCS and zeta potential

4.4.1.1. Dendrimer profiles

The three dendrimer species (DAB-16-Am, cDAB-16 and cDAB-16 vesicles) were prepared at 0.5 – 60 molar N: P ratios in 1 mM phosphate buffer at pH 7.4 and the hydrodynamic diameter and surface charge of the resulting complexes were measured. The resulting profiles are shown in Figure 35, Figure 36 and Figure 37 below.

The hydrodynamic diameters of the dendrimer-DNA complexes have reached minima by 30 N: P under these conditions and are determined to be 95.2 ± 1.9 nm for DAB-16-Am, 105.7 ± 1.1 nm for cDAB-16 and 176.4 ± 14.6 nm for cDAB-16 vesicles. There is little size difference between the DAB-16-Am and cDAB-16 complexes, however the cDAB-16 vesicles remain significantly larger which can be ascribed to the bulk of cholesterol within the internal structure. This ratio is also the limit of surface charging of the DAB-16-Am-DNA complexes (at 30 N: P ζ = +34.7 ± 1.0 mV; at 60 N: P, ζ = +36.2 ± 2.7 mV), but the surface charge accumulated by the amphiphiles continues to escalate and at the final measurement (60 N: P) cDAB-16 complexes achieve ζ = 45.8 ± 1.7 mV and cDAB-16 vesicles ζ = 64.2 ± 1.5 mV. It appears that amphiphile monomer or bilayer components remain able to attach to the surface of the complex beyond the earlier solubility-limiting ratio. This is logical as the electrostatic repulsion that exists between individual dendrimer molecules is ameliorated by hydrophobic interactions. Resolubilisation phenomena arise when dendrimer species are complexed at high N: P ratios as sufficient charge density now exists on the particle surface to resist further aggregation [85]. Stability is generally conferred to a colloidal system when the zeta potential value exceeds -30mV or +30mV [105].

It is important that the parameter of polydispersity index (PI) is considered; this value is unacceptable (>0.7) in unstable formulations therefore the sizes calculated for aggregated complexes (above ~1 μm) cannot be quoted absolutely. The mean PI is an excellent corroborator of stable complex formation, first dropping to 0.043 ±

0.03 at 5 N: P for DAB-16-Am indicating a near monodisperse, stable size population beyond this ratio. The mean PI for the cDAB-16 vesicle formulation drops to 0.203 ± 0.012 at 1 N: P, although these complexes remain more polydisperse than the DAB-16-am-DNA complexes. cDAB-16 does not achieve an especially low mean PI until 30 N: P is attained and all aggregation events are overcome (0.169 ± 0.015), which highlights the stabilising role of cholesterol within the previous formulation.

It is also informative to examine these profiles to determine the approximate N: P ratio that the complexes are at isoelectric point; from the figures below it can be seen that this occurs for DAB-16-Am at 3 N: P, cDAB-16 at 1 N: P, whereas cDAB-16 vesicles are already in a neutral complex with DNA at 0.5 N: P. This data is of value as it suggests that the cDAB-16 vesicle formulation is able to bind DNA most efficiently overall. A further amphiphile aggregation event as detected by ITC (section 3.4.2.3) is confirmed by these profiles, occurring at 4 N: P for cDAB-16 and 5 N: P for cDAB-16 vesicles. The extent of this aggregation (based on the relative size of the aggregates) also appears to be less for the cDAB-16 vesicles.

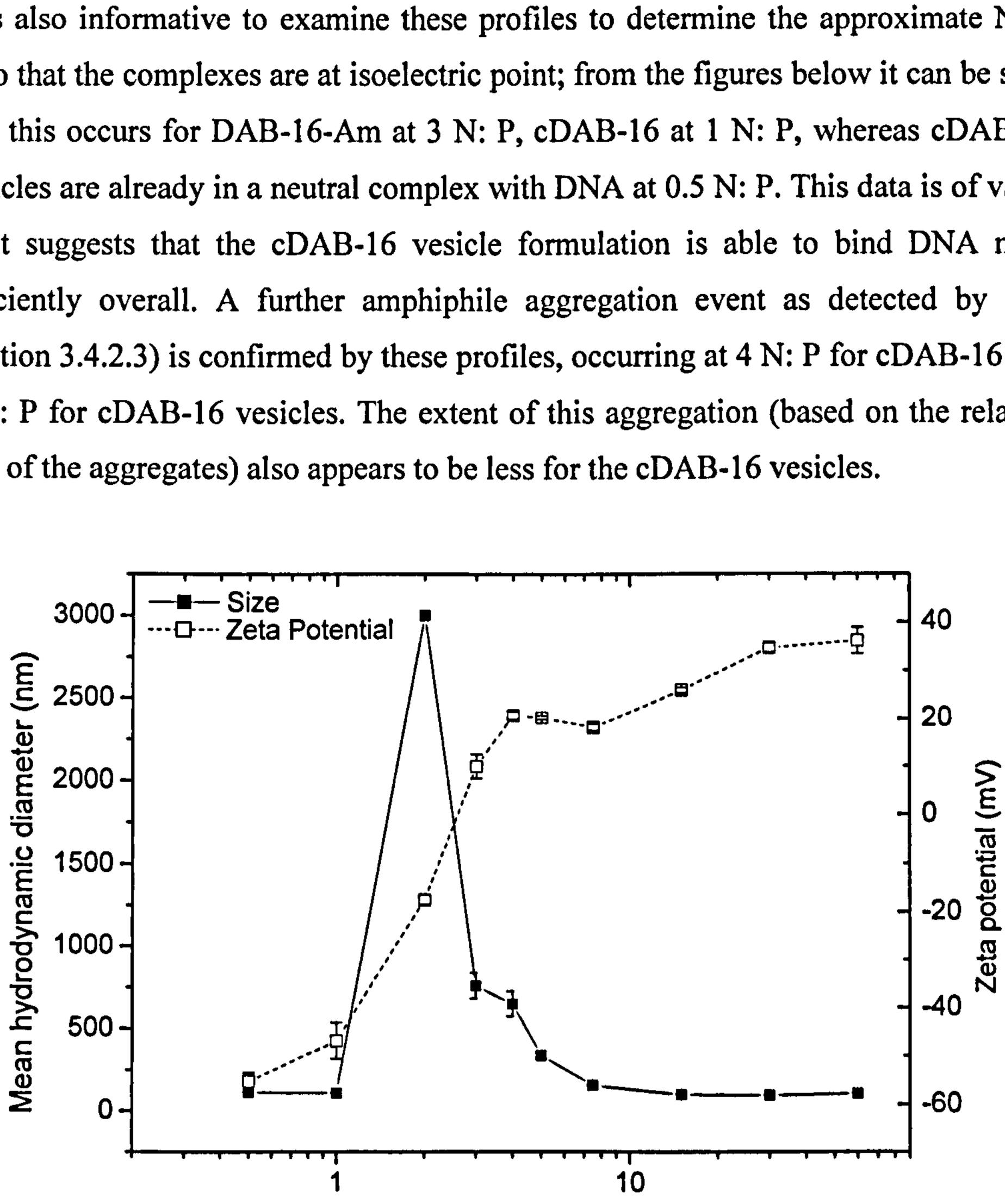

Figure 35 Size and zeta potential analysis of DAB-16-Am-DNA complexes 0.5-60 N:P pH 7.4

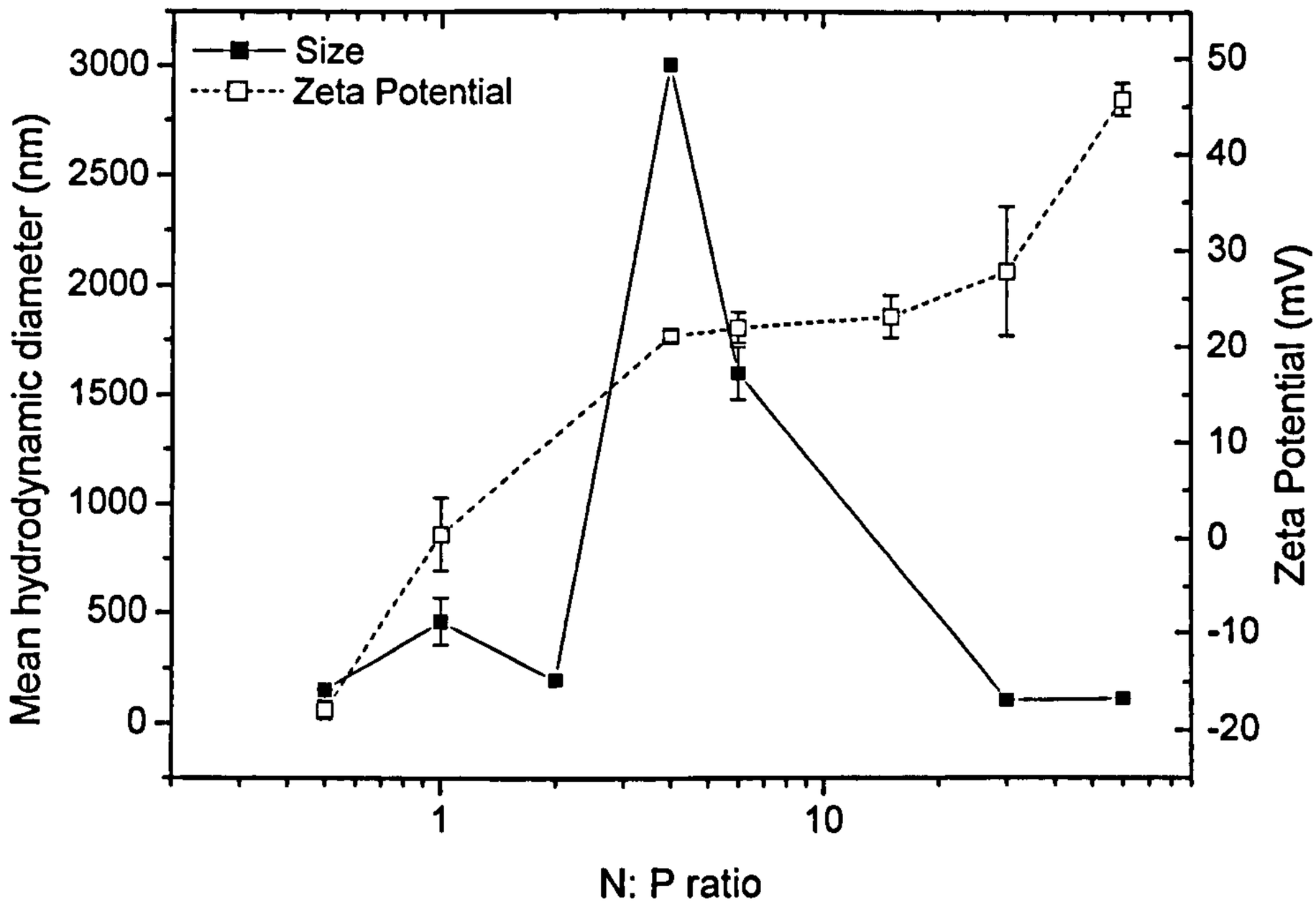

Figure 36 Size and zeta potential analysis of cDAB-16 -DNA complexes 0.5-60 N: P pH 7.4

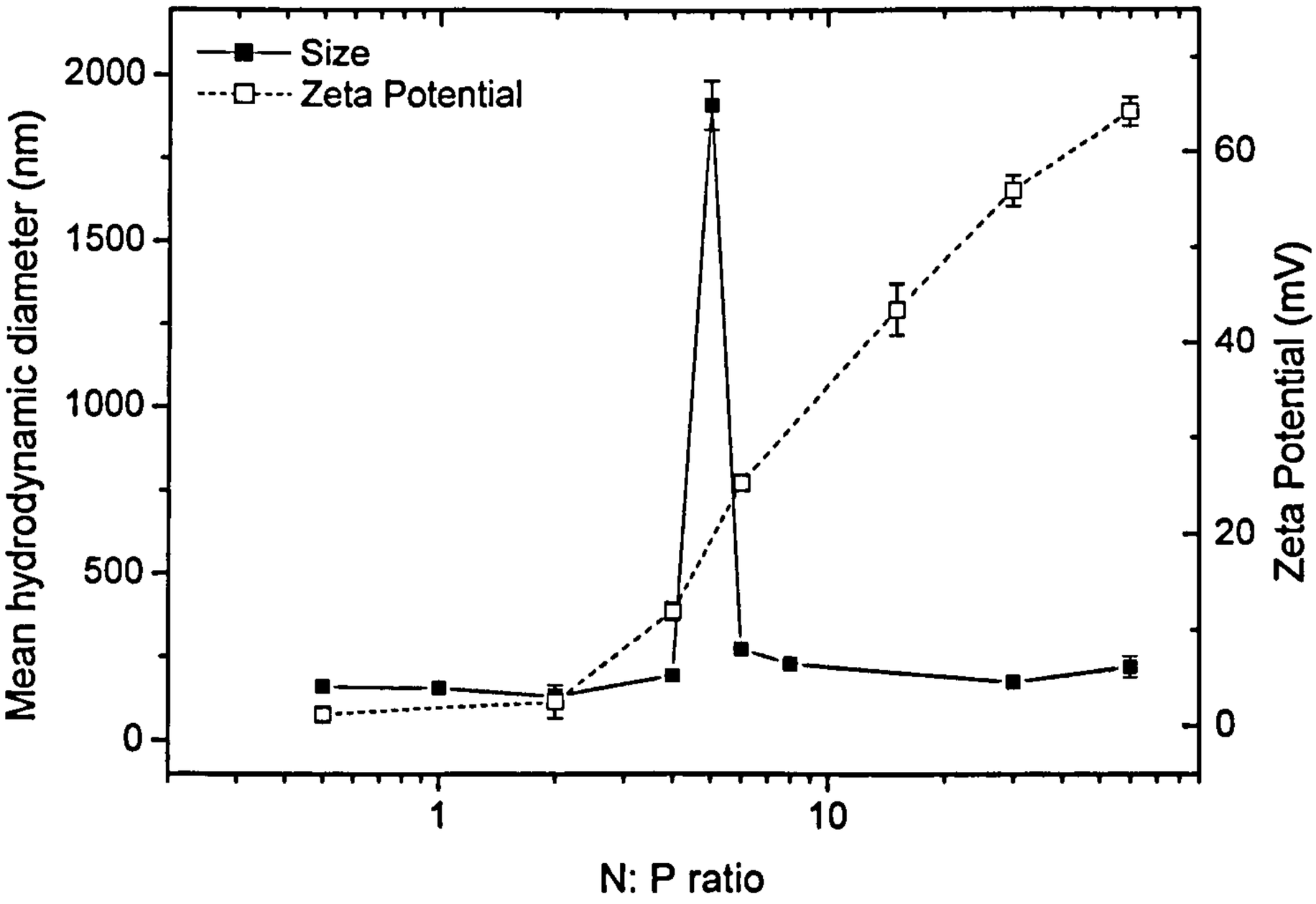

Figure 37 Size and zeta potential analysis of cDAB-16 vesicles -DNA complexes 0.5-60 N: P pH 7.4

4.4.1.2. Environmental conditions – pH

Complexes were analysed for size and surface zeta potential at the molar dendrimer nitrogen: DNA phosphate ratios recommended for transfection studies; 30 N: P for DAB-16-Am and its derivatives and 6 N: P for ExGen 500. Dendrimer and ExGen formulations are prepared in sterile 5% dextrose solution for *in vivo* administration. Under these conditions, the DAB-16-Am primary amines buffer the resulting solution at approximately pH 10 and these moderately cationic complexes (Table 11) have been used successfully for *in vivo* gene delivery [53]. The surface charge of these complexes increases dramatically from pH 10 to pH 7.4 as the outer primary amines become completely protonated.

Interestingly, cDAB-16 formulations produce more highly charged, smaller complexes than DAB-16-Am at pH 10 and when considering only these parameters, the amphiphile formulations are indistinguishable from each other. However, at pH 7.4 the effect of inclusion of cholesterol in the complex is observed (Table 11). It is possible that the lamellar DNA packing arrangement produced by the cDAB-16 vesicles cannot be reduced in volume as much as the other dendrimer-DNA arrangements upon the increased charge density resulting from the lower pH, although these charges have clearly been concentrated together on the surface of the structure ($\zeta = +55.9 \pm 1.6$mV). These pH profiles have implications for *in vivo* use of complexes.

The surface charge of DAB-16-Am complexes is unaltered from pH 7.4 to pH 3 (Table 11) as all outer shell (primary) amines are charged as the pH is reduced to neutrality. However the size of DAB-16-Am-DNA complexes formed at pH 3 does decrease slightly; this tighter complex could be a result of the interaction of protonated tertiary amines with the DNA backbone and concurs with the results of DNA binding studies (Chapter 3). This effect is recorded in the literature for the cationic polymer poly(2-(dimethylamino)ethyl methacrylate) (pDMAEMA) which consists of tertiary amines [126]. A similar principle can be applied to the ExGen 500 (linear PEI) formulation, as the acidic pH results in complete protonation of secondary amines within the polymer network (although this does also lead to a

significant increase in complex surface charge). Like ExGen 500, complexes of DAB-16-Am could also be formulated in low pH conditions for experimental work to exploit improved complex stabilities.

	pH 3		pH 7.4		pH 10	
	Size (nm)	**Z.P. (mV)**	**Size (nm)**	**Z.P. (mV)**	**Size (nm)**	**Z.P. (mV)**
DAB-16-Am	64.9 ± 4.4	+40.0 ± 3.0	95.2 ± 1.9	+34.7 ± 1.0	310.2 ± 4.0	+11.4 ± 0.8
cDAB-16	-	-	105.7 ± 1.1	+27.9 ± 6.7	244.7 ± 4.9	+32.8 ± 0.9
cDAB-16 vesicles	-	-	176.4 ± 14.6	+55.9 ± 1.6	244.3 ± 13.0	+33.9 ± 0.2
ExGen 500	87.8 ± 1.0	+47.9 ± 2.9	130.7 ± 7.5	+40.1 ± 2.4	-	-

Table 11 Hydrodynamic diameter (nm) and surface zeta potential (mV) of complexes (PPI 30 N: P/ PEI 6 N: P, pDNA 50 μg.mL^{-1}) in differing solution pH.

4.4.1.3. Environmental conditions – salt and serum

As a further indicator of complex stability, hydrodynamic diameters of complexes were examined under a series of differing environmental conditions. Complexes were formed in low (HBD; I = 10mM) and high (DMEM; physiological) ionic strength media and incubated for 15 min at 25°C before size analysis. Complexes produced in HBD were also further diluted 10 x in HBD, DMEM or DMEM: FBS (1:1 v/v). These give an estimation as to the effect of simple dilution, dilution into DMEM (as in *in vitro* transfection experiments) or dilution into 50% FBS in DMEM (a mimic of *in vivo* injection conditions) respectively.

It is important to note that 50% FBS in HBD produces detectable particulates of 44.0 ± 1.7 nm Z average mean hydrodynamic diameter which can be attributed to aggregates of serum proteins. 10 x dilution of complexes into HBD alone can increase the complex size by more than 50% (e.g. DAB-16-Am-DNA complexes

increase from 90.3 ± 12.8 nm to 143.7 ± 0.6 nm). However, this is still an order of magnitude lower than the size of complexes formed in or diluted into physiological salt solution (DMEM) which rapidly grow to micrometer sizes (for DAB-16-Am, 1247.8 ± 73.3 nm, cDAB-16, 1345.5 ± 29.2 nm). Dilution into 50% FBS stabilises these complexes against salt-induced aggregation; this is commonly attributed to binding of negatively charged serum proteins to the surface of the complexes forming a protective 'coating'. However, if the presence of a strong surface cationic charge is critical for cell internalisation of the complexes then transfection efficiencies can be ameliorated under these conditions [223]. Also, in the blood this process can lead to opsonisation of complexes by complement components and inactivation [223, 224].

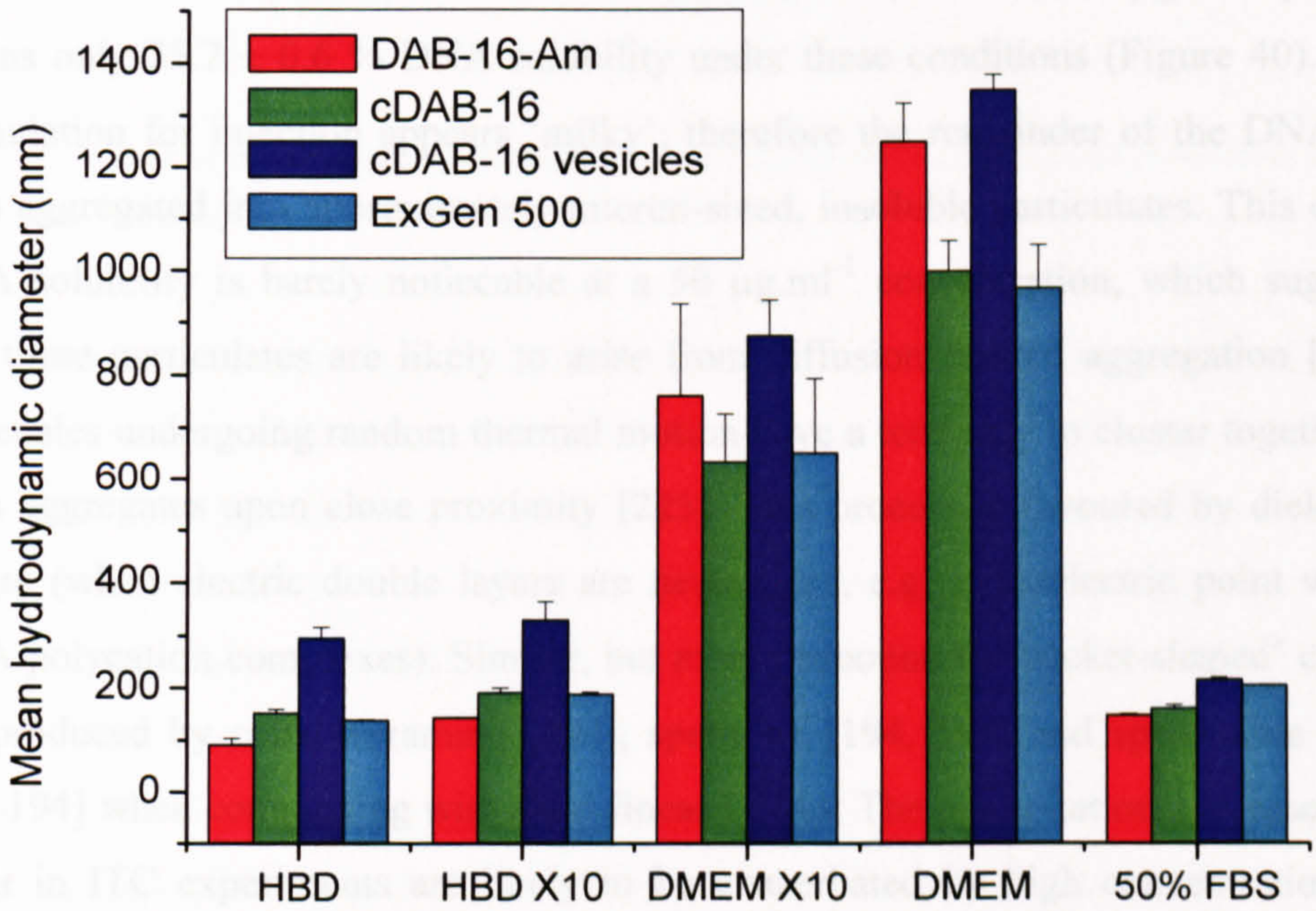

Figure 38 Hydrodynamic diameter (nm) of carriers at a final DNA concentration of 25 μg.mL^{-1} (PPI 30 N: P/ PEI 6 N: P) in differing environments. HBD = formed in HEPES buffered dextrose; HBD x10 = formed in HBD, diluted x10 into HBD; DMEM x10 = formed in HBD, diluted x10 into DMEM; DMEM = formed in DMEM; 50% FBS = formed in HBD, diluted x10 into DMEM: FBS 1: 1 v/v.

4.4.2. Precipitation profiling

Figure 39 shows the fraction of soluble DNA (without distinction between that complexed by DAB-16-Am or free in solution) as a function of molar ratio (varying from 0.1 – 30 N: P) and DNA concentration (50, 250 and 500 $\mu g.mL^{-1}$ pDNA).

The majority of pDNA present at the lowest N: P ratios is in a soluble state, and known to be uncondensed from Eth Br studies. A transition phase spans 0.2 – 1 N: P and DNA solubility reaches a nadir for all three DNA concentrations at 1 – 2 N: P. A further transition (resolubilisation) phase spans 2 – 5 N: P at which point a solubility plateau is reached. Using information from gel retardation studies and size analysis this plateau indicates that stable, soluble DNA complexes have been formed.

The successful *in vivo* DAB-16-Am-DNA formulation (30 N: P, 250 $\mu g.mL^{-1}$ pDNA) retains only 55.7 ± 0.6 % DNA solubility under these conditions (Figure 40). This formulation for injection appears 'milky'; therefore the remainder of the DNA has been aggregated into approximately micron-sized, insoluble particulates. This dip in DNA solubility is barely noticeable at a 50 $\mu g.ml^{-1}$ concentration, which suggests that these particulates are likely to arise from diffusion limited aggregation [225]. Molecules undergoing random thermal motion have a tendency to cluster together to form aggregates upon close proximity [225]. This process is favoured by dielectric failure (when electric double layers are neutralised, e.g. at isoelectric point within DNA-polycation complexes). Similar, but more pronounced, 'bucket-shaped' curves are produced by cobalthexamine [194], spermine [194, 195] and spermidine [118, 120, 194] when complexing with short linear DNAs. The precipitation processes that occur in ITC experiments are likely to be exacerbated by high concentrations of pDNA ($500\mu g.mL^{-1}$) (Figure 39).

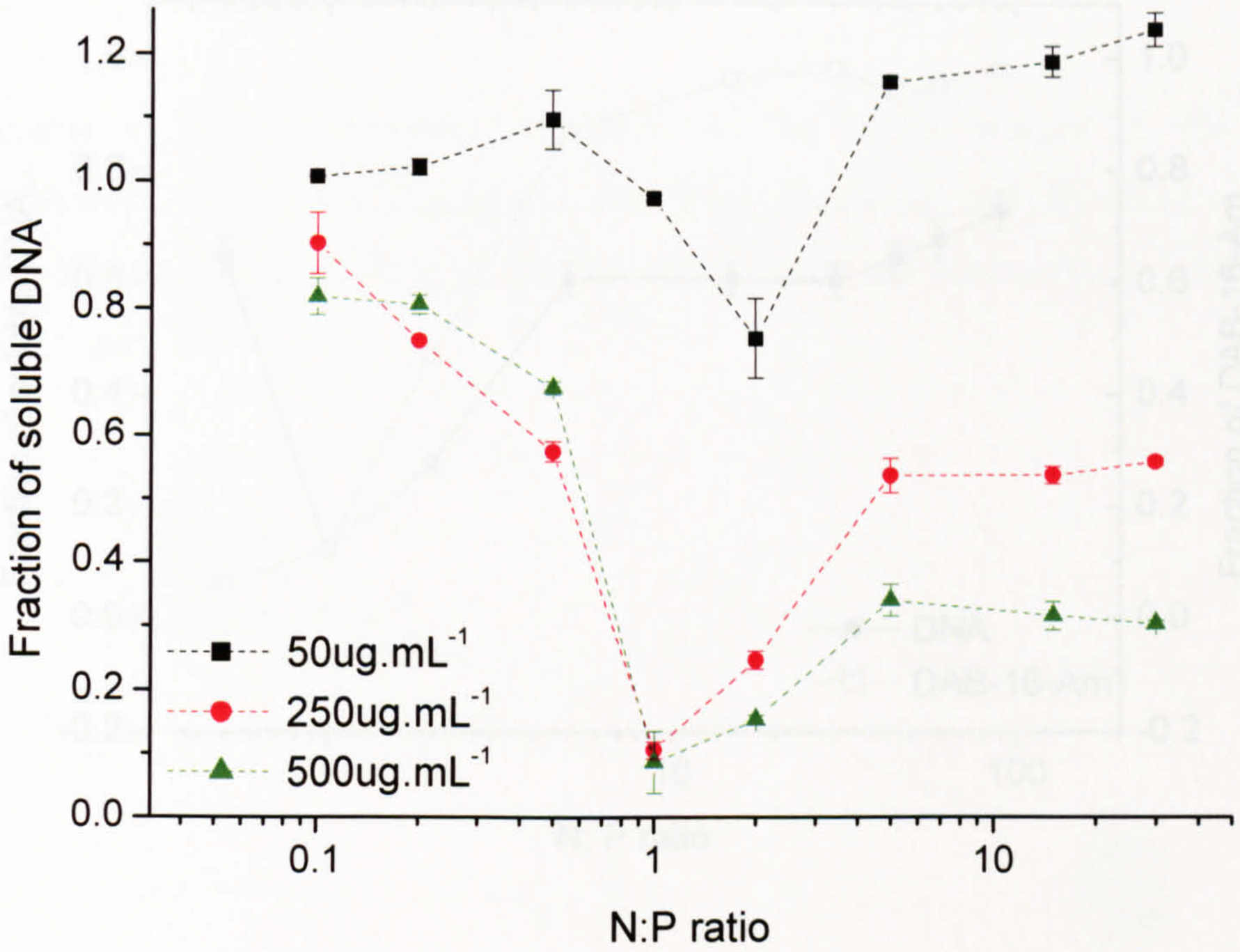

Figure 39 Variation in DNA solubility complexed with DAB-16-Am at N: P ratios 0.1-30 at three DNA concentrations.

A comparison of the profiles for DAB-16-Am (Figure 40) and cDAB-16 (Figure 41) below at *in vivo* DNA concentration are very informative. The fraction of soluble DNA, and therefore the concentration of soluble DNA complexes, reaches a plateau at approximately 30 N: P within both formulations. Cetyl DAB-16 produces the largest fraction of soluble DNA (75.4 ± 1.9% versus 60.4 ± 3.0% for DAB-16-Am) at this molar ratio and DNA concentration. Upon stoichiometric binding with cetyl DAB-16 (0.5 – 1 N: P), approximately two thirds of pDNA remains in soluble complexes after ultracentrifugation (67.4 ± 2.9%). This is in stark contrast with the solubility of pDNA within DAB-16-Am complexes, which at the same ratio drops to 11.9 ± 0.6%. It should be noted that this does not imply that global precipitation occurred at this ratio, but the formulation did become visibly opaque.

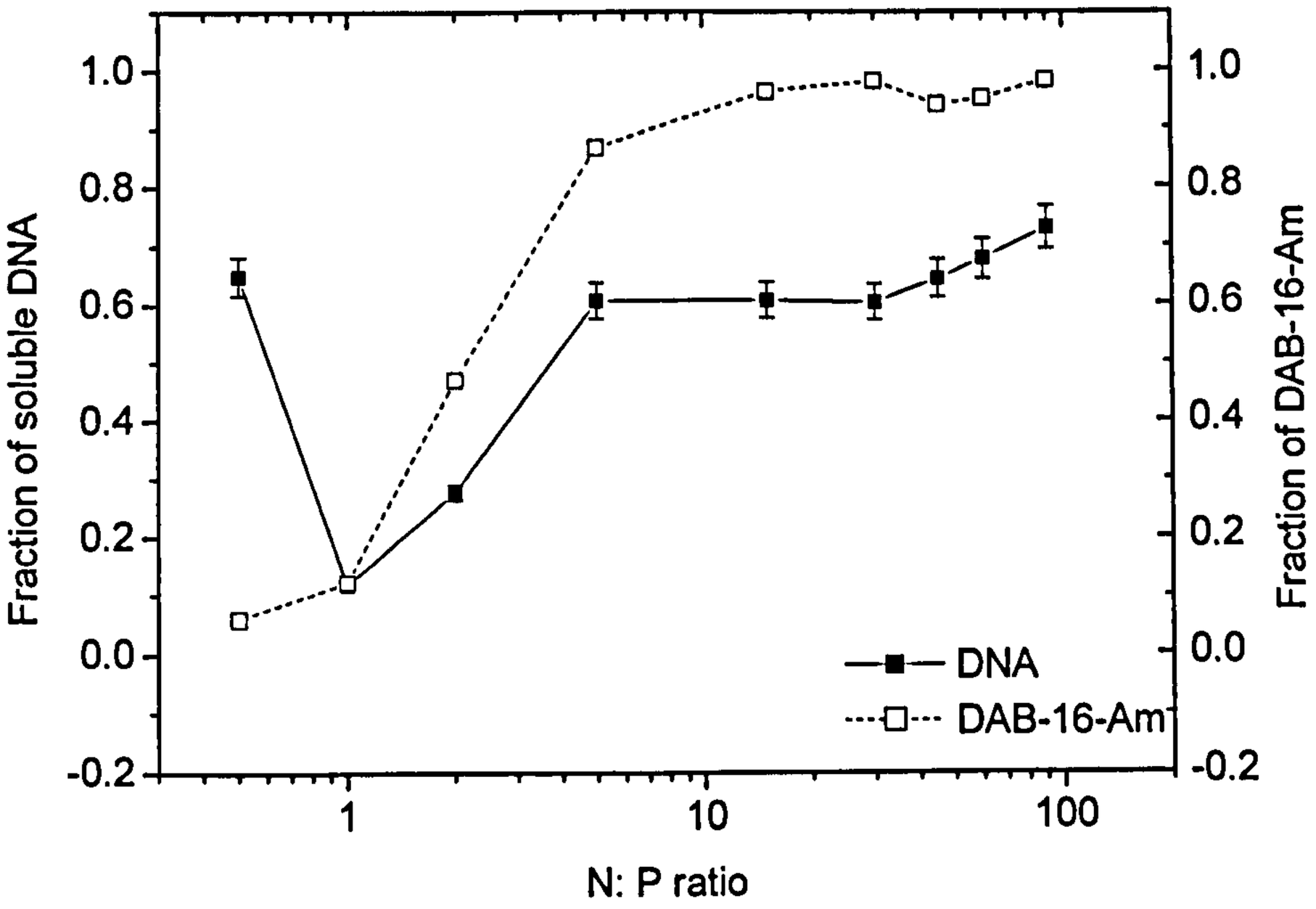

Figure 40 DAB-16-Am NP 0.5-30 (250μg.ml^{-1} DNA) and amine levels (pH 7.4)

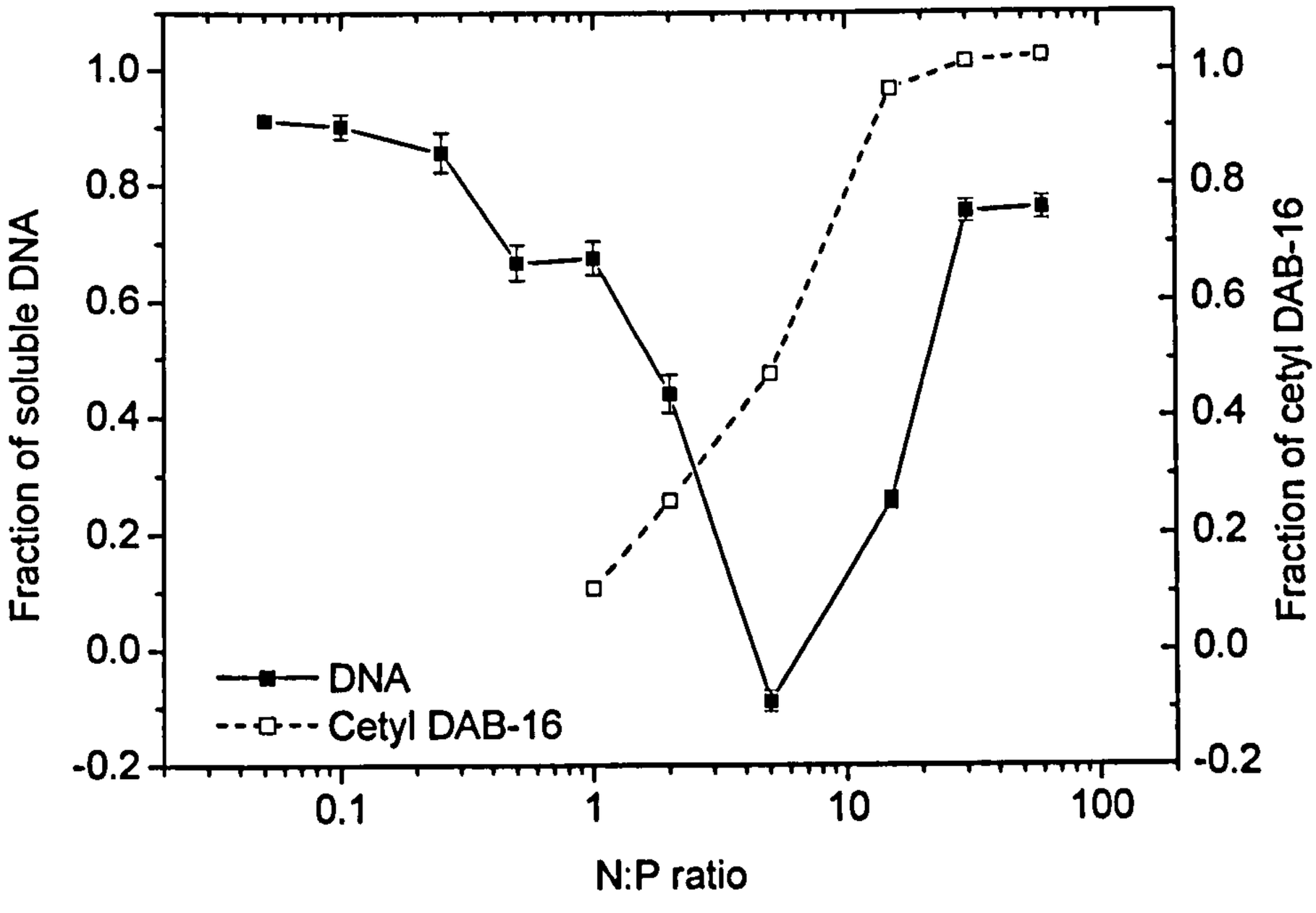

Figure 41 cDAB-16 NP 0.05-30 (250μg.ml^{-1} DNA) and amine levels (pH 7.4)

4.4.3. AFM

Structures of DNA complexes identified in TM AFM images of the three formulations DAB-16-Am (Figure 43), cDAB-16 (Figure 44) and cDAB-16 vesicles (Figure 45) formed at 30 N: P in 5% dextrose solution are schematically illustrated below (Figure 42).

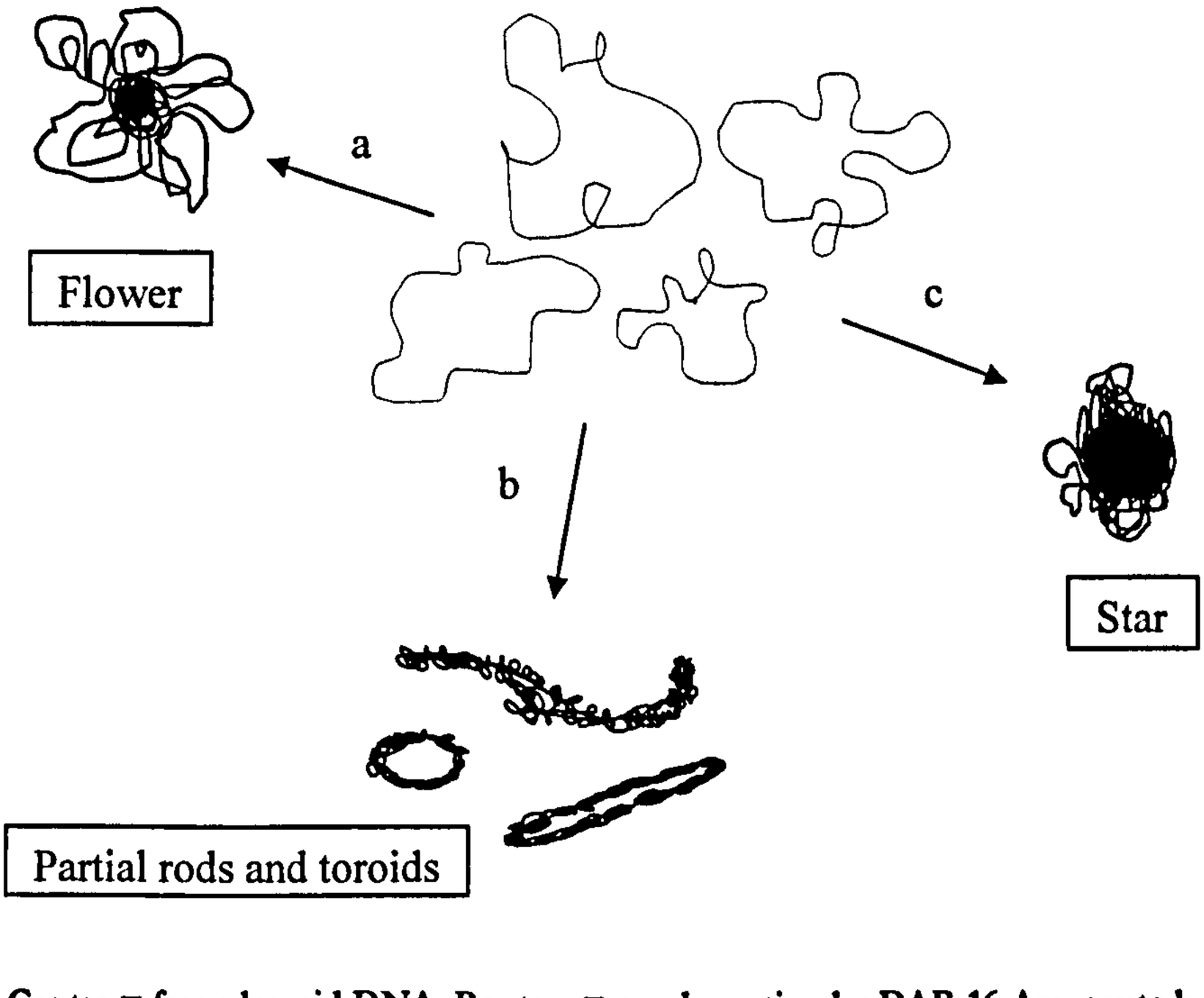

Figure 42 Centre = free plasmid DNA. Route a = condensation by DAB-16-Am, route b = condensation by cDAB-16 and route c = condensation by cDAB-16 vesicles (all after 15 min incubation).

These structures are each very different. 'Flowers' (Figure 43) are formed by DAB-16-Am after a 15 min incubation, with long loops extending from a tightly wound core. It should be observed that the thickness of these DNA 'loops' is approximately 10nm; much greater than the B-DNA duplex (~2nm). Therefore, these larger loops exhibit a degree of supercoiling (winding). Flowers are known to form at sub-saturating concentrations of PEI, with progressive condensation shown to occur through DNA folding upon addition of polycation [183]. It is known that polyethylenimines, fractured PAMAM dendrimer and poly-L-lysines finally

condense DNA into small toroids [41]. Abdelhady *et al.* found that if a PAMAM generation 4 dendrimer was allowed to form complexes with DNA (5: 1 w/w) for 2 h rather than 15 min, loops were no longer visible on AFM images [203]. Such early intermediates have also been observed for spermines using AFM, for which toroidal and rod shapes are the only well defined end points *in vitro* [207]. The existence of intermediate structures recorded by Bottcher *et al.* (parallel DNA bundles and frequent partial toroids) is also consistent with the idea that there is a slow-post collapse rearrangement of DNA into final rod or toroid forms [226]. Increasing the spermidine concentration did not accelerate the path to these end points.

A 'toroid' consists of a series of spiral DNA supercoils wound about an (imaginary) ring structure. Seemingly contradictory, this highly curved structure usually arises in nature as a result of underwinding of the B-form of DNA by the binding agent, producing one fewer than the natural number of twists. Minagawa *et al.* were the first to suggest that basic polypeptides caused these circular structures because cross - linking between phosphate groups restricts stretching motion leading to a decrease in persistence length [227]. A 'rod' also consists of a series of interwound supercoils and may terminate in a curved portion forming end loops as seen in Fig. 12 for cDAB-16. The rods and toroids seen here are only partially formed, similar to transitional structures observed for pDMAEMA [228]. This suggests that cDAB-16 had progressed further along the compaction pathway to these equilibrium rod and toroidal structures than DAB-16-Am under these conditions, possibly through more efficient DNA chain cross-linking.

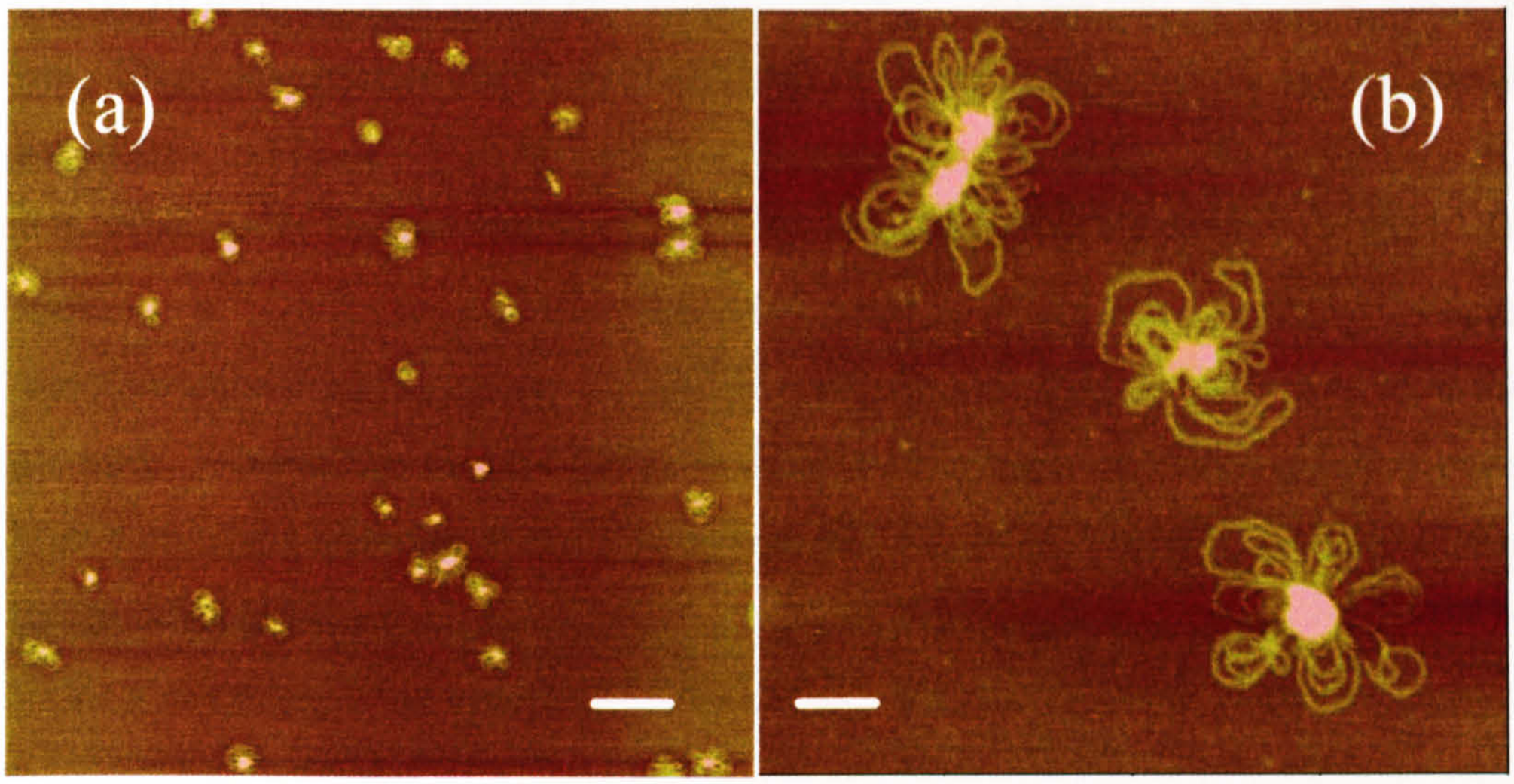

Figure 43 TM-AFM images in 5% dextrose solution (pH 10). DAB 16-Am –DNA complex at 30 N: P ratio; where scale bar in (a) is 500 nm and (b) is 100 nm. Z = 10 nm in (a) and Z = 15 nm in (b)

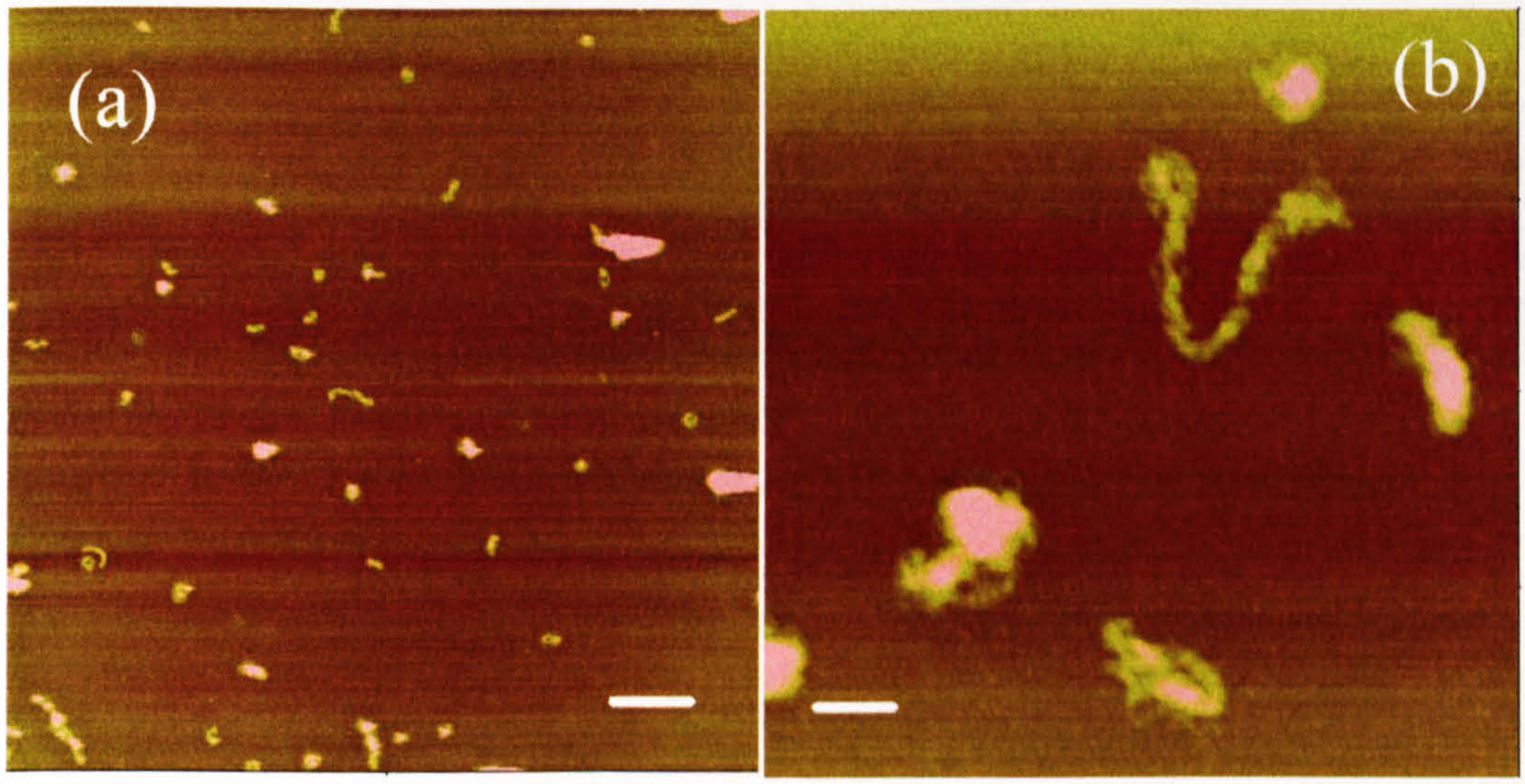

Figure 44 TM-AFM images in 5% dextrose solution (pH 10). Cetyl-DAB 16 –DNA complexes at 30 N: P ratio; where scale bar in (a) is 500 nm and (b) is 100 nm. Z = 10 nm in (a) and Z = 15 nm in (b)

Although upon examination of hydrodynamic diameter and surface charge the two cDAB-16 formulations could be virtually identical, morphologically, this is not the case. Sizes do correlate well with the PCS data; however partial rods and toroids are not visible in Figure 45. Rather there are very dense, globular, 'star' structures. The star structure is representative of cationic liposomal binding to DNA [229]. The addition of DNA to cationic liposomes results in a fascinating topological transformation from liposomes to optically birefringent liquid-crystalline condensed globules. X-ray diffraction (X-RD) and small angle neutron scattering (SANS) have been carried out showing alternating monolayers of cationic bilayer and DNA within the globules [154].

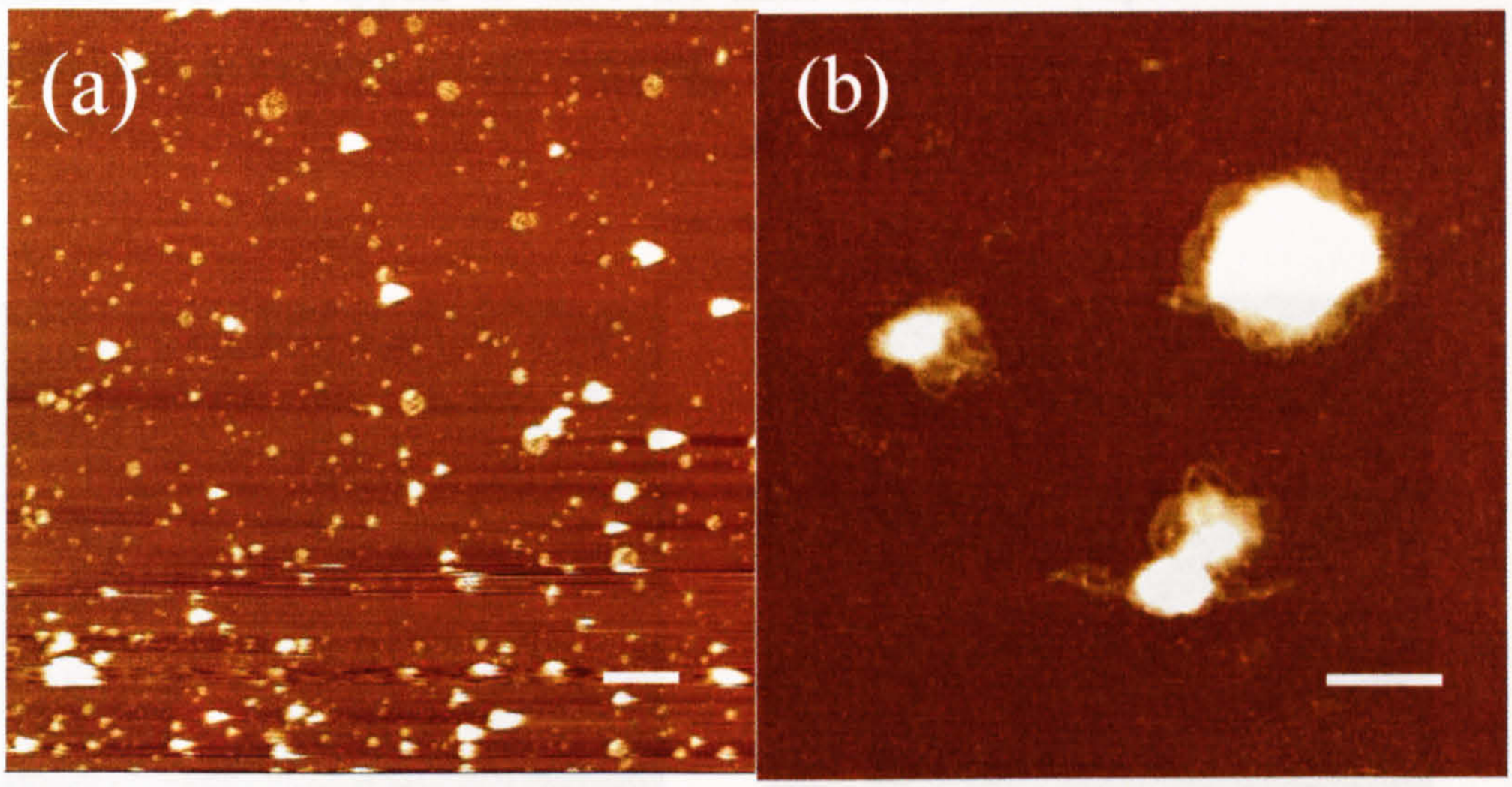

Figure 45 TM-AFM images in 5% dextrose solution (pH 10). Cetyl DAB 16-vesicles –DNA complexes at 30 N: P ratio. Where scale bar in (a) is 500 nm and (b) is 100 nm. Z-scale for (a) = 35 nm and (b) = 15 nm

Interestingly, the hydrodynamic diameters calculated for DAB-16-Am and cDAB-16 – DNA complexes using PCS are corroborated by TM AFM of complexes formed at physiological pH (Figure 46 & Figure 47). Both species produce very densely packed complexes of approximately 100nm in size, in appearance more like the cationic – hydrophobic star structures. The increased charge density in this pH environment appears to have enhanced the interaction between the DNA strands and the dendrimer species. It would suggest that the hydrophobic chains present in the cDAB-16 formulation have little influence on morphology at this pH when electrostatic interactions dominate. Interestingly, DAB-16-Am terminally quaternised with methyl groups is also a flower structure (image supplied by Y. T. Chim, University of Nottingham), therefore modification with permanent cationic charges does not appear to have the same effect on compaction of DNA as formulation in a neutral pH environment.

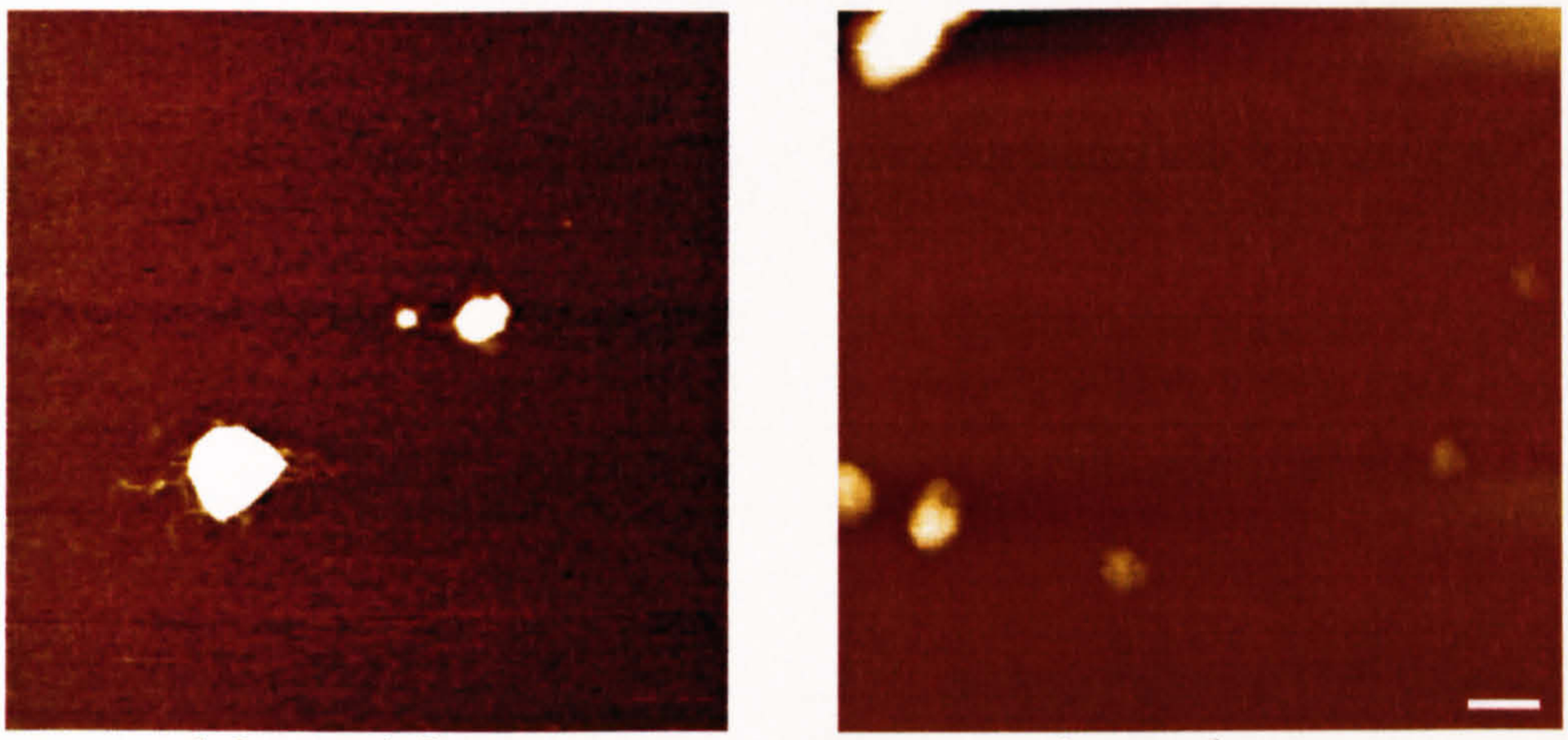

1.5 μm x 1.5 μm

1 μm x 1 μm

Figure 46 DAB-16-Am-DNA complexes, 30 N: P, pH 7.4, 15-20 min incubation Z = 10nm for both images.

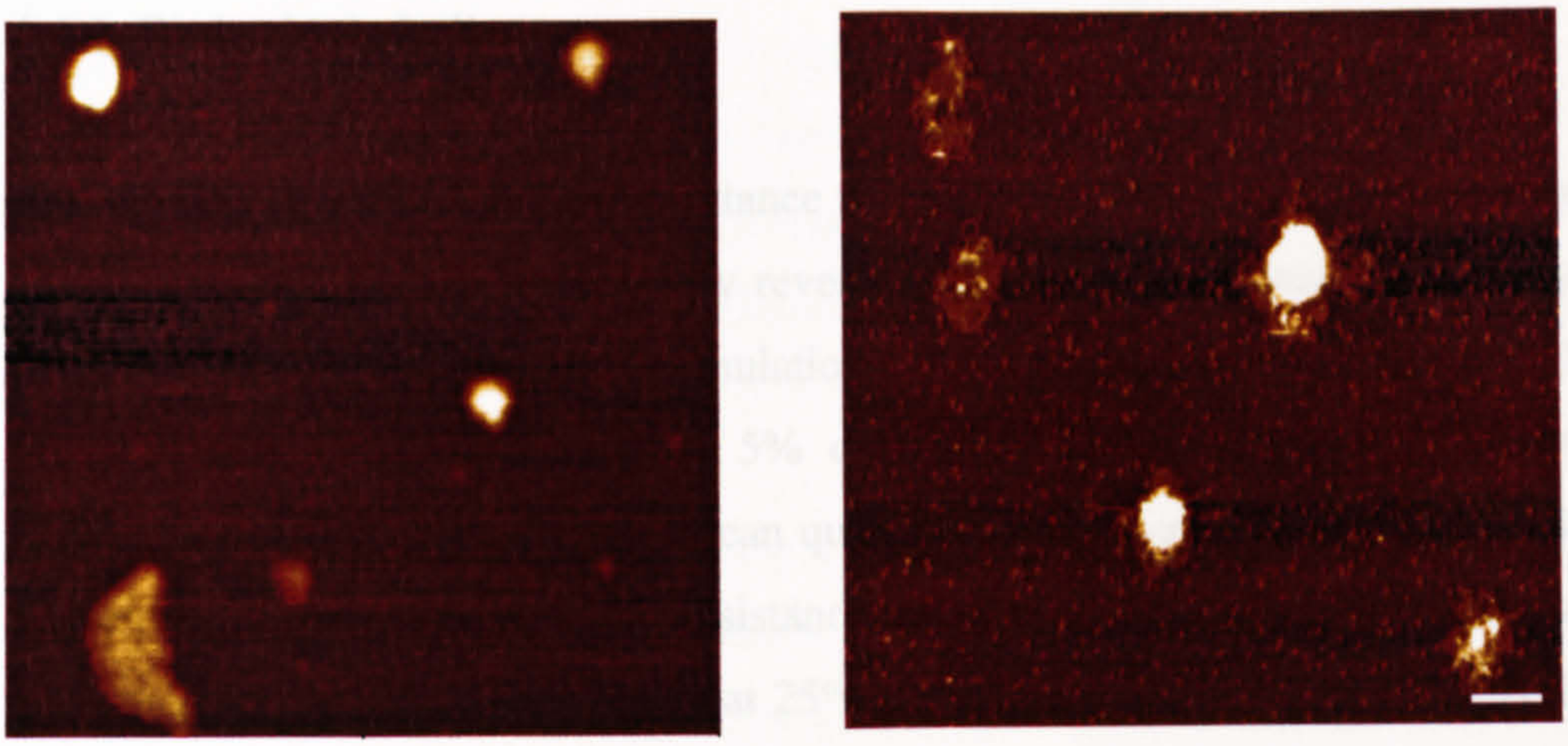

1.5 μm x 1.5 μm

1 μm x 1 μm

Figure 47 Cetyl-DAB-16-DNA complexes, 30 N: P, pH 7.4, 15-20 min incubation. Z = 10nm for both images.

4.4.4. Biological challenge

4.4.4.1. Heparin

The use of Eth Br to probe the resistance of complexed DNA against disruption by heparin (a synthetic GAG) was very revealing. A comparison was drawn between DAB-16-Am, its amphiphilic formulations, ExGen 500 and the cationic lipid DOTAP, conducted in unbuffered 5% dextrose solution. Heparin is a densely negatively charged molecule which can quite literally rip cationic species off DNA. Therefore, it served to rank the resistance of these agents to strong electrostatic disrupting forces below (Figure 48) at 25°C. Incubation at 70°C was included in an effort to completely remove the cationic species and also for applicability to later studies when enzyme inactivation would also be required.

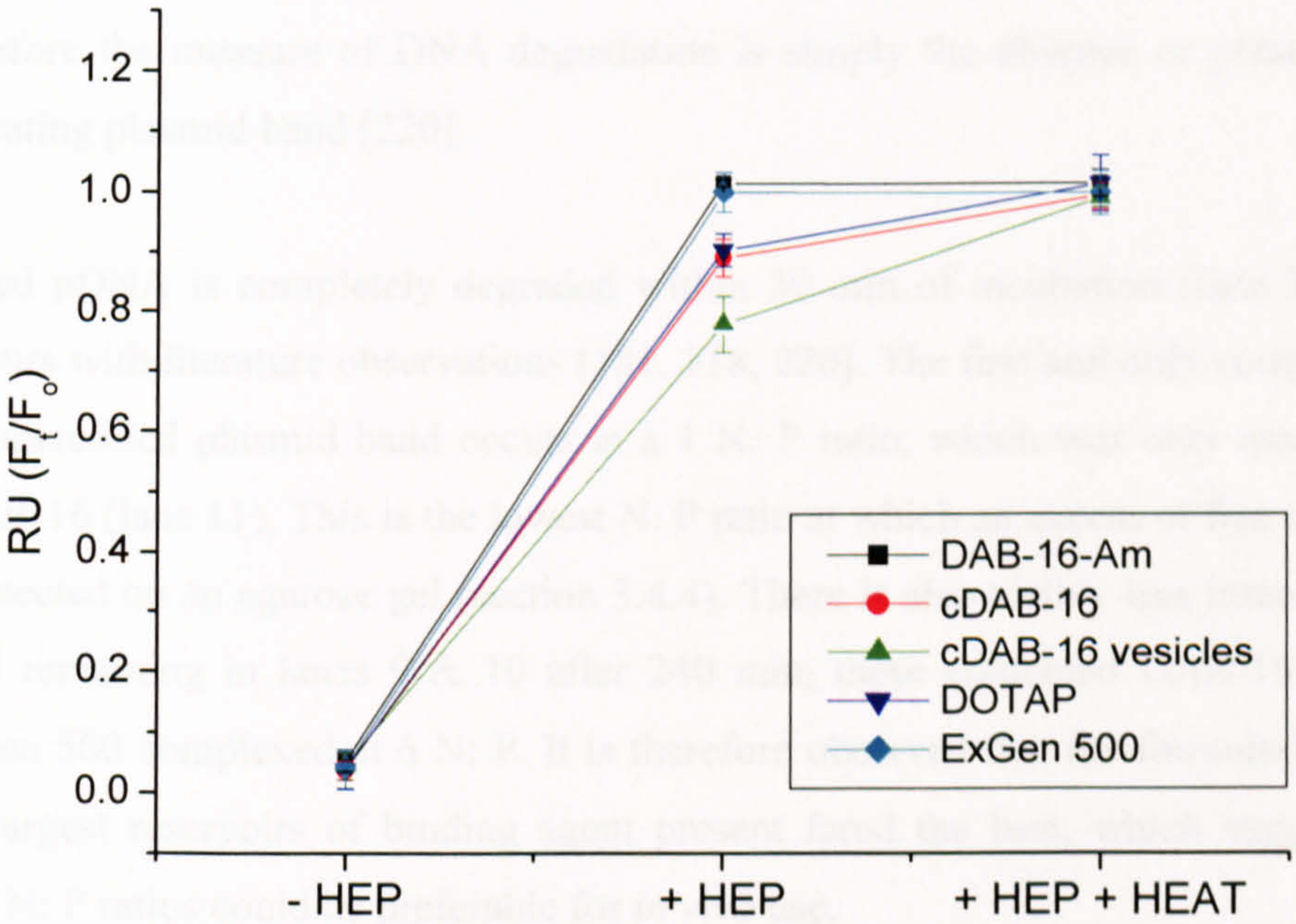

Figure 48 '– HEP' = carriers at 30 N: P (DAB-16-Am, cDAB-16 and cDAB-16 vesicles), 6N:P (ExGen 500) and 2 N:P (DOTAP); '+ HEP' = carrier complexes with 1% w/v heparin sodium (25°C, 10 min); '+ HEP + HEAT' = with 1% w/v heparin sodium (70°C, 16 h)

The carriers were ranked after incubation for 10 min at 25°C as follows: DAB-16-Am = ExGen 500 < cDAB-16 = DOTAP < cDAB-16 vesicles. Interestingly, each of

the three 'groups' represents a structure from TM AFM studies (Figure 43, Figure 44 & Figure 45). As the hydrophobic content of complexes increases, so does the resistance to electrostatic disruption. Heparin was later used in combination with Triton X-100 and heating at 70°C to disrupt hydrophobic interactions and completely release DNA from all complexes for further analysis.

4.4.4.2. Nuclease resistance

Resistance to degradation by DNase I is very relevant to the intravenous delivery of gene therapeutics. In this work, resistance to degradation of DAB-16-Am, cDAB-16, cDAB-16 vesicles and PEI complexes has been explored in various pH environments over a period of 4 hours in the presence of 2 units of DNase I per microgram of pDNA (Figure 49). It is important to note that degradation products of pDNA e.g. oligonucleotide fragments will not intercalate Eth Br to the same extent as dsDNA, therefore the measure of DNA degradation is simply the absence or presence of a migrating plasmid band [220].

Naked pDNA is completely degraded within 30 min of incubation (lane 3), which concurs with literature observations [181, 218, 220]. The first and only complete loss of supercoiled plasmid band occurs at a 1 N: P ratio, which was only assessed for cDAB-16 (lane 11). This is the lowest N: P ratio at which an excess of free cDAB-16 is detected on an agarose gel (section 3.4.4). There is also visibly less intact plasmid band remaining in lanes 9 & 10 after 240 min, these contained DAB-16-Am and ExGen 500 complexed at 6 N: P. It is therefore observed that the formulations with the largest reservoirs of binding agent present fared the best, which suggests that high N: P ratios could be preferable for *in vivo* use.

DNase I degradation of complexed DNA does not follow any trend which can align it with morphological information in this work. It is speculated in the literature that 'petals' of flower structures are where DNase I attacks first [228] but petals known to be formed in DAB-16-Am-DNA complexes (at pH 10, lane 6) are still protected from very high amounts of DNase I. This agrees with the work of Bielinska *et al.* which finds that DNA complexed with large PAMAM dendrimers is substantially

resistant to DNase I degradation at N: P ratios exceeding unity and these data could not be correlated with AFM structural information [181].

Importantly, other serum components such as proteins could interact with these complexes and either stabilise or destabilise complexes to nuclease action [220], therefore the effect of serum on DNA integrity will be considered next.

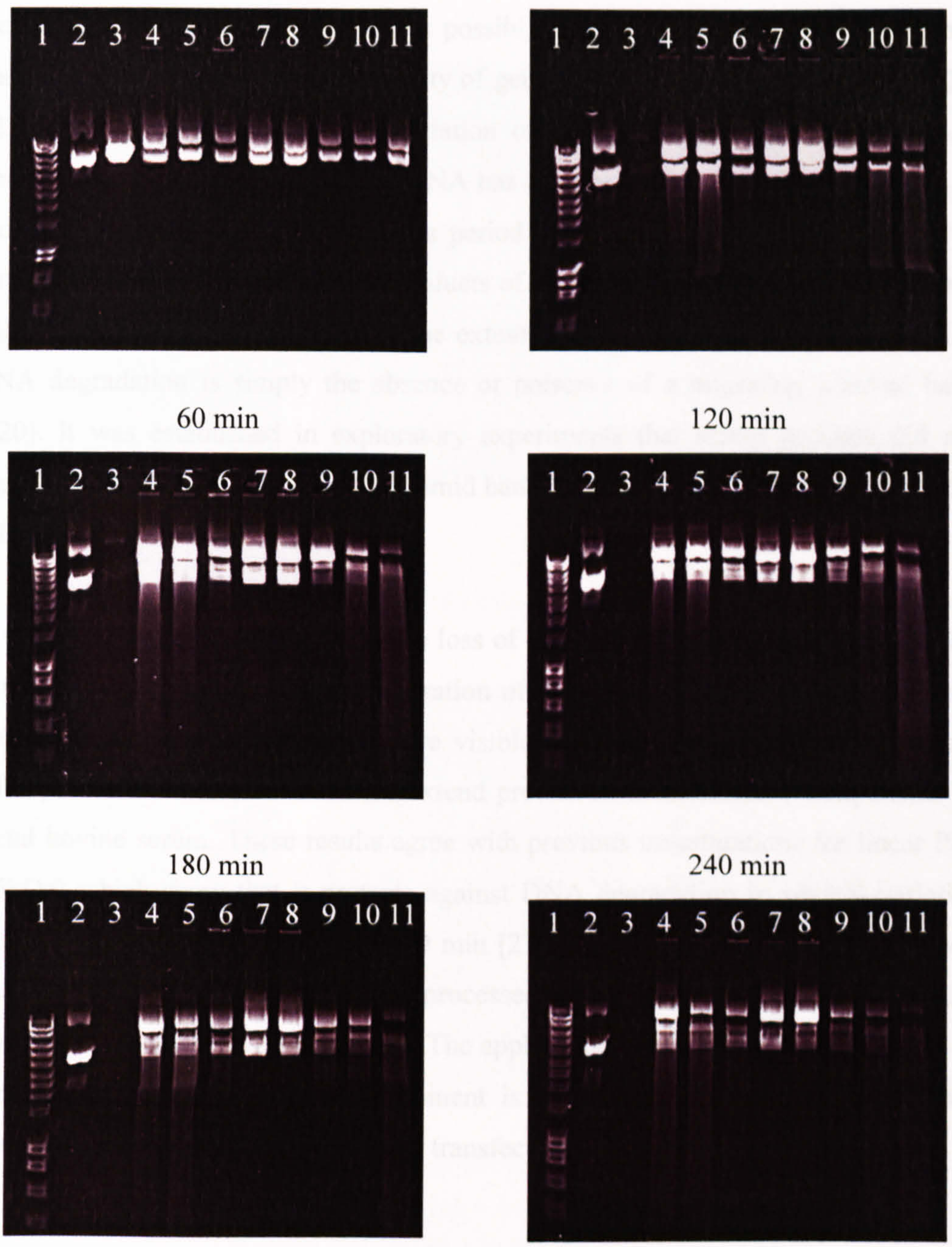

Figure 49 DNase I sensitivity of pDNA in the presence of carriers.

Lane 1: ladder. Lane 2: pDNA alone. Lane 3: pDNA + 2U/ μg DNase I. Lanes 4-6: DAB-16-Am, N: P ratio = 30, pH 3.5, 7.4, 10 respectively. Lane 7: cDAB-16, N: P ratio = 30, pH 10. Lane 8: cDAB-16 vesicles, N: P ratio = 30, pH 10. Lane 9: ExGen, N: P ratio = 6, pH 7.4. Lane 10: DAB-16-Am, N: P ratio = 6, pH 7.4. Lane 11: cDAB-16, N: P ratio = 1, pH 7.4.

4.4.4.3. Serum resistance

Resistance to degradation by serum is possibly more relevant than synthetic DNase challenge for the assessment of stability of gene therapeutics in the circulation [221, 223]. Therefore, resistance to degradation of DAB-16-Am, cDAB-16, cDAB-16 vesicles and L-PEI complexes with DNA has been explored following incubation in the presence of 50% v/v FBS over a period of 4 hours (Figure 50). Again, it is important to note that degradation products of pDNA e.g. oligonucleotide fragments will not intercalate Eth Br to the same extent as dsDNA, therefore the measure of DNA degradation is simply the absence or presence of a migrating plasmid band [220]. It was established in exploratory experiments that serum proteins did not significantly alter the migration of plasmid bands or prevent Eth Br intercalation with dsDNA.

In this experiment there is a complete loss of pDNA band after 180 min incubation (lane 2); this is not seen over the duration of the experiment for DNA complexed with these carriers, although there are visible losses of supercoiled plasmid band density. These carriers do therefore extend protection to DNA from components of foetal bovine serum. These results agree with previous investigations for linear PEI (25kDa) which show that it protects against DNA degradation in several varieties and proportions of sera for at least 30 min [218]. The presence of serum stabilised these complexes against aggregation processes rather than disrupting them in PCS studies, which concur with these data. The application of these findings to the fate of complexes in the circulatory environment is uncertain, but these will be further examined in the context of *in vitro* cell transfection in chapter 5.

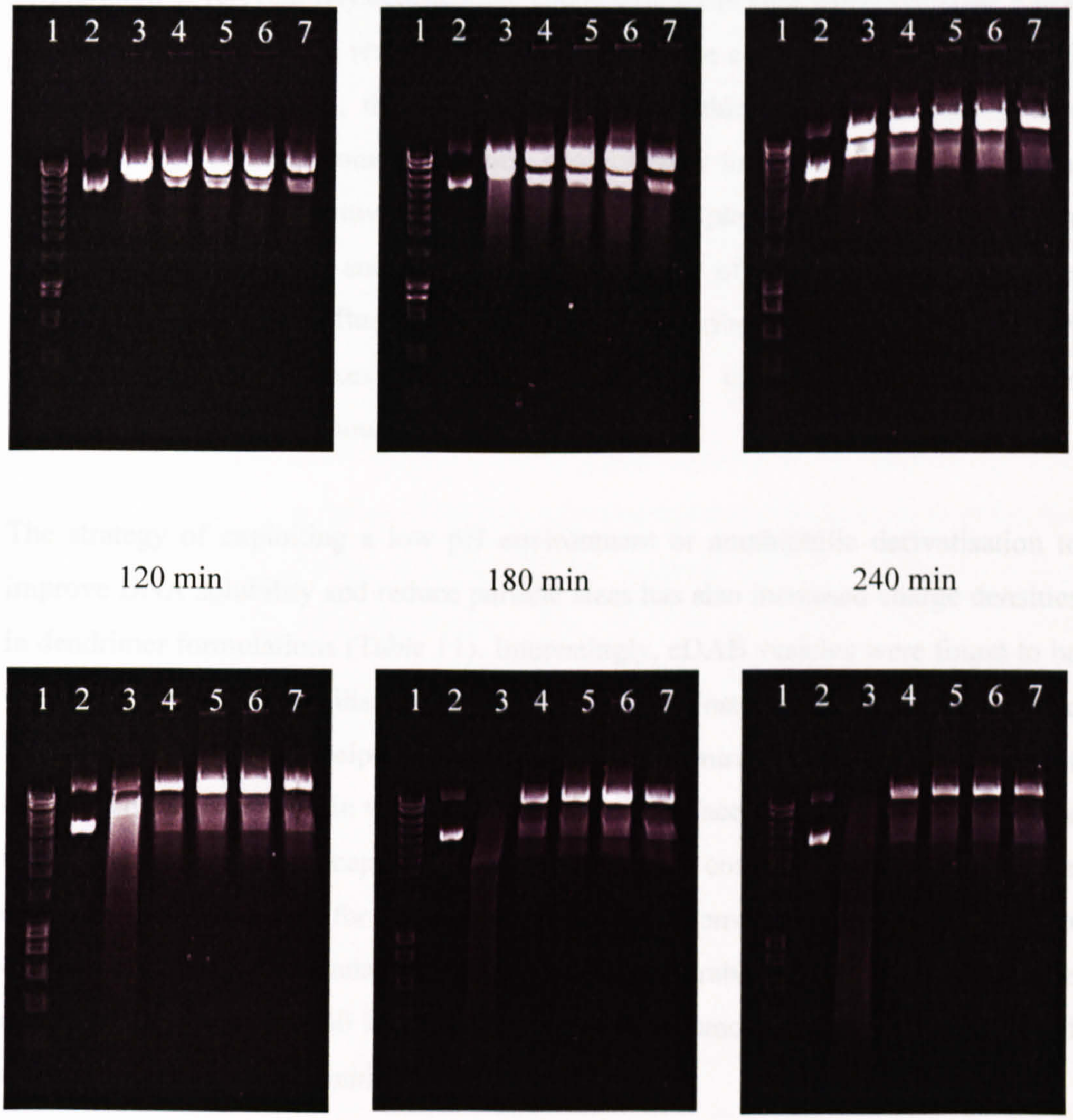

Figure 50 DNA degradation in the presence of 50% v/v foetal bovine serum (FBS) with carriers. Lane 1: Ladder. Lane 2: pDNA. Lane 3: pDNA + 50%FBS. Lane 4: + DAB-16-Am N: P ratio = 30, pH 7.4. Lane 5: + cDAB-16 N: P ratio = 30, pH 7.4. Lane 6: +cDAB-16 vesicles N:P ratio = 30 pH 7.4. Lane 7: + ExGen 500 N: P ratio = 6, pH 7.4.

4.5. Discussion and conclusions

Exploration of relevant physicochemical characteristics is vital when assessing a new gene delivery agent for *in vivo* use. There is likely to be a fine balance of parameters that are most favourable; the solubility of DNA within complexes, the size and surface charge of these complexes, their susceptibility to degradation by biological agents and the tendency towards precipitation under physiological salt conditions. The small dendrimer size and moderate surface charge of resulting DNA complexes appear to favourably influence the *in vivo* biodistribution profile [74] of PPI dendrimer-DNA complexes, which escape capture in the first capillary bed encountered upon intravenous injection – the lung.

The strategy of exploiting a low pH environment or amphiphilic derivatisation to improve DNA solubility and reduce particle sizes has also increased charge densities in dendrimer formulations (Table 11). Interestingly, cDAB vesicles were found to be the most effective at stabilising complexed DNA against aggregation events as the inclusion of the neutral helper lipid cholesterol concentrates the highest density of cationic charge measured in this study onto vesicle surfaces. Therefore, this may be a more pharmaceutically acceptable formulation at high concentrations of pDNA (for example, those required for *in vivo* applications). Conversely, it is possible that cetylated dendrimer formulations may not be favourable for *in vivo* use at the established charge ratio (30 N: P) as there may be enhanced interactions with blood components. This will be initially assessed in chapter 5.

The morphology of complexes as determined by TM AFM has been shown to be strongly dependent upon the composition of vector (Figure 43, Figure 44 & Figure 45). The DNA 'flowers' produced by the least hydrophobic species (DAB-16-Am) and the partial DNA rods and toroids formed after 15 min incubation in the presence of cDAB-16 support the widely held view that these varying structures are intermediates within the same pathway to equilibrium polyplex structure [41]. cDAB-16 vesicles, however, do appear to condense DNA the most efficiently,

evidenced by the most stable particle sizes (Figure 37) and tight 'star' morphologies (Figure 45).

Cetylated formulations displayed increasingly better resistance against electrostatic disruption by a synthetic GAG (Figure 48) than the parent dendrimer as the amount of hydrophobic component increased. However, it has been confirmed with confocal microscopy that GAGs taken up with complexes and free carrier molecules alter intracellular behaviours as well. For example, buffering and swelling of the endosome may be affected by the presence of acidic GAGs, leading to non-transcriptive compartmentalisation [210]. In this situation, complete relaxation of DNA is not required for transfection to be adversely affected but any change in mobility and size can affect uptake [210], therefore again it is very hard to describe an *in vitro – in vivo* correlation. Although essential that complexed DNA is protected from biological degradation, it must also be released through a reversal of this process into cell cytoplasm and nucleus. The ability of a synthetic GAG to release pDNA from the dendrimer derivatives also suggests that these carriers are suitable to examine for transfection ability.

Interestingly, neither complex structural features nor hydrophobicities were able to be correlated with DNase I or whole serum activity (Figure 49 & Figure 50). It seems rather that high cationic surface charge densities are protective of DNA, possibly due to the presence of a large reservoir of interacting free polycation in the incubation mixture. DAB-16-Am and its derivatives produced significant protection of plasmid DNA under these conditions, which was anticipated following the success of DAB-16-Am as an *in vivo* DNA carrier. The reduced susceptibility to electrostatic disruption of the cDAB-16 complexes by GAGs could ultimately lead to enhanced DNA preservation *in vivo*.

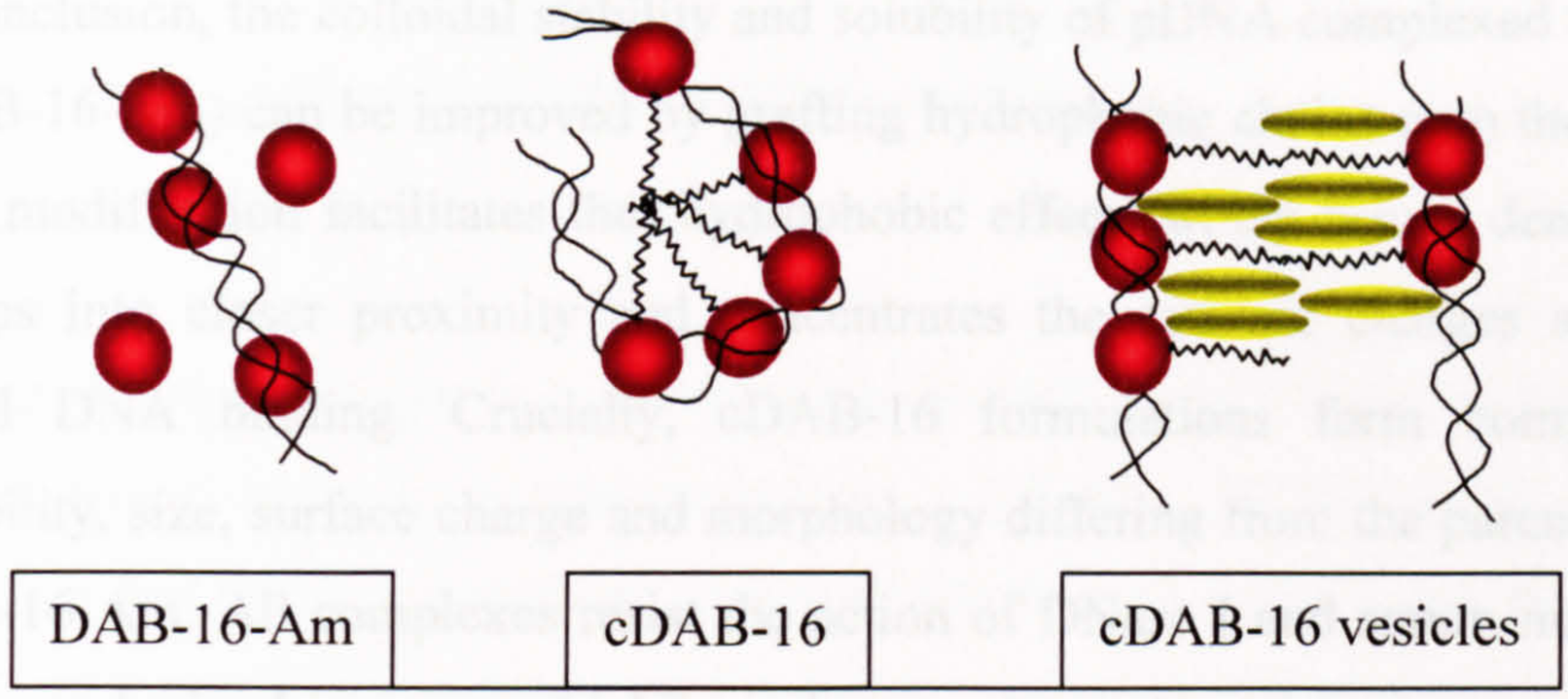

Figure 51 Suggested initial binding configurations for the three dendrimer species based on studies in Chapter 3 and Chapter 4.

Using structural and chemical information gathered about the three dendrimer species investigated, and established theory about the internal packing of cationic lipid-DNA complexes [154], the above modes of DNA binding are speculated (Figure 51). Dunlap *et al.* suggest from their observations that the threshold point of condensation is as a result of cation crosslinking i.e. electrostatic bridging of adjacent helices by multivalent cations [183] so it should not be assumed that binding of DAB-16-Am remains uncooperative in later stages of complexation. It is hypothesised that the slow equilibrium rearrangement observed in Eth Br intercalation studies involves approach of amine groups (primary or tertiary) to DNA phosphate groups on separate strands, extending intermolecular bridging and condensation. As previously mentioned, cetylation facilitates this process through long-range coordination of hydrophobic domains.

In conclusion, the colloidal stability and solubility of pDNA complexed with PPI G3 (DAB-16-Am) can be improved by grafting hydrophobic chains onto the dendrimer. This modification facilitates the 'hydrophobic effect' which brings dendrimer head groups into closer proximity and concentrates the cationic charges available for initial DNA binding. Crucially, cDAB-16 formulations form complexes with solubility, size, surface charge and morphology differing from the parent dendrimer, DAB-16-Am. All complexes resist the action of DNase I and serum nuclease upon DNA and dendrimer amphiphiles show enhanced resistance to electrostatic disruption by a model glycosaminoglycan. These features may allow links to be forged between the physicochemical properties of the dendrimers and their biological effects.

5. In vitro biological characterisation

5.1. Introduction

Cells from original tissue (e.g. a tumour), a primary culture or from a cell strain can be cultured in an artificial environment as a cell line. Termed tissue culture, this technique has found especial use in investigations into intracellular processes (e.g. DNA replication, transcription and translation) and extracellular activities (e.g. drug-cell and cell-cell interactions) [230]. In this work it forms the basis of an *in vitro* model of likely *in vivo* conditions. The major advantage of tissue culture is the ease of use in screening tests with many variables and replicates. A homogenous cell monolayer adhered to a substrate can be directly exposed to a reagent at defined concentrations with constant control of the physicochemical environment and (pH, temperature, partial gas tensions) and physiological conditions (nutrient concentrations) [230].

Human tumours (malignantly transformed cells) can give rise to continuous, immortalised cell lines. These are insensitive to density limitation of growth and often tumourigenic themselves. The origin of the bulk population lies with a small pool of transformed stem cells which retain significant phenotypic elements of the parental cells. However, phenotypic instability is a problem with many continuous cell lines as subculture (propagation) can produce differential populations; therefore even immortalised cell lines have a finite lifetime [230]. Also, many differences in cell behaviour from those *in vivo* arise as a result of their two-dimensional geometry and a loss of certain cell-cell interactions and wider nervous and endocrine control. However, with appreciation of these differences, immortalised tissue culture is a valuable tool [230].

The aim of this chapter is to assess the *in vitro* biological effects of DAB-16-Am and its amphiphilic derivatives before advancing to *in vivo* studies. The haemocompatibility of each dendrimer species will be examined, along with cytotoxic effects and the efficiency of transfection of three immortalised cell lines:

A431 (skin sarcoma), PC-3 (prostate carcinoma) and B16 F10 (malignant melanoma). Haemocompatibility studies take the form of an erythrocyte lysis assay; cytotoxicity will be assessed using an MTT ((3-(4, 5-Dimethylthiazol-2-yl)-2, 5-diphenyltetrazolium bromide) reduction assay. ExGen 500 will serve as a 'gold standard' positive control for *in vitro* transfection of these cell lines with plasmids containing either β-galactosidase or luciferase reporter genes.

5.1.1. Biocompatibility

Biocompatibility testing of new bioactive molecules required before licensing is extensive. Many tests for toxic effects may be carried out in animals, although the principle of the three 'Rs' was established almost fifty years ago – replacement, reduction and refinement [231]. There is pressure to at least perform part of toxicity testing *in vitro*. The establishment of specialised cell cultures has made this possible [230] as long as the differences between the *in vitro* and *in vivo* responses are appreciated (e.g. the influence of pharmacokinetic effects and systemic responses).

5.1.1.1. Haemocompatibility

The first concern for any agent that is to be injected intravenously must be whether it is blood-compatible. Intravenous (i.v.) injection of polycation can result in interactions with blood components such as erythrocytes and plasma proteins [232] and has the potential to cause cell aggregation and embolism as well as cell lysis. The extent of cell damage has been shown to be dependent not only on the surface charge density of the polycation [61, 233-235] but also the distribution of anionic domains on the cell surface [234], therefore erythrocytes are extremely susceptible to this damage. The measurement of disruption of the erythrocyte lipid bilayer often takes the form of a UV-Vis spectrophotometric assay [39, 232, 235, 236] which monitors haemoglobin release via red light absorbance at 570nm. Cationic amphiphiles have long been implicated in toxic bilayer effects [237] therefore it is necessary to examine the haemolytic potential of the amphiphilic forms of DAB-16-Am.

5.1.1.2. Cytotoxicity

Toxicity is a complex event *in vivo*, so most assays determine effects at the cellular level via cytotoxicity measurements. The induction of cell signalling or other cell interactions that may give rise to an inflammatory response, for example, are very difficult to detect, whereas gross tests of cell death are cheap, relatively facile and reproducible [230]. (3-(4,5-Dimethylthiazol-2-yl)-2,5-diphenyltetrazolium bromide (MTT) reduction assay is one of the most widely used methods of quantifying the toxicity of novel polymeric delivery systems [39, 59, 61, 64, 143, 236, 238]. It was first described as a technique by Mosmann in 1983 [239] who used it as an indirect measure of cell viability in immunological studies. The MTT reagent is a water-soluble, yellow dye containing a tetrazolium ring which is cleaved by mitochondrial dehydrogenases in living cells to produce an insoluble, purple product. These purple formazan salts can be dissolved in a suitable organic solvent (in this work, DMSO) to give a peak intensity at 570nm which reflects the viable (metabolically active) cell number within the sample.

This system has since been optimised further. After treatment with the agents under investigation cell populations are given opportunity to proliferate; distinguishing between true cell death and metabolic perturbation [230]. Cell densities used are optimised so that non-treated controls do not reach a growth plateau within the time frame of the experiment, as cell sensitivity to an agent would then be underestimated [240]. As the uptake of MTT is maximal in metabolically active cells [240-242] any nutrient deficit prior to analysis should be addressed with replacement of exhausted culture medium [243]. Sufficient MTT solution must be used so that, again, cell sensitivity is not underestimated [244]. Another important factor investigated by Plumb *et al.* is the pH environment of the dissolved formazan product, which alters with the metabolically active cell density within each well. They recommend the addition of a glycine buffer to solublised formazan products producing a final solution pH of 10.5. At this pH only a single absorption maxima is produced at 570nm, unlike at lower pH values when the peak can split into two components, which can again cause the extent of dye reduction to be underestimated. Using this

method a positive correlation between cell number and formazan production is established independent of cell densities, which is supremely important.

5.1.2. Cell transfection

As discussed in chapter 1, transfection refers to the process of introducing foreign DNA into host cells resulting in the expression of the desired protein by the host organism. Genetic reporters are commonly used to study gene expression, two widely used reporter genes are β-galactosidase and firefly luciferase [15, 42, 59, 64, 73, 74, 77, 83, 85, 123, 158, 166, 167, 245-247]. Some of the parameters that have been shown to influence non-viral gene transfer are outlined in section 4.1. The most successful methods exploit knowledge of the mechanism of gene transfer and design carriers with features to overcome key biological barriers. One important choice is the plasmid construct and within this, the selection of a promoter.

For cell transfection with firefly luciferase, an enhanced pGL3 plasmid construct is selected with non-specific, strong promoters: in this work, CMV (cytomegalovirus) and ElF1α/HTLV (Elongation Factor One Alpha linked to a Human T-cell Lentivirus) are compared. pCMV is ubiquitously used to enhance transcription of reporter genes; ElF1α/HTLV is lesser used although it has found application in transfection of resistant stem cell populations [248, 249]. Human ElF1α itself has been implicated in DNA replication and severing of microtubules [250]. The two plasmid constructs to be compared in the luciferase transfection assay are in Figure 52 & Figure 53. The structure of pCMVsport- β-galactosidase can be found in section 3.3.1.

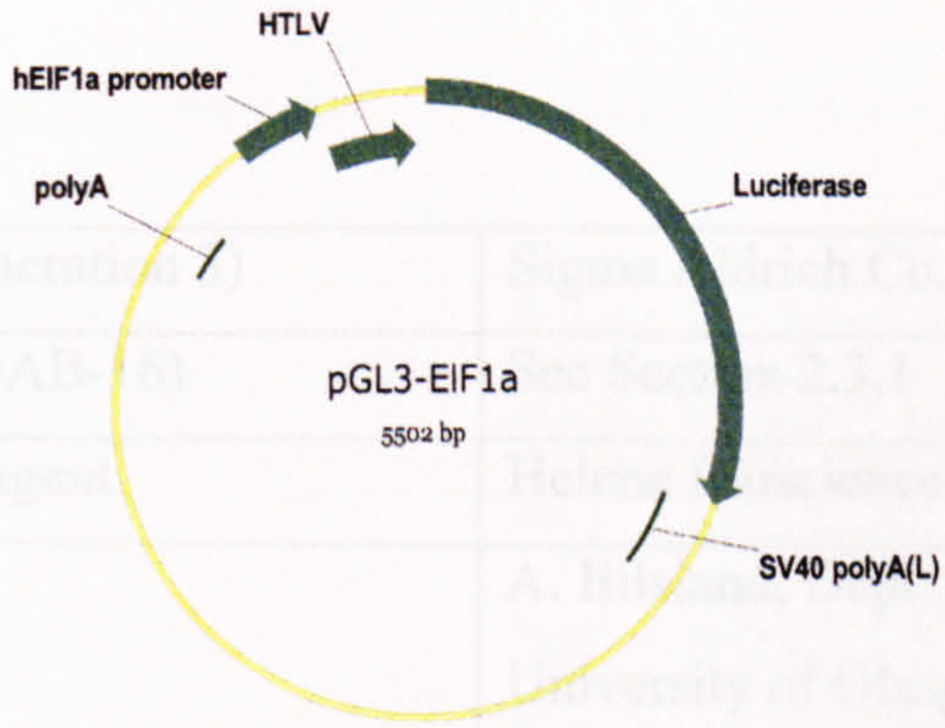

Figure 52 The EIF1α/HTLV Luc (enhanced) expression plasmid

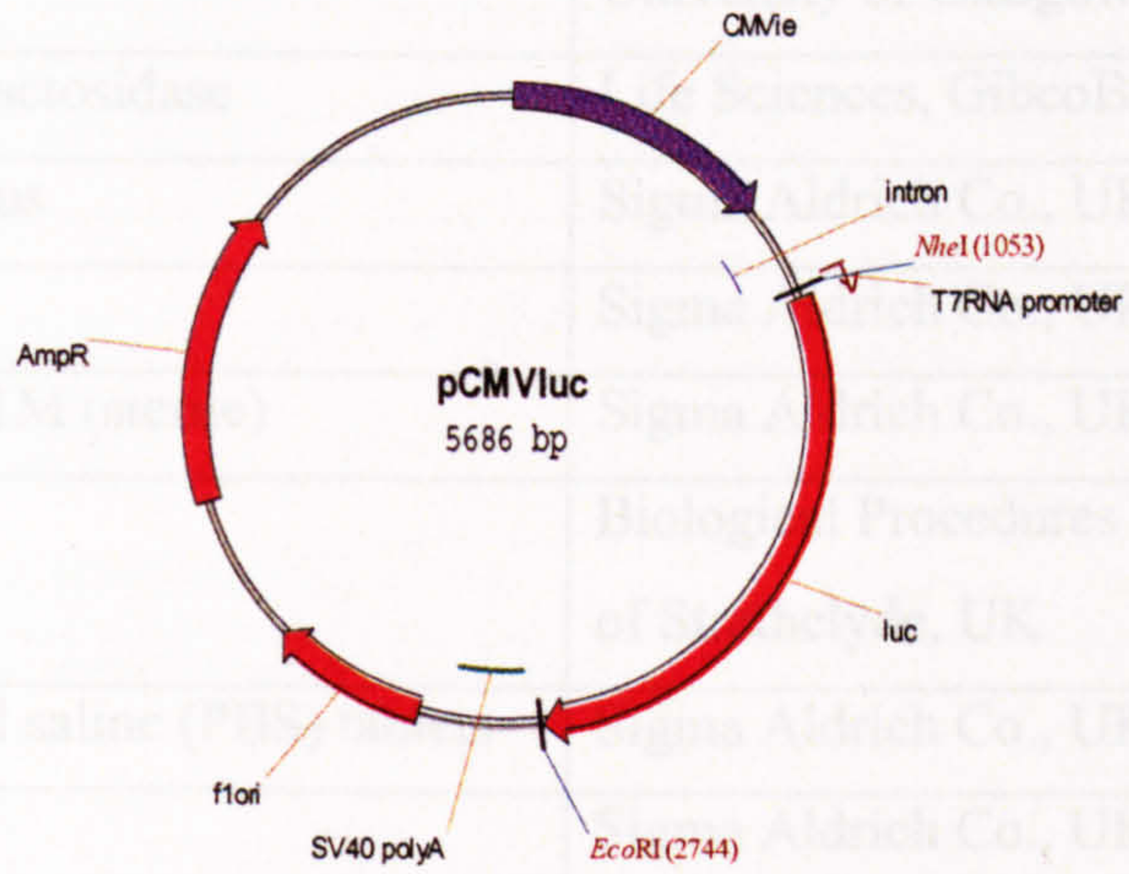

Figure 53 The CMV Luc (enhanced) expression plasmid

Cell transfection efficiencies are adjusted according to the average level of protein produced by the cells, gaining an indirect measure of cell viability and a level of reporter protein production proportionate to the metabolic activity of the cell overall. Protein determination using bicinchoninic acid relies upon the formation of a Cu^{2+} - protein complex which directly induces reduction of Cu^{2+} to Cu^{1+} and the formation of a purple BCA-Cu^{1+} complex under alkaline conditions [251, 252]. The BCA assay is more sensitive than biuret or Lowry procedures and less variable than the Bradford assay. Importantly, it has less susceptibility to detergents, although their inclusion should be minimised.

5.2. Materials

DAB-16-Am (PPI Generation 3)	Sigma Aldrich Co., UK
cDAB-16 (cetylated DAB-16)	See Section 2.3.1
ExGen 500 in vitro reagent	Helena Biosciences, UK
pEIF1α/HTLV-Luc	A. Bilsland, Dept. Medical Oncology, University of Glasgow
pCMV-Luc	M. Brown, Dept. Medical Oncology, University of Glasgow
pCMVsport β-Galactosidase	Life Sciences, GibcoBRL, UK
Dextrose, anhydrous	Sigma Aldrich Co., UK
Cholesterol	Sigma Aldrich Co., UK
HEPES free acid, 1M (sterile)	Sigma Aldrich Co., UK
Fresh rat blood	Biological Procedures Unit, University of Strathclyde, UK
Phosphate buffered saline (PBS) tablets	Sigma Aldrich Co., UK
Triton X-100	Sigma Aldrich Co., UK
Polysorbate (TWEEN®) 80	Sigma Aldrich Co., UK
A431 skin sarcoma cells	ATCC, CRL-1555
PC-3 prostate carcinoma cells	ATCC, CRL-1435
B16 F10 malignant melanoma cells	ATCC, CRL-6475
Foetal Bovine Serum (FBS)	Life Sciences, GibcoBRL, UK
Dulbecco's Modified Eagles Medium (DMEM)	Life Sciences, GibcoBRL, UK
L-glutamine (2mM)	Life Sciences, GibcoBRL, UK
Trypsin	Life Sciences, GibcoBRL, UK
EDTA	Life Sciences, GibcoBRL, UK
Passive Lysis Buffer 5x (PLB)	Promega Ltd, UK
Bicinchoninic acid (MicroBCA) protein assay solution	Pierce, IL, USA
Copper (II) sulphate pentahydrate 4%	Sigma Aldrich Co., UK

solution	
o-nitrophenyl β-D-galactopyranoside (ONPG)	Sigma Aldrich Co., UK
Recombinant β-Galactosidase	Sigma Aldrich Co., UK
Sodium phosphate (dibasic)	Sigma Aldrich Co., UK
Magnesium chloride	Sigma Aldrich Co., UK
β-mercaptoethanol (thioglycol)	Sigma Aldrich Co., UK
Luciferase Assay Reagent	Promega Ltd, UK
QuantiLum® Recombinant Luciferase	Promega Ltd, UK
Bovine Serum Albumin (BSA)	Sigma Aldrich Co., UK
Dimethyl sulfoxide (DMSO)	Fisher Scientific, UK
Glycine	Fisher Scientific, UK
Sodium chloride (NaCl)	Sigma Aldrich Co., UK
(3-(4,5-Dimethylthiazol-2-yl)-2,5-diphenyltetrazolium bromide (MTT)	Sigma Aldrich Co., UK

Table 12 Materials and suppliers used in Chapter 5

5.3. Methods

5.3.1. Cell culture maintenance (A431, PC-3, B16 F10)

Cell lines were grown aseptically in DMEM supplemented with 10% FBS and 1% L-glutamine under 10% CO_2 (A431) or 5% CO_2 (PC-3 and B16-F10) in air at 37°C and 95% relative humidity. Cell lines were subcultured via trypsinisation and EDTA chelation every 7 days with the exception of PC-3 cells which required subculture every 3 days. Experiments were performed on cells with morphologically confirmed identities, subcultured between four and twelve times.

5.3.2. pDNA synthesis and purification

Plasmids (pCMVsport β-Gal, pCMV-Luc and pEIF1α/ HTLV-Luc) were propagated and purified as previously described in section 3.3.1.

5.3.3. Preparation of complexes

All complexes were formed or diluted in DMEM for cell viability and transfection studies (unless stated otherwise) and prepared in PBS for erythrocyte lysis assay as described in section 3.3.3.

5.3.4. Haemocompatibility assay

Rat blood (freshly drawn, 5mL) was diluted to a final volume of 50mL in phosphate buffered saline (PBS, pH 7.4) before centrifugation at 1000g for 10 min at 4°C (Hermle Z323K centrifuge, Hermle Labortechnik, Germany). The resulting erythroctye pellet was washed twice with PBS under centrifugation then weighed and resuspended 3% w/v in PBS.

Carriers with or without DNA were prepared in PBS at concentrations ranging from 0.001 – 10 $mg.mL^{-1}$ in PBS, dependent on solubility. Each preparation (80μL) was added 1: 1 v/v to fresh erythrocyte suspension in a 96 well microtitre plate (for each concentration, n = 6 wells). Triton X-100 (1% v/v) and PBS were positive and

negative controls respectively. The haemolytic profile of polysorbate (TWEEN®) 80, a popular solubilising agent included in formulations for intravenous injection [253], was also determined for the purposes of comparison. Four hours of incubation at 37°C preceded a further round of centrifugation to pellet erythrocyte debris, after which the supernatant (80μL) from each well was transferred to fresh microtitre plates and the absorbance of each well read at 570nm (EL_x808 plate reader, Bio-tek Instruments Inc., USA).

Results obtained were expressed as a percentage of the haemolytic activity of Triton X-100 (designated 100%) normalised to the haemolysis produced by PBS (designated 0%) (Equation 3) where A = absorbance:

$$\% \text{ haemolysis} = [(A_{sample} - A_{PBS})/(A_{Triton\ X\text{-}100} - A_{PBS})].100 \qquad \text{Equation 3}$$

5.3.5. MTT reduction assay

As a measure of cytotoxicity, the 50% inhibitory concentration (IC_{50}) is well established and this is the value to be determined for each carrier, alone or complexed with pDNA, using the MTT reduction assay.

A431 and PC-3 cells (1000 cells/ well) and B16 F10 cells (500 cells/ well) were seeded into each well of a 96-well microtitre plate in 200 μL DMEM supplemented with 10% FBS and 1% L-glutamine. The cells were then incubated for 72 h under 10% CO_2 (A431) or 5% CO_2 (PC-3 and B16-F10) in air at 37°C and 95% relative humidity.

Solutions of DAB-16-Am and its amphiphilic forms (0.05 – 1000 $\mu g.mL^{-1}$) were prepared by serial dilution into DMEM. Carrier-DNA complexes were prepared as section 3.3.3. Each preparation (200 μL) was added to five replicate wells (n = 5) per plate after aspiration of growth media. The cells were then further incubated under the conditions specified above for 4 h. Triton X-100 (20% v/v) and DMEM formed the positive and negative controls respectively. After incubation the treatments were aspirated off and replaced with fresh DMEM (200 μL) supplemented with 10% FBS

and 1% L-glutamine. Incubation for a further 96 h preceded the addition of MTT reagent (50 μL, 5 $mg.mL^{-1}$) and incubation for 4 h in the dark at 37°C. Finally, all solutions were aspirated; the cells were lysed using DMSO (200 μL) and 25 μL Sorensen's glycine buffer (0.1 M glycine, 0.1 M NaCl, pH 10.5) added before reading plates at A = 570nm (E_{max} plate reader, Molecular Devices Ltd., UK). Results were expressed as percentage cell viability for each sample concentration (Equation 4):

$$\% \text{ cell viability} = [A_{sample} - A_{Triton\ X\text{-}100})/\ (A_{DMEM} - A_{Triton\ X\text{-}100})].100 \qquad \textbf{Equation 4}$$

IC_{50} values were obtained from sigmoidal fitting of Log (base 10) plots of concentration versus percentage cell viability for each carrier (as an average of at least three replicate plates) using Microcal Origin® Version 7.

5.3.6. Reporter gene assays

A431 cells (10,000 cells/ well), PC-3 cells (10,000 cells/ well) or B16 F10 cells (7500 cells/ well) or were seeded into 96-well microtitre plates and maintained in DMEM supplemented with FBS (10% v/v) and L-glutamine, 2mM (1% v/v) for 24 h under the prescribed conditions in section 5.3.1. Dendrimer-DNA complexes at a range of N: P ratios (1 - 30) were prepared in DMEM (serum-free) or HBD (pH 7.4), depending upon the application, at 10x the final concentration required. Complexes (20 μL) were inoculated into wells containing DMEM or DMEM: FBS 1: 1 v/v (200 μL; 0.2, 0.5 or 1μg pDNA/ well) and incubated with cells for 4 h under the same conditions. All were treated in replicates of 5 wells per plate (n = 5). ExGen 500 (6 N: P, 0.3 μg pDNA/ well) and DMEM (200 μL) served as positive and negative controls respectively. pDNA (1μg/ well) was included for further comparison.

Treatments were aspirated off and replaced with DMEM supplemented with FBS and L-glutamine as above (200 μL) and the cells incubated for a further 48 h again under the specified conditions. In all cases the treated cells were washed three times with sterile PBS (200 μL) before lysis with PLB 1x (50 μL) at 37°C for at least 20 min (lysis confirmed microscopically).

5.3.6.1. β-Galactosidase activity

To assess β-galactosidase activity following cell uptake of pCMVsport β-galactosidase plasmid a photometric assay was employed, utilising the coloured cleavage product of the action of β-galactosidase on the substrate o-nitrophenyl β-D-galactopyranoside (ONPG).

The lysates from section 5.3.6 were transferred to new 96-well microtitre plates containing 50 μL ONPG (1.33 $mg.mL^{-1}$) in 2x assay buffer (sodium dibasic phosphate 60mM; magnesium chloride, 1mM; β-mercaptoethanol 50mM; pH 7.3). Plates were then incubated for 2 h in the dark at 37°C before reading the absorbance of each well at 405nm using a plate reader (E_{max} plate reader, Molecular Devices Ltd., UK). Results were compared with an on-plate standard curve (0 – 5 mU recombinant β-galactosidase).

5.3.6.2. Firefly Luciferase activity

Firefly luciferase (61 kDa protein) catalyses the oxidation of luciferin using $ATP.Mg^{2+}$ as a co-substrate; as a result of this reaction light is produced by converting the chemical energy of oxidation through an electron transition. Assay of cell lysates for luciferase activity following cell transfection with luciferase expression plasmid was carried out according to the Luciferase Assay System (microtitre plate) protocol provided by Promega Ltd.

Cell lysate (20 μL) was transferred into a white luminometer plate and protected from light. A standard curve was included on each plate containing 10^{-20} – 10^{-12} mol recombinant luciferase in 20 μL PLB 1x supplemented with $1mg.mL^{-1}$ BSA. Each well was read for 10 s with 2 s measurement delays using a luminometer (Veritas® Microplate Luminometer, Turner Biosystems, USA) immediately after injection of 100 μL Luciferase Assay Reagent (proprietary formula, Promega Ltd). Reported luciferase activities were normalised with respect to total cell protein (relative light units per microgram cell protein per second; RLU/ μg/ s).

5.3.6.3. Total cell protein

Total cell protein was measured using a microBCA assay. Working assay reagent was prepared according to the manufacturer's instructions (Pierce, USA). Cell lysate (10 µL) from section 5.3.6 was diluted 10x onto a second microtitre plate (final volume assayed = 25 µL, PLB 0.1x). Bovine serum albumin (BSA) 0 – 800µg/mL^{-1} in PLB 0.1x formed a standard curve. Working assay reagent (200 µL; sample: reagent ratio 1: 8) was added, the plates sealed and incubated at 37°C for 2h before reading the absorbance of each well at 570nm (E_{max} plate reader, Molecular Devices Ltd., UK).

5.3.7. Statistical analysis

Statistical significances were assessed using the statistical software package Minitab® (version 10) using one-way analysis of variance (one-way ANOVA).

5.4. Results

5.4.1. Haemocompatibility

A comparison of haemolytic potential was performed using the previously described haemolysis assay and the carriers were ranked as follows: TWEEN® 80 > cDAB-16 > cDAB-16 vesicles > DAB-16-Am (Figure 54). The fact that PPI dendrimer formulations are haemolytic has been reported [236]. The toxicity of other polycation species such as PLL and PEI are well documented [39].

In this work, the first measured concentration of carrier that exceeds 20% haemolysis is deemed to be too toxic for i.v. injection. With respect to free cDAB-16, the final concentration in the circulation should not exceed 0.1mg.mL^{-1}; however DAB-16-Am and cDAB-16 vesicles could be safely administered up to a final concentration of 0.5mg.mL^{-1} (Figure 54). TWEEN® 80 is included for comparison, a non-ionic detergent commonly used as a stabilising agent in drug formulations for injection [253]; this could not be recommended for use at a concentration above that which would deliver more than 0.01mg.mL^{-1} into the circulation.

These data do not comment directly upon aggregation effects caused by the agents, however, lytic and aggregation events are both likely to arise as a result of carrier electrostatic interaction with anionic species in the cell membrane [110]. Some membrane perturbation will exist prior to detectable lysis according to the polycation 'flip flop' theory of Kabanov and Yaraslov [110]. Anionic lipids in a model cell membrane (a vesicle) were shown to rearrange themselves within the membrane in order to maintain contact with adsorbed polycations, although the biological significance of this is unclear. It was at a critical concentration of adsorbed polycation however that a reversible disruption and aggregation of the vesicles occurred. Hydrophobic domains present in cationic amphiphilic species caused irreversible events, possibly due to permanent bilayer incorporation, explaining the increased haemolytic potential of cDAB-16. cDAB-16 vesicles are likely to retain biocompatibility due to stabilisation of these flexible hydrophobic domains via the inclusion of cholesterol and assembly into stable vesicle systems.

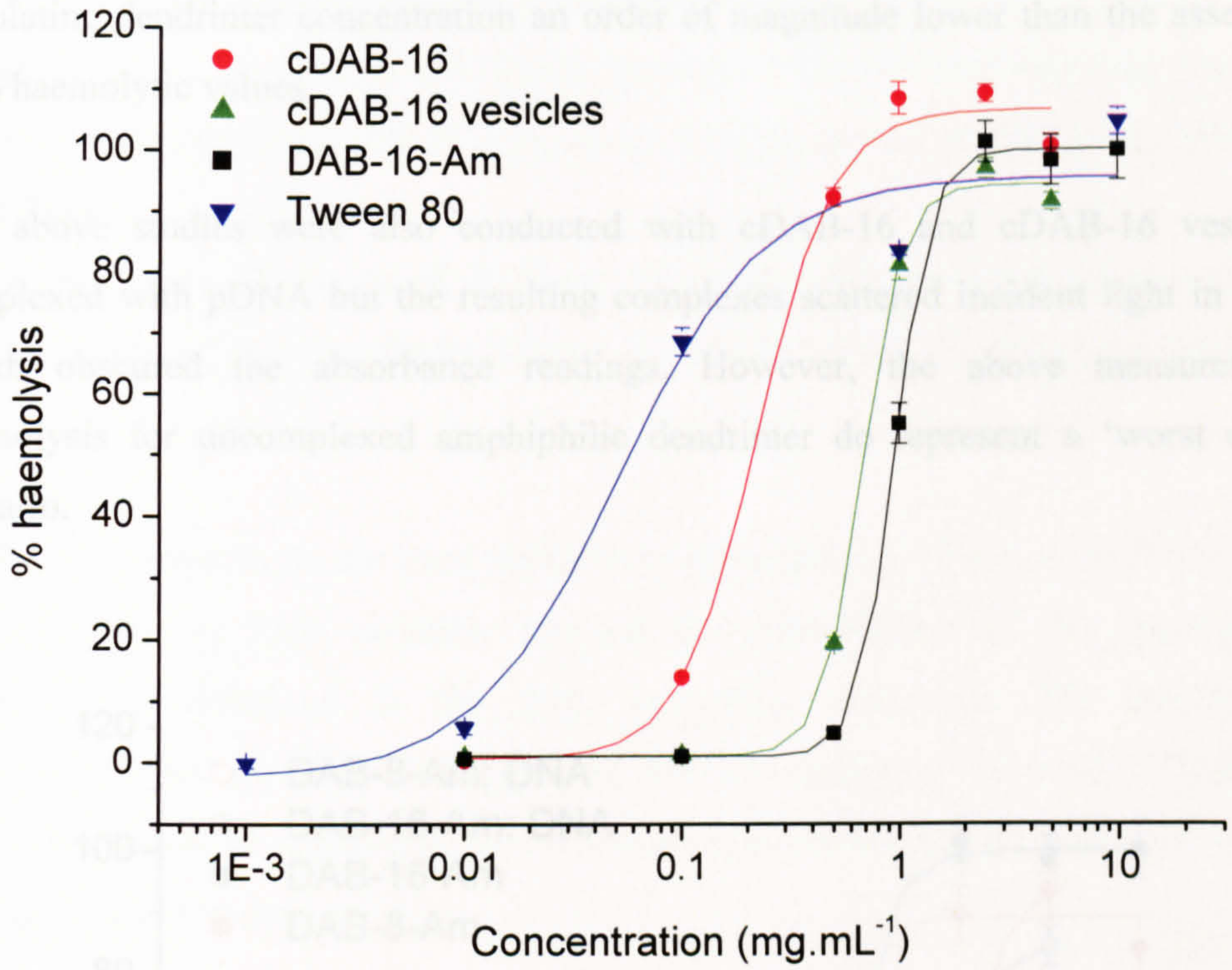

Figure 54 Mean ± SE haemolytic activity (%) of carriers at concentrations from 0.001 – 10 mg.mL^{-1}. 0% = PBS solution, 100% = Triton-X 100 1% v/v (n=3).

Further to this, the generation 2 PPI dendrimer, DAB-8-Am, was included in the experiment to determine the effect of an increase in dendrimer generation (a doubling from eight to sixteen surface primary amines) on haemolytic potential (Figure 55). Increasing dendrimer generation has been shown previously in cytotoxicity studies to enhance cell damage [59, 74]. The dendrimers were examined alone or complexed with pDNA (pCMVsport-β-galactosidase) at 30 N: P.

DAB-8-Am produced improved haemocompatibilities when compared with DAB-16-Am (below 20% haemolysis at 1 mg.mL^{-1} versus 0.5 mg.mL^{-1}). The haemocompatibility of both dendrimers was improved upon complexation with pDNA and neither complexed nor free lower generation PPI dendrimers pose a haemolytic risk at the likely concentrations required in the blood for therapeutic

effect. DAB-16-Am was previously administered to nude mice at a dose of 12.5mg/kg [53]; therefore, assuming a total blood volume of 2mL, this equates with a circulating dendrimer concentration an order of magnitude lower than the assessed 20% haemolytic values.

The above studies were also conducted with cDAB-16 and cDAB-16 vesicles complexed with pDNA but the resulting complexes scattered incident light in PBS which obscured the absorbance readings. However, the above measures of haemolysis for uncomplexed amphiphilic dendrimer do represent a 'worst case' scenario.

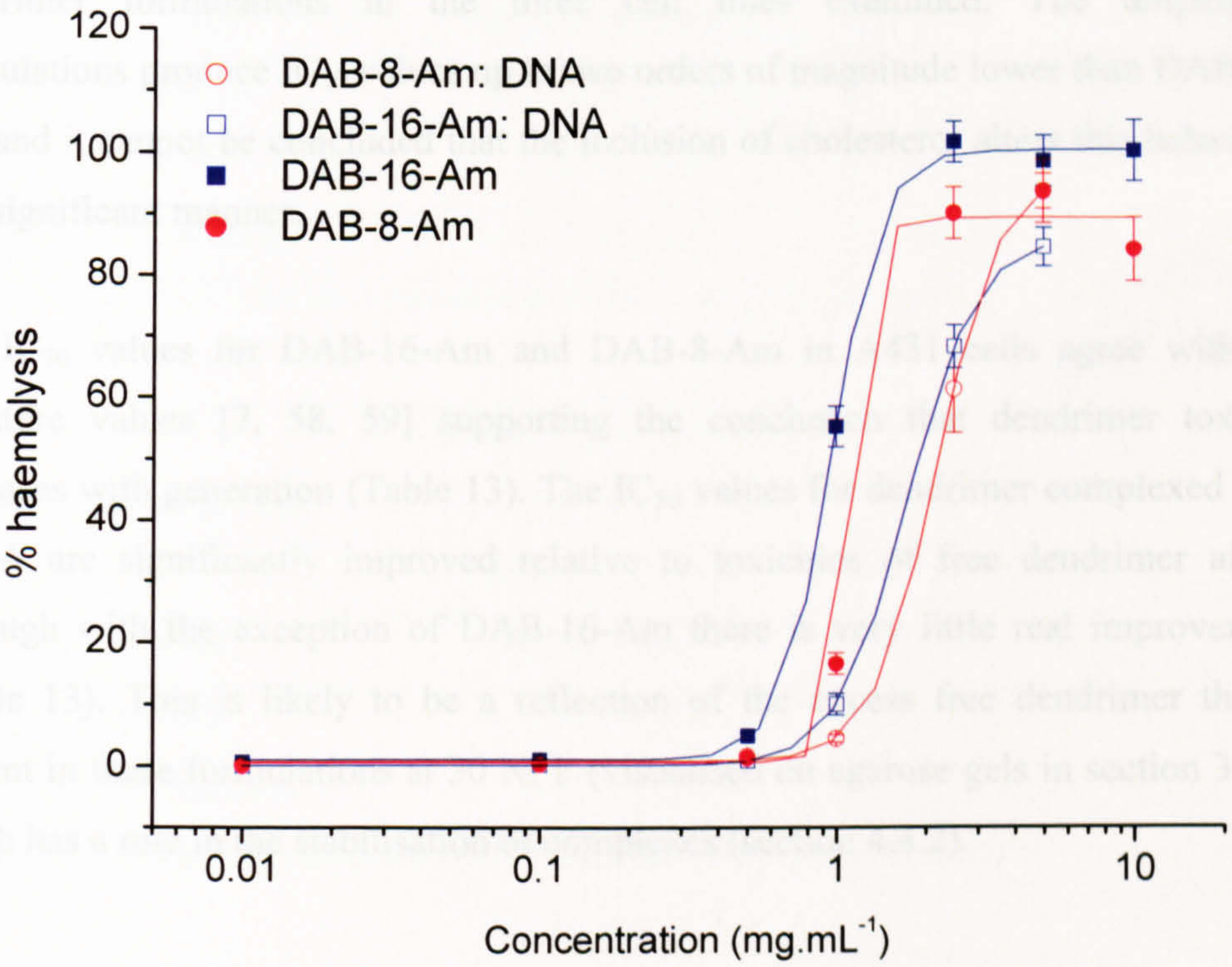

Figure 55 Mean ± SE haemolytic activity (%) of lower generation PPI dendrimers free or complexed with pDNA (30 N: P) (n=3)

5.4.2. Cytotoxicity

The MTT reduction assay was used to determine 50% cell viability (CV) (IC_{50}) values for A431, PC-3 and B16 F10 cells incubated with PPI dendrimers for four hours at least in triplicate. The IC_{50} values are summarised below (Table 13, Table 14 & Table 15) and plotted in
Figure 56, Figure 57, Figure 58 & Figure 59. Overall, the dendrimer species can be ranked in order of cytotoxicity as follows: cDAB-16 ≥ cDAB-16 vesicles > DAB-16-Am.

A431 cells appear to be the most sensitive to the inhibitory effects of DAB-16-Am, however there is little variation between the cytotoxicities of the amphiphilic dendrimer formulations in the three cell lines examined. The amphiphile formulations produce IC_{50} values up to two orders of magnitude lower than DAB-16-Am and it cannot be concluded that the inclusion of cholesterol alters this behaviour in a significant manner.

The IC_{50} values for DAB-16-Am and DAB-8-Am in A431 cells agree with the literature values [7, 58, 59] supporting the conclusion that dendrimer toxicity increases with generation (Table 13). The IC_{50} values for dendrimer complexed with pDNA are significantly improved relative to toxicities of free dendrimer alone, although with the exception of DAB-16-Am there is very little real improvement (Table 13). This is likely to be a reflection of the excess free dendrimer that is present in these formulations at 30 N: P (visualised on agarose gels in section 3.4.4) which has a role in the stabilisation of complexes (section 4.4.2).

Dendrimer species	Mean IC_{50} value ± SE ($\mu g.mL^{-1}$) free dendrimer	Mean IC_{50} value ± SE ($\mu g.mL^{-1}$) 30 N: P with pDNA
DAB-8-Am	202.54 ± 13.78	-
DAB-16-Am	43.12 ± 3.57	92.70 ± 11.87
cDAB-16	7.61 ± 0.35	8.77 ± 0.34
cDAB-16 vesicles	10.66 ± 0.39	17.24 ± 0.36

Table 13 Mean IC_{50} values for dendrimer formulations in A431 cells (n=3)

Dendrimer species	Mean IC_{50} value ± SE ($\mu g.mL^{-1}$) free dendrimer
DAB-16-Am	417.54 ± 637.87
cDAB-16	12.20 ± 0.55
cDAB-16 vesicles	13.71 ± 1.05

Table 14 Mean IC_{50} values for dendrimer formulations in PC-3 cells (n=3)

Dendrimer species	Mean IC_{50} value ± SE ($\mu g.mL^{-1}$) free dendrimer
DAB-16-Am	372.64 ± 10.06
cDAB-16	6.98 ± 0.18
cDAB-16 vesicles	9.71 ± 0.22

Table 15 Mean IC_{50} values for dendrimer formulations in B16 F10 cells (n=3)

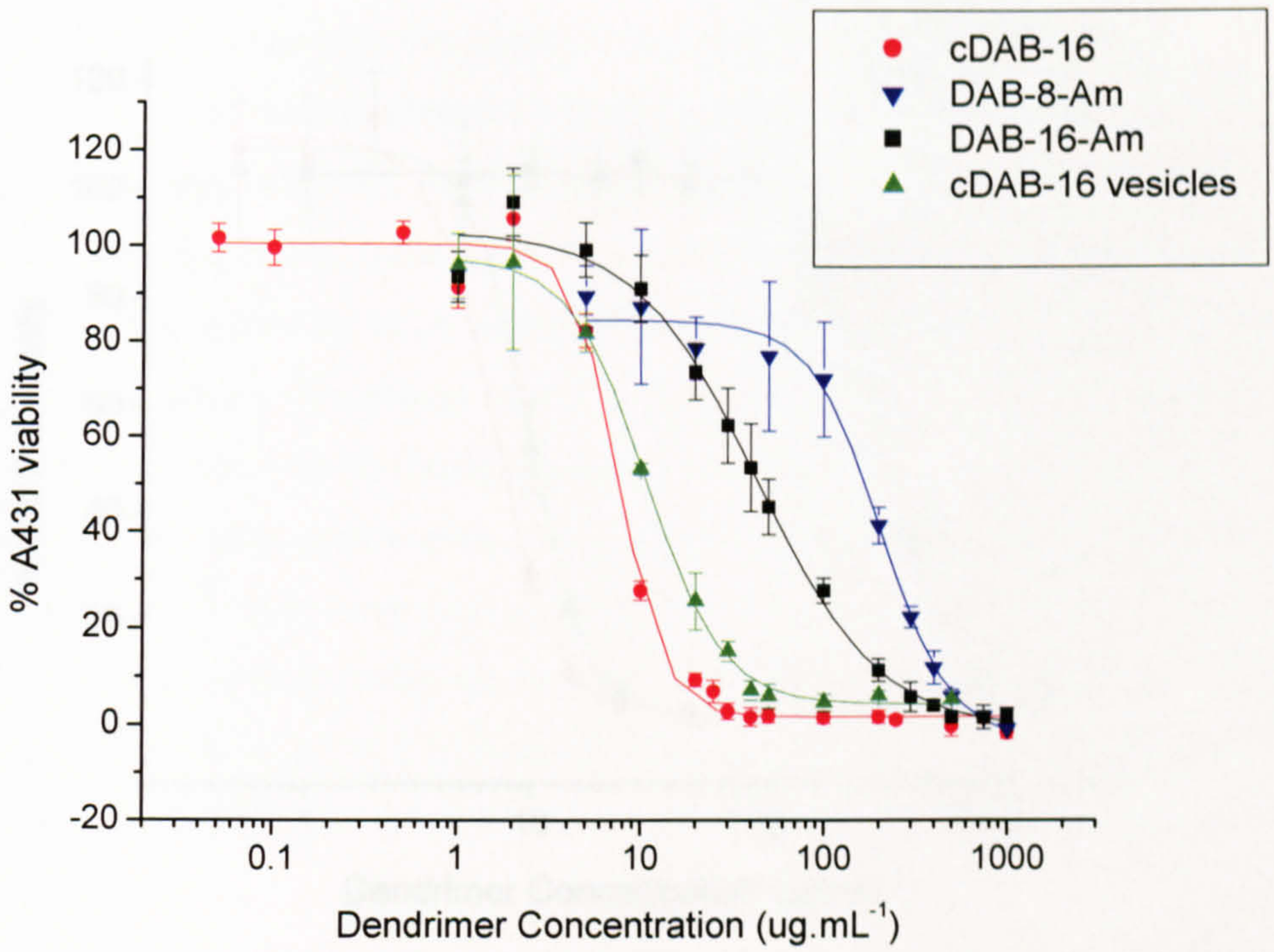

Figure 56 Mean ± SE A431 % cell viability (CV) versus free dendrimer concentration (n=3)

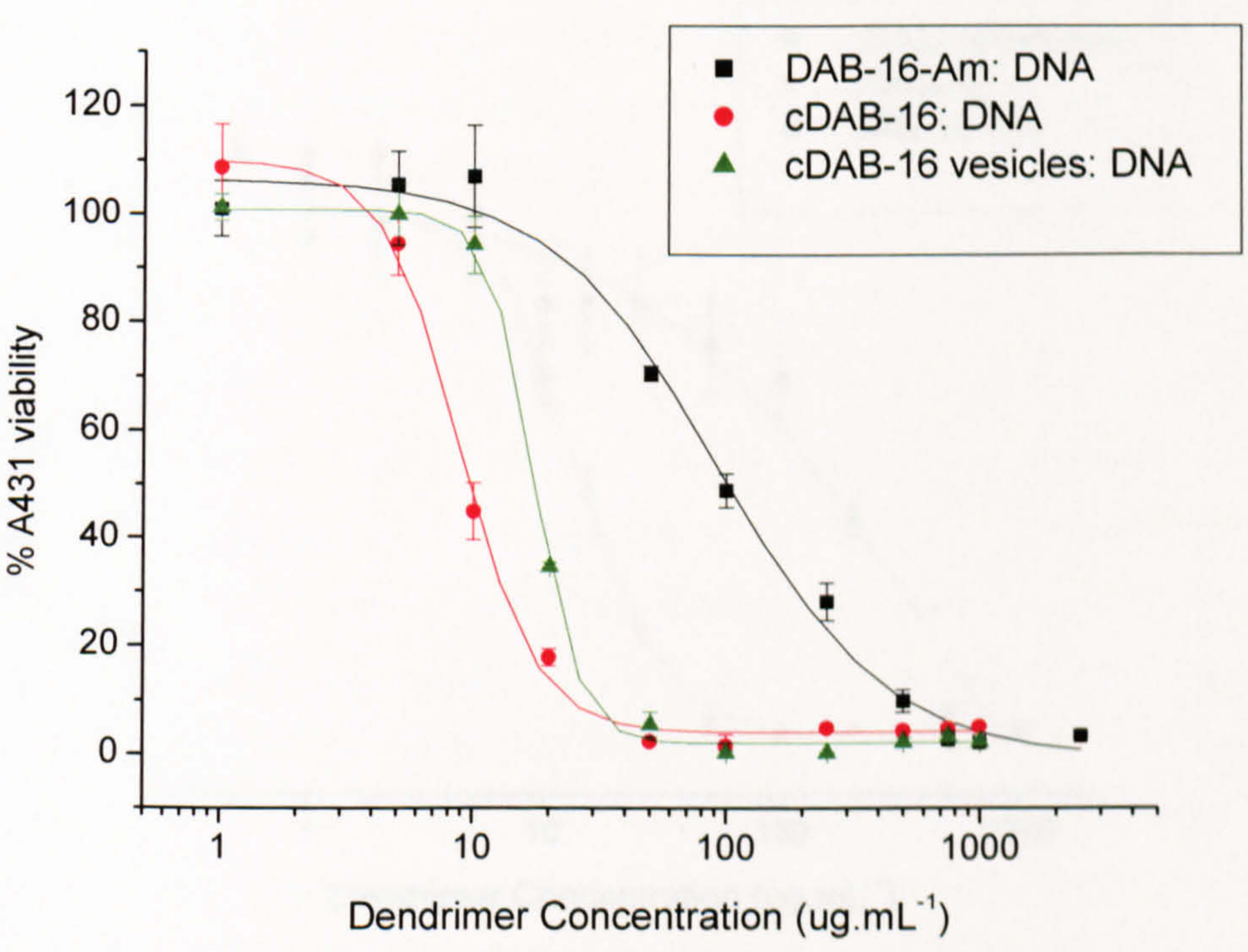

Figure 57 Mean ± SE A431 % CV versus dendrimer complexed with pDNA (30 N: P) (n=3)

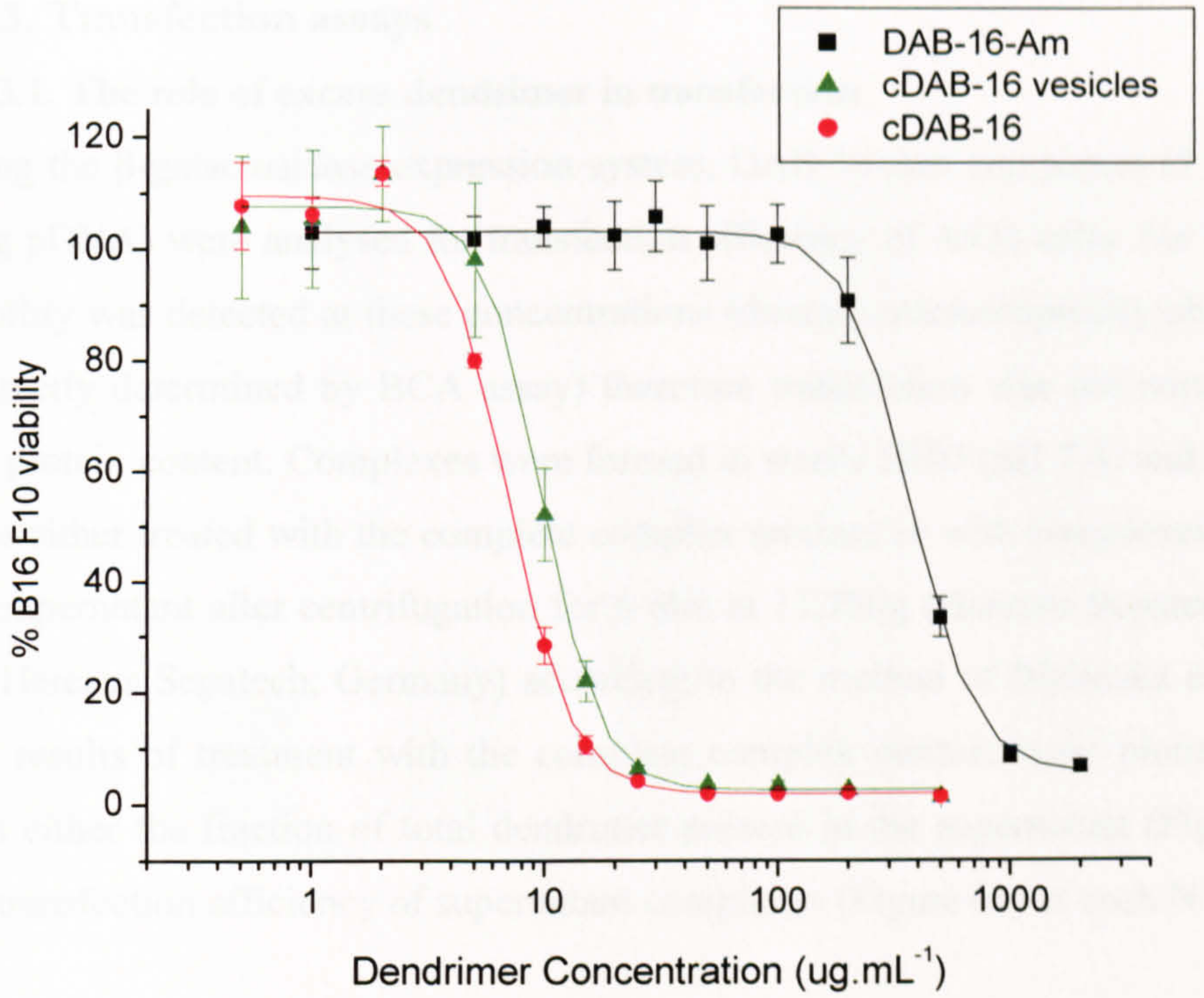

Figure 58 Mean ± SE B16 F10 % cell viability (CV) versus free dendrimer concentration (n=3)

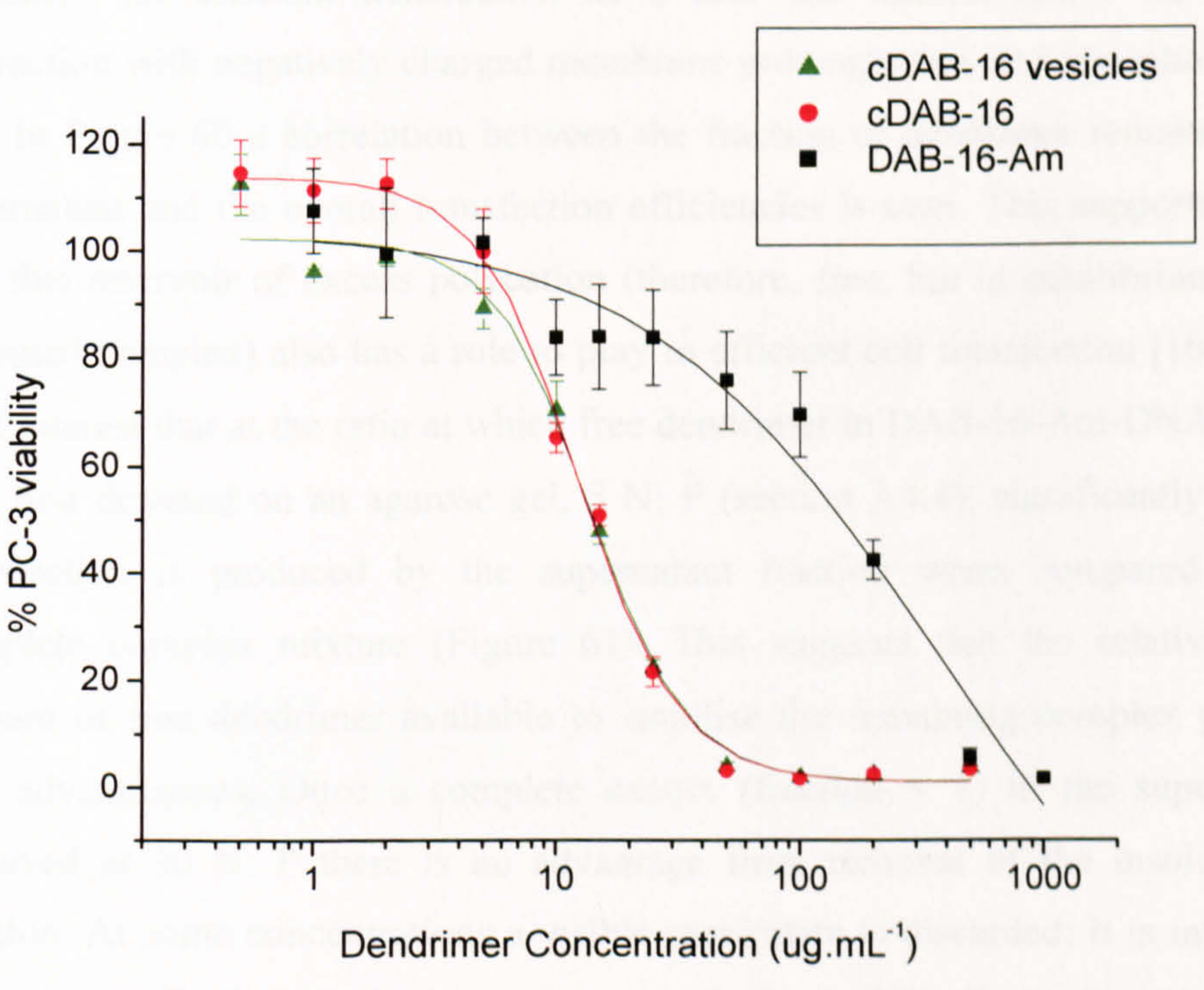

Figure 59 Mean ± SE PC-3 % cell viability (CV) versus free dendrimer concentration (n=3)

5.4.3. Transfection assays

5.4.3.1. The role of excess dendrimer in transfection

Using the β-galactosidase expression system, DAB-16-Am complexes (1 – 30 N: P, 1 μg pDNA) were analysed for transfection efficiency of A431 cells. No loss in cell viability was detected at these concentrations (directly microscopically observed and indirectly determined by BCA assay) therefore transfection was not normalised for cell protein content. Complexes were formed in sterile HBD (pH 7.4) and A431 cells were either treated with the complete complex mixture or with complexes present in the supernatant after centrifugation for 6 min at 11,750g (Hereaus Sepatech Biofuge 15, Hereaus Sepatech, Germany) according to the method of Bielinska *et al.* [167]. The results of treatment with the complete complex mixture were plotted together with either the fraction of total dendrimer present in the supernatant (Figure 60) or the transfection efficiency of supernatant complexes (Figure 61) at each N: P ratio.

As expected, transfection efficiencies of DAB-16-Am increase with increasing N: P ratio. It is commonly held that a cationic charge excess on the surface of a complex is necessary for efficient transfection as it aids cell internalisation via reversible interaction with negatively charged membrane proteoglycans and phospholipids [57, 59]. In Figure 60 a correlation between the fraction of dendrimer remaining in the supernatant and the overall transfection efficiencies is seen. This supports the view that this reservoir of excess polycation (therefore, free, but in equilibrium with the saturated complex) also has a role to play in efficient cell transfection [167, 254]. It is of interest that at the ratio at which free dendrimer in DAB-16-Am-DNA solutions was first detected on an agarose gel, 5 N: P (section 3.4.4), significantly enhanced transfection is produced by the supernatant fraction when compared with the complete complex mixture (Figure 61). This suggests that the relatively larger amount of free dendrimer available to stabilise the remaining complex population was advantageous. Once a complete excess (fraction = 1) in the supernatant is achieved at 30 N: P there is no advantage from removal of the insoluble DNA fraction. At some concentrations a visible precipitate is discarded; it is inferred that this is not useful for transfection purposes as the loss of this plasmid content does not detrimentally affect transfection efficiencies.

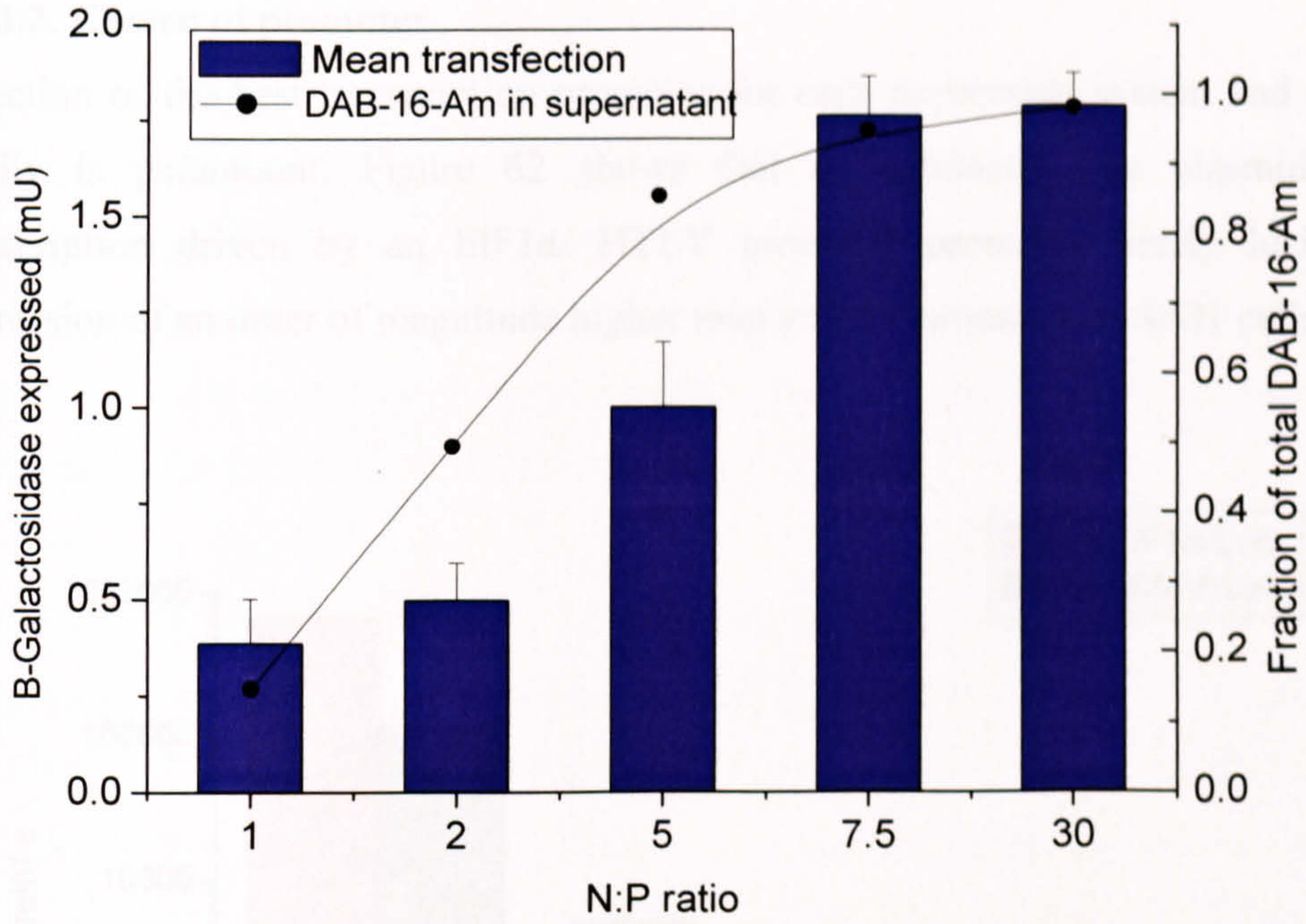

Figure 60 Mean ± SE (n = 6) transfection efficiency of DAB-16-Am with varied N: P ratio (columns); with fraction of total dendrimer in supernatant (line)

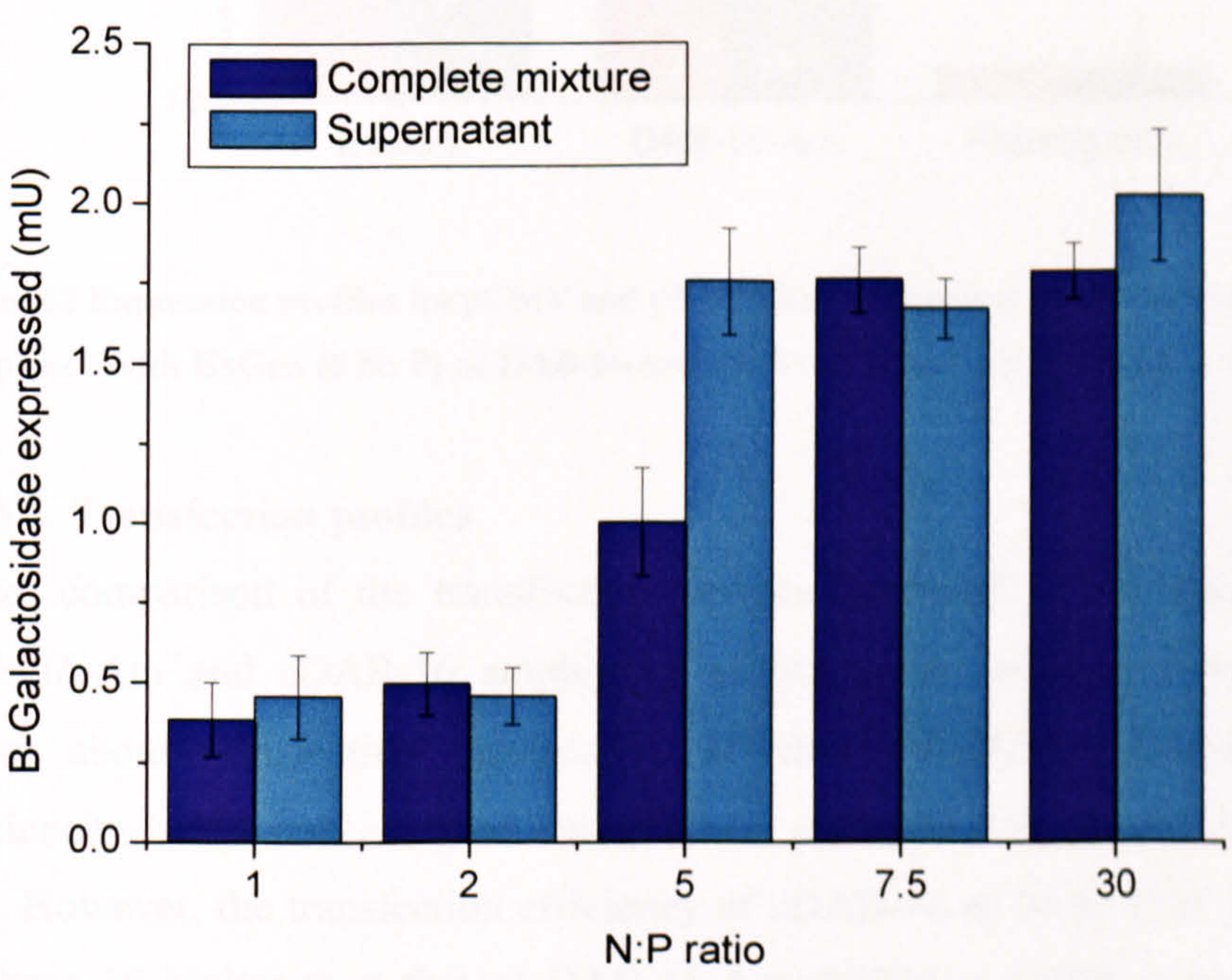

Figure 61 Comparison of transfection efficiencies (mean ± SE) of complete DAB-16-Am-pDNA complexes versus supernatant complexes with varied N: P ratio (n = 6).

5.4.3.2. Choice of promoter

Selection of the best transcription promoter for each expression system and vector family is paramount. Figure 62 shows that an enhanced Luc plasmid with transcription driven by an ElF1α/ HTLV promoter promotes firefly luciferase expression of an order of magnitude higher than a CMV promoter in A431 cells.

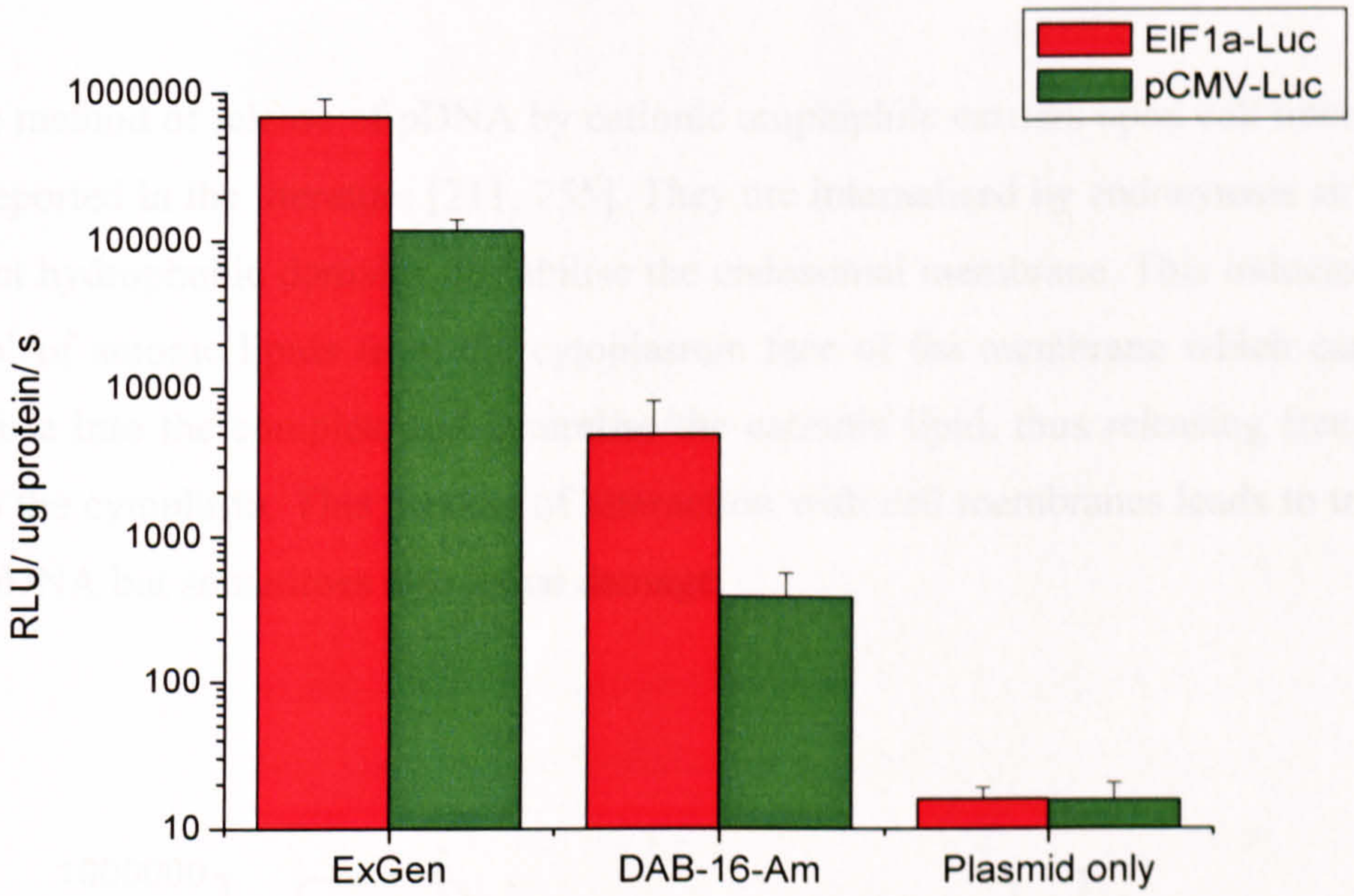

Figure 62 Expression profiles for pCMV and pElF1α-Luc plasmid (1 μg DNA) alone or complexed with ExGen (6 N: P) or DAB-16-Am (30 N: P) (Mean values ± SE, n = 3).

5.4.3.3. Transfection profiles

Direct comparison of the transfection profiles produced by the parent dendrimer DAB-16-Am and cDAB-16 amphiphile allows some tentative conclusions to be drawn about transfection mechanism. cDAB-16 displays minimal transfection efficiencies below concentration values which cause measurable cell damage (Figure 63). However, the transfection efficiency of cDAB-16 at 30 N: P in A431 cells is a log base 10 higher than that of DAB-16-Am (87720 ± 31974 versus 1660 ± 672 RLU/ μg) (Figure 63 & Figure 64). This fact is not observed unless the levels of reporter protein are corrected for total cell protein as cDAB-16 has ceased 90% of

the protein synthesis measured in the control cell population. Perturbation of the cell monolayer by cDAB-16 was observed at this ratio upon microscopic inspection and also the concentration applied to the cells (5 μg cDAB-16 / 200 μL) is in reach of cytotoxic levels according to MTT assay (Figure 57). DAB-16-Am induces steadily increasing transfection levels at increasing N: P ratio with no significant loss in cell viability (Figure 64). In these studies ExGen 500 is used as a positive control and dosed into wells at the levels recommended by the manufacturer; 0.3 μg pDNA complexed with ExGen 500 *in vitro* at 6 N: P.

The method of release of pDNA by cationic amphiphile carriers upon cell interaction is reported in the literature [211, 255]. They are internalised by endocytosis at which point hydrophobic domains destabilise the endosomal membrane. This induces 'flip-flop' of anionic lipids from the cytoplasmic face of the membrane which can then diffuse into the complex and neutralise the cationic lipid, thus releasing free DNA into the cytoplasm. This process of interaction with cell membranes leads to transfer of pDNA but sometimes also lethal damage.

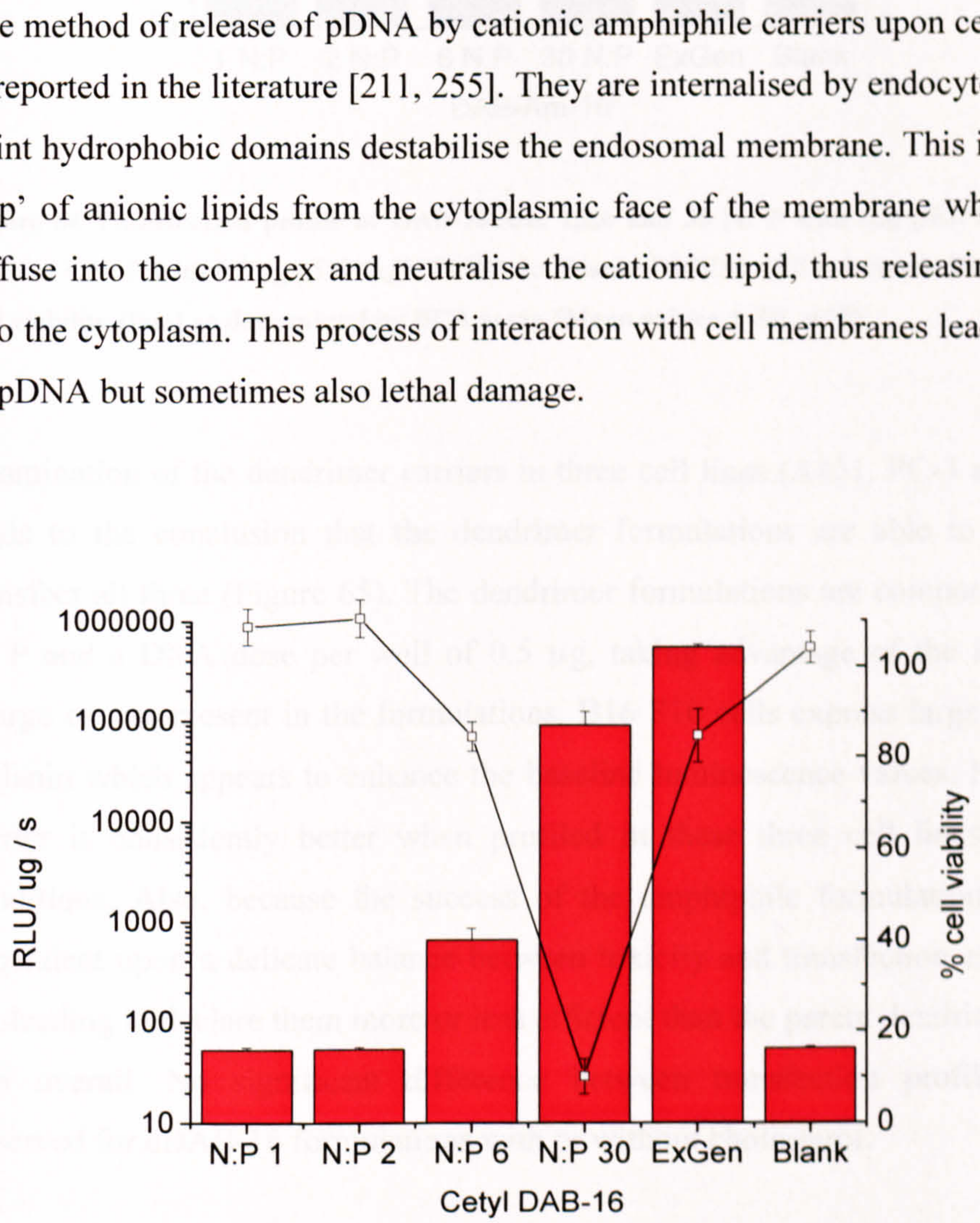

Figure 63 Transfection profile of cDAB-16: 1,2,6 and 30 N: P with 1μg pEIF1α/HTLV-Luc. ExGen: 6 N: P with 0.3 μg pEIF1α/HTLV-Luc. Blank: DMEM. (All columns). Plotted against % cell viability (line) as determined by BCA assay (Mean values ± SE, n=5)

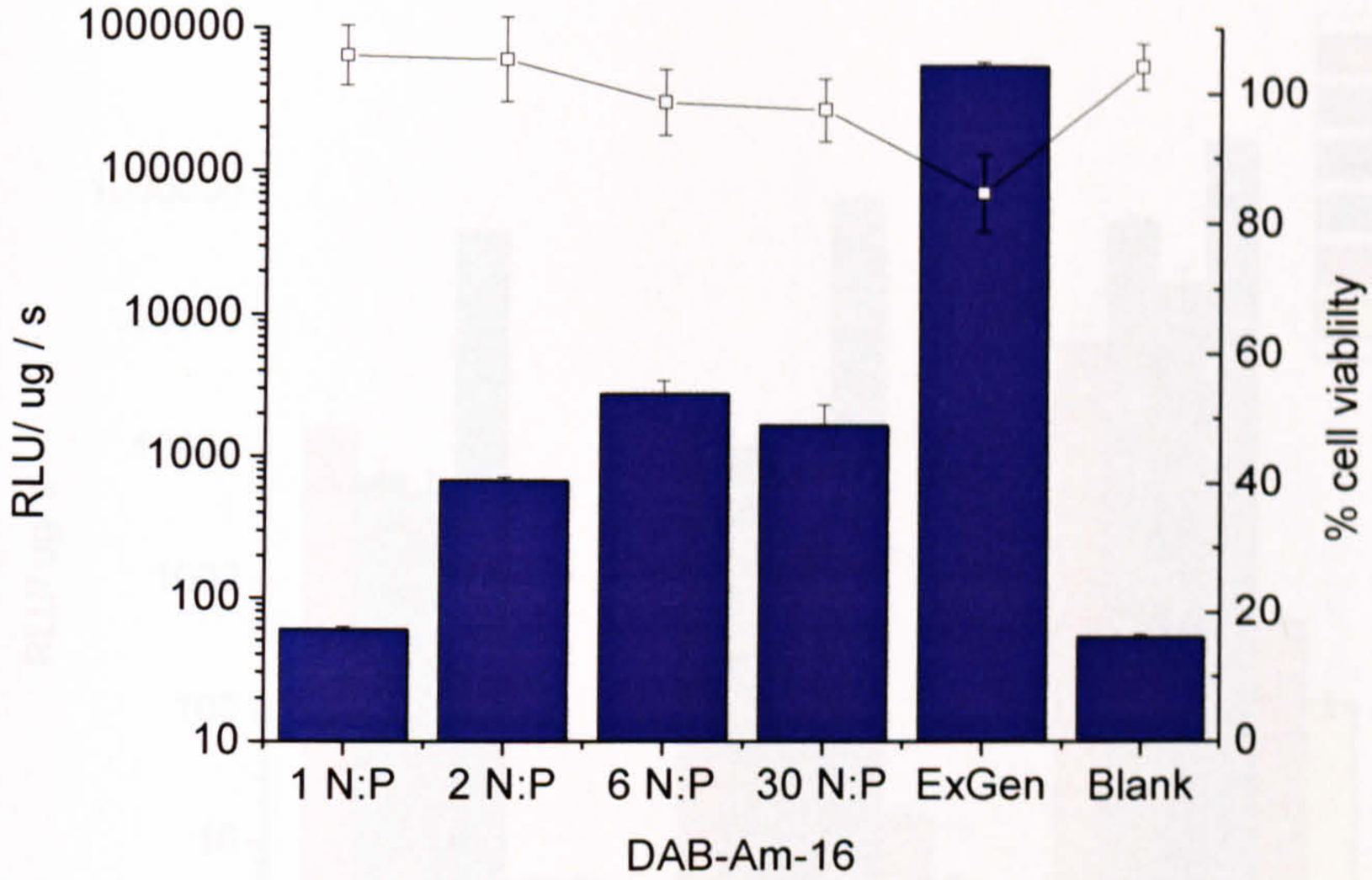

Figure 64 Transfection profile of DAB-16-Am: 1,2,6 and 30 N: P with 1μg pElF1α/HTLV-Luc. ExGen: 6 N: P with 0.3 μg pElF1α/HTLV-Luc. Blank: DMEM. (All columns). Plotted against % cell viability (line) as determined by BCA assay (Mean values ± SE, n=5)

Examination of the dendrimer carriers in three cell lines (A431, PC-3 and B16 F10) leads to the conclusion that the dendrimer formulations are able to significantly transfect all three (Figure 65). The dendrimer formulations are compared here at 30 N: P and a DNA dose per well of 0.5 μg, taking advantage of the large cationic charge excess present in the formulations. B16 F10 cells express large quantities of melanin which appears to enhance the baseline luminescence values. No dendrimer carrier is consistently better when profiled in these three cell lines under these conditions. Also, because the success of the amphiphile formulations is strongly dependent upon a delicate balance between toxicity and transfection efficiency it is misleading to declare them more or less efficient than the parent dendrimer DAB-16-Am overall. No significant difference between transfection profiles could be observed for cDAB-16 formulations with or without cholesterol.

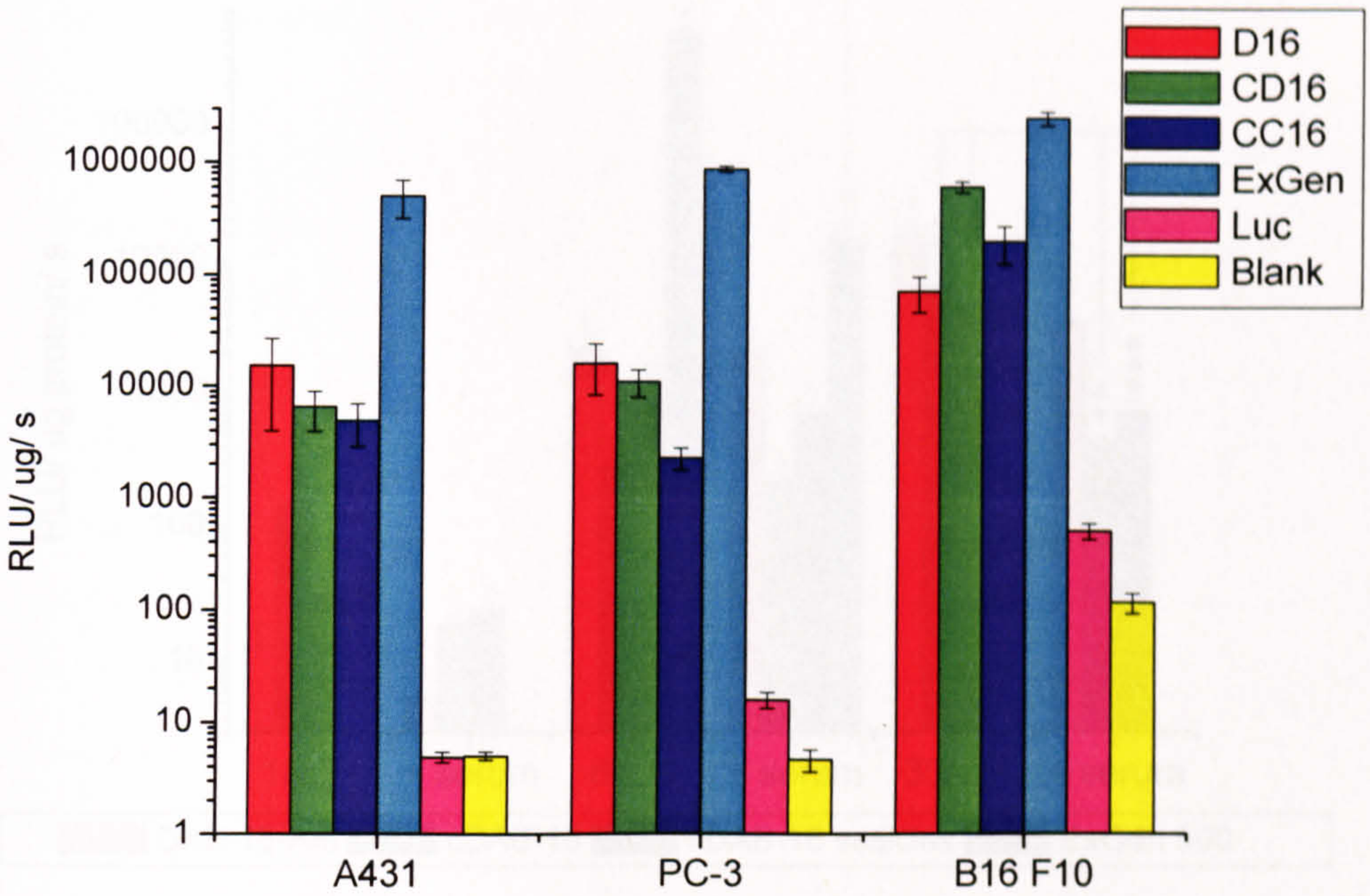

Figure 65 Luciferase expression achieved by carriers in A431, PC-3 and B16 F10 cells. BL = DMEM. Luc = EIF1α/HTLV-Luc 0.5 μg. ExGen = ExGen 500: pLuc (6 N: P, 0.3 μg). D16 = DAB-16-Am: pLuc (30 N: P, 0.5 μg). CD16 = cDAB-16: pLuc (30 N: P, 0.5 μg). CC16 = cDAB-16 vesicles: pLuc (30 N: P, 0.5 μg) (Mean values ± SE, n = 6)

5.4.3.4. Serum effects

The dendrimer species most significantly affected by the presence of 50% v/v FBS is cDAB-16 (Figure 66) which correlates with the strongest haemolytic activity in section 5.4.1. DAB-16-Am shows no significant decrease in transfection efficiency in the presence of 50% v/v FBS at any N: P ratio; this would suggest that amphiphilicity has enhanced the interaction of the dendrimer with serum components. The transfection efficiency of ExGen 500 is reduced by more than an order of magnitude upon addition of serum, producing a transfection efficiency in A431 cells at the manufacturer's recommended ratio (6 N: P) similar to those of the dendrimer carriers at 30 N: P (Figure 66).

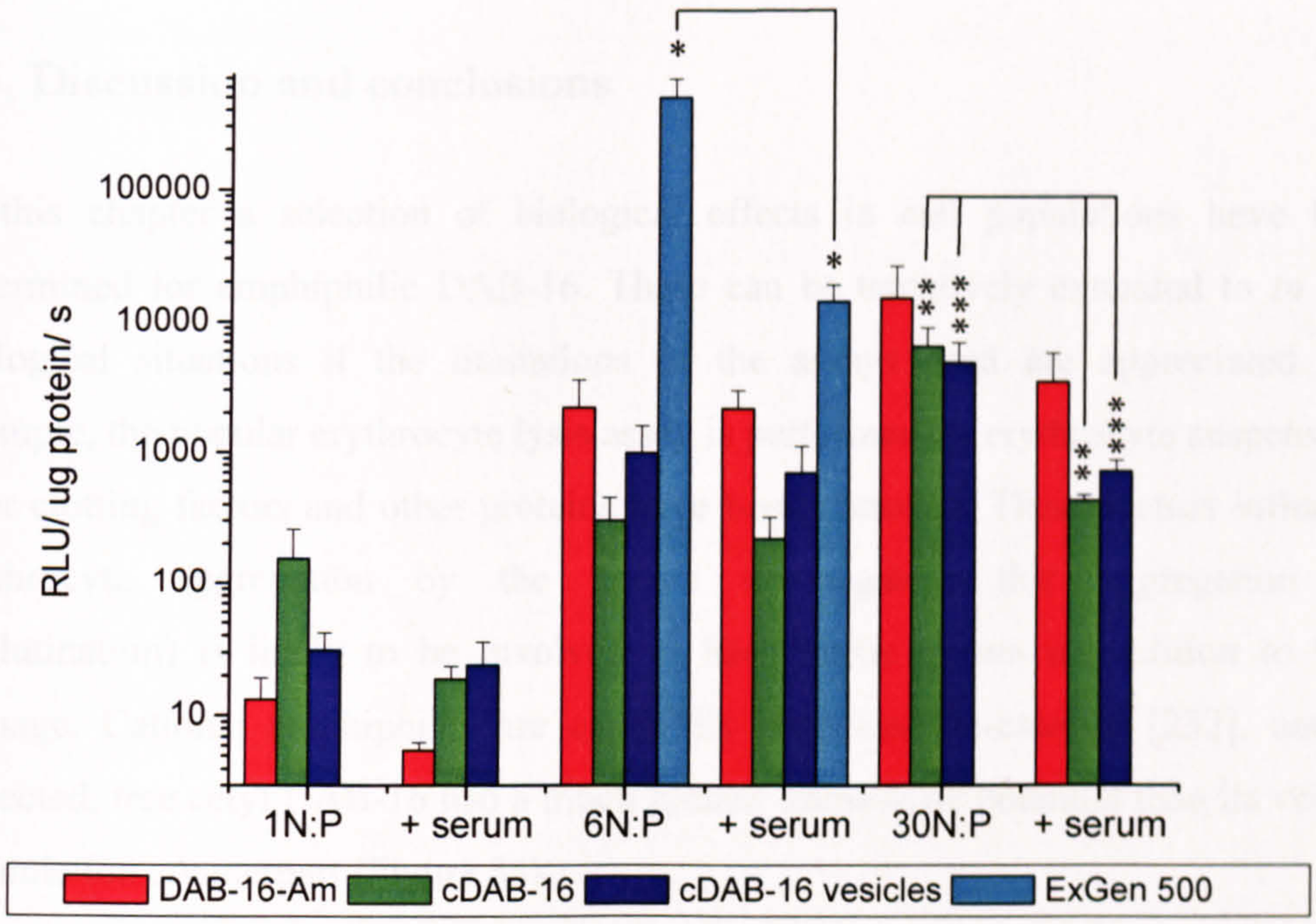

Figure 66. The reduction of carrier transfection efficiencies in A431 cells (0.5 μg pEIF1α/HTLV-Luc) upon addition of 50% v/v serum (statistical significances are as follows: * p = 0.001 ** p ≤ 0.02 *** p ≤ 0.05) (Mean values ± SE, n = 3)

5.5. Discussion and conclusions

In this chapter a selection of biological effects in cell populations have been determined for amphiphilic DAB-16. These can be tentatively extended to *in vivo* biological situations if the limitations of the assays used are appreciated. For example, the popular erythrocyte lysis assay is performed on erythrocyte suspensions after clotting factors and other proteins have been removed. These factors influence erythrocyte aggregation by the agents investigated; this aggregation (or agglutination) is likely to be involved in haemotoxic events in addition to lytic damage. Cationic amphiphiles are especially agglutination-causing [232], and as expected, free cetyl DAB-16 had a much greater haemolytic potential than its vesicle formulation counterpart (Figure 54).

Interestingly this reduction in toxicity upon formulation into vesicle structures was not as pronounced in MTT reduction assay measurements (Table 13, Table 14 & Table 15), suggesting that metabolic activity as an indirect measure of cell viability may not be as applicable for the amphiphilic dendrimer compared with DAB-16-Am. This cytotoxicity is likely to be a result of predominantly membrane effects therefore measurement of cytosolic lactate dehydrogenase (LDH) release may be a more valuable technique to quantify and compare cell toxicity [39, 256]. The MTT assay is also disadvantaged by the toxicity of the reagent to the cells and the need for organic solvent extraction. There are alternative reagents available to measure changes in cell metabolic activity such as the non-toxic, water-soluble indicator dye AlamarBlue® [257]. The particular cell line (B16 F10, PC-3 or A431) treated with the dendrimer formulation did not affect the resulting toxicities of DAB-16-Am, cDAB-16 or cDAB-16 vesicles in real terms (Table 13, Table 14 & Table 15). A comparison of the viability of a non-transformed cell line following treatment would be more representative of 'normal' cellular effects; however there are inherent difficulties in the culture of these cells. It should be noted that serum was not included in the treatments of cells for MTT measurement which might in the *in vivo* situation ameliorate some of the toxicity due to neutralisation of non-specific cationic charge

interactions by anionic serum proteins. Also, the mode of cell death (e.g. apoptotic or necrotic) was not determined.

When carriers are complexed in, or diluted into, DMEM micron-sized complexes are rapidly formed according to PCS studies (section 4.4.1.2). It has been shown in the literature that micron sized complexes can enhance the transfection of certain cell lines by polycation carriers such as PEI [171, 174] simply due to the enhanced gravitation of complexes onto the cell monolayer during incubation. This may also apply to PPI dendrimer; therefore complexes of PPI dendrimer and DNA were usually formed in physiological salt solution for these studies.

Purification of polyplexes (i.e. removal of free polymer) has been shown to reduce transfection efficiencies, which were restored upon readdition of free polycation [254]. Excess soluble DAB-16-Am and cDAB-16 dendrimer also helps to solubilise complexes retaining soluble DNA (section 4.4.2). From this work it is concluded that DAB-16-Am also fits this trend with a large excess of free polycation required for efficient transfection (Figure 60). Supernatants run on an agarose gel with or without heparin confirmed the presence of complexed DNA in this portion.

Again, examination of the dendrimer carriers in three cell lines (A431, PC-3 and B16 F10) leads to the conclusion that the dendrimer formulations are able to significantly transfect all three (Figure 65) however no dendrimer carrier performs consistently better. It would appear that the overall mechanism of transfection has been altered by hydrophobic derivatisation and that the success of the amphiphile formulations is strongly dependent upon finding a delicate balance between toxicity and access to the cell cytoplasm [258]. It has been reported previously that the inclusion of cholesterol in a cationic lipid formulation did not enhance transfection efficiencies [14].

Unlike in this study, the presence of serum did not affect the transfection efficiency of PEI in A549 cells according to Bragonzi *et al.* However, only a final concentration of 10% FBS was used [245] and is not sufficient to mimic *in vivo* conditions.

Enhanced interaction with serum components is to be expected for flexible amphiphile monomers and the inclusion of cholesterol in the cDAB-16 formulation does result in a lesser reduction in the given transfection efficiency which seems to support this theory [221]. Interestingly, susceptibility to serum reduction is not seen under these conditions for DAB-16-Am although it can bind serum components (evidenced as a reduction in particle size, section 4.4.1.3). The susceptibility of ExGen 500 to serum reduces its transfection efficiency of A431 cells to a level similar to that produced by DAB-16-Am (Figure 66), which may mean that this high *in vitro* level of ExGen 500 transfection would not be of advantage *in vivo*. Susceptibilities to inactivation by serum components may be attributable to the higher cationic charge density of the large (22KDa) PEI molecules when compared with the small (<2KDa) PPI dendrimer molecules.

In conclusion, cDAB-16 and cDAB-16 vesicles are able to transect three immortalised cell lines. The dose of amphiphilic dendrimer applied to cells must carefully balance transfection efficiencies with the toxicity that they can produce. The amphiphilic dendrimer formulations are in all cases an order of magnitude more toxic to the cell lines than the parent dendrimer DAB-16-Am according to an MTT reduction assay. These features suggest that cetylated DAB-16 has a potential application in anti-tumour gene therapy. However, cDAB-16 also has pronounced haemolytic activity, which is partially ameliorated following incorporation into stable vesicles. It is now important to ascertain the relevance of these findings in the *in vivo* situation, particularly with respect to the biodistribution of transgene expression upon intravenous injection.

6. In vivo biological characterisation

6.1. Introduction

Medical research has its ultimate goal in improvement of human health, and research using animals has brought benefits not realised in any other way. It has been legislated since 1876 (Cruelty to Animals Act) that this work should be regulated to minimise any distress or pain that might be caused. The researcher has a responsibility to avoid the use of animals whenever possible and give sound scientific reasons for their use. Experimental aims should be well defined and the simplest organisms possible used (with the appropriate physiology) in the least numbers required. Finally, procedures should be of the lowest possible severity and animal welfare and health must constantly be maintained and monitored [259].

This work seeks to determine the *in vivo* toxicity and organ biodistribution profile of gene expression produced by an amphiphilic dendrimer gene carrier in order to determine whether it could be a suitable gene delivery agent for human use; particularly with a view towards therapeutic cancer gene therapy [53]. Non-invasive optical imaging of a bioluminescent gene product will be used in order to limit animal distress.

6.1.1. Toxicity determination

As mentioned in chapter 5, extensive biocompatibility testing of new chemical entities is required before licensing. Following initial *in vitro* biological assessment of the toxicity of agents they may be transferred into a mouse model, as in this work, as there is much pharmacological knowledge of this species and mice can be inbred with specific characteristics (e.g. transgenic or athymic mice) aiding experimental reproducibility. In this work, dose escalation was initiated at a fiftieth of the lowest dose shown to cause a significant (up to 20%) haemolytic effect. Doses were escalated approximately following a Fibonacci number series (e.g. 1,2,3,5,8,13 ...) every 24 hours. After injection of the required agent the animals must be observed for toxicity reactions. These may be acute reactions within a time frame of minutes,

but animals may also be monitored for sub-acute and chronic effects (over a period of years). Abnormal reactions such as rapid, extreme weight loss (> 20% body weight) or convulsions upon dose escalation are indicative that maximum tolerated dose has been reached.

6.1.2. Quantification of Luciferase transgene expression

6.1.2.1. In vivo

Non-invasive, *in vivo* (whole animal) imaging has been used to accelerate preclinical model validation for gene carriers and may allow clinical monitoring of human gene therapy [260]. These imaging techniques include positron emission tomography (PET), single photon emission computed tomography (SPECT), magnetic resonance imaging (MRI) and optical imaging. Optical (bioluminescent) imaging using a cooled CCD camera has a very high sensitivity with minimal background, making it most suitable for study of transient transfection by non-viral gene carriers [261-263]. Bioluminescent imaging has also been more widely used in the design of pharmaceuticals targeted to modulate protein-protein interactions [264], clinical immunology [265] and cancer biology [266].

The Xenogen IVIS® Imaging System is a highly sensitive, low light-level system used in conjunction with the custom Living Image® software package [267] to detect and quantify photons (bioluminescence) emitted from a subject in this work. The nature of the propagation of light through tissue must be considered when using this technique. Tissue is a highly scattering medium and as a result photons emitted from tissues deep within the animal may scatter many times before reaching the surface (Figure 67). The IVIS imaging system measures this surface radiance, which depends therefore upon both the brightness and the depth of the source. Generally, the surface radiance is directly proportional to the brightness of the source but this assumes that the position of the source within the animal does not vary [267]. Quantitative analysis of bioluminescent images is achieved by drawing regions of interest (ROIs) on the images and integrating the signal within the regions, therefore the equipment must be carefully calibrated and background emission must be taken into account [267].

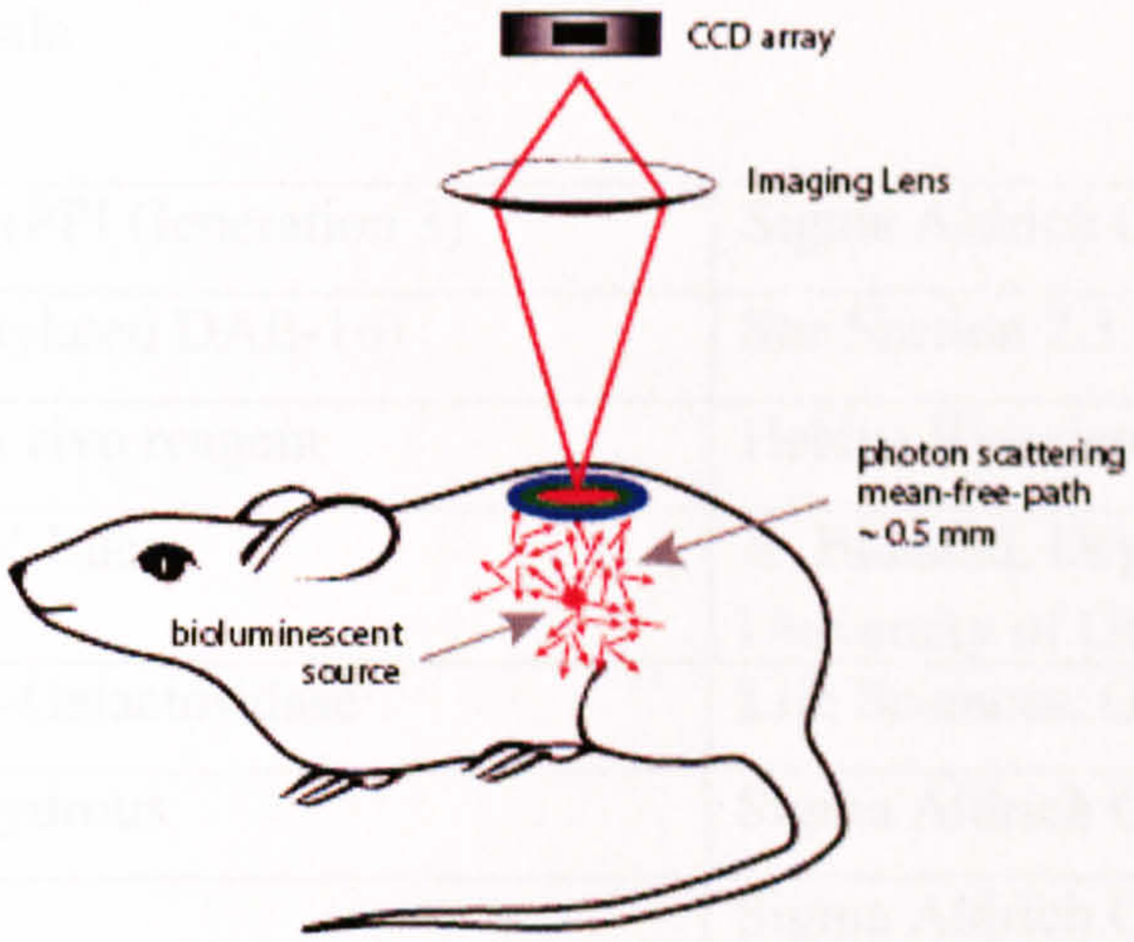

Figure 67. Illustration of photon transport of light from an internal source to the visible position on the surface of the animal. This surface image is observed [267].

6.1.2.2. Ex vivo

Ex vivo analysis of organs is often used to validate *in vivo* detection data gained from imaging systems [261-263, 268, 269]. This is principally because only a two dimensional image can currently be produced using this technique, as mentioned previously, therefore the exact source of the signal should be confirmed ex vivo when first examining an agent. Analysis of luciferase activity in organ lysates is however subject to error, principally due to the variable blood (and protein) content of organs [269, 270]. Haemoglobin contamination results in a considerable decrease in detectable luciferase activity and perfusion of the required tissues may be performed [268, 270, 271] to reduce this effect.

6.2. Materials

DAB-16-Am (PPI Generation 3)	Sigma Aldrich Co., UK
cDAB-16 (cetylated DAB-16)	See Section 2.3.1
ExGen 500 in vivo reagent	Helena Biosciences, UK
pEIF1α/HTLV-Luc	A. Bilsland, Dept. Medical Oncology, University of Glasgow
pCMVsport β-Galactosidase	Life Sciences, GibcoBRL, UK
Dextrose, anhydrous	Sigma Aldrich Co., UK
Cholesterol	Sigma Aldrich Co., UK
HEPES free acid, 1M (sterile)	Sigma Aldrich Co., UK
Phosphate buffered saline (PBS) tablets	Sigma Aldrich Co., UK
A431 skin sarcoma cells	ATCC, CRL-1555
Foetal Bovine Serum (FBS)	Life Sciences, GibcoBRL, UK
Dulbecco's Modified Eagles Medium (DMEM)	Life Sciences, GibcoBRL, UK
L-glutamine (2mM)	Life Sciences, GibcoBRL, UK
Trypsin	Life Sciences, GibcoBRL, UK
EDTA	Life Sciences, GibcoBRL, UK
Bicinchoninic acid (BCA) protein assay solution	Sigma Aldrich Co., UK
Copper (II) sulphate pentahydrate (4%)	Sigma Aldrich Co., UK
Luciferase Assay Reagent	Promega Ltd, UK
QuantiLum® Recombinant Luciferase	Promega Ltd, UK
Bovine Serum Albumin (BSA)	Sigma Aldrich Co., UK
D-luciferin (sodium salt)	Xenogen, CA, USA
Dulbecco's PBS 10x (Ca^{2+} /Mg^{2+} free)	Sigma Aldrich Co., UK
Isoflurane-Vet	Merial Animal Health Ltd, UK
Passive Lysis Buffer 5x (PLB)	Promega Ltd, UK
Phenylmethylsulphonyl fluoride (PMSF)	Sigma Aldrich Co., UK
Protease Inhibitor Cocktail (PIC)	Sigma Aldrich Co., UK

Table 16 Materials and suppliers used in Chapter 6

6.3. Methods

6.3.1. Dose ranging

Two female balb/c mice with initial weights ca. 20g were obtained and housed at 19°C to 23°C with a 12 hour light-dark cycle. They were fed conventional diet and mains water *ad libitum*.

cDAB-16 or cDAB-16 vesicles (100 µL) were mixed with pCMVsport-β-galactosidase pDNA (100 µL) at a 5:1 w/ w ratio in sterile 5% dextrose solution. Dendrimer-DNA complexes were injected immediately (200 µL) via the tail vein (i.v.). Doses were administered daily, ranging from 2 µg pDNA on Day 0 to 50 µg pDNA on Day 4. Animals were monitored carefully after injection; transient reactions lasting a few minutes (e.g. hunched posture and reduced activity) were deemed acceptable whilst persistent behavioural changes such as prostration, rapid shallow breathing or vocalisation would indicate that the animal should be removed from the study and euthanised by a schedule 1 method. Body weights were also monitored daily: a loss of 20% body weight also would necessitate removal from the study.

6.3.2. Cell culture and tumour induction

Thirty-nine female CD-1 nude mice with initial mean weights of 20g each were obtained and housed in groups of six at 19°C to 23°C with a 12 hour light-dark cycle. They were fed conventional diet and mains water *ad libitum*.

A431 cells (subculture 4- 8) were maintained in DMEM supplemented with 10% v/ v FBS and 1% v/ v L-glutamine (2mM) under the prescribed conditions in section 5.3.1. At ca. 80% confluence cells were harvested in PBS (final concentration $5x10^6$ cells) and injected subcutaneously (200 µL) into each flank of 15 CD1-nude female mice. Tumour size was monitored and imaging conducted with tumours of 5mm or larger diameter.

6.3.3. Preparation and administration of treatments

All treatments administered for biodistribution studies were prepared in sterile filtered HBD pH 7.4 (HEPES free acid 20mM in 5% dextrose solution, adjusted to pH 7.4). HBD served as a blank. pEIF1α/HLTV-Luc (50 μg) in 200 μL was the pLuc control. DAB-16-Am, cDAB-16 and cDAB-16 vesicles were complexed at 30 N: P (5: 1 w/w) with 50 μg pEIF1α/HLTV-Luc per 200 μL. ExGen 500 in vivo was complexed with 50 μg pEIF1α/HLTV-Luc per 200 μL at 6 N: P according to the manufacturer's instructions. Treatments (200 μL) were administered to each mouse in the non-tumour bearing group (24 animals) and tumour bearing group (15 animals) on day 0 via the tail vein (i.v.). At least 3 mice were assigned to each treatment group. Animal weights were recorded at 0, 24 and 48 h at which point the experiment was terminated.

6.3.4. Quantification of Luciferase transgene expression

6.3.4.1. Living Imaging®

Animals were imaged *in vivo* in batches of 3 animals at 24 h and 48 h following i.v. injection before sacrifice for *ex vivo* analysis of luciferase activity. Twenty minutes prior to the first image, animals received 200 μL of 30 mg.mL^{-1} D-luciferin (6 mg) in 1x Dulbecco's PBS (without Mg^{2+} or Ca^{2+}) via intraperitoneal (i.p.) injection. They were then transferred to a holding chamber containing vapourised isofluorane and when anaesthetised (ca. 2 min) removed to the imaging chamber of the Xenogen IVIS® Imaging System 50 Series (Xenogen, CA) which includes a cooled CCD camera. Anaesthesia was maintained with low levels of isofluorane delivered via nose tubes. A greyscale photograph of each animal was taken in a supine position then a bioluminescent image acquired for 10 min. A second image of the flank (10 min) was taken if the animal was tumour-bearing. Regions of interest (ROIs) were drawn over particular regions (the tumour and those with the greatest intensity upon imaging, the tail and lungs) of a consistent size and shape. The photon counts from regions of 'no signal' of the same size were used as a background reading and subtracted from the RLUs detected. The corrected RLUs were then divided by the acquisition time and expressed as RLU/ min.

6.3.4.2. Ex vivo analysis

After imaging at 48 h post-injection the animals were euthanised via a schedule 1 method. Three mice (non-tumour bearing) treated with either DAB-16-Am, ExGen 500 or blank (HBD) were randomised to receive transcardiac perfusion before organ removal. The heart was accessed under terminal anaesthesia and sterile PBS was pumped via a needle into the left ventricle and relieved by right cardiac puncture. The lungs, liver, spleen, heart, kidneys, tail and tumour (if present) were harvested and flash frozen in liquid N_2 prior to analysis. Each organ was weighed and freshly prepared mash buffer added (5 mL 5x PLB, 1 mL PMSF 50mM in methanol and 0.5 mL PIC made up to 25 mL with distilled water) 0.2 mL per 0.1 g organ weight. Each sample was homogenised on ice (Ultra-Turrax® T-25 basic, IKA, USA) and 100 µL transferred to a centrifuge tube and centrifuged at 11,750g for 10 min at 4°C (Hereaus Sepatech Biofuge 15, Hereaus Septatech, Gemany). Supernatant (20 µL) was transferred to white luminometer plates for luciferase analysis and a second aliquot diluted 1/100 in water (final concentration x0.01 PLB) and 25 µL plated on a 96 well microtitre plate for BCA assay.

Luciferase analysis was carried out using a Veritas Microplate Luminometer (Turner Biosystems Inc, USA) with a pre-programmed Promega single injection protocol (injection of 100 µL Luciferase Assay Reagent with a 2 s delay and a 10 s integration time). A standard curve was included on each plate containing 10^{-20} – 10^{-12} mol recombinant luciferase in 20 µL PLB 0.01x supplemented with $1mg.mL^{-1}$ BSA. The RLUs obtained were normalised to RLU/ mg/ min. All data are reported as a mean ± standard deviation (n = 3).

BCA analysis was carried out on 25 µL diluted lysate by the addition of 200 µL working reagent (BCA assay solution: copper (II) sulphate pentahydrate 50: 1) and incubation at 37°C for 30 min before reading plates at λ = 570nm (E_{max} plate reader, Molecular Devices Ltd., UK). Bovine serum albumin (BSA) 0 – $800\mu g/mL^{-1}$ in PLB 0.01x formed a standard curve.

6.4. Results

6.4.1. Dose ranging

The maximum dose of cDAB-16 and cDAB-16 vesicles administered to balb/c mice in dose ranging was 250μg complexed with 50 μg pDNA. The animals exhibited no toxic effects and were observed for a further two weeks before euthanisation by a schedule 1 method. The maximum tolerated dose of DAB-16-Am (12.5 $mg.kg^{-1}$) was previously established [53]. All dendrimer complexes were formed at 30 N: P (the equivalent of DAB-16-Am: DNA 5: 1 w/w) as per the literature [53], therefore each animal (weight 20-25g) was dosed with 50μg DNA and 250μg dendrimer.

6.4.2. Luciferase transgene expression

6.4.2.1. Animal weights

Animal weights recorded just before tail vein injection (t = 0 h) with carrier complexes (50μg DNA and 250μg dendrimer) then at 24 h and 48 h post injection were stable, indicating that acute toxicity did not occur following injection (Figure 68). One animal from the cDAB-16 treatment arm was removed from the study at t = 0 h.

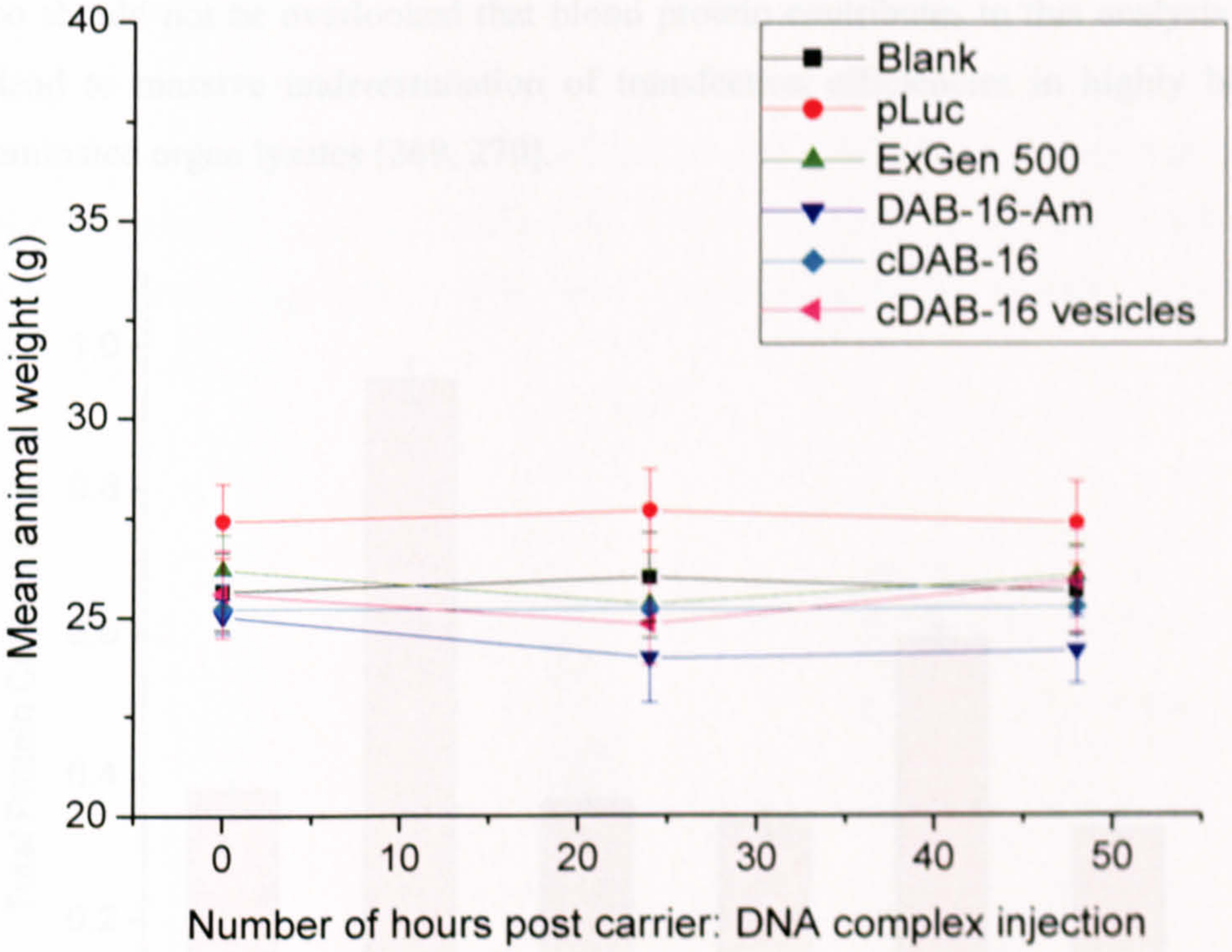

Figure 68 Animal weights (g) recorded at 0, 24 and 48h post i.v. injection with carrier formulations: Blank = HBD pH 7.4, pLuc = EIF1α/HTLV –Luc (50 μg), ExGen 500 = ExGen 500: pLuc (6 N: P), DAB-16-Am = DAB-16-Am: pLuc (30 N: P), cDAB-16 = cDAB-16: pLuc (30 N: P), cDAB-16 vesicles = cDAB-16 vesicles: pLuc (30 N: P). (Mean values ± SE, n=3 animals/group)

6.4.2.2. Total cell protein

As previously mentioned, the total level of protein produced by a given organ is an important parameter that must be accounted for in *ex vivo* analysis of organ lysates to accurately determine the efficiency of *in vivo* transfection of the organ.

For example, liver samples in this work (Figure 69) contain two and a half times the total protein level of the lungs and threefold that of the induced A431 tumours. Without normalising for total protein, reported transfection efficiencies could potentially be skewed in favour of highly metabolically active organs such as the liver.

It also should not be overlooked that blood protein contributes to this analysis; this can lead to massive underestimation of transfection efficiencies in highly blood-contaminated organ lysates [269, 270].

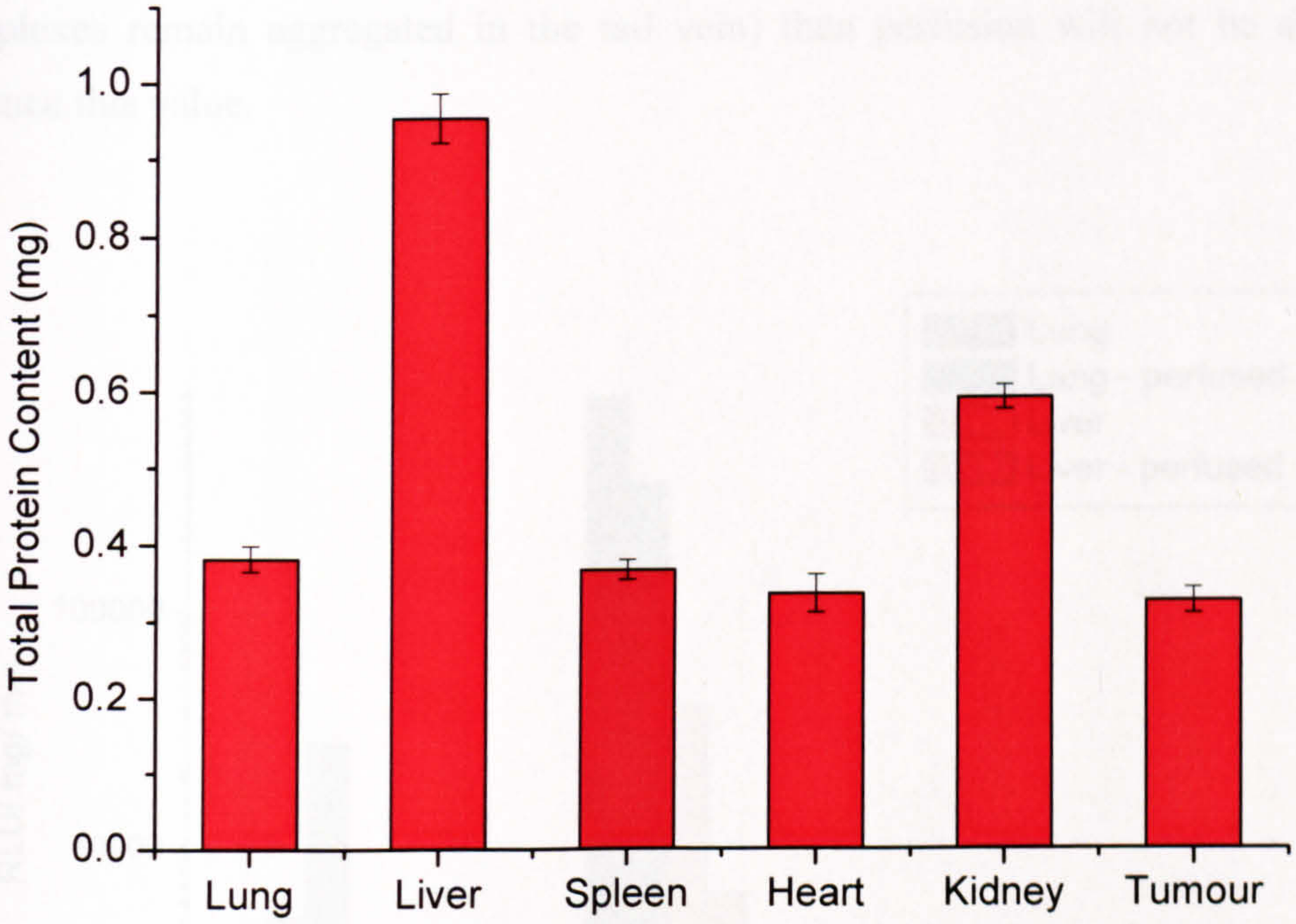

Figure 69 Total protein content (mg) per 0.2 mL organ lysate measured by BCA assay (Mean values ± SE, n = 15 animals)

6.4.2.3. Whole animal perfusion

CD-1 nude mice (six in total) were randomly assigned to receive DAB-16-Am complexes, ExGen 500 complexes or HBD (pH 7.4) and 3/ 6 animals received transcardiac perfusion with sterile PBS before sacrifice and organ removal 24 h following injection. This technique enhanced the signal produced by DAB-16-Am in the lung over five times and in the liver one and a half times (Figure 70). The increased efficiency of lung perfusion is expected, in agreement with Colin *et al.* [270] who recorded an eight-fold increase in lung transfection measurements but much less improvement for other organs. Hepatic portal vein access can be used to perfuse the liver more efficiently.

However, the same trend is not seen for the ExGen treated mice. This can be explained by the corresponding Living Image® data (not shown) which shows that the non-perfused mouse received a significantly more effective injection (exhibiting widespread gene expression). Therefore, if the injection is not successful (e.g. complexes remain aggregated in the tail vein) then perfusion will not be able to enhance this value.

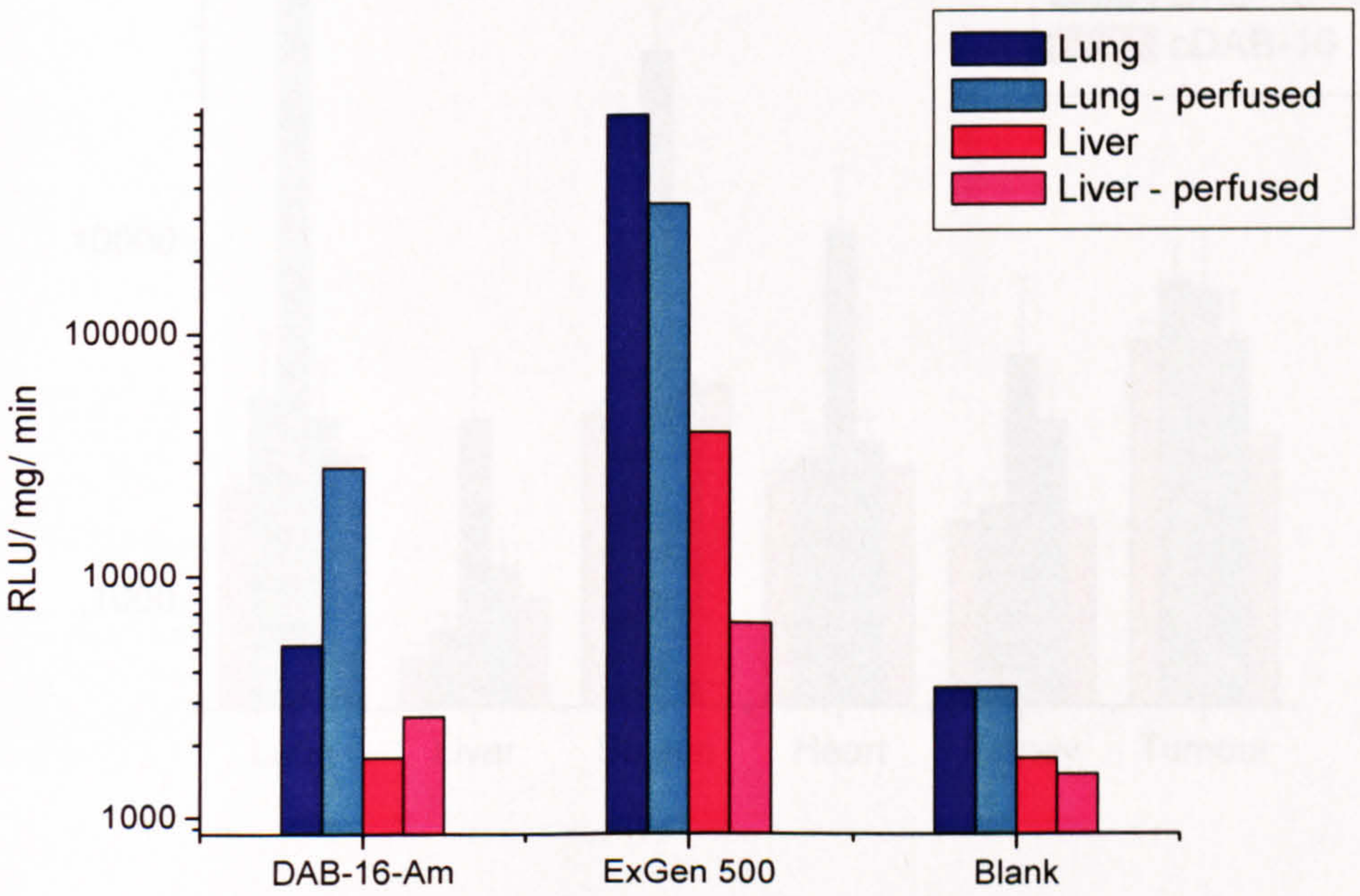

Figure 70 Ex vivo luciferase analysis of liver or lung lysates 24 h after injection with DAB-16-Am 30 N: P with ElF1α/HTLV –Luc (50 μg) (n=2), ExGen 500 6N: P with ElF1α/HTLV –Luc (50 μg) (n=2) or Blank = HBD (pH 7.4) (n=2) with or without whole animal perfusion.

6.4.2.4. Ex vivo biodistribution analysis

The *ex vivo* analysis of organ lysates at 48 h after injection was used to describe a correlation between *in vivo* images and assayed luciferase quantities in the lysates (Figure 68). Luciferase activity in any particular area on the image is limited by the two dimensional format of the technique, therefore the exact origin of the signal cannot be ascertained with complete certainty.

At 48 h a statistically significant increase in luciferase activity (when compared with plasmid alone) is found to reside in the lungs, liver, spleen and heart of animals treated with ExGen 500 (lung; $p = 0.012$) and in the liver of animals treated with DAB-16-Am (liver; $p = 0.042$).

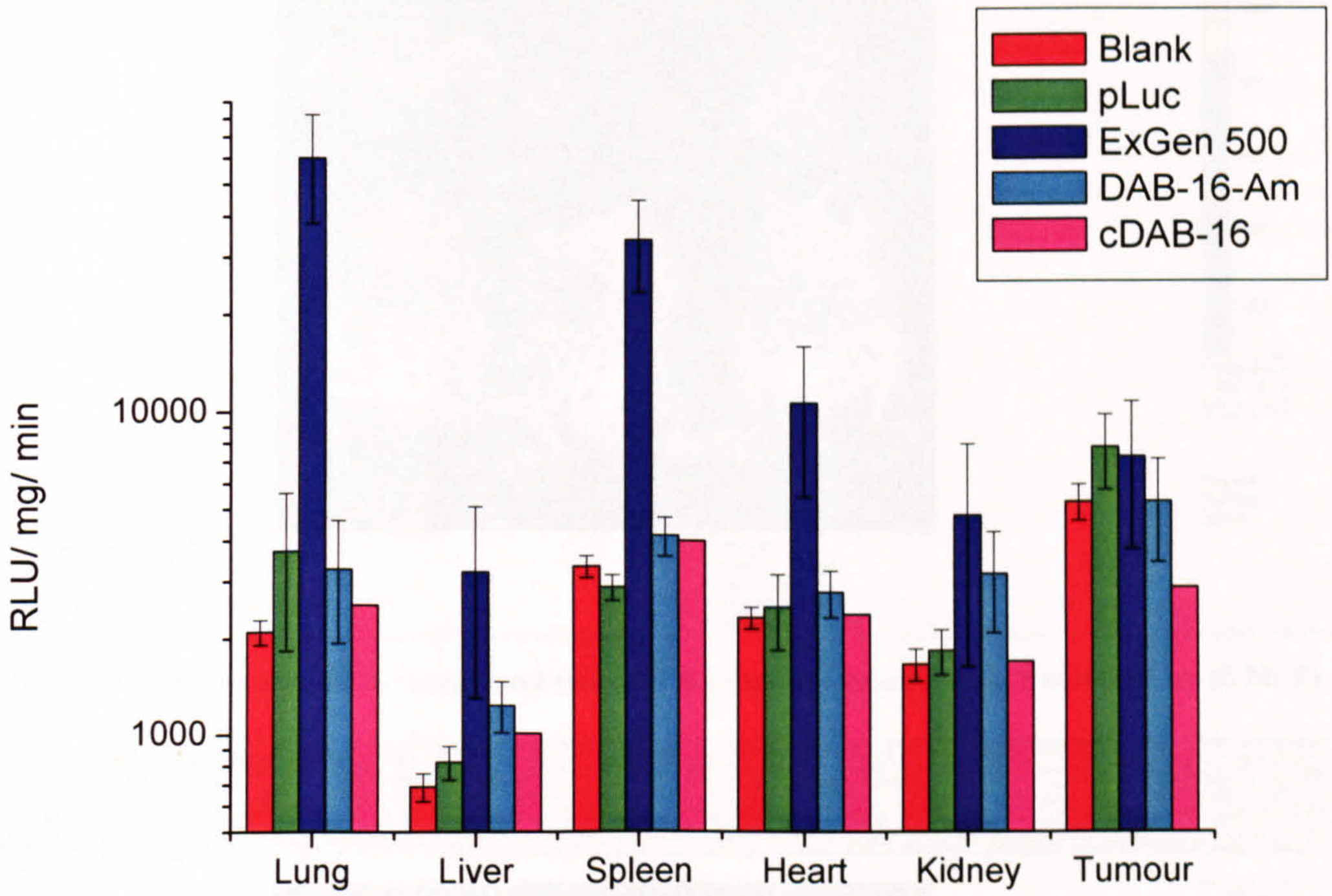

Figure 71 Ex vivo luciferase analysis of organ lysates 48 h after injection with: Blank = HBD pH 7.4, pLuc = ElF1α/HTLV –Luc (50 μg), ExGen 500 = ExGen 500: pLuc (6 N: P), DAB-16-Am = DAB-16-Am: pLuc (30 N: P), cDAB-16 = cDAB-16: pLuc (30 N: P) (Mean values ± SE, n = 3 with the exception of one animal in the cDAB-16 group removed from the study).

6.4.2.5. IVIS® quantitative analysis

As stated previously, regions of interest (ROIs) were drawn using the Living Image® analysis software to cover the tumour and any other ROIs seen, which in this work existed over the lungs and the tail at 24 h and 48 h after injection. Unfortunately, no significant counts from the tumour location were detectable for any group. Example

ROI calculations for lung and tail at 24 and 48 h are shown below for the ExGen 500 treatment group (Figure 72 & Figure 73).

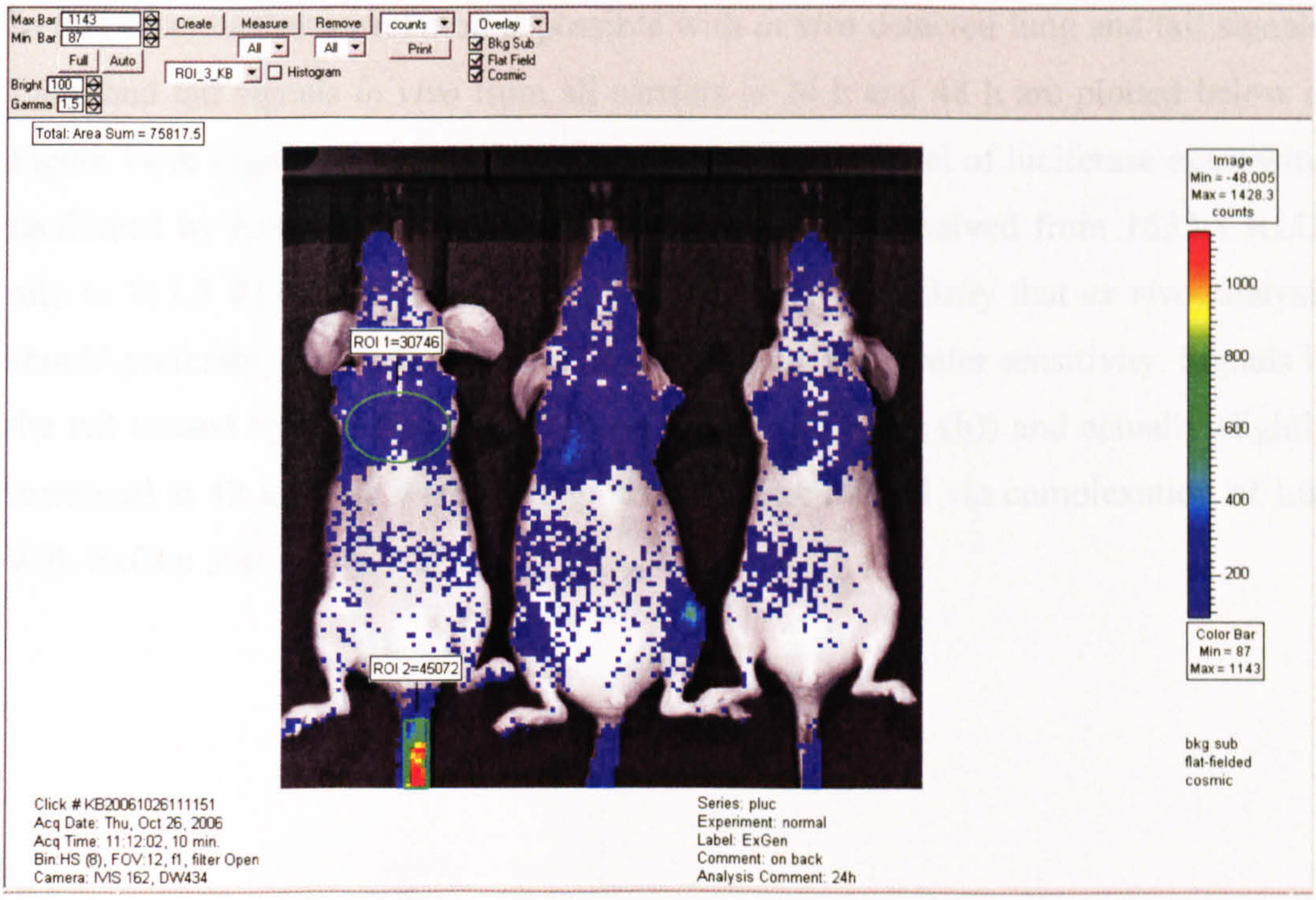

Figure 72 ROIs measured for lungs and tail at 24 h in mouse treated with ExGen-pLuc (6 N: P)

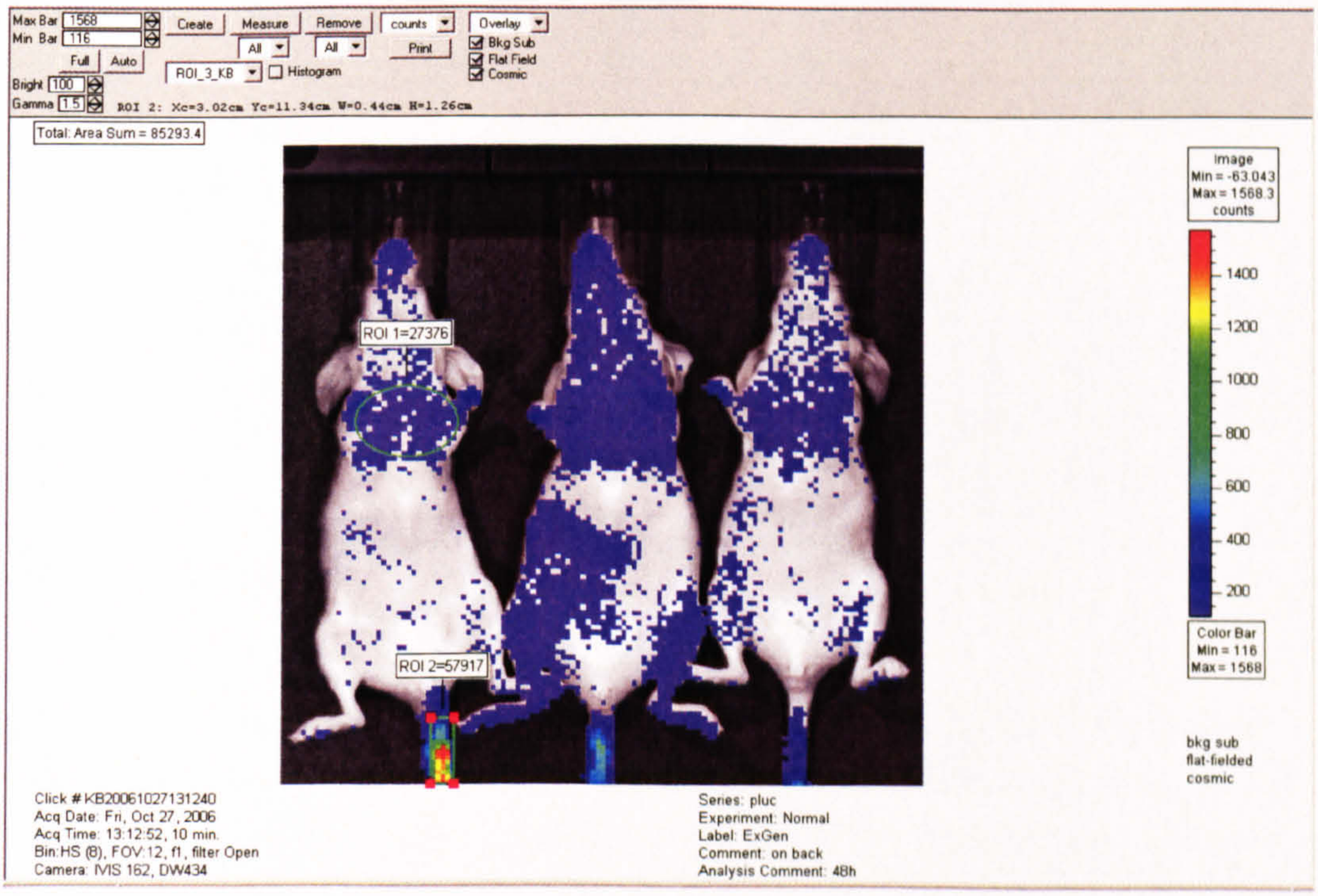

Figure 73 ROIs measured for lungs and tail at 48 h in mouse treated with ExGen-pLuc (6 N: P)

In this case, further correlation is possible with *in vivo* detected lung and tail signals. Lung and tail signals *in vivo* from all carriers at 24 h and 48 h are plotted below in Figure 74 & Figure 75. After 48 h the measured *in vivo* level of luciferase expression facilitated by ExGen 500 in the lung has approximately halved from 1632.3 RLU/ min to 811.3 RLU/ mg/ min (Figure 74 (a) & (b)). It is likely that *ex vivo* analysis should preferably be carried out at a 24 h time point for greater sensitivity. Signals in the tail caused by Luc alone were strong (Figure 75 (a) & (b)) and actually slightly increased at 48 h; these were not significantly ameliorated via complexation of Luc with ExGen 500.

(a)

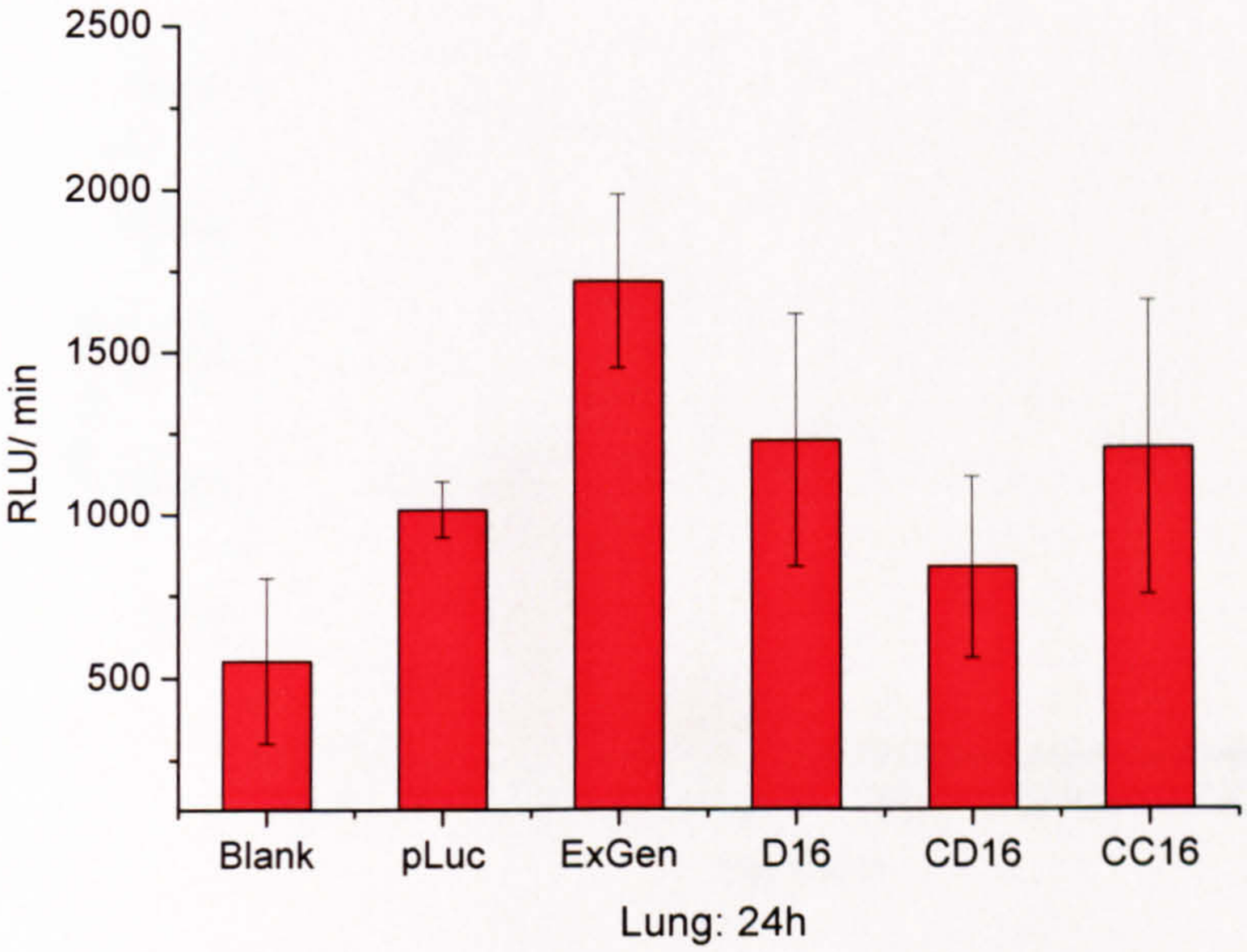

(b)

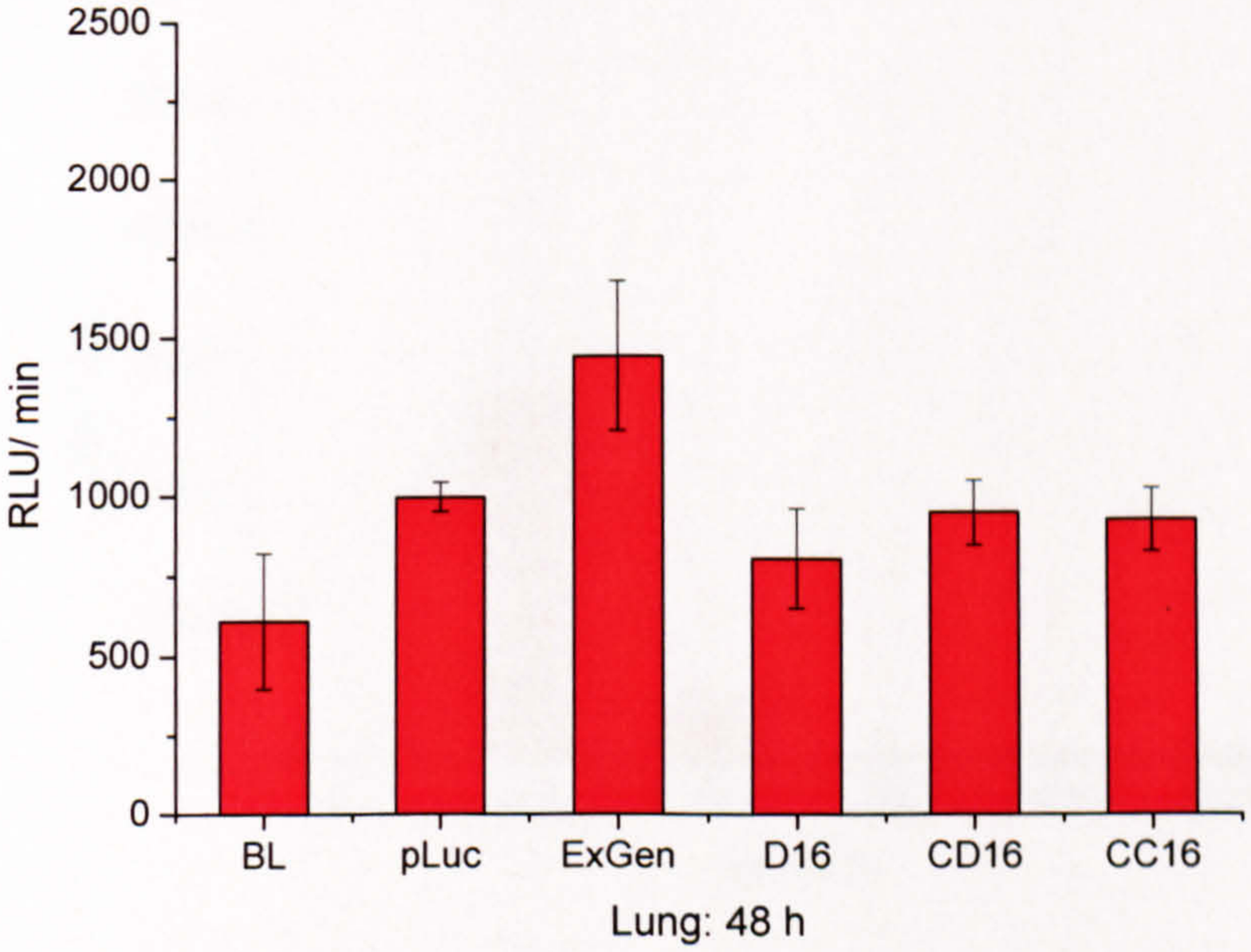

Figure 74 In vivo luciferase activity in the lung for carriers BL = blank, pLuc = EIF1α/HTLV – Luc (50 μg), ExGen = ExGen 500: pLuc (6 N: P), D16 = DAB-16-Am: pLuc (30 N: P), CD16 = cDAB-16: pLuc (30 N: P), CC16 = cDAB-16 vesicles: pLuc (30 N: P) (Mean values ± SE, n=3) at (a) 24 h and (b) 48 h.

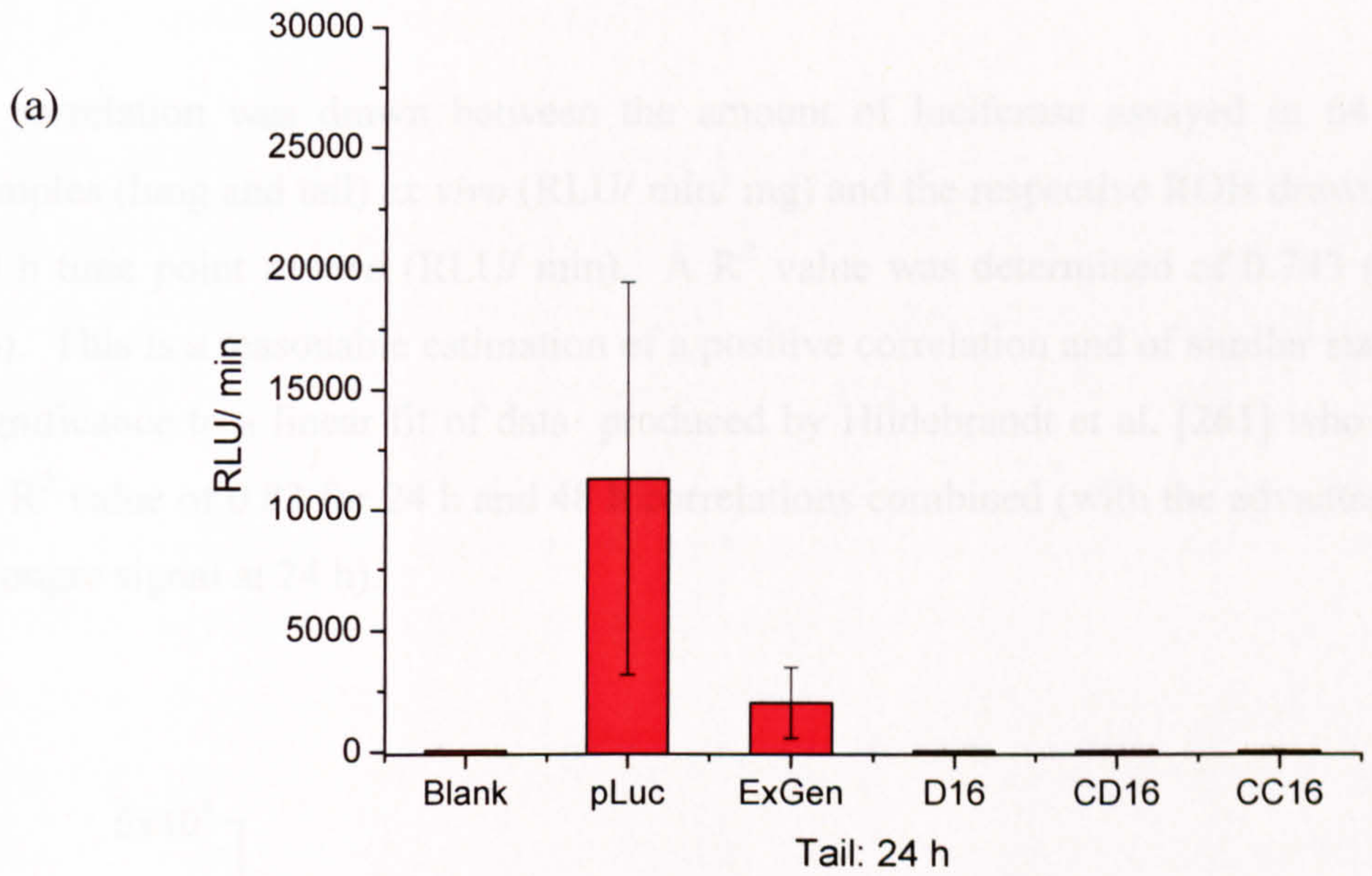

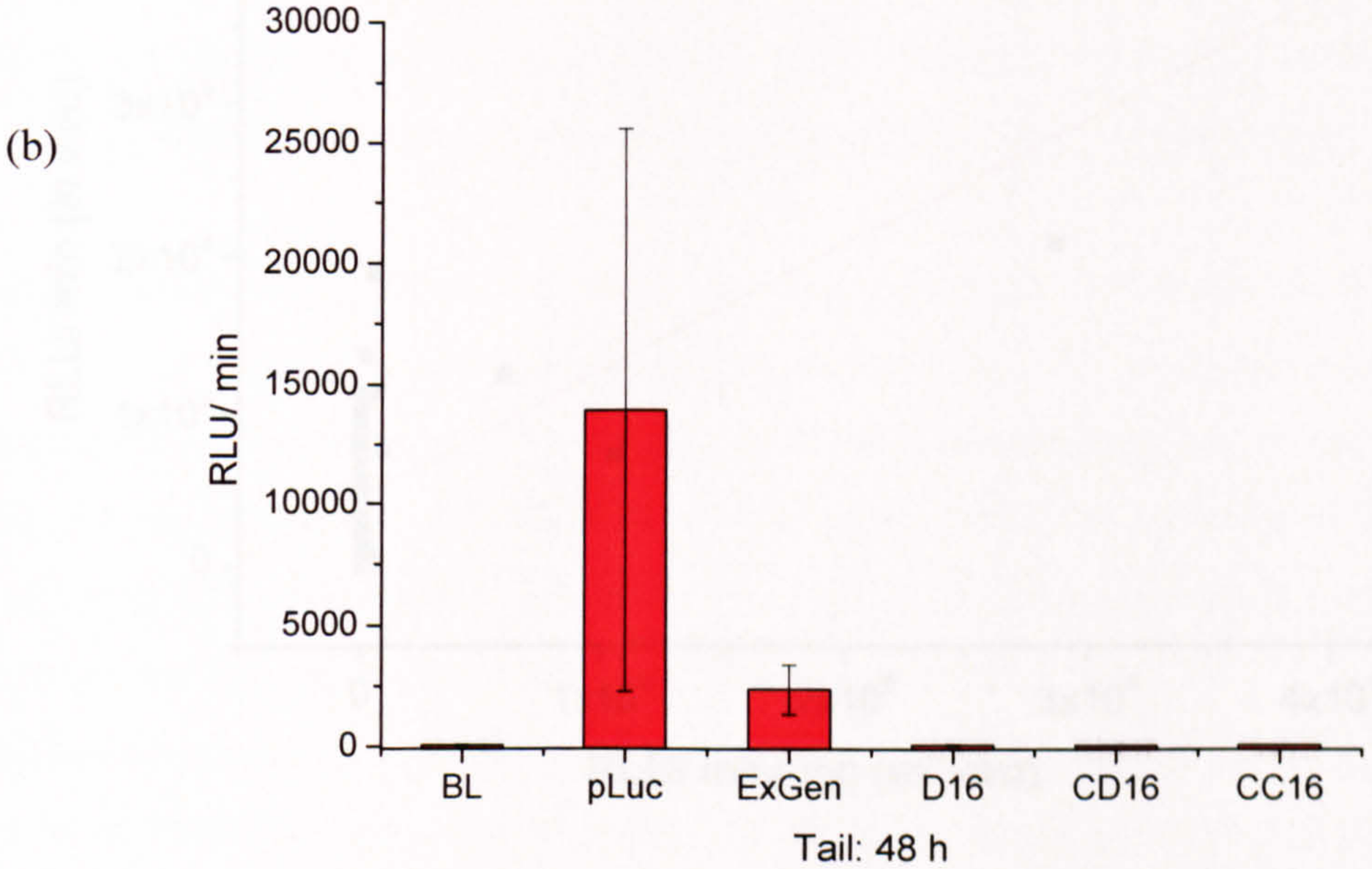

Figure 75 In vivo luciferase activity in the tail for carriers BL = blank, pLuc = ElF1α/HTLV-Luc, ExGen = ExGen 500: pLuc (6 N: P), D16 = DAB-16-Am: pLuc (30 N: P), CD16 = cDAB-16: pLuc (30 N: P), CC16 = cDAB-16 vesicles: pLuc (30 N: P) (Mean values ± SE, n=3) at (a) 24 h and (b) 48 h.

6.4.2.6. *Ex vivo/ in vivo* correlation

A correlation was drawn between the amount of luciferase assayed in 64 organ samples (lung and tail) *ex vivo* (RLU/ min/ mg) and the respective ROIs drawn at the 48 h time point *in vivo* (RLU/ min). A R^2 value was determined of 0.743 (Figure 76). This is a reasonable estimation of a positive correlation and of similar statistical significance to a linear fit of data produced by Hildebrandt et al. [261] who record an R^2 value of 0.83 for 24 h and 48 h correlations combined (with the advantage of a stronger signal at 24 h).

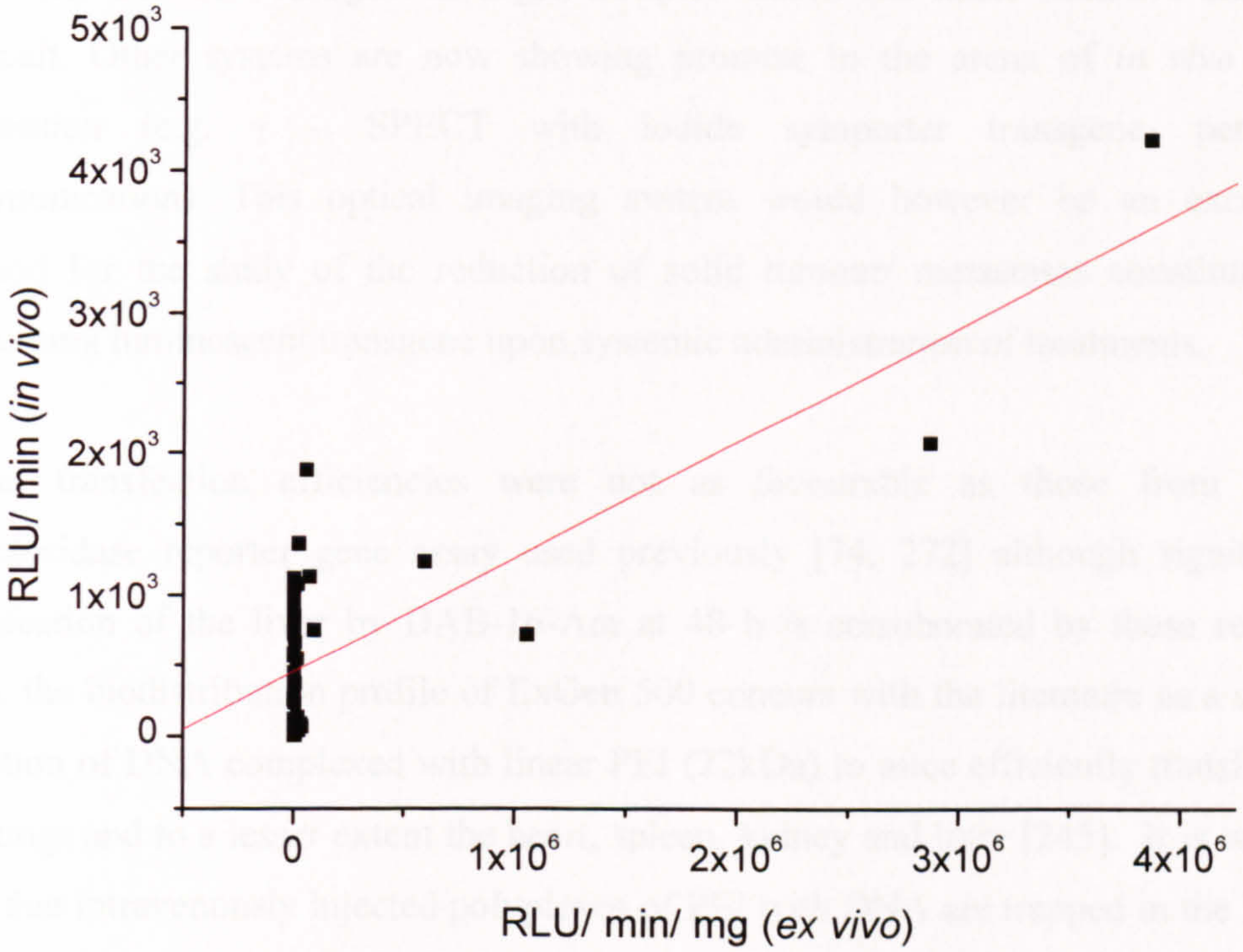

Figure 76 *Ex vivo – in vivo* correlation between 64 tail and lung samples at 48 h post injection.

6.5. Discussion and conclusions

In dose ranging studies, cDAB-16 was less toxic than might have been expected from haemolysis and cytotoxicity assays; therefore it is important to confirm these data in a whole organism. Animals under study were monitored for signs of acute toxicity and weighed each day. Animal weights remained stable throughout.

From the biodistribution studies in this chapter it can be concluded that unfortunately luciferase expression analysis is not a good technique for measurement of PPI dendrimer *in vivo* gene expression. Also inherent to this assay is a great deal of variability between background organ samples which has made sensitive analysis difficult. Other systems are now showing promise in the arena of *in vivo* gene expression (e.g. γ – SPECT with iodide symporter transgene, personal communication). This optical imaging system would however be an excellent method for the study of the reduction of solid tumour/ metastases constitutively expressing luminescent transgene upon systemic administration of treatments.

Organ transfection efficiencies were not as favourable as those from a β-galactosidase reporter gene assay used previously [74, 272] although significant transfection of the liver by DAB-16-Am at 48 h is corroborated by these results. Also, the biodistribution profile of ExGen 500 concurs with the literature as a single injection of DNA complexed with linear PEI (22kDa) to mice efficiently transfected the lungs and to a lesser extent the heart, spleen, kidney and liver [245]. It is widely held that intravenously injected polyplexes of PEI with DNA are trapped in the lungs due to erythrocyte agglutination upon contact with the large available capillary surface area, producing expression in the vasculature of this organ [273, 274]. Also, large amounts of gene expression are seen at the point of injection, usually in the tail vein vasculature. However, these commonly observed effects are detrimental to transfection of distant organs and for example, a xenograft [261].

It may be possible to further improve these transfection efficiencies using alternative injection protocols. Bragonzi *et al*. used a double injection protocol with a 15 min

interval; two doses of 22 kDa PEI/ luciferase produced a log increase in transfection efficiencies [245]. It is uncertain whether loss of dendrimer expression in the circulation is due to degradation by serum nuclease or protein/ glycosaminoglycan disruption, for example, or aggregation leading to compartmentalisation in non-expressing pathways. Strong complement activation has been recorded for a fifth generation PAMAM dendrimer, although further information that complement activation by poly-L-lysine was dependent on chain length may have bearing on the relative toxicity of the small, lower generation PPI dendrimers. The extent of this effect was also dependent on charge ratio [224].

In conclusion, assessment of luciferase transgene expression may not find application in further *in vivo* study of PPI dendrimers, however *in vivo* imaging techniques are improving rapidly in resolution and signal mapping [260] and alternative transgene expression systems are available. cDAB-16 and cDAB-16 vesicles were found to be safe for *in vivo* use which supports further investigation of their potential as cancer gene therapeutics.

7. Conclusions and further work

7.1. Conclusions

As introduced previously, the purpose of synthesising amphiphilic DAB-16 was to produce an improved transfection agent derived from DAB-16-Am based on rational principles set down in the literature. Inclusion of hydrophobic parts can improve interaction with the membrane of a target cell facilitating uptake [110]. The colloidal stability of PPI G3 (DAB-16-Am) complexes with DNA can also be poor [74] due to areas of weak charge on the complex surface [59]. It was postulated that this could also be overcome by grafting hydrophobic chains onto the dendrimer as the 'hydrophobic effect' [104] would bring the dendrimer head groups into closer proximity and concentrate the cationic charges available for DNA binding.

The cDAB-16 product contains a statistical distribution of low levels of cetylation based around a mean value. ^{1}H NMR and EA agree an average level of derivatisation of ~ 1.1 cetyl chains per dendrimer molecule. ESIMS data (Table 3 & Figure 13) give some indication that there is very little tri-cetylated product in the mixture although this cannot be taken as quantitative. As anticipated, the 3.75 mol % average substitution level is very low and cDAB-16 favours association into vesicle structures upon inclusion of cholesterol.

Probe sonication was successfully employed to produce self-assembled systems from cDAB-16 [80]. A small CAC value (0.32mM) has been estimated (Figure 14) for cDAB-16 in aqueous, low ionic strength media using the hydrophobic probe, MO. Further proof of the presence of these assemblies is taken from PCS measurements as a particulate population is detected with a low mean Z average hydrodynamic diameter (Table 5). Importantly though, this potential for hydrophobic interaction altered the microstructures that were formed upon complexation of cDAB-16 with plasmid DNA.

The Z average mean hydrodynamic diameter of cDAB-16 vesicles (2:1 cDAB-16: cholesterol weight ratio) correlated well with the estimated diameter of the main vesicle population from TEM images. The size peak with the most intensity was that of 50nm, uni-lamellar vesicles which appeared disc-like on the image along with visible coalescence of individual vesicles to form multi-lamellar vesicles (Figure 17 iii). These vesicles behaved differently from the cDAB-16 aggregates in biological systems, again providing a tool for the formation of structure-activity relationships.

After examination of linked proton effects of DAB-16-Am-DNA binding using ITC it was concluded that only dendrimer primary amines are involved in initial DNA binding under the experimental conditions (I = 10mM, pH 7.4, 25°C) and that this process is virtually enthalpically neutral (Figure 23) consistent with the hydrophobic effect dominating the complexation process [123, 133]. This hydrophobic binding effect signature is produced by a variety of synthetic gene delivery systems, suggestive that these systems may have more in common mechanistically than first thought [275-277]. Equilibrium dissociation constants were not derived for the binding interaction between DAB-16-Am and pDNA but could in future be approximated by fitting the initial exothermic, binding phase (where a sigmoidal shape is exhibited) to a single-affinity binding site model [275-277].

ITC, Eth Br exclusion assay, gel retardation studies and PCS all provide consistent information about the pDNA-dendrimer complexation process [278]. A loss of approximately 90% Eth Br binding sites corresponds with the onset of global pDNA collapse (condensation) detectable using ITC, the onset of retardation of DNA-dendrimer complex migration through an agarose gel, transition through neutral surface zeta potential conditions and a maxima in complex hydrodynamic diameter. Using all the available biophysical techniques it can be concluded that the complexation process is complete for cDAB-16 and cDAB-16 vesicles at 1 N: P (30 mol of phosphate are bound by 1 mol of amphiphilic dendrimer), tripling the binding capacity of the parent dendrimer DAB-16-Am, and that the presence of hydrophobic alkyl chains did improve the packaging of pDNA by the dendrimer. On the basis of

accumulated evidence cDAB-16 vesicles (cholesterol- stabilised cDAB-16 aggregates) appear to condense DNA the most efficiently overall.

DAB-16-Am binds DNA more efficiently than the 'gold standard' *in vitro* transfection agent, linear PEI, under the experimental conditions examined, as less complexing agent is required to induce condensation (Figure 24). It is concluded that the increased nitrogen density of linear PEI does not pose an advantage at this stage of the process, perhaps limited by the separation distance between DNA phosphate groups (~3.3Å) [87, 113]. The more 'natural' propylene group amine separation (exhibited by the polyamines spermine and spermidine) has in fact been shown to strengthen cationic liposome-pDNA interactions in comparison with ethylene spacings [278]. This work also supports early findings by Kabanov *et. al.* [149] who reported that PPI dendrimers can condense DNA increasingly efficiently as the environmental pH decreases towards pH 3. It is known that PPI dendrimers swell into extended conformations upon protonation of primary and tertiary amine groups [70] therefore it is plausible that inner tertiary amines now have improved access to the DNA backbone. DAB-16-Am-DNA complexes could therefore benefit from formation at an acidic pH prior to use in other applications.

Further examination of these complexes using a fluorescent probe over one week reveals that at least two stages occur; first, a fast binding and condensation event (occurs within milliseconds of mixing dendrimer and DNA), followed by a slow equilibrium condensation rearrangement. After one week of incubation at 25°C cDAB-16 formulations are able to completely exclude Eth Br at approximately 0.25 N: P (Figure 26 & Figure 27) and DAB-16-Am at approximately 0.5 N: P (Figure 25). This suggests that these dendrimer-pDNA complexes are structurally plastic (metastable) complexes, a property also identified in cationic liposome-pDNA particles that retain unprotonated amine groups at neutral pH [275]. This rearrangement process can be attributed to the tertiary amines of the inner dendrimer branches (pKa, unbound = 5.7) which when incubated at pH 7.4 within proximity to pDNA can extend amine group protonation and energise dendrimer structural rearrangement creating further binding sites. It is apparent that substantial

rearrangements take place; therefore, this dynamic process must be better understood in order to identify the ideal incubation conditions and produce well-defined and reproducible formulations [275].

Exploration of relevant physicochemical characteristics is vital when assessing a new gene delivery agent for *in vivo* use. Formulation in a low pH environment or amphiphilic derivatisation significantly increased the surface charge density of these dendrimer formulations and therefore improved the solubility and reduced particle sizes of dendrimer-DNA complexes. These modifications produced a more pharmaceutically acceptable formulation but this may be problematic *in vivo*, however, as serum interactions are known to destabilise highly cationic species and prevent transfection from taking place [275]. Dendrimer amphiphile formulations were importantly able to stabilise DNA against precipitation at charge neutrality. There is a precedent for the use of slightly negatively charged or neutral pDNA particles for *in vivo* transfection purposes, which cDAB-16 would facilitate. In all cases, the tendency for complexes to aggregate in physiological media was dramatically reduced in the presence of 50% w/ w serum, a very good prognostic indicator for *in vivo* use.

Cetylated formulations displayed increasingly better resistance against electrostatic disruption by a synthetic GAG (Figure 48) than the parent dendrimer as the amount of hydrophobic component increased. Although essential that complexed DNA is protected from biological degradation, it must also be released through a reversal of this process into cell cytoplasm and nucleus for translation. The ability of a synthetic GAG to release pDNA from the dendrimer derivatives also suggested that these carriers were suitable to examine for transfection ability.

The morphology of complexes as determined by TM AFM has been shown to be dependent upon the composition of vector (Figure 43, Figure 44 & Figure 45). Interestingly, neither complex structural features visualised using AFM nor hydrophobicities were able to be correlated with DNase I or whole serum DNA degradation (Figure 49 & Figure 50). It seems rather that the existing high cationic

surface charge densities are protective of DNA, possibly due to the presence of a large reservoir of interacting free dendrimer in the incubation mixture. This warrants further examination of the process of DNase I degradation of DNA complexed by these dendrimers using a technique such as AFM [228].

A selection of biological effects in cell populations has been determined for amphiphilic DAB-16. These can be tentatively extended to *in vivo* biological situations if the limitations of the assays used are appreciated. For example, free cetyl DAB-16 had a much greater haemolytic potential than its vesicle formulation counterpart (Figure 54) which was partially reversed by assembly into vesicle structures. Interestingly this reduction in toxicity upon formulation into vesicle structures was not as pronounced in MTT reduction assay measurements (Table 13, Table 14 & Table 15), suggesting that metabolic activity as an indirect measure of cell viability may not be as sensitive to the effects of the amphiphilic dendrimer as those of DAB-16-Am. The amphiphilic dendrimer formulations were in all cases an order of magnitude more toxic to the cell lines than the parent dendrimer DAB-16-Am according to the MTT reduction assay. The particular cell line (B16 F10, PC-3 or A431) treated with the dendrimer formulation did not affect the resulting toxicities of DAB-16-Am, cDAB-16 or cDAB-16 vesicles in real terms. A comparison of the viability of a non-transformed cell line following treatment would be more representative of 'normal' cellular effects however there are inherent difficulties in the culture of these cells. It should be noted that serum was not included in the treatments of cells for MTT measurement and serum components were removed prior to haemolytic assay; in the *in vivo* situation some of this toxicity may be ameliorated by neutralisation of non-specific cationic charge interactions by anionic serum proteins.

Examination of the transfection efficiencies of the dendrimer carriers in these three cell lines leads to the conclusion that the dendrimer formulations are able to significantly transfect all three (Figure 65) however no dendrimer carrier performs consistently better. It would appear that the overall mechanism of transfection is altered by hydrophobic derivatisation and that the success of the amphiphile

formulations is strongly dependent upon finding a delicate balance between toxicity and transfection efficiency [258].

Enhanced interaction with serum components was to be expected for flexible amphiphile monomers [279] and the inclusion of cholesterol in the cDAB-16 formulation did produce a smaller reduction in the given transfection efficiency upon exposure to 50% v/v serum, which seems to support this theory [221]. Interestingly, susceptibility to serum reduction is not seen under these conditions for DAB-16-Am although it can bind serum components (evidenced as a reduction in particle size, section 4.4.1.3). The susceptibility of ExGen 500 to serum reduces its transfection efficiency of A431 cells to a level similar to that produced by DAB-16-Am (Figure 66), which may mean that this high level of ExGen 500 *in vitro* transfection would not be of advantage *in vivo*. Susceptibilities to inactivation by serum components may be attributable to the higher cationic charge density of the large (22KDa) PEI molecules when compared with the small (<2KDa) PPI dendrimer molecules.

In dose ranging studies, cDAB-16 was less toxic than might have been expected from haemolysis and cytotoxicity assays and found to be safe for *in vivo* use; therefore it is important to confirm these data in a whole organism. From the *in vivo* biodistribution studies it was concluded that unfortunately luciferase expression analysis is not a good technique for measurement of PPI dendrimer *in vivo* gene expression. Organ transfection efficiencies were not as favourable as those from a β-galactosidase reporter gene assay used previously [74, 272] although significant transfection of the liver by DAB-16-Am at 48 h is corroborated by these results. The biodistribution profile of ExGen 500 did concur with the literature as a single injection of DNA complexed with linear PEI (22kDa) to mice efficiently transfected the lungs and to a lesser extent the heart, spleen, kidney and liver [245]. It remains uncertain whether loss of dendrimer expression in the circulation was due to degradation by serum nuclease following protein/ glycosaminoglycan disruption, for example, or gross aggregation leading to compartmentalisation in non-expressing pathways.

Although data were initially promising, cDAB-16 has not yet fulfilled its potential as an *in vivo* gene delivery agent. This is likely to be due to the strong cationic surface charges exhibited by cDAB-16-pDNA complexes at the N: P ratio examined (N: P 30) and the resulting potential for interaction with biological milieu. This thesis has presented some evidence to support the formulation of these complexes at lower N: P ratios for *in vivo* applications. However, a reassessment of amphiphilic dendrimer chemical structure could be undertaken using a tested paradigm with a view to engineering a simple yet more stable complex for these purposes [280, 281].

7.2. Further work

As mentioned above, cDAB-16 was safe for *in vivo* use at 12.5 $mg.kg^{-1}$ and was more cytotoxic to immortalised cells than DAB-16-Am, so first and foremost it should be more thoroughly investigated as an anti-cancer gene medicine in a suitable biological model such as A431 xenograft in nude mice and used to deliver a therapeutic plasmid such as TNFα [53]. Reporter gene biodistribution models able to align chemical and physical characteristics of complexes with biological disposition deserve further investigation and the technique of SPECT has shown some promise in this area [260].

Thermodynamic characterisation was limited to direct examination of binding enthalpies using ITC. Ideally a mathematical model should be derived for elucidation of binding parameters to the dendrimer binding curve following ITC analysis; one that does not require equilibrium attainment and takes into account cooperative and specific ion exchange effects between these spherical dendrimers [136].

Techniques such as SANS could be used to probe the interior of cetylated dendrimer complexes as certain packing arrangements have been shown to result in improved transfection [41, 176].

As binding studies utilising exclusion of ethidium bromide showed that DNA condensation by DAB-16-Am and cDAB-16 was continuing over a period of several days, transfection studies using complexes formed over longer time periods than 30 min should now be conducted to determine an optimum incubation period.

Investigation into the long term stability of complexes upon storage will be vital, and as this preparation is likely to require freeze drying for use in the clinic. The selection of cryoprotectants for improved reconstitution should be investigated, perhaps beginning with the addition of sucrose to the complex formulation [282].

Bibliography

1. Watson, J.D. and F.H. Crick, *Genetical implications of the structure of deoxyribonucleic acid.* Nature, 1953. **171**(4361): p. 964-7.
2. Watson, J.D. and F.H. Crick, *Molecular structure of nucleic acids; a structure for deoxyribose nucleic acid.* Nature, 1953. **171**(4356): p. 737-8.
3. Human Genome Project. *Genomics and Its Impact on Science and Society: A 2003 Primer*. 2003 [cited 08 September 2007]; Available from: www.ornl.gov/hgmis.
4. Lever, A.M.L. and P. Goodfellow, *Gene Therapy*. British Medical Bulletin. Vol. 51. 1995, Edinburgh: Churchill Livingstone.
5. Journal of Gene Medicine. *Gene therapy clinical trials worldwide*. Journal of Gene Medicine 2007 [cited 08 September 2007]; Available from: http://www.wiley.co.uk/genmed.
6. Anderson, K.P., et al., *Inhibition of human cytomegalovirus immediate-early gene expression by an antisense oligonucleotide complementary to immediate-early RNA.* Antimicrob. Agents Chemother., 1996. **40**(9): p. 2004-2011.
7. *A randomized controlled clinical trial of intravitreous fomivirsen for treatment of newly diagnosed peripheral cytomegalovirus retinitis in patients with AIDS.* Am J Ophthalmol, 2002. **133**(4): p. 467-74.
8. Pearson, S., H. Jia, and K. Kandachi, *China approves first gene therapy.* Nat Biotechnol, 2004. **22**(1): p. 3-4.
9. Huang, L., M.-C. Hung, and E. Wagner, *Non-Viral Vectors for Gene Therapy Second Edition Part 1*. 2nd ed. Advances in Genetics, ed. J. Hall and J.F. Dunlap, T. Vol. 53. 2005, San Diego: Elsevier Academic Press.
10. Robbins, P.D., H. Tahara, and S.C. Ghivizzani, *Viral vectors for gene therapy.* Trends Biotechnol, 1998. **16**(1): p. 35-40.
11. Lehrman, S., *Virus treatment questioned after gene therapy death.* Nature, 1999. **401**(6753): p. 517-8.
12. Kaiser, J., *Gene therapy. Seeking the cause of induced leukemias in X-SCID trial.* Science, 2003. **299**(5606): p. 495.

13. Wolff, J.A., et al., *Direct gene transfer into mouse muscle in vivo.* Science, 1990. **247**(4949 Pt 1): p. 1465-8.
14. Song, Y.K., et al., *Characterization of cationic liposome-mediated gene transfer in vivo by intravenous administration.* Hum Gene Ther, 1997. **8**(13): p. 1585-94.
15. Ogris, M., et al., *PEGylated DNA/transferrin-PEI complexes: reduced interaction with blood components, extended circulation in blood and potential for systemic gene delivery.* Gene Ther, 1999. **6**(4): p. 595-605.
16. Ruponen, M., et al., *Extracellular and intracellular barriers in non-viral gene delivery.* J Control Release, 2003. **93**(2): p. 213-7.
17. Kawabata, K., Y. Takakura, and M. Hashida, *The fate of plasmid DNA after intravenous injection in mice: involvement of scavenger receptors in its hepatic uptake.* Pharm Res, 1995. **12**(6): p. 825-30.
18. Ward, C.M., M.L. Read, and L.W. Seymour, *Systemic circulation of poly(L-lysine)/DNA vectors is influenced by polycation molecular weight and type of DNA: differential circulation in mice and rats and the implications for human gene therapy.* Blood, 2001. **97**(8): p. 2221-9.
19. Khalil, I.A., et al., *Uptake pathways and subsequent intracellular trafficking in nonviral gene delivery.* Pharmacol Rev, 2006. **58**(1): p. 32-45.
20. Pollard, H., et al., *Ca2+-sensitive cytosolic nucleases prevent efficient delivery to the nucleus of injected plasmids.* J Gene Med, 2001. **3**(2): p. 153-64.
21. Pante, N. and M. Kann, *Nuclear pore complex is able to transport macromolecules with diameters of about 39 nm.* Mol Biol Cell, 2002. **13**(2): p. 425-34.
22. Schaffer, D.V., et al., *Vector unpacking as a potential barrier for receptor-mediated polyplex gene delivery.* Biotechnol Bioeng, 2000. **67**(5): p. 598-606.
23. Mislick, K.A. and J.D. Baldeschwieler, *Evidence for the role of proteoglycans in cation-mediated gene transfer.* Proc Natl Acad Sci U S A, 1996. **93**(22): p. 12349-54.
24. Zabner, J., et al., *Cellular and molecular barriers to gene transfer by a cationic lipid.* J Biol Chem, 1995. **270**(32): p. 18997-9007.

25. Lukacs, G.L., et al., *Size-dependent DNA mobility in cytoplasm and nucleus.* J Biol Chem, 2000. **275**(3): p. 1625-9.
26. Okuda, T., T. Niidome, and H. Aoyagi, *Cytosolic soluble proteins induce DNA release from DNA--gene carrier complexes.* J Control Release, 2004. **98**(2): p. 325-32.
27. Arigita, C., et al., *Association and dissociation characteristics of polymer/DNA complexes used for gene delivery.* Pharm Res, 1999. **16**(10): p. 1534-41.
28. Zhang, G., et al., *Hydroporation as the mechanism of hydrodynamic delivery.* Gene Ther, 2004. **11**(8): p. 675-82.
29. Thanaketpaisarn, O., et al., *Tissue-specific characteristics of in vivo electric gene: transfer by tissue and intravenous injection of plasmid DNA.* Pharm Res, 2005. **22**(6): p. 883-91.
30. Nabel, G.J., et al., *Direct gene transfer with DNA-liposome complexes in melanoma: expression, biologic activity, and lack of toxicity in humans.* Proc Natl Acad Sci U S A, 1993. **90**(23): p. 11307-11.
31. Brown, M.D., A.G. Schatzlein, and I.F. Uchegbu, *Gene delivery with synthetic (non viral) carriers.* Int J Pharm, 2001. **229**(1-2): p. 1-21.
32. Farhood, H., N. Serbina, and L. Huang, *The role of dioleoyl phosphatidylethanolamine in cationic liposome mediated gene transfer.* Biochim Biophys Acta, 1995. **1235**(2): p. 289-95.
33. Audouy, S. and D. Hoekstra, *Cationic lipid mediated transfection in vitro and in vivo.* Molecular Membrane Biology, 2001. **18**(2): p. 129-143.
34. da Cruz, M.T., et al., *Kinetic analysis of the initial steps involved in lipoplex--cell interactions: effect of various factors that influence transfection activity.* Biochim Biophys Acta, 2001. **1510**(1-2): p. 136-51.
35. Thomas, M. and A.M. Klibanov, *Non-viral gene therapy: polycation-mediated DNA delivery.* Appl Microbiol Biotechnol, 2003. **62**(1): p. 27-34.
36. Brown, M.D., et al., *Preliminary characterization of novel amino acid based polymeric vesicles as gene and drug delivery agents.* Bioconjug Chem, 2000. **11**(6): p. 880-91.

37. Ohana, P., et al., *Regulatory sequences of the H19 gene in DNA based therapy of bladder cancer.* Gene Therapy and Molecular Biology, 2004. **8**: p. 181-192.

38. Pollard, H., et al., *Polyethylenimine but not cationic lipids promotes transgene delivery to the nucleus in mammalian cells.* J Biol Chem, 1998. **273**(13): p. 7507-11.

39. Fischer, D., et al., *In vitro cytotoxicity testing of polycations: influence of polymer structure on cell viability and hemolysis.* Biomaterials, 2003. **24**(7): p. 1121-31.

40. Sonawane, N.D., F.C. Szoka, Jr., and A.S. Verkman, *Chloride accumulation and swelling in endosomes enhances DNA transfer by polyamine-DNA polyplexes.* J Biol Chem, 2003. **278**(45): p. 44826-31.

41. Tang, M.X. and F.C. Szoka, *The influence of polymer structure on the interactions of cationic polymers with DNA and morphology of the resulting complexes.* Gene Ther, 1997. **4**(8): p. 823-32.

42. Brown, M.D., et al., *In vitro and in vivo gene transfer with poly(amino acid) vesicles.* J Control Release, 2003. **93**(2): p. 193-211.

43. Yamazaki, Y., et al., *Polycation liposomes, a novel nonviral gene transfer system, constructed from cetylated polyethylenimine.* Gene Ther, 2000. **7**(13): p. 1148-55.

44. Zhou, X.H., A.L. Klibanov, and L. Huang, *Lipophilic polylysines mediate efficient DNA transfection in mammalian cells.* Biochim Biophys Acta, 1991. **1065**(1): p. 8-14.

45. Al-Jamal, K.T., T. Sakthivel, and A.T. Florence, *Dendrisomes: cationic lipidic dendron vesicular assemblies.* Int J Pharm, 2003. **254**(1): p. 33-6.

46. Wagner, E., *Strategies to improve DNA polyplexes for in vivo gene transfer: will "artificial viruses" be the answer?* Pharm Res, 2004. **21**(1): p. 8-14.

47. Wagner, E., et al., *Influenza virus hemagglutinin HA-2 N-terminal fusogenic peptides augment gene transfer by transferrin-polylysine-DNA complexes: toward a synthetic virus-like gene-transfer vehicle.* Proc Natl Acad Sci U S A, 1992. **89**(17): p. 7934-8.

48. Wagner, E., et al., *Coupling of adenovirus to transferrin-polylysine/DNA complexes greatly enhances receptor-mediated gene delivery and expression of transfected genes.* Proc Natl Acad Sci U S A, 1992. **89**(13): p. 6099-103.
49. Dufes, C., et al., *Niosomes and polymeric chitosan based vesicles bearing transferrin and glucose ligands for drug targeting.* Pharm Res, 2000. **17**(10): p. 1250-8.
50. Kunath, K., et al., *Galactose-PEI-DNA complexes for targeted gene delivery: degree of substitution affects complex size and transfection efficiency.* J Control Release, 2003. **88**(1): p. 159-72.
51. Petersen, H., et al., *Polyethylenimine-graft-poly(ethylene glycol) copolymers: influence of copolymer block structure on DNA complexation and biological activities as gene delivery system.* Bioconjug Chem, 2002. **13**(4): p. 845-54.
52. Fisher, K.D., et al., *A versatile system for receptor-mediated gene delivery permits increased entry of DNA into target cells, enhanced delivery to the nucleus and elevated rates of transgene expression.* Gene Ther, 2000. **7**(15): p. 1337-43.
53. Dufes, C., et al., *Synthetic anticancer gene medicine exploits intrinsic antitumor activity of cationic vector to cure established tumors.* Cancer Res, 2005. **65**(18): p. 8079-84.
54. Buhelier, E., W. Wehner, and F. Vogtle, Synthesis, 1978: p. 155.
55. Bosman, A.W., H.M. Janssen, and E.W. Meijer, *About Dendrimers: Structure, Physical Properties, and Applications.* Chem Rev, 1999. **99**(7): p. 1665-1688.
56. Bielinska, A., et al., *Regulation of in vitro gene expression using antisense oligonucleotides or antisense expression plasmids transfected using starburst PAMAM dendrimers.* Nucleic Acids Res, 1996. **24**(11): p. 2176-82.
57. Eichman, J.D., et al., *The use of PAMAM dendrimers in the efficient transfer of genetic material into cells.* Pharm Sci Technolo Today, 2000. **3**(7): p. 232-245.
58. Hollins, A.J., et al., *Evaluation of generation 2 and 3 poly(propylenimine) dendrimers for the potential cellular delivery of antisense oligonucleotides*

targeting the epidermal growth factor receptor. Pharm Res, 2004. **21**(3): p. 458-66.

59. Zinselmeyer, B.H., et al., *The lower-generation polypropylenimine dendrimers are effective gene-transfer agents.* Pharm Res, 2002. **19**(7): p. 960-7.

60. Boas, U. and P.M. Heegaard, *Dendrimers in drug research.* Chem Soc Rev, 2004. **33**(1): p. 43-63.

61. Jevprasesphant, R., et al., *Engineering of dendrimer surfaces to enhance transepithelial transport and reduce cytotoxicity.* Pharm Res, 2003. **20**(10): p. 1543-50.

62. Shah, D.S., et al., *DNA transfection and transfected cell viability using amphipathic asymmetric dendrimers.* Int J Pharm, 2000. **208**(1-2): p. 41-8.

63. Ramaswamy, C., et al., *Dendriplexes and their characterisation.* Int J Pharm, 2003. **254**(1): p. 17-21.

64. Gebhart, C.L. and A.V. Kabanov, *Evaluation of polyplexes as gene transfer agents.* J Control Release, 2001. **73**(2-3): p. 401-16.

65. Florence, A.T. and N. Hussain, *Transcytosis of nanoparticle and dendrimer delivery systems: evolving vistas.* Adv Drug Deliv Rev, 2001. **50 Suppl 1**: p. S69-89.

66. Lee, C.C., et al., *Designing dendrimers for biological applications.* Nat Biotechnol, 2005. **23**(12): p. 1517-26.

67. Shaunak, S., et al., *Polyvalent dendrimer glucosamine conjugates prevent scar tissue formation.* Nat Biotechnol, 2004. **22**(8): p. 977-84.

68. Chen, C.Z., et al., *Quaternary ammonium functionalized poly(propylene imine) dendrimers as effective antimicrobials: structure-activity studies.* Biomacromolecules, 2000. **1**(3): p. 473-80.

69. Van-Quynh, A., et al., *NMR relaxation study of molecular dynamics in columnar and smectic phases of a PAMAM liquid-crystalline co-dendrimer.* Eur Phys J E Soft Matter, 2005. **18**(2): p. 149-58.

70. Frechet, J.M.J. and D.A. Tomalia, *Dendrimers and Other Dendritic Polymers.* 2001.

71. Santhakumaran, L.M., T. Thomas, and T.J. Thomas, *Enhanced cellular uptake of a triplex-forming oligonucleotide by nanoparticle formation in the presence of polypropylenimine dendrimers.* Nucleic Acids Res, 2004. **32**(7): p. 2102-12.
72. Kan, P.L., et al., *Tumour gene expression from C12 spermine amphiphile gene delivery systems.* J Drug Target, 2005. **13**(6): p. 345-57.
73. Uchegbu, I.F., et al., *Quaternary ammonium palmitoyl glycol chitosan--a new polysoap for drug delivery.* Int J Pharm, 2001. **224**(1-2): p. 185-99.
74. Schatzlein, A.G., et al., *Preferential liver gene expression with polypropylenimine dendrimers.* J Control Release, 2005. **101**(1-3): p. 247-58.
75. Dash, P.R., et al., *Factors affecting blood clearance and in vivo distribution of polyelectrolyte complexes for gene delivery.* Gene Ther, 1999. **6**(4): p. 643-50.
76. Bell, H.S., et al., *A p53-derived apoptotic peptide derepresses p73 to cause tumor regression in vivo.* J Clin Invest, 2007. **117**(4): p. 1008-18.
77. Han, S.O., R.I. Mahato, and S.W. Kim, *Water-Soluble Lipopolymer for Gene Delivery.* Bioconjugate Chem., 2001. **12**(3): p. 337-345.
78. Kim, S., et al., *Hydrophobic modification of polyethylenimine for gene transfectants.* Bull. Korean. Chem. Soc., 2001. **22**(10): p. 1069-1075.
79. Uchegbu, I.F., et al., *Gene transfer with three amphiphilic glycol chitosans--the degree of polymerisation is the main controller of transfection efficiency.* J Drug Target, 2004. **12**(8): p. 527-39.
80. Wang, W., L. Tetley, and I.F. Uchegbu, *The Level of Hydrophobic Substitution and the Molecular Weight of Amphiphilic Poly-L-lysine-Based Polymers Strongly Affects Their Assembly into Polymeric Bilayer Vesicles.* J Colloid Interface Sci, 2001. **237**(2): p. 200-207.
81. Sansone, F., et al., *DNA condensation and cell transfection properties of guanidinium calixarenes: dependence on macrocycle lipophilicity, size, and conformation.* J Am Chem Soc, 2006. **128**(45): p. 14528-36.
82. Kurisawa, M., M. Yokoyama, and T. Okano, *Transfection efficiency increases by incorporating hydrophobic monomer units into polymeric gene carriers.* J Control Release, 2000. **68**(1): p. 1-8.

83. Brownlie, A., I.F. Uchegbu, and A.G. Schatzlein, *PEI-based vesicle-polymer hybrid gene delivery system with improved biocompatibility.* Int J Pharm, 2004. **274**(1-2): p. 41-52.

84. Templeton, N.S., et al., *Improved DNA: liposome complexes for increased systemic delivery and gene expression.* Nat Biotechnol, 1997. **15**(7): p. 647-52.

85. Kabanov, A.V. and V.A. Kabanov, *DNA complexes with polycations for the delivery of genetic material into cells.* Bioconjug Chem, 1995. **6**(1): p. 7-20.

86. Patel, M.M. and T.J. Anchordoquy, *Contribution of hydrophobicity to thermodynamics of ligand-DNA binding and DNA collapse.* Biophys J, 2005. **88**(3): p. 2089-103.

87. Howard, K.A., et al., *Influence of hydrophilicity of cationic polymers on the biophysical properties of polyelectrolyte complexes formed by self-assembly with DNA.* Biochim Biophys Acta, 2000. **1475**(3): p. 245-55.

88. Wang, W., et al., *Self-Assembly of Cetyl Linear Polyethylenimine To Give Micelles, Vesicles, and Dense Nanoparticles.* Macromolecules, 2004. **37**(24): p. 9114-9122.

89. Nöding, G., Heitz, W., *Amphiphilic poly(ethyleneimine) based on long-chain alkyl bromides.* Macromol. Chem. Phys., 1998. **199**: p. 1637-1644.

90. Sykes, P., *A guidebook to mechanism in organic chemistry*. 6th ed. 1997, Singapore: Longman.

91. Akitt, J.W. and B.E. Mann, *NMR and chemistry: an introduction to modern NMR spectroscopy*. 4th ed. 2000, Cheltenham: Stanley Thornes.

92. Williams, D.H. and I. Fleming, *Spectroscopic Methods in Organic Chemistry*. 5th ed. 1995, London: McGraw-Hill.

93. Kusumi, T., T. Iwashita, and H. Naoki, *One-dimensional and Two-dimensional NMR Spectra by Modern Pulse Techniques*, ed. K. Nakanishi. 1990, Sausalito, California: University Science Books.

94. Willard, H.H., *Instrumental Methods of Analysis*. 7th ed. 1988: Wadsworth Publishing.

95. Harris, D.C., *Quantitative Chemical Analysis*. 5th ed. 1999, New York: W. H. freeman.

96. Ingram, G., *Methods of Organic Elemental Microanalysis*. 1962, London: Chapman & Hall.
97. Dutta, R.K. and S.N. Bhat, *Interaction of phenazinium dyes and methyl orange with micelles of various charge types.* Colloids and Surfaces A: Physicochemical and Engineering Aspects, 1996. **106**: p. 127-134.
98. Franceschi, S., et al., *Synthesis and aggregation behaviour of two-headed surfactants contaning the urocanic acid moiety.* New J Chem, 1998. **22**: p. 225-231.
99. Gehlen, M.H., M. Ferreira, and M.G. Neumann, *Interaction of methyl orange with cationic micelles and its effect on dye photochemistry.* Journal of Photochemistry and Photobiology A: Chemistry, 1995. **87**: p. 55-60.
100. Karukstis, K.K., et al., *Spectroscopic studies of the interaction of methyl orange with cationic alkyltrimethylammonium bromide surfactants.* Journal of Colloid and Interface Science, 1998. **203**: p. 157-163.
101. Kuiper, J.M., et al., *Novel pyridinium surfactants with unstaurated alkyl chains: Aggregation Behavior and interactions methyl orange in aqueous solution.* Langmuir, 2001. **17**: p. 5216-5224.
102. Lin, Y. and P. Alexandridis, *Cosolvent effects on the micellisation of an amphiphilic siloxane graft copolymer in aqueous solution.* Langmuir, 2002. **18**: p. 4220-4231.
103. Buwalda, R.T. and J.B.F.N. Engberts, *Aggregation of Dicationic Surfactants with Methyl Orange in Aqueous Solution.* Langmuir, 2001. **17**: p. 1054-1059.
104. Shaw, D., *Introduction to Colloid and Surface Chemistry*. 4th edition ed. 1992, Oxford: Butterworth Heinemann.
105. Malvern, *ZetaSizer Manual MAN0149 Making Size Measurements*. Issue 1.1 ed. M.I. Ltd. 2000.
106. Chai, M., Niu, Y., Youngs, W. J. and Rinaldi, P. L., *Structure and Conformation of DAB Dendrimers in Solution via Multidimensional NMR Techniques.* J. Am. Chem. Soc., 2001. **123**: p. 4670-4678.
107. Murugan, E., et al., *Catalysis by hydrophobically modified poly(propylenimine) dendrimers having quaternary ammonium and tertiary amine functionality.* Langmuir, 2004. **20**(19): p. 8307-12.

108. Pistolis, G., et al., *Poly(propylenimine) Dendrimers as pH-Sensitive Controlled-Release Systems.* Chem Eur J, 1999. **5**(5): p. 1440-1444.
109. Wang, D. and T. Imae, *Fluorescence emission from dendrimers and its pH dependence.* J Am Chem Soc, 2004. **126**: p. 13204-13205.
110. Kabanov, V.A. and A.A. Yaroslavov, *What happens to negatively charged lipid vesicles upon interacting with polycation species?* J Control Release, 2002. **78**(1-3): p. 267-71.
111. Israelachvili, J.N., *Intermolecular Surface Forces*. 2nd ed. 1992: Academic Press.
112. Podesta, A., et al., *Positively charged surfaces increase the flexibility of DNA.* Biophys J, 2005. **89**(4): p. 2558-63.
113. Saenger, W., *Principles of Nucleic Acid Structure*. Springer advanced texts in chemistry, ed. C.R. Cantor. 1984, New York: Springer-Verlag.
114. Podgornik, R., et al., *Watching molecules crowd: DNA double helices under osmotic stress.* Biophys Chem, 1995. **57**(1): p. 111-21.
115. Wilson, R.W. and V.A. Bloomfield, *Counterion-induced condesation of deoxyribonucleic acid. a light-scattering study.* Biochemistry, 1979. **18**(11): p. 2192-6.
116. Raspaud, E., et al., *Precipitation of DNA by polyamines: a polyelectrolyte behavior.* Biophys J, 1998. **74**(1): p. 381-93.
117. Manning, G.S., *The molecular theory of polyelectrolyte solutions with applications to the electrostatic properties of polynucleotides.* Q Rev Biophys, 1978. **11**(2): p. 179-246.
118. Braunlin, W.H., T.J. Strick, and M.T. Record, Jr., *Equilibrium dialysis studies of polyamine binding to DNA.* Biopolymers, 1982. **21**(7): p. 1301-14.
119. Haq, I., et al., *Parsing free energies of drug-DNA interactions.* Methods Enzymol, 2000. **323**: p. 373-405.
120. Teif, V.B., *Ligand-induced DNA condensation: choosing the model.* Biophys J, 2005. **89**(4): p. 2574-87.
121. Watson, J.D., et al., *Recombinant DNA*. 2nd edition ed. 1992, New York: Scientific American Books.

122. Ladbury, J.E. and M.L. Doyle, *Biocalorimetry 2: Applications of calorimetry in the biological sciences*. 2004, Chichester: John Wiley & Sons Ltd.

123. Braun, C.S., et al., *Structure/function relationships of polyamidoamine/DNA dendrimers as gene delivery vehicles.* J Pharm Sci, 2005. **94**(2): p. 423-36.

124. Chen, W., N.J. Turro, and D.A. Tomalia, *Using Ethidium Bromide to Probe the Interactions between DNA and Dendrimers.* Langmuir, 2000. **16**: p. 15-19.

125. Imzumrudov, V.A., M.V. Zhiryakova, and A.A. Goulko, *Ethidium Bromide as a Promising Probe for Studying DNA Interaction with Cationic Amphiphiles and Stability of the Resulting Complexes.* Langmuir, 2002. **18**: p. 10348-10356.

126. Rungsardthong, U., et al., *Effect of polymer ionization on the interaction with DNA in nonviral gene delivery systems.* Biomacromolecules, 2003. **4**(3): p. 683-90.

127. Boussif, O., et al., *A versatile vector for gene and oligonucleotide transfer into cells in culture and in vivo: polyethylenimine.* Proc Natl Acad Sci U S A, 1995. **92**(16): p. 7297-301.

128. Feinbaum, R., *Vectors derived from plasmids*. Current Protocols in Molecular Biology. 1998: John Wiley & Sons Inc. 1.5.1-1.5.17.

129. Budelier, K. and J. Schorr, *Purification of DNA by anion-exchange chromotography*. Current Protocols in Molecular Biology. 1998.

130. QIAGEN, *QIAGEN plasmid purification handbook.* 2nd edition 2003, Crawley: QIAGEN. p86.

131. Wilfinger, W.W., K. Mackey, and P. Chomczynski, *Effect of pH and ionic strength on the spectrophotometric assessment of nucleic acid purity.* Biotechniques, 1997. **22**(3): p. 474-6, 478-81.

132. Chaires, J.B., *Energetics of drug-DNA interactions.* Biopolymers, 1997. **44**(3): p. 201-15.

133. Choosakoonkriang, S., et al., *Biophysical characterization of PEI/DNA complexes.* J Pharm Sci, 2003. **92**(8): p. 1710-22.

134. Ehtezazi, T., U. Rungsardthong, and S. Stolnik, *Thermodynamic Analysis of Polycation-DNA Interaction Applying Titration Microcalorimetry.* Langmuir, 2003. **19**: p. 9387-9394.

135. McGhee, J.D. and P.H. von Hippel, *Theoretical aspects of DNA-protein interactions: co-operative and non-co-operative binding of large ligands to a one-dimensional homogeneous lattice.* J Mol Biol, 1974. **86**(2): p. 469-89.

136. Gurtovenko, A.A., et al., *Molecular dynamics study of charged dendrimers in salt-free solution: effect of counterions.* J Chem Phys, 2006. **124**(9): p. 94904.

137. Baker, B.M. and K.P. Murphy, *Evaluation of linked protonation effects in protein binding reactions using isothermal titration calorimetry.* Biophys J, 1996. **71**(4): p. 2049-55.

138. Ellis, K.J. and J.F. Morrison, *Buffers of constant ionic strength for studying pH-dependent processes.* Methods Enzymol, 1982. **87**: p. 405-26.

139. Fukada, H. and K. Takahashi, *Enthalpy and heat capacity changes for the proton dissociation of various buffer components in 0.1M potassium chloride.* Proteins: Structure, Function and Genetics, 1998. **33**: p. 159-166.

140. Lobo, B.A., et al., *Thermodynamic analysis of binding and protonation in DOTAP/DOPE (1:1): DNA complexes using isothermal titration calorimetry.* Biophys Chem, 2003. **104**(1): p. 67-78.

141. Widom, J. and R.L. Baldwin, *Inhibition of cation-induced DNA condensation by intercalating dyes.* Biopolymers, 1983. **22**(6): p. 1621-32.

142. Budker, V., V. Trubetskoy, and J.A. Wolff, *Condensation of nonstochiometric DNA/polycation complexes by divalent cations.* Biopolymers, 2006. **83**(6): p. 646-57.

143. Zinselmeyer, B.H., *Evaluation of polypropylenimine dendrimers and their quaternary amino derivatives as non-viral gene transfer agents*, in *Department of Pharmaceutical Sciences*. 2006, University of Strathclyde: Glasgow.

144. Ritort, F., et al., *Condensation transition in DNA-polyaminoamide dendrimer fibers studied using optical tweezers.* Phys Rev Lett, 2006. **96**(11): p. 118301.

145. Trubetskoy, V.S., et al., *Quantitative assessment of DNA condensation.* Anal Biochem, 1999. **267**(2): p. 309-13.

146. Clonotech Laborotories Inc. *pCMVBeta vector information Protocol PT2004-5.* 2006 [cited 08 July 2007]; Available from: http://www.clontech.com/images/pt/PT2004-5.pdf.

147. Moore, S., *Amino acid analysis: aqueous dimethyl sulfoxide as solvent for the ninhydrin reaction.* J Biol Chem, 1968. **243**(23): p. 6281-6283.

148. Moore, S. and W.H. Stein, *A modified ninhydrin reagent for the photometric determination of amino acids and related compounds.* J Biol Chem, 1954. **211**(2): p. 907-13.

149. Kabanov, V.A., et al., *Interpolyelectrolyte complexes formed by DNA and Astramol poly(propylenimine) dendrimers.* Macromolecules, 2000. **33**(9587-9593).

150. Florence, A.T. and D. Attwood, *Physicochemical Principles of Pharmacy.* 4th edition ed. 2006, London: Pharmaceutical Press.

151. Lobo, B.A., et al., *Isothermal titration calorimetric analysis of the interaction between cationic lipids and plasmid DNA.* Arch Biochem Biophys, 2001. **386**(1): p. 95-105.

152. Matulis, D., I. Rouzina, and V.A. Bloomfield, *Thermodynamics of DNA binding and condensation: isothermal titration calorimetry and electrostatic mechanism.* J Mol Biol, 2000. **296**(4): p. 1053-63.

153. Matulis, D., I. Rouzina, and V.A. Bloomfield, *Thermodynamics of cationic lipid binding to DNA and DNA condensation: roles of electrostatics and hydrophobicity.* J Am Chem Soc, 2002. **124**(25): p. 7331-42.

154. Koltover, I., T. Salditt, and C.R. Safinya, *Phase diagram, stability, and overcharging of lamellar cationic lipid-DNA self-assembled complexes.* Biophys J, 1999. **77**(2): p. 915-24.

155. Braun, C.S., et al., *A stopped-flow kinetic study of the assembly of nonviral gene delivery complexes.* Biophys J, 2005. **88**(6): p. 4146-58.

156. Ales Prokop, E.K.W.M.J.M.D., *Maximizing the <I>in vivo</I> efficiency of gene transfer by means of nonviral polymeric gene delivery vehicles.* Journal of Pharmaceutical Sciences, 2002. **91**(1): p. 67-76.

157. Jones, N.A., et al., *Polymer chemical structure is a key determinant of physicochemical and colloidal properties of polymer-DNA complexes for gene delivery.* Biochim Biophys Acta, 2000. **1517**(1): p. 1-18.
158. Kunath, K., et al., *Low-molecular-weight polyethylenimine as a non-viral vector for DNA delivery: comparison of physicochemical properties, transfection efficiency and in vivo distribution with high-molecular-weight polyethylenimine.* J Control Release, 2003. **89**(1): p. 113-25.
159. Gabrielson, N.P. and D.W. Pack, *Acetylation of Polyethylenimine Enhances Gene Delivery via Weakened Polymer/DNA Interactions.* Biomacromolecules, 2006. **7**(8): p. 2427-2435.
160. Mannisto, M., et al., *Structure-activity relationships of poly(L-lysines): effects of pegylation and molecular shape on physicochemical and biological properties in gene delivery.* J Control Release, 2002. **83**(1): p. 169-82.
161. Doody, A.M., et al., *Characterizing the structure/function parameter space of hydrocarbon-conjugated branched polyethylenimine for DNA delivery in vitro.* J Control Release, 2006. **116**(2): p. 227-37.
162. Kono, K., et al., *Transfection activity of polyamidoamine dendrimers having hydrophobic amino acid residues in the periphery.* Bioconjug Chem, 2005. **16**(1): p. 208-14.
163. Sochanik, A., et al., *In vivo gene transfer using cetylated polyethylenimine.* Acta Biochim Pol, 2004. **51**(3): p. 693-702.
164. Uchegbu, I.F., et al., *Polymeric chitosan-based vesicles for drug delivery.* J Pharm Pharmacol, 1998. **50**(5): p. 453-8.
165. Sato, T., T. Ishii, and Y. Okahata, *In vitro gene delivery mediated by chitosan. effect of pH, serum, and molecular mass of chitosan on the transfection efficiency.* Biomaterials, 2001. **22**(15): p. 2075-80.
166. Ohsaki, M., et al., *In vitro gene transfection using dendritic poly(L-lysine).* Bioconjug Chem, 2002. **13**(3): p. 510-7.
167. Bielinska, A.U., et al., *DNA complexing with polyamidoamine dendrimers: implications for transfection.* Bioconjug Chem, 1999. **10**(5): p. 843-50.

168. Prasad, T.K., V. Gopal, and N. Madhusudhana Rao, *Structural changes in DNA mediated by cationic lipids alter in vitro transcriptional activity at low charge ratios.* Biochim Biophys Acta, 2003. **1619**(1): p. 59-69.
169. Ahmad, A., et al., *New multivalent cationic lipids reveal bell curve for transfection efficiency versus membrane charge density: lipid-DNA complexes for gene delivery.* J Gene Med, 2005. **7**(6): p. 739-48.
170. Honore, I., et al., *Transcription of plasmid DNA: influence of plasmid DNA/polyethylenimine complex formation.* J Control Release, 2005. **107**(3): p. 537-46.
171. Ogris, M., et al., *The size of DNA/transferrin-PEI complexes is an important factor for gene expression in cultured cells.* Gene Ther, 1998. **5**(10): p. 1425-33.
172. Emi, N., et al., *Gene transfer mediated by polyarginine requires a formation of big carrier-complex of DNA aggregate.* Biochem Biophys Res Commun, 1997. **231**(2): p. 421-4.
173. Ross, P.C. and S.W. Hui, *Lipoplex size is a major determinant of in vitro lipofection efficiency.* Gene Ther, 1999. **6**(4): p. 651-9.
174. Godbey, W.T., K.K. Wu, and A.G. Mikos, *Size matters: molecular weight affects the efficiency of poly(ethylenimine) as a gene delivery vehicle.* J Biomed Mater Res, 1999. **45**(3): p. 268-75.
175. Lleres, D., et al., *Dependence of the cellular internalization and transfection efficiency on the structure and physicochemical properties of cationic detergent/DNA/liposomes.* J Gene Med, 2004. **6**(4): p. 415-28.
176. Koltover, I., et al., *An inverted hexagonal phase of cationic liposome-DNA complexes related to DNA release and delivery.* Science, 1998. **281**(5373): p. 78-81.
177. Evans, H.M., et al., *Structural polymorphism of DNA-dendrimer complexes.* Phys Rev Lett, 2003. **91**(7): p. 075501.
178. Ewert, K.K., et al., *A columnar phase of dendritic lipid-based cationic liposome-DNA complexes for gene delivery: hexagonally ordered cylindrical micelles embedded in a DNA honeycomb lattice.* J Am Chem Soc, 2006. **128**(12): p. 3998-4006.

179. Oberle, V., et al., *Lipoplex formation under equilibrium conditions reveals a three-step mechanism.* Biophys J, 2000. 79(3): p. 1447-54.

180. Kreiss, P., et al., *Plasmid DNA size does not affect the physicochemical properties of lipoplexes but modulates gene transfer efficiency.* Nucleic Acids Res, 1999. **27**(19): p. 3792-8.

181. Bielinska, A.U., J.F. Kukowska-Latallo, and J.R. Baker, Jr., *The interaction of plasmid DNA with polyamidoamine dendrimers: mechanism of complex formation and analysis of alterations induced in nuclease sensitivity and transcriptional activity of the complexed DNA.* Biochim Biophys Acta, 1997. **1353**(2): p. 180-90.

182. Okuda, T., et al., *Time-dependent complex formation of dendritic poly(L-lysine) with plasmid DNA and correlation with in vitro transfection efficiencies.* Org Biomol Chem, 2003. 1(8): p. 1270-3.

183. Dunlap, D.D., et al., *Nanoscopic structure of DNA condensed for gene delivery.* Nucleic Acids Res, 1997. **25**(15): p. 3095-101.

184. Volcke, C., et al., *Influence of DNA condensation state on transfection efficiency in DNA/polymer complexes: an AFM and DLS comparative study.* J Biotechnol, 2006. **125**(1): p. 11-21.

185. Cherng, J.Y., et al., *Effect of DNA topology on the transfection efficiency of poly((2-dimethylamino)ethyl methacrylate)-plasmid complexes.* J Control Release, 1999. **60**(2-3): p. 343-53.

186. Godbey, W.T., et al., *Improved packing of poly(ethylenimine)/DNA complexes increases transfection efficiency.* Gene Ther, 1999. 6(8): p. 1380-8.

187. Maksimenko, A.V., et al., *Optimisation of dendrimer-mediated gene transfer by anionic oligomers.* J Gene Med, 2003. 5(1): p. 61-71.

188. Kichler, A., C. Leborgne, and O. Danos, *Dilution of reporter gene with stuffer DNA does not alter the transfection efficiency of polyethylenimines.* J Gene Med, 2005. 7(11): p. 1459-67.

189. Kichler, A., et al., *Influence of the DNA complexation medium on the transfection efficiency of lipospermine/DNA particles.* Gene Ther, 1998. 5(6): p. 855-60.

190. Ruponen, M., S. Yla-Herttuala, and A. Urtti, *Interactions of polymeric and liposomal gene delivery systems with extracellular glycosaminoglycans: physicochemical and transfection studies.* Biochim Biophys Acta, 1999. **1415**(2): p. 331-41.
191. Malvern, *Making zeta potential measurements - Zetasizer 2000/3000. Manual 0150.* 2000.
192. Ramos, J.E., Jr., R. de Vries, and J. Ruggiero Neto, *DNA psi-condensation and reentrant decondensation: effect of the PEG degree of polymerization.* J Phys Chem B, 2005. **109**(49): p. 23661-5.
193. Jary, D. and J.L. Sikorav, *Cyclization of globular DNA. Implications for DNA-DNA interactions in vivo.* Biochemistry, 1999. **38**(11): p. 3223-7.
194. Pelta, J., F. Livolant, and J.L. Sikorav, *DNA aggregation induced by polyamines and cobalthexamine.* J Biol Chem, 1996. **271**(10): p. 5656-62.
195. Saminathan, M., et al., *Ionic and structural specificity effects of natural and synthetic polyamines on the aggregation and resolubilization of single-, double-, and triple-stranded DNA.* Biochemistry, 1999. **38**(12): p. 3821-30.
196. Yang, J. and D.C. Rau, *Incomplete ion dissociation underlies the weakened attraction between DNA helices at high spermidine concentrations.* Biophys J, 2005. **89**(3): p. 1932-40.
197. Neugebauer, W.A., E. Neugebauer, and R. Brzezinski, *Determination of the degree of N-acetylation of chitin-chitosan with picric acid.* Carbohydrate Res, 1989. **189**: p. 363-367.
198. Snyder, S.L. and P.Z. Sobocinski, *An improved 2,4,6-trinitrobenzenesulfonic acid method for the determination of amines.* Analytical Biochemistry, 1975. **64**(1).
199. Wang, W., L. Tetley, and I. Uchegbu, *A new class of amphiphilic poly-L-lysine based polymers forms nanoparticles on probe sonication in aqueous media.* Langmuir, 2000. **16**(7859-7866).
200. Widom, J. and R.L. Baldwin, *Monomolecular condensation of lambda-DNA induced by cobalt hexamine.* Biopolymers, 1983. **22**(6): p. 1595-620.
201. Oberle, V., U. Bakowsky, and D. Hoekstra, *Lipoplex assembly visualized by atomic force microscopy.* Methods Enzymol, 2003. **373**: p. 281-97.

202. Martin, A.L., et al., *Observation of DNA-polymer condensate formation in real time at a molecular level.* FEBS Lett, 2000. 480(2-3): p. 106-12.

203. Abdelhady, H.G., et al., *Direct real-time molecular scale visualisation of the degradation of condensed DNA complexes exposed to DNase I.* Nucleic Acids Res, 2003. 31(14): p. 4001-5.

204. Pope, L., et al., *Intercalation-induced changes in DNA supercoiling observed in real-time by atomic force microscopy.* Analytica Chimica Acta, 1999. 400: p. 27-32.

205. Lichtman, J.W. and J.A. Conchello, *Fluorescence microscopy.* Nat Methods, 2005. 2(12): p. 910-9.

206. Betley, T., et al., *Tapping mode atomic force microscopy investigation of poly(amidoamine) dendrimers: Effects of substrate and pH on dendrimer deformation.* Langmuir, 2001. 17: p. 2768-2773.

207. Fang, Y. and J.H. Hoh, *Cationic silanes stabilize intermediates in DNA condensation.* FEBS Lett, 1999. 459(2): p. 173-6.

208. Itaka, K., et al., *Evaluation by fluorescence resonance energy transfer of the stability of nonviral gene delivery vectors under physiological conditions.* Biomacromolecules, 2002. 3(4): p. 841-5.

209. Itaka, K., et al., *In situ single cell observation by fluorescence resonance energy transfer reveals fast intra-cytoplasmic delivery and easy release of plasmid DNA complexed with linear polyethylenimine.* J Gene Med, 2004. 6(1): p. 76-84.

210. Ruponen, M., et al., *Extracellular glycosaminoglycans modify cellular trafficking of lipoplexes and polyplexes.* J Biol Chem, 2001. 276(36): p. 33875-80.

211. Xu, Y. and F.C. Szoka, Jr., *Mechanism of DNA release from cationic liposome/DNA complexes used in cell transfection.* Biochemistry, 1996. 35(18): p. 5616-23.

212. Pan, C.Q., et al., *Mutational analysis of human DNase I at the DNA binding interface: implications for DNA recognition, catalysis, and metal ion dependence.* Protein Sci, 1998. 7(3): p. 628-36.

213. Suck, D., *DNA recognition by structure-selective nucleases.* Biopolymers, 1997. **44**(4): p. 405-21.

214. Kunitz, M., *Crystalline desoxyribonuclease; isolation and general properties; spectrophotometric method for the measurement of desoxyribonuclease activity.* J Gen Physiol, 1950. **33**(4): p. 349-62.

215. Eichhorn, G.L., P. Clark, and E. Tarien, *The interaction of metal ions with polynucleotides and related compounds. 13. The effect of metal ions on the enzymatic degradation of ribonucleic acid by bovine pancreatic ribonuclease and of deoxyribonucleic acid by bovine pancreatic deoxyribonuclease I.* J Biol Chem, 1969. **244**(3): p. 937-42.

216. Gosse, C., et al., *Initial degradation of deoxyribonucleic acid after injection in mammals.* Cancer Res, 1965. **25**(6): p. 877-83.

217. Lechardeur, D., et al., *Metabolic instability of plasmid DNA in the cytosol: a potential barrier to gene transfer.* Gene Ther, 1999. **6**(4): p. 482-97.

218. Moret, I., et al., *Stability of PEI-DNA and DOTAP-DNA complexes: effect of alkaline pH, heparin and serum.* J Control Release, 2001. **76**(1-2): p. 169-81.

219. Harada, A., H. Togawa, and K. Kataoka, *Physicochemical properties and nuclease resistance of antisense-oligodeoxynucleotides entrapped in the core of polyion complex micelles composed of poly(ethylene glycol)-poly(L-lysine) block copolymers.* Eur J Pharm Sci, 2001. **13**(1): p. 35-42.

220. Hill, I.R., et al., *Determination of protection from serum nuclease activity by DNA-polyelectrolyte complexes using an electrophoretic method.* Anal Biochem, 2001. **291**(1): p. 62-8.

221. Audouy, S., et al., *Serum as a modulator of lipoplex-mediated gene transfection: dependence of amphiphile, cell type and complex stability.* J Gene Med, 2000. **2**(6): p. 465-76.

222. Cherng, J.Y., et al., *Effect of size and serum proteins on transfection efficiency of poly ((2-dimethylamino)ethyl methacrylate)-plasmid nanoparticles.* Pharm Res, 1996. **13**(7): p. 1038-42.

223. Lian, T. and R.J. Ho, *Design and characterization of a novel lipid-DNA complex that resists serum-induced destabilization.* J Pharm Sci, 2003. **92**(12): p. 2373-85.

224. Plank, C., et al., *Activation of the complement system by synthetic DNA complexes: a potential barrier for intravenous gene delivery.* Hum Gene Ther, 1996. 7(12): p. 1437-46.

225. Witten, T.A. and L.M. Sander, *Diffusion-Limited Aggregation, a Kinetic Critical Phenomenon.* Physical Review Letters, 1981. 47(19): p. 1400.

226. Bottcher, C., et al., *High-Yield Preparation of Oligomeric C-Type DNA Toroids and Their Characterization by Cryoelectron Microscopy.* J. Am. Chem. Soc., 1998. 120(1): p. 12-17.

227. Minagawa, K., et al., *Direct observation of the biphasic conformational change of DNA induced by cationic polymers.* FEBS Lett, 1991. 295(1-3): p. 67-9.

228. Chim, Y.T.A., et al., *Structural Study of DNA Condensation Induced by Novel Phosphorylcholine-Based Copolymers for Gene Delivery and Relevance to DNA Protection.* Langmuir, 2005. 21(8): p. 3591-3598.

229. Radler, J.O., et al., *Structure of DNA-cationic liposome complexes: DNA intercalation in multilamellar membranes in distinct interhelical packing regimes.* Science, 1997. 275(5301): p. 810-4.

230. Freshney, I.R., *Culture of Animal Cells: A Manual of Basic Technique.* 5th ed. 2005: John Wiley & Sons Inc.

231. Goldberg, A.M., J. Zurlo, and D. Rudacille, *The three Rs and biomedical research.* Science, 1996. 272(5267): p. 1403.

232. Moreau, E., et al., *Interactions between red blood cells and a lethal, partly quaternized tertiary polyamine.* J Control Release, 2000. 64(1-3): p. 115-28.

233. Bottega, R. and R.M. Epand, *Inhibition of protein kinase C by cationic amphiphiles.* Biochemistry, 1992. 31(37): p. 9025-30.

234. Morgan, D.M., V.L. Larvin, and J.D. Pearson, *Biochemical characterisation of polycation-induced cytotoxicity to human vascular endothelial cells.* J Cell Sci, 1989. 94 (Pt 3): p. 553-9.

235. Senior, J.H., K.R. Trimble, and R. Maskiewicz, *Interaction of positively-charged liposomes with blood: implications for their application in vivo.* Biochim Biophys Acta, 1991. 1070(1): p. 173-9.

236. Malik, N., et al., *Dendrimers: relationship between structure and biocompatibility in vitro, and preliminary studies on the biodistribution of 125I-labelled polyamidoamine dendrimers in vivo.* J Control Release, 2000. **65**(1-2): p. 133-48.
237. Ryser, H.J., *A membrane effect of basic polymers dependent on molecular size.* Nature, 1967. **215**(5104): p. 934-6.
238. Krishna, T.R. and N. Jayaraman, *Synthesis of poly(propyl ether imine) dendrimers and evaluation of their cytotoxic properties.* J Org Chem, 2003. **68**(25): p. 9694-704.
239. Mosmann, T., *Rapid colorimetric assay for cellular growth and survival: application to proliferation and cytotoxicity assays.* J Immunol Methods, 1983. **65**(1-2): p. 55-63.
240. Hansen, M.B., S.E. Nielsen, and K. Berg, *Re-examination and further development of a precise and rapid dye method for measuring cell growth/cell kill.* J Immunol Methods, 1989. **119**(2): p. 203-10.
241. Liu, Y., et al., *Mechanism of cellular 3-(4,5-dimethylthiazol-2-yl)-2,5-diphenyltetrazolium bromide (MTT) reduction.* J Neurochem, 1997. **69**(2): p. 581-93.
242. Vistica, D.T., et al., *Tetrazolium-based assays for cellular viability: a critical examination of selected parameters affecting formazan production.* Cancer Res, 1991. **51**(10): p. 2515-20.
243. Jabbar, S.A., P.R. Twentyman, and J.V. Watson, *The MTT assay underestimates the growth inhibitory effects of interferons.* Br J Cancer, 1989. **60**(4): p. 523-8.
244. Plumb, J.A., R. Milroy, and S.B. Kaye, *Effects of the pH dependence of 3-(4,5-dimethylthiazol-2-yl)-2,5-diphenyl-tetrazolium bromide-formazan absorption on chemosensitivity determined by a novel tetrazolium-based assay.* Cancer Res, 1989. **49**(16): p. 4435-40.
245. Bragonzi, A., et al., *Comparison between cationic polymers and lipids in mediating systemic gene delivery to the lungs.* Gene Ther, 1999. **6**(12): p. 1995-2004.

246. Huang, C.Y., et al., *Enhancements in gene expression by the choice of plasmid DNA formulations containing neutral polymeric excipients.* J Pharm Sci, 2002. **91**(5): p. 1371-81.

247. Tang, M.X., C.T. Redemann, and F.C. Szoka, Jr., *In vitro gene delivery by degraded polyamidoamine dendrimers.* Bioconjug Chem, 1996. 7(6): p. 703-14.

248. Serafini, M., et al., *Elongation factor 1 (EF1alpha) promoter in a lentiviral backbone improves expression of the CD20 suicide gene in primary T lymphocytes allowing efficient rituximab-mediated lysis.* Haematologica, 2004. **89**(1): p. 86-95.

249. Hong, S., et al., *Functional analysis of various promoters in lentiviral vectors at different stages of in vitro differentiation of mouse embryonic stem cells.* Mol Ther, 2007. **15**(9): p. 1630-9.

250. Frum, R., et al., *HDM2-binding partners: interaction with translation elongation factor EF1alpha.* J Proteome Res, 2007. **6**(4): p. 1410-7.

251. Smith, P.K., et al., *Measurement of protein using bicinchoninic acid.* Anal Biochem, 1985. **150**(1): p. 76-85.

252. Wiechelman, K.J., R.D. Braun, and J.D. Fitzpatrick, *Investigation of the bicinchoninic acid protein assay: identification of the groups responsible for color formation.* Anal Biochem, 1988. **175**(1): p. 231-7.

253. Varma, R.K., et al., *Polysorbate 80: a pharmacological study.* Arzneimittelforschung, 1985. **35**(5): p. 804-8.

254. Boeckle, S., et al., *Purification of polyethylenimine polyplexes highlights the role of free polycations in gene transfer.* J Gene Med, 2004. **6**(10): p. 1102-11.

255. Bhattacharya, S. and S.S. Mandal, *Evidence of interlipidic ion-pairing in anion-induced DNA release from cationic amphiphile-DNA complexes. Mechanistic implications in transfection.* Biochemistry, 1998. **37**(21): p. 7764-77.

256. Hong, S., et al., *Interaction of poly(amidoamine) dendrimers with supported lipid bilayers and cells: hole formation and the relation to transport.* Bioconjug Chem, 2004. **15**(4): p. 774-82.

257. Al-Nasiry, S., et al., *The use of Alamar Blue assay for quantitative analysis of viability, migration and invasion of choriocarcinoma cells.* Hum Reprod, 2007. **22**(5): p. 1304-9.

258. Pouton, C.W., et al., *Polycation-DNA complexes for gene delivery: a comparison of the biopharmaceutical properties of cationic polypeptides and cationic lipids.* J Control Release, 1998. **53**(1-3): p. 289-99.

259. Smyth, D.H., *Alternatives to animal experiments*. 1978, London: Scolar Press, in association with The Research Defence Society.

260. Min, J.J. and S.S. Gambhir, *Gene therapy progress and prospects: noninvasive imaging of gene therapy in living subjects.* Gene Ther, 2004. **11**(2): p. 115-25.

261. Hildebrandt, I.J., et al., *Optical imaging of transferrin targeted PEI/DNA complexes in living subjects.* Gene Ther, 2003. **10**(9): p. 758-64.

262. Iyer, M., et al., *Bioluminescence imaging of systemic tumor targeting using a prostate-specific lentiviral vector.* Hum Gene Ther, 2006. **17**(1): p. 125-32.

263. Shin, J.H., et al., *Noninvasive imaging for monitoring of viable cancer cells using a dual-imaging reporter gene.* J Nucl Med, 2004. **45**(12): p. 2109-15.

264. Ray, P., et al., *Noninvasive quantitative imaging of protein-protein interactions in living subjects.* Proc Natl Acad Sci U S A, 2002. **99**(5): p. 3105-10.

265. Hildebrandt, I.J. and S.S. Gambhir, *Molecular imaging applications for immunology.* Clin Immunol, 2004. **111**(2): p. 210-24.

266. Thorne, S.H. and C.H. Contag, *Using in Vivo Bioluminescence Imaging to Shed Light on Cancer Biology.* Prceedings of the IEEE, 2005. **50**(4): p. 750-762.

267. Xenogen, *Living Image® Software Version 2.50 Manual PN40072*. 2004, Xenogen Corporation: Alameda.

268. Pringle, I.A., et al., *Detection of plasmid DNA vectors following gene transfer to the murine airways.* Gene Ther, 2005. **12**(15): p. 1206-14.

269. Smith, A.D. and J.P. Trempe, *Luminometric quantitation of photinus pyralis firefly luciferase and Escherichia coli beta-galactosidase in blood-contaminated organ lysates.* Anal Biochem, 2000. **286**(1): p. 164-72.

270. Colin, M., et al., *Haemoglobin interferes with the ex vivo luciferase luminescence assay: consequence for detection of luciferase reporter gene expression in vivo.* Gene Ther, 2000. 7(15): p. 1333-6.
271. Regnstrom, K., et al., *Gene Expression Profiles in Mouse Lung Tissue after Administration of Two Cationic Polymers Used for Nonviral Gene Delivery.* Pharm Res, 2005. **23**(3): p. 475-482.
272. Zinselmeyer, B.H., et al., *Quantification of beta-galactosidase activity after non-viral transfection in vivo.* J Control Release, 2003. **91**(1-2): p. 201-8.
273. Eliyahu, H., et al., *Lipoplex-induced hemagglutination: potential involvement in intravenous gene delivery.* Gene Ther, 2002. **9**(13): p. 850-8.
274. Zou, S.M., et al., *Systemic linear polyethylenimine (L-PEI)-mediated gene delivery in the mouse.* J Gene Med, 2000. **2**(2): p. 128-34.
275. Keller, M., et al., *Thermodynamic aspects and biological profile of CDAN/DOPE and DC-Chol/DOPE lipoplexes.* Biochemistry, 2003. **42**(20): p. 6067-77.
276. Keller, M., et al., *Biophysical characterization of the DNA binding and condensing properties of adenoviral core peptide mu.* Biochemistry, 2002. **41**(2): p. 652-9.
277. Preuss, M., et al., *Comparison between the interactions of adenovirus-derived peptides with plasmid DNA and their role in gene delivery mediated by liposome-peptide-DNA virus-like nanoparticles.* Org Biomol Chem, 2003. **1**(14): p. 2430-8.
278. Stewart, L., et al., *Physico-chemical analysis of cationic liposome-DNA complexes (lipoplexes) with respect to in vitro and in vivo gene delivery efficiency.* J. Chem. Soc., Perkin Trans. 2, 2001: p. 624-632.
279. Schenning, A.P.H.J., et al., *Amphiphilic Dendrimers as Building Blocks in Supramolecular Assemblies.* J Am Chem Soc, 1998. **120**: p. 8199-8208.
280. Fletcher, S., et al., *In vivo studies of dialkynoyl analogues of DOTAP demonstrate improved gene transfer efficiency of cationic liposomes in mouse lung.* J Med Chem, 2006. **49**(1): p. 349-57.

281. Fletcher, S., et al., *Biophysical properties of CDAN/DOPE-analogue lipoplexes account for enhanced gene delivery.* Chembiochem, 2008. 9(3): p. 455-63.

282. Talsma, H., et al., *Stabilization of gene delivery systems by freeze-drying.* Int J Pharm, 1997. **157**(2): p. 233-238.